Right Ventricular Pressure Overload: hemodynamic and proteomic changes

Matthijs Jan Faber

Financial support for this thesis was generously provided by:

Afdeling kindercardiologie, Sophia Kinderziekenhuis Erasmus MC

Erasmus Universiteit Rotterdam

ISBN: 978-90-5335-525-1

Layout: Simone Vinke, Ridderprint BV, Ridderkerk, The Netherlands
Print: Ridderprint BV, Ridderkerk, The Netherlands

Right Ventricular Pressure Overload: hemodynamic and proteomic changes

Drukoverbelasting van de rechter hartkamer:
veranderingen in hemodynamiek en het proteoom

Proefschrift

ter verkrijging van de graad van doctor aan de
Erasmus Universiteit Rotterdam

op gezag van de
rector magnificus

Prof.dr. H.G. Schmidt

en volgens besluit van het College voor Promoties.
De openbare verdediging zal plaatsvinden op

donderdag 12 april 2012 om 13:30 uur

door

Matthijs Jan Faber

geboren te Terneuzen

Promotiecommissie

Promotoren:	Prof.dr. W.A. Helbing Prof.dr. J.M.J. Lamers
Overige leden:	Prof.dr. D.J.G.M. Duncker Prof.dr. D. Tibboel Prof.dr. J.W. Roos-Hesselink
Copromotor:	Dr. M. Dalinghaus

Contents:

Chapter 1

General introduction and outline thesis

Introduction

Background

The incidence of congenital heart disease (CHD) is estimated to vary between 4 to 50 per 1000 live births [1, 2] . This wide range of incidence is due to different phenotypes of CHD, as well as the inclusion criteria used. All together, CHD can be seen as the most common birth defect worldwide with approximately 1 million children born with a CHD each year [3]. Epidemiological studies in the Netherlands report an incidence of 6 per 1000 children born with a CHD each year [4].

When looking at causes of infant death, congenital anomalies are the leading cause. One third of these deaths are due to CHD [5]. However, the introduction of modern surgery as well as improved treatment strategies for CHD resulted in a decline in mortality from CHD [6]. In addition, death resulting form CHD shifted from newborns to young adults [7]. Thus, this prolonged survival results in an increase in patients with CHD that need treatment not only at birth, but also during adolescence and even during their adult live. In a selected group of these patients, the structural abnormalities that define a particular CHD phenotype results in prolonged RV pressure overload, such as Tetralogy of Fallot, left hypoplastic heart syndrome or congenitally corrected transposition of the great vessels. In addition, other diseases such as pulmonary hypertension or even ischemic heart disease can result in increased RV loading conditions. The effects of prolonged RV pressure overload on the heart's function, as well as the effects on molecular and cellular level is not yet fully understood. However, patient data suggest that the RV is unable to cope with prolonged periods of (systemic) overload resulting in RV failure [8-12]. Therefore, it is of utmost importance to understand the effects of prolonged pressure overload on the RV in terms of ventricular function, as well as at the molecular level.

Right ventricular properties

The effects of prolonged pressure overload on the left ventricle (LV) have been widely studied. The results of those studies, however, cannot be simply translated to the RV. The RV distinguishes from the LV in various ways. First of all, the stroke volume of the RV is similar to the LV but using approximately 25% of the stroke work because of the low resistance of the pulmonary vasculature [13]. Given Laplace's law, which states that the pressure within a sphere is proportional to the wall tension (wall stress times wall thickness) and is inversely proportional to the internal diameter, the RV is thin walled under normal physiological circumstances. In addition, the geometry of the RV is different from the LV. Where the LV is more round shaped, the RV has a more crescent shape with an inlet (sinus) portion and an outlet (conus) section, separated by the crista supraventricularis. The RV stroke volume mostly results from longitudinally shortening

of the RV wall, whereas in the LV circumferential shortening is more important [14]. The two chambers cannot be seen as two separate units since they are linked by a shared wall, the interventricular septum, and are encircled by common muscle fibers. Therefore, alterations in the geometry of one ventricle by for instance hypertrophy of dilatation can influence the systolic or diastolic function of the contralateral ventricle [15].

Right ventricular adaptation to prolonged afterload

Prolonged elevations in RV afterload result in extensive remodelling of the RV. An important first adaptation mechanism is the development of hypertrophy [16]. This initial increase in ventricular mass helps the RV to cope with the increased afterload but gradually progressive contractile dysfunction will set in. Eventually, the right ventricle will dilate to allow for compensatory preload in order to maintain stroke volume despite reduced fractional shortening. When the contractile function deteriorates even further, clinical signs of RV failure (systemic congestion) will become eminent [17].

This adaptive process of RV hypertrophy to increased afterload and the subsequent development of RV failure is a complex, dynamic process which evolves over time. The characterisation of the hypertrophic response is not uniform. Several classifications and definitions of the type of hypertrophic response, such as physiological and pathological hypertrophy, have been proposed [18-22]. Despite the different point of views, it is acknowledged that the process of hypertrophy is, in addition to an increase in muscle mass, accompanied by various changes in both physiological behaviour of the myocardium as well as biochemical changes.

Biochemical changes in right ventricular hypertrophy

Until recently, most research available on the molecular mechanisms involved in cardiac hypertrophy and the progression to failure is derived from studies on the LV. This was merely due to underestimation of the pivotal role of the RV in the systemic circulation [13]. Some of the mechanisms involved in LV hypertrophy may be present in the RV, however, given the various structural, functional and even developmental differences between RV and LV, it is also reasonable to assume that other mechanisms are involved. Therefore, to increase our understanding of the transition from RV hypertrophy to failure, it is mandatory to conduct studies specifically aimed at RV pathobiology and -physiology.

In general, (pathological) cardiac hypertrophy is accompanied by changes at the cellular level such as changes in calcium handling [23], β-adrenergic signalling [24], mitochondrial energy metabolism [25], and the activation of several signal transduction cascades that in turn can lead to altered gene-transcription activity with alteration in gene expression levels [26].

Research on most of these aforementioned mechanisms has been done in either *in vitro* experiments or in *in vivo* models of LV hypertrophy. At present, little is known about the contribution of each of these mechanisms in RV hypertrophy. In addition, RV hypertrophy that develops after prolonged periods of pressure overload is a continuous process in which the pathological changes at the molecular level are time related. In particular, crucial changes can be expected in the transition phase of compensated hypertrophy to decompensated hypertrophy, i.e. heart failure.
In this present thesis, the protein changes after various periods of RV pressure overload are studied using proteomics technologies.

Analyzing protein changes in right ventricular hypertrophy - proteomics

As mentioned above, during the development of RV hypertrophy or heart failure, many alterations occur in signal transduction cascades that eventually will lead to alterations in gene expression. The total number of genes present in a cell at a given time and condition is called a genome. The determination of these genes can be done using genomics technologies, such as micro array experiments. Data from these genomics experiments on heart hypertrophy and failure have provided insight on gene expression profiles that are present in various stages of hypertrophy [27]. However, alterations in gene expression levels during hypertrophy do not necessarily correlate with changes in the protein level since not all gene alterations will lead to protein syntheses. In addition, proteins can undergo modifications after their translation (so-called post-translational modifications (PTMs)). The eventual phenotype of the cells is a result of the proteins present. In analogy to genomics, the complement of proteins that are present in the cell in a given time and under certain conditions (the proteome), can be studied using proteomics. One of the main characteristics of the proteomics approach is the holistic view on the protein changes. Unlike the "classical" or "reductionists" approach which involved the study of single proteins at the time with for instance Western blotting, proteomics aims to display changes in groups of proteins. The resulting advantage of proteomics is that changes can be detected in proteins that were formerly unknown to be involved in certain diseases. In addition, many proteomics techniques also allow the study of proteins with PTMs. A detailed review on proteomics in general and the application in cardiovascular research is given in chapter 2

Right ventricular physiology

RV physiology differs substantially from LV physiology due to multiple factors, such as difference in wall thickness and degree of afterload. Given its position in the circulatory system, between systemic venous and the pulmonary circulation, the main function

is to provide adequate pulmonary perfusion. In addition, a sufficient pump function of the RV also prevents congestion of tissues and organs by maintaining low systemic venous pressures [17]. Furthermore, the RV also influences the LV via the shared intraventricular septum, thereby playing a role in maintaining global cardiac function. Due to its positioning within the circulatory system, the RV is subject to a lower afterload as compared to the LV. The pressures generated by the RV under normal physiological circumstances are also lower. As a result, the RV uses approximately 5 times less energy to pump the same amount of blood [28]. The mechanisms involved in RV contraction and subsequent ejection of blood are also different from the LV. The RV free wall will move toward the interventricular septum, thereby reducing the septal-to-free wall distance [29]. The majority of blood will be ejected by this motion. The complete emptying will result from the contraction of circular LV fibers that enhance the convexity of the interventricular septum.

The cardiac cycle can be defined in periods such as isovolumic relaxation, diastolic filling phase, isovolumic contraction and finally ejection. For the LV, these periods are well defined. In the RV the isovolumic contraction is less well defined as it is rapidly followed by RV ejection. In addition, the RV ejection is still ongoing while RV pressures already start to decline [30]. In addition, the amount of stoke work is about 5 times less as compared to the LV [28]. Despite the physiological differences between both ventricles, there is also a great deal of interaction between LV and RV. In the diastolic phase, the filling of RV will lead to reduced LV chamber dimensions and result in upward displacement of diastolic pressure-volume relations [31, 32]. The systolic ventricular interaction mainly consists of LV contraction contributing to the generation of RV systolic pressure [33]. It is thought that approximately 20-40% of total RV systolic pressure development is the result of LV contraction [34].

Analyzing right ventricular function by pressure-volume loops

The assessment of right ventricular function is a challenging task. The continuos measurement of RV pressure has been possible for a long time, but the pressure changes alone are not sufficient for determining the RV performance. In addition to pressure, one should also measure RV volume. This parameter, however, is challenging to obtain since the geometry of the RV is rather complex. In addition, there is a great deal of inter-individual variation in the size of the RV [33]. A precise volumetric analysis should therefore consist of techniques that measure volume independent of geometrical assumptions [35-37]. Preferably, the RV volume and pressure should be measured continuously and simultaneously so pressure-volume (PV) relations can be constructed that give insight into the mechanical function of the heart.

In this present thesis we have used PV-relations to describe cardiac function.

In figure one a schematical pressure-volume loop is shown. On the horizontal axis ventricular volume is plotted, on the vertical axis ventricular pressure. Segment A-B reflects the diastolic filling phase, followed by the isovolumic contraction phase (B-C), ejection phase (B-C) and the isovolumic relaxation (C-D). From these loops the end-diastolic and end-systolic points (resp. point B and D) can be derived. The width of each loop represents stroke volume, the surface area represents stroke work. For the RV, the pressure-volume loops are smaller in size and more triangular due to the more difficult definition of isovolumic contraction and relaxation intervals.

Figure 1: Schematic representation of a Pressure-Volume loop. See text for more details.

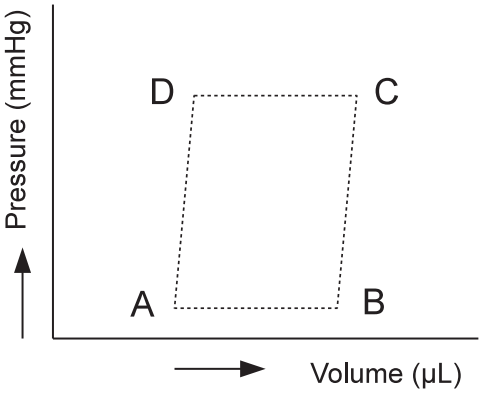

When preload is reduced, for instance by partial occlusion of the vena cava inferior, the ventricular pressure- and volume both decrease. This results in a downward- and leftward shift of the PV-loops. This manoeuvre enables us to derive several parameters that can be used to determine ventricular function. One of these parameters is the end-systolic pressure-volume relation (ESPVR). The ESPVR is a linear relation between pressure and volume at end-systole (also termed: elastance) and is a relative load independent measure of end-systolic performance [38-40]. A leftward or upward displacement of the ESPVR reflects an increase in myocardial contractility, whereas an opposite displacement reflects a decreased level of contractility. Besides the slope of the ESPVR, also the intercept with the volume-axis at a certain pressure can be used to determine changes in inotropy [41-43]. Besides the ESPVR, also other parameters can be used to describe systolic function. The preload recruitable stroke work (PRSW) relation is a preload-independent measure of systolic function and is relative insensitive to changes in afterload [44-46]. It's a ventricular function curve using stroke work and end-diastolic volume. A third parameter is the dP/dtmax-Ved (end-diastolic volume) relation. Whereas the dP/dtmax is commonly used as an isovolumic parameter of

contractile function, it is very sensitive to changes in preload. To correct for the preload-dependence, the dP/dtmax was linearly related to the end-diastolic volume [47]. This resulted in a very sensitive parameter of systolic function with minor dependence on preload. However, the large variations observed in the dP/dtmax make it a less stable parameter of contractile function as compared to the ESPVR [44]. As all three parameters of systolic function have their own limitations, we have used more than one parameter to describe the systolic function of the RV.
The diastolic function can also be derived from the PV-loops. When constructing the end-diastolic pressure and - volume points during a preload reduction manoeuvre, one obtains the end-diastolic pressure-volume relation (EDPVR). This parameter reflects the passive characteristics of the ventricle, ie. chamber stiffness [48, 49]. A second parameter used to describe diastolic function is tau. This index reflects isovolumic relaxation by describing the time needed for ventricular pressure to fall to 1/e (approximately 37%) of its initial value [50]. In addition, the dP/dtmin was used as a determinant of early diastolic performance as it reflects the peak rate of pressure decline during isovolumic relaxation.

Outline of this thesis

This present thesis consist of several studies that aim to elucidate biochemical and physiological changes that occur during (prolonged) right ventricular pressure overload. As an introduction to the biochemical techniques used, a review on proteomics methods is presented in chapter two. The application of proteomics technologies on RV protein changes after 6 weeks of PAB is presented in chapter three. The application of biventricular PV-loops is presented in chapter four, where the effects of PAB on RV and LV physiology are described. A detailed study on longitudinal protein changes during RV pressure overload is presented in chapter 5. Chapter 6 describes the changes in LV and RV systolic and diastolic function that occur after various time periods of PAB. Finally, chapter 7 presents a method for assessing cardiac myofilament changes using HPLC.

References

1. Hoffman, J.I., S. Kaplan, and R.R. Liberthson, Prevalence of congenital heart disease. Am Heart J, 2004. 147(3): p. 425-39.
2. Hoffman, J.I. and S. Kaplan, The incidence of congenital heart disease. J Am Coll Cardiol, 2002. 39(12): p. 1890-900.
3. Foundation, M.o.D.B.D., Global report on birth defects. The hidden toll of dying and disabled children. White plains. 2006, New York, USA. 28.
4. EUROCAT, Prevalence of congenital malformations in the Northern Netherlands, 1981-2005. 2007, University Medical Center Groningen: Groningen, The Netherlands.
5. Organization, W.H. Infant deaths: number of deaths by cause, sex and age. 2006; Available from: http://www.who.int/healthinfo/morttables/en/index.html.
6. Boneva, R.S., et al., Mortality associated with congenital heart defects in the United States: trends and racial disparities, 1979-1997. Circulation, 2001. 103(19): p. 2376-81.
7. Organization, W.H. WHO Mortality Database. 2009 21-4-2009; Available from: http://www.who.int/whosis/mort/download/en/index.html.
8. Graham, T.P., Jr., Ventricular performance in congenital heart disease. Circulation, 1991. 84(6): p. 2259-74.
9. Helbing, W.A., et al., Long-term results of atrial correction for transposition of the great arteries. Comparison of Mustard and Senning operations. J Thorac Cardiovasc Surg, 1994. 108(2): p. 363-72.
10. Redington, A.N., et al., Right ventricular function 10 years after the Mustard operation for transposition of the great arteries: analysis of size, shape, and wall motion. Br Heart J, 1989. 62(6): p. 455-61.
11. Cochrane, A.D., T.R. Karl, and R.B. Mee, Staged conversion to arterial switch for late failure of the systemic right ventricle. Ann Thorac Surg, 1993. 56(4): p. 854-61; discussion 861-2.
12. Wong, K.Y., et al., Longitudinal study of ventricular function after the Mustard operation for transposition of the great arteries: a long term follow up. Br Heart J, 1988. 60(4): p. 316-23.
13. Voelkel, N.F., et al., Right ventricular function and failure: report of a National Heart, Lung, and Blood Institute working group on cellular and molecular mechanisms of right heart failure. Circulation, 2006. 114(17): p. 1883-91.
14. Kukulski, T., et al., Normal regional right ventricular function and its change with age: a Doppler myocardial imaging study. J Am Soc Echocardiogr, 2000. 13(3): p. 194-204.
15. Maruyama, Y., et al., Mechanical interactions between four heart chambers with and without the pericardium in canine hearts. Circ Res, 1982. 50(1): p. 86-100.
16. Dias, C.A., et al., Reversible pulmonary trunk banding. II. An experimental model for rapid pulmonary ventricular hypertrophy. J Thorac Cardiovasc Surg, 2002. 124(5): p. 999-1006.
17. Furey, S.A., 3rd, H.A. Zieske, and M.N. Levy, The essential function of the right ventricle. Am Heart J, 1984. 107(2): p. 404-10.
18. Grossman, W., Cardiac hypertrophy: useful adaptation or pathologic process? Am J Med, 1980. 69(4): p. 576-84.
19. Krayenbuehl, H.P., et al., Physiologic or pathologic hypertrophy. Eur Heart J, 1983. 4 Suppl A: p. 29-34.
20. Wikman-Coffelt, J., W.W. Parmley, and D.T. Mason, The cardiac hypertrophy process. Analyses of factors determining pathological vs. physiological development. Circ Res, 1979. 45(6): p. 697-707.
21. Meerson, F.Z., The myocardium in hyperfunction, hypertrophy and heart failure. Circ Res, 1969. 25(1): p. Suppl 2:1-163.

22. Weber, K.T., et al., Physiologic versus pathologic hypertrophy and the pressure-overloaded myocardium. J Cardiovasc Pharmacol, 1987. 10 Suppl 6: p. S37-50.
23. Brunner, F., G. Wolkart, and S. Haleen, Defective intracellular calcium handling in monocrotaline-induced right ventricular hypertrophy: protective effect of long-term endothelin-A receptor blockade with 2-benzo[1,3]dioxol-5-yl-3-benzyl-4-(4-methoxy-phenyl-)- 4-oxobut-2-enoate-sodium (PD 155080). J Pharmacol Exp Ther, 2002. 300(2): p. 442-9.
24. Dorn, G.W., 2nd and J.D. Molkentin, Manipulating cardiac contractility in heart failure: data from mice and men. Circulation, 2004. 109(2): p. 150-8.
25. Huss, J.M. and D.P. Kelly, Mitochondrial energy metabolism in heart failure: a question of balance. J Clin Invest, 2005. 115(3): p. 547-55.
26. Frey, N. and E.N. Olson, Cardiac hypertrophy: the good, the bad, and the ugly. Annu Rev Physiol, 2003. 65: p. 45-79.
27. Buermans, H.P., et al., Microarray analysis reveals pivotal divergent mRNA expression profiles early in the development of either compensated ventricular hypertrophy or heart failure. Physiol Genomics, 2005. 21(3): p. 314-23.
28. Redington, A., Right ventricular function, in The right heart in congenital heart disease, A.N. Redington, Brawn W.J., Deanfield J.E., Anderson R.H. , Editor. 1998, Greenwich Medical Media Ltd.: London. p. 17-24.
29. Santamore, W.P., G.D. Meier, and A.A. Bove, Effects of hemodynamic alterations on wall motion in the canine right ventricle. Am J Physiol, 1979. 236(2): p. H254-62.
30. Redington, A.N., et al., Characterisation of the normal right ventricular pressure-volume relation by biplane angiography and simultaneous micromanometer pressure measurements. Br Heart J, 1988. 59(1): p. 23-30.
31. Santamore, W.P., et al., Myocardial interaction between the ventricles. J Appl Physiol, 1976. 41(3): p. 362-8.
32. Bemis, C.E., et al., Influence of right ventricular filling pressure on left ventricular pressure and dimension. Circ Res, 1974. 34(4): p. 498-504.
33. Dell'Italia, L.J., The right ventricle: anatomy, physiology, and clinical importance. Curr Probl Cardiol, 1991. 16(10): p. 653-720.
34. Yamaguchi, S., et al., Comparative significance in systolic ventricular interaction. Cardiovasc Res, 1991. 25(9): p. 774-83.
35. Kaul, S., et al., Assessment of right ventricular function using two-dimensional echocardiography. Am Heart J, 1984. 107(3): p. 526-31.
36. Oldershaw, P., Assessment of right ventricular function and its role in clinical practice. Br Heart J, 1992. 68(1): p. 12-5.
37. Jiang, L., et al., Three-dimensional echocardiography: in vivo validation for right ventricular free wall mass as an index of hypertrophy. J Am Coll Cardiol, 1994. 23(7): p. 1715-22.
38. Suga, H., K. Sagawa, and A.A. Shoukas, Load independence of the instantaneous pressure-volume ratio of the canine left ventricle and effects of epinephrine and heart rate on the ratio. Circ Res, 1973. 32(3): p. 314-22.
39. Suga, H. and K. Sagawa, Instantaneous pressure-volume relationships and their ratio in the excised, supported canine left ventricle. Circ Res, 1974. 35(1): p. 117-26.
40. Kass, D.A. and W.L. Maughan, From 'Emax' to pressure-volume relations: a broader view. Circulation, 1988. 77(6): p. 1203-12.
41. van der Velde, E.T., et al., Nonlinearity and load sensitivity of end-systolic pressure-volume relation of canine left ventricle in vivo. Circulation, 1991. 83(1): p. 315-27.

42. Little, W.C., et al., Response of the left ventricular end-systolic pressure-volume relation in conscious dogs to a wide range of contractile states. Circulation, 1988. 78(3): p. 736-45.
43. Steendijk, P., et al., Effects of critical coronary stenosis on global systolic left ventricular function quantified by pressure-volume relations during dobutamine stress in the canine heart. J Am Coll Cardiol, 1998. 32(3): p. 816-26.
44. Little, W.C., et al., Comparison of measures of left ventricular contractile performance derived from pressure-volume loops in conscious dogs. Circulation, 1989. 80(5): p. 1378-87.
45. Glower, D.D., et al., Linearity of the Frank-Starling relationship in the intact heart: the concept of preload recruitable stroke work. Circulation, 1985. 71(5): p. 994-1009.
46. Takeuchi, M., et al., Comparison between preload recruitable stroke work and the end-systolic pressure-volume relationship in man. Eur Heart J, 1992. 13 Suppl E: p. 80-4.
47. Little, W.C., The left ventricular dP/dtmax-end-diastolic volume relation in closed-chest dogs. Circ Res, 1985. 56(6): p. 808-15.
48. Grossman, W. and W.H. Barry, Diastolic pressure-volume relations in the diseased heart. Fed Proc, 1980. 39(2): p. 148-55.
49. Kass, D.A., Assessment of diastolic dysfunction. Invasive modalities. Cardiol Clin, 2000. 18(3): p. 571-86.
50. Weiss, J.L., J.W. Frederiksen, and M.L. Weisfeldt, Hemodynamic determinants of the time-course of fall in canine left ventricular pressure. J Clin Invest, 1976. 58(3): p. 751-60.

Chapter 2

New perspectives offered by proteomics and its implementation in the study of cardiac hypertrophy and failure

Matthijs J. Faber, Giulio Agnetti, Karel Bezstarosti, Inge M. Lankhuizen, Michiel Dalinghaus, Carlo Guarnieri, Claudio M. Caldarera, Willem A. Helbing, Jos M.J. Lamers

Adapted from:
M.J. Faber et al. *Cell Biochem Biophys. 2006;44(1):11-29. Review*

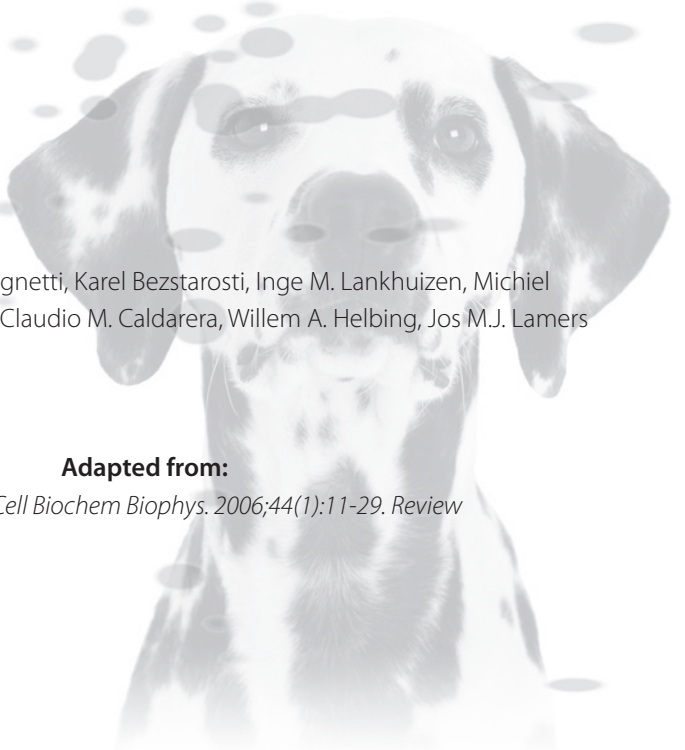

Abstract

The key components to the molecular understanding of the pathophysiology of various forms of heart failure involve global and/or large-scale identifications of proteins, their patterns of expression, post-translational modifications, and functional characterization. Particularly, proteins involved in the induction of cardiac (mal) adaptive hypertrophic growth, the interstitial fibrosis, and contractile dysfunction, are of interest. In general, with the accumulation of vast amounts of DNA sequences in databases, researchers have become aware that merely having complete sequences of genomes and transcriptional changes for thousands of genes simultaneously, will not be sufficient to elucidate, in molecular terms, the etiology and pathophysiology of cardiovascular disease. In the last decade, a new technology called proteomics, has become available that allows biological and (patho)physiological questions to be approached exclusively from the protein perspective. Proteomics may enable us to map the entire complement of proteins expressed by the heart at any time and condition. This approach creates the unique possibility to identify, by differential analysis, protein alterations associated with the etiology of heart disease and its progression, outcome, and response to therapy. In order to illustrate the true power of proteomics, most of the current available methodologies are first reviewed including their limitations. In this review will also be dealt with the current status and the perspectives of proteomics applications in research on heart failure in general. Furthermore, examples of recent own data on global protein profiling of the pressure-overloaded rat right ventricle, and of endothelin-1 stimulated cultures of neonatal rat cardiac myocytes, will be provided. A last section is devoted to the continuous advances in proteomic technologies, including protein separation methods, MS instrumentation, computational analysis and bioinformatic tools, together with integrative databases.

Introduction

Cardiovascular diseases remain the most common cause of mortality in adults worldwide [1]. In the past few decades, however, the clinical expression of cardiovascular disease has changed considerably. Significantly less people now succumb in the immediate aftermath of a cardiovascular event, such as acute myocardial infarction or stroke. This results in an increased burden of chronic manifestations of slowly progressive heart failure on the aging population. Heart failure is not a uniform disease entity, but a syndrome with various causes such as cardiomyopathy, congenital heart disease, hypertension, and myocardial infarction. The molecular basis of this syndrome remains poorly understood. The heart failure syndrome is largely treated symptomatically by a complex regimen of drugs. However, the effect of pharmacotherapy is not always satisfying [1]. The identification of single gene mutations that are responsible for inherited forms of hypertrophic and dilated cardiomyopathy, has allowed to pinpoint several of the initiating events that can lead to features of heart failure in humans [2]. However, even in these rare forms of cardiomyopathy, there is still a broad gap between the mutation and the understanding how the abnormality in the encoded protein leads to cardiac failure. Likewise, the molecular basis of chronic overload-induced heart failure is only slowly emerging. A key component to the molecular understanding of the pathophysiology is the identification and characterization of proteins. Particularly, those proteins involved in the induction of cardiac (mal)adaptive hypertrophic growth, the interstitial fibrosis, and contractile dysfunction are of interest. Changes in cardiac phenotype, i.e. quantitative (amount) and qualitative (isoform and post-translational modifications (PTMs)) alterations in protein expression, are likely to be the main determinants in the deterioration of cardiac function. The classical approach of molecular research, such as measurement of activities or quantities of already known proteins and/or enzymes in normal and diseased myocardium, typically focus on the analysis of one or a few known proteins per experiment. However, the key to the understanding of the molecular regulators of cardiac function in health and disease, lies in the identification of the complex interplay between global protein expression and modification patterns associated with clinical phenotype. The concept of mapping the human proteome was already put forward almost 20 years ago, but rapid advances in molecular biology techniques shifted the emphasis towards to the genome, ultimately leading to the human genome project [3]. Nowadays, sequence information on numerous proteins can be inferred from the open reading frames from the more than 50 complete genome sequences, including human and rodents (www.tigr.org/tdb/tgi) [3, 4]. Microarrays, or DNA "chips", have emerged as another powerful tool that now is applied to many areas in cardiovascular physiology and pathology [5]. This genomic approach allows large-scale parallel assessment of gene expression

profiles in various stages of developing cardiac hypertrophy and heart failure [5]. Additionally, the ability to engineer precise mutations in the heart, coupled with the ability to quantitate the effects of these mutations on cardiac function *in vivo*, has led to the recognition of a previously unsuspected set of signalling pathways and proteins that stimulate specific effects of cardiac hypertrophic growth [2]. The effects of both over-expression and knock-out of individual genes in animals have provided models that replicate human heart diseases [6-8]. Taken together, understanding the failing heart at a molecular level seems approachable by breaking down this complex disease into specific endpoints, and identifying key pathways and checkpoints for each important clinical phenotype during heart failure progression [1]. The *in vivo* models are very often (partially) extended to, and refined by, cell culture models. In this approach, homogeneous preparations of one cardiac cell type (myocytes, fibroblasts, etc.) are studied with respect to e.g. neurohormonal-, pacing-, or stretch specific cellular responses [9, 10]. The present state of knowledge on key signalling pathways, master switch proteins, and critical enzymes, may give the impression that the overall molecular characterization of several heart diseases will be complete in the near future. However, only the known pieces of a puzzle are described at a detailed level, neither knowing nor investigating which part of the puzzle has been resolved. Proteomics allows to map the entire complement of proteins expressed by the heart at any time and condition, which creates the unique possibility to identify, by differential analysis, protein alterations associated with the etiology of heart disease and its progression, outcome, and response to therapy.

This review will address the current status of proteomics applications in research on heart failure in general, together with a description of some of our recent data. To illustrate the true power of proteomics, an overview of the current status of the methodologies is provided, including the last new technological advances in this rapidly growing field. The potential pay-off of global proteomic analysis is the identification of novel therapeutic targets by uncovering distinctive protein signatures associated with heart failure. If such a protein is discovered, information on amino-acid sequence, obtained by tandem mass spectrometry (MS/MS), can be rapidly obtained. This can be used for designing nucleic acid based vectors specifically overexpressing or silencing protein production. Furthermore, protein action can be blocked specifically by a dominantly negative mutant protein [11, 12].

Why proteomics approach?

With the accumulation of vast amounts of DNA sequences in databases, researchers are increasingly realizing that merely having complete sequences of genomes is not sufficient to elucidate biological function. The existence of an open reading frame in

genomic sequences does not necessarily imply the existence of a functional gene. Thus, verification of a gene product by proteomic methods is an essential step in "annotating the genome" [13]. There are several other compelling reasons to approach biological and (patho)physiological questions exclusively from the protein perspective:
1) Proteins, not genes, are responsible for the phenotype of cells. Proteins are the functional output of the cell and therefore are expected to provide the most relevant information for molecular understanding of (patho)physiological processes. The level of complexity resulting from co- and post-translational modification events can only be dissected and understood through qualitative and quantitative studies at the level of the functional proteins themselves [14]. Particularly, when interpretation of protein expression takes into account the dynamics of this expression in specific biological contexts (see also point 4) [15].
2) It will be impossible to elucidate mechanisms of disease, aging, and effects of environment, solely by studying the genome and its expression at the level of mRNA [16]. For the study of proteins in bodily fluids, such as serum and urine, this is most evident in view of the remote mRNA source. The cellular expression or function of proteins is modulated at many steps from transcription to post-translation. Indeed, there generally is a poor correlation between the abundance of mRNA transcribed from the DNA and the respective proteins translated from that mRNA. Many different protein isoforms can be generated from a single gene at the first step of formation of mRNA. The initial transcript can be spliced in various ways to yield different protein forms [17]. Extensive alterations can also be introduced during or after translation. Indeed, the concept of "one gene, one protein" is an oversimplification. It is estimated that up to 200 different types of PTMs exist, such as the addition of specific carbohydrate side-chains (glycosylation) or phosphorylation of serine, threonine or tyrosine groups. Mechanisms, such as regulation of protein function by proteolysis, recycling, recruitment, and sequestration in cell compartments, affects gene products, not genes [15].
3) Protein-protein interactions and molecular composition of cellular structures, can be determined only at the cellular level. The human body may contain more than half a million modified proteins [17]. Understanding of their interplay is a formidable undertaking, even at the cellular level, where only 5,000 – 10,000 genes (although many more proteins) may be expressed. A key question about a protein is: with which other protein(s) does it interact [16]? Interaction partners are an immediate lead into biological function and can also be potentially exploited for therapeutical purposes. Biological function usually arises from the interaction of several proteins in tight complexes rather than as an intrinsic feature of an individual protein [18]. The systematic investigation of protein interactions for the purpose of elucidating protein

functions is termed "functional or interaction proteomics", and its application can make an important contribution to the study of protein-protein interaction [19].
4) The cell's proteome consists of all (modified) proteins present within the cell at any given time and/or any condition, which dictates the phenotype at a precise moment and/or under a specific condition [20]. Unlike the static information contained within the genome, the transcriptome and proteome are dynamic, reflecting the conditions to which a cell is exposed or, for example, a specific disease process. There are potentially huge numbers of proteomes for each cell type and its condition at a given time.
The execution of a proteomics-based study involves the integration of a number of technologies and expertise in biochemistry/molecular biology, physiology, bioinformatics/statistics and analytical protein chemistry. The term "proteome", defined as the protein complement of a genome, was first coined by Wilkins in 1995 at the Siena meeting for protein separation based on 2-DE [21]. Today, the field of proteomics covers essentially all efforts in separation, detection, quantification, identification and (functional) characterization of proteins and protein-protein interactions [16]. The most significant breakthrough in proteomics has been the MS identification of gel-separated proteins, which extends analysis far beyond the mere display of proteins on 2-DE, feasible since the seventies [22, 23]. For this major advance in proteomics, John Fenn and Koichi Tanaka shared the Nobel Prize in Chemistry in 2002 [24, 25].

Proteomic technologies including its current limitations

Protein separation by 2-DE

The initial step in global proteomic analysis is the separation of a complex protein mixture derived from e.g. a total tissue extract, a derived subfraction, or a homogenate of a primary cell culture or cell line. The use of 2-DE remains one of the best techniques to separate complex protein mixtures. Proteins are first separated based on their pI, by iso-electric focusing (IEF). In the second, perpendicular dimension, they are further resolved based on their relative molecular mass (M_r), by SDS-PAGE. One can routinely resolve 2,000 to 3,000 proteins from a single sample preparation, or up to 10,000 proteins when using large-scale custom gels [26]. Today's standard 2-DE technique is rather simple to perform, has a reasonable reproducibility, and is in principle the same as the method originally described 25 years ago [23]. Its reproducibility is improved by the introduction of immobilized pH gradients [27, 28]. An even further development of these so-called IPG strips was the development of narrow-ranged pH gradients which increased the resolving power and enabled "zooming at the proteome" [27, 29]. Also the sensitivity of protein detection was greatly enhanced by the introduction of novel staining protocols (discussed below). Although 2-DE analysis of proteomes

is conceptually simple, it suffers from several limitations that preclude widespread application for proteome analysis. It is technically demanding, labor intensive, and fraught with potential artifacts that hamper gel comparisons. Hydrophobic proteins and basic proteins are poorly solubilized in buffers used for 2-DE. Likewise, very high- and low-molecular weight proteins are poorly resolved by this technique. Basic proteins have the tendency to form pronounced streaks rather than spots due to electro-endoosmotic effects, the migration of reducing agents, and the potential hydrolysis of acrylamide at basic pH values [30]. These effects can be partially overcome using dithiothreitol replenishment during IEF and inclusion of glycerol to suppress electro-endoosmosis. Membrane-associated proteins pose a particular challenge with respect to solubilization and are therefore significantly underrepresented on 2-DE gels. One attempt to improve their solubility has been the use of alternative detergents [31]. Since many of the important regulatory proteins in cardiac muscle are highly charged (e.g. troponin I, pI 9.8), hydrophobic (e.g. SR membrane protein SERCA), or hydrophobic and large (e.g. ryanodine receptor in SR), or soluble but large (heavy-chain myosin), the global 2-DE patterns will surely not be complete. The higher resolution of 2-DE, compared to 1-DE, allows to detect proteins with alterations in mass and/or charge due to PTMs. This excellent resolving power of 2-DE can, however, work as a "dual-edged sword" [32] because artifactual modifications such as protein carbamylation can be picked up as well [33].

Methods for protein detection

Coomassie blue is a beloved staining dye for 2-DE gels [34, 35]. The low costs, ease of use, and probably most noteworthy, the good compatibility with downstream protein identification on MS, contributed to its popularity [36]. The dye is moderately sensitive (detection level: 8-10 ng), but its linear dynamic range makes it suitable for quantitation in a certain range of protein concentration. Silver staining has much higher sensitivity, approximately 0.1 ng protein per spot [37]. However, its dynamic range is nonlinear and PTMs can interfere with the staining [38]. Another drawback of the silver staining is its interference with MS-identification [36]. However, some studies have shown that minor modifications to the staining protocol can improve the compatibility with peptide mass profiling methods, however, at the expense of detection sensitivity [39, 40]. Radiolabelling, if applicable, such as when active protein phosphorylation occurs, can also achieve very high sensitivity, whereas western immunoblotting techniques makes it possible to detect as few as 1,000 molecules per cell [14]. Recently, as a typical example of radiolabelling, a first elegant analysis of β-adrenergic agonist-dependent phosphoproteome of isolated cardiomyocytes was reported by Chu et al., using 2-DE in combination with ^{32}P-autoradigraphy and MALDI-MS in conjunction with computer-

assisted protein spot matching [41]. A novel development in protein detection for 2-DE is called fluorescence 2-D difference gel electrophoresis technology (2D-DIGE) using pre-electrophoretic labeling with fluorescent dyes (Figure 1). It has the potential to improve the sensitivity and to increase the dynamic range of protein detection [42, 43]. Moreover, molecular weight and charge matched cyanine dyes enable multiplex labeling of different samples to be run in the same 2-DE gel allowing more accurate relative protein quantitation than the conventional methods. The most common used labels are amine reactive cyanine dyes (Cy2, Cy3, Cy5), allowing up to 3 different protein mixtures (e.g. control, treated and mixed plus treated as internal standard) to be labeled individually prior to mixing them and running them simultaneously on the same 2-DE gel. This experimental design reduces gel-to-gel variation over conventional 2-DE and facilitates the use of 2-D analysis software (DeCyder (Amersham Biosciences)) for automated and accurate spot quantitation, gelmatching, and statistical analysis. A major concern is still the detection sensitivity. For optimal solubilization of the proteins, only 1-2 % of the lysine residues in the proteins can be labeled with the fluorescent dyes [44]. Optimized DIGE can detect up to four times as many proteins as Coomassie blue staining, but only half the amount of proteins that can be detected by conventional silver staining [42]. However, DIGE technology is surpassing the MS adjusted silver staining with regard to sensitivity, although the SYPRO Ruby staining remains superior to DIGE [45]. Another issue that should be taken into account is the slight mass difference between the fluorescent labeled and unlabeled proteins. Registration errors between labeled and unlabeled proteins occur in 95% of the spots complicating the excision of the spots which may give erroneous results on MS [42, 44]. Post-staining can solve this problem but the detection sensitivity of this stain should be high enough to reveal all differentially displayed proteins that were initially detected by the cyanine dye. Therefore, the fluorescent (SYPRO Ruby) dye prevails the Coomassie blue staining and has been accepted as the post-staining of choice for DIGE analysis [42, 45, 46].

Figure 1: Schematical illustration of the basic principles of the DIGE (gel-dependent-), ICAT, and ^{16}O to ^{18}O exchange (both gel-independent-) technologies for relative protein quantitation *(see text for details)*.

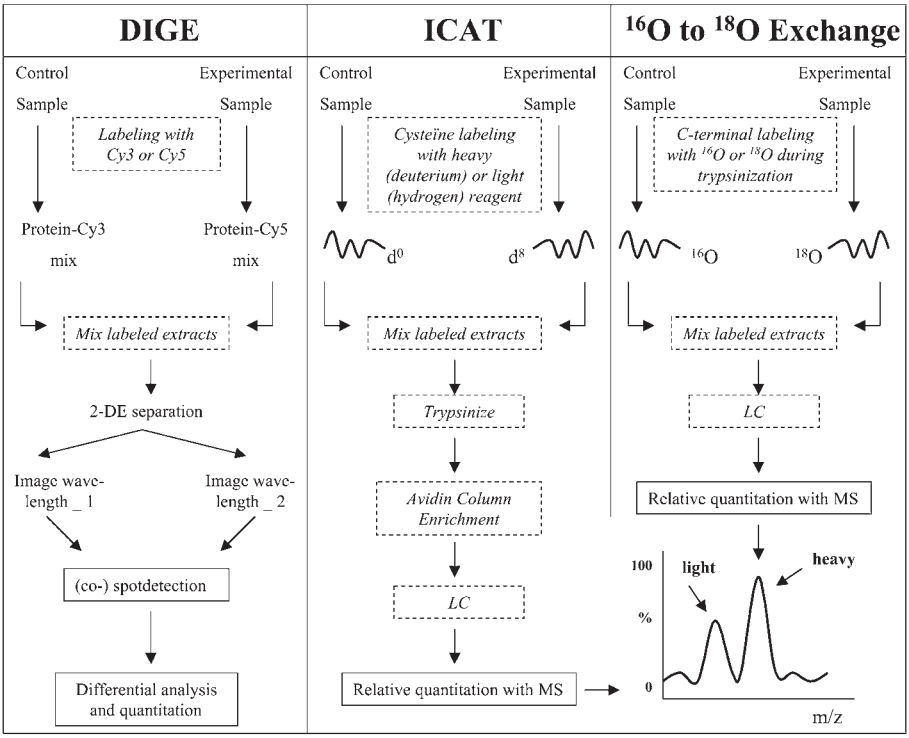

(m/z = mass to charge ratio).

Qualitative and quantitative analysis including differential display

The main purpose of the application of 2-DE in proteomics is to carry out differential protein profiling and/or creation of 2-DE gel protein databases. Coomassie blue dyes, designated as G-250 and R-250, are conventionally used to stain for proteins separated by 2-DE for quantitative purposes. Image acquisition is most often accomplished with an imaging densitometer resulting in a digital image of the 2-DE gel [14]. Software packages are currently commercially available for analysis of 2-DE gel images. The current generation of packages include e.g. PDQUEST (BioRad Laboratories, Hercules, Ca, USA) and Progenesis (Nonlinear Dynamics, Newcastle-upon-Tyne, UK). Image analysis entails detection of spots on the gel-image, quantification of abundance, and matching of protein spots on different gels [14]. Matching requires the definition of several "anchor points" or "landmarks" used as reference on all gels. In practice, depending on the type of software used, about 30 spots are chosen across the full

length and width of the images. Although spot detection is an automated procedure, inherent variations in the 2-DE process invariably necessitate a considerable manual editing. In the differential profiling approach, protein expression levels between two samples are compared, both qualitatively and quantitatively. By process of subtraction, differences (e.g. presence, absence, intensity of proteins, or different forms) can be found [15]. The gain or loss of protein spots yields information on the differential protein expression, while the spot intensities are used for calculating the relative up- or downregulation. Examples of such type of proteomics studies in the cardiovascular field will be described below. On the other hand, the creation of 2-DE gel protein databases, which started in the 1990s, has been essential for proteomics in the heart to become a powerful tool in the research of heart diseases. Pioneering proteomic work by the laboratories of Dunn and Jungblut led to the creation of several online 2-DE databases of human, dog, rat, and mouse atrial and ventricular myocardium [26, 47-49]. The three main databases are HEART-2D-PAGE [26, 48], HSC-2D-PAGE [47, 49, 50], and HP-2D-PAGE [51]. Over the years many groups have contributed to these databases (reviewed by [32]). However, these databases are still far from complete with roughly 200 proteins identified. Nevertheless, these freely accessible protein inventories are tremendously important because they provide researchers with a basis for visualization of changes in protein patterns resulting from conditions of their particular study [32].

MS identification and characterization of proteins

Two-DE provides information on the abundance, pI, and M_r of the separated proteins, but most often gives no direct clues as to their identities or functions [14]. Over the past few years, MS methods have become increasingly important for the analysis of proteins and peptides. This was made possible by the development of matrix assisted laser desorption (MALDI) and electrospray ionization methods (ESI) that are capable of ionizing very large molecules such as peptides with little or no fragmentation. If the excised spot is first in-gel digested with trypsin, which cleaves proteins at specific amino-acid sequences (if present), the proteins can be broken into a mixture of peptides. The mass of each of these peptides can then be measured by MS to produce a so-called "peptide mass fingerprint" (PMF) [15]. This discriminating signature is compared to the peptide masses predicted from theoretical digestion or protein sequences currently contained within databases allowing protein identification. If necessary, actual sequence information can be obtained by MS/MS, in which discrete peptide ions can be selected and fragmented and complex algorithms are used to correlate the experimental data derived from peptide sequences with protein databases. The MS/MS method is technically more complex and less scalable than MALDI fingerprinting. The main advantage of MS/MS is that sequence information

derived from several peptide fragments is much more specific for the identification of the protein, than a list of peptide masses [13]. The success of PMF is highly dependent on the existence of comprehensive, searchable databases (e.g. Mascot search engine at http://www.matrixscience.com), for the species under investigation [20]. Besides these databases that allow for identification of proteins, also other internet-based databases are available that facilitate further characterization ranging from the calculation of their physicochemical properties to the prediction of potential PTMs and 3-dimensional structures (links from http://www.expasy.org). Annotated protein and 2-DE databases are the bioinformatic core of proteome research For example, a database of human cardiac proteins has been established on http://www.expasy.ch/ch2d/2d-index.html [15]. PMF data are often coupled with MS/MS to increase the degree of confidence of identification. One approach, termed peptide sequence tagging, is based on interpretation of a portion of the electrospray ionization (ESI)-MS/MS fragmentation data to generate a short sequence or "tag". This is used in combination with the mass of the intact parent peptide ion to provide significant additional information. A second approach uses the database searching algorithm SEQUEST to match uninterpreted experimental MS/MS spectra with predicted fragment patterns generated *in silico* from sequences in protein and nucleotide databases [14, 15].

Isolation of subproteomes to detect low-abundance proteins and to reduce complexity

Because of the limited resolution power of separation technologies presently applied in proteomics research, additional fractionation steps upstream of 2-DE and MS are required [52]. Subcellular fractionation consists of disruption of the cellular organization (homogenization) and fractionation of the homogenate to separate different populations of organelles. A major limitation in successful subcellular fractionation is the association of organelles with cytoskeletal elements surrounding the nucleus or their entrapment in large aggregates, which readily sediment. In cardiac muscle there is also a wide difference in abundance between the myofilament proteins and the vast majority of other cellular proteins, which makes organelle proteomics necessary [17]. Reproducible subcellular fractionation methods will therefore become essential for enrichment of organelle-specific or low-abundance proteins for proteomic analysis [52]. A simple cardiac homogenate subfractionation includes separation of myofilament proteins from all the other cellular proteins by isolation and detergent extraction of the isolated myofilament fraction [53]. This approach has also been used in our setting for subfractionation of right ventricular homogenates (see later). A different approach, now called "functional proteomics", is prior protein fractionation based on specific affinity of multiple low-abundant proteins for a common interaction

partner. The latter has recently been successfully applied on the PKC-signaling network in the heart [18, 54]. This affinity-based separation is based on the fact that PKC-ε forms functional complexes with numerous structural proteins, signaling molecules, and stress-activated proteins to accomplish task-specific signal transduction. These complexes can be isolated by a gluthation-S transferase (GST)-based affinity pull-down method using recombinant GST-PKC-ε proteins. Alternatively, immunoprecipitation by PKC-ε antibody on protein G-Sepharose beads can be used. The comprehensive list of cardiac proteins identified in PKC-ε complexes presently contains a total of 93 proteins, which includes also proteins involved in metabolism and transcription and translation processes [18, 54].

Multi-dimensional liquid phase based separations

Taken into account the drawbacks of 2-DE, together with the lack of on-line integration with MS, various multi-dimensional (MuD) liquid-phase based separation techniques have recently been explored [55]. These systems separate proteins based on a variety of properties, such as pI and relative molecular mass, size and charged state, or hydrophobicity and charged state. In particular, with the emergence of techniques such as nanoflow capillary high-performance liquid chromatography (HPLC) in conjunction with MS/MS (HPLC-ESI-MS/MS), attention is gradually refocusing on developing comprehensive MuD-liquid chromatography-based separation techniques. The latter techniques will soon dominate the field of protein identification [55]. Nevertheless, there are still only few examples of 2-D HPLC, in which proteins are separated using two sequential steps [53]. The first dimension separations are carried out based on protein's pI, through ion exchange chromatography [56], chromatofocussing [57], or based on protein mass, such as in the case of size-exclusion LC [58]. Each of these separation methods are followed by reversed phase (RP) HPLC, the second dimension. In each case, the power of protein separation is primarily achieved in the first dimension. Neverova et al. used the RP-HPLC to resolve extremely complex protein mixtures, including cardiac muscle proteome, on the basis of hydrophobicity [53]. The HPLC fractions, collected within distinct regions of the chromatograms, were analyzed by MS and immunoblot analysis. Two myofilament proteins, troponin T and myosin heavy chain, which are known to be problematic for separation on 2-DE only, were identified and found differentially modified in the failing swine heart. Therefore, RP-HPLC used in conjunction with 2-DE provides additional information, particularly about the myofilament proteome [53]. Limitation of the latter approach, however, is the inability to accurately quantitate the relative protein abundances on a global scale. In principle, using HPLC-ESI-MS/MS in proteomics, quite a few different strategies may be undertaken [59]. In one approach, close to the conventional one, 2-DE is still

employed for the separation of intact proteins. Subsequently, the excised spots are digested and analyzed by LC-MS or LC-MS/MS, which is complementary to the results obtained on MALDI-TOF-MS. Such a parallel MALDI peptide mapping and ESI-LC-MS/MS approach therefore typically enhances protein coverage [59]. Using another approach, the proteins in the total proteome are only separated and resolved by molecular mass using 1-DE. Subsequently, this 1-DE gel is cut into pieces, all proteins in a band digested, and the mixture of proteins is analyzed by LC-MS and/or LC-MS/MS. This approach provides several advantages over 2-DE gels; it is less elaborate, very large and basic proteins are much easier to handle, and the non-abundant, as well as many, if not all, membrane proteins are included. However, an important disadvantage of 1-DE is that it is not amenable for differential analysis of protein abundancy comparing extracts from e.g. control versus diseased tissue. In a third, non-gel "shotgun" approach, whole protein extracts are digested by proteases generating a very complex set of peptides which is beyond the separation capacity of 1-DE and 2-DE gels [59, 60]. Especially the Yates' group has introduced the so-called multidimensional protein identification technology (MudPIT) by employing for instance a biphasic column with a section of RP material flanked by a strong cation-exchange-resin for e.g. proteome wide analysis (e.g. 1484 identified proteins of *Sacharomyces Cerevisiae*) [61]. Compared to the conventional 2-DE based approach, MuD-LC has proven to be profitable for the analysis of membrane proteins [62, 63]. The MuDPIT accomplishes the need to obtain the largest protein coverage of a biological sample, but again, as it is feasible with images of 2-DE gel, the MudPIT does not really offer an alternative for quantification of relative expression levels of individual proteins.

Identification and mapping of PTMs(ites)

As already mentioned in this review, detection and site-identification of co- or post-translational modifications of proteins is the domain of proteomics research where it surpasses genomics [60]. These modifications are likely to be the most intriguing part of the puzzle in understanding disease processes. As an illustration, various toxic reactions, such as oxidation of proteins by generated reactive oxygen species (ROS) belong to the covalent protein modifications occurring during ischemia-reperfusion injury in the heart or advanced glycation of proteins associated with a number of the diabetic complications. The evolution of the concept of oxidative stress triggered by ROS has led to therapeutic strategies consisting in the administration of anti-oxidant molecules in a variety of pathological conditions. Likewise, nitrosative stress, defined as excessive or deregulated NO formation, leads to an increase of reactive nitrogen species production and has been associated with a number of cardiovascular disorders [64, 65]. The so-called "redox proteomics" is the collection of technologies presently available

for identifying proteins based on their redox state. The modifications include e.g. lysine- and arginine carbonylation, tyrosine nitration and thiol-disulfide chemistry of cysteines. Most of the detection methods are conceptually based either on derivatization or conjugation of the modified group prior to 2-DE and/or immunoblotting with a specific antibody. Until now, only the relatively stable modifications, such as nitration of specific tyrosine residues, are suitable to be identified by MS [64].

Since the discovery of O-linked β-N-acetylglucosamine (O-Glc-NAc) more than 20 years ago, the recognition of O-GlcNAc as a PTM has been slow, albeit similar to phosphorylation, because of the lack of tools available for its study [66-68]. For instance, serine/threonine-O-GlcNAc is as abundant and dynamic as O-phosphate on nucleocytosolic proteins site. Interestingly, the recently discovered novel regulator of cardiac development and pathological hypertrophy [69], glycogen synthase kinase-3β (GSK-3β), has been shown to be not only O-phosphorylated but also O-Glc-Nac modified [70]. A complete understanding of the complex regulation of protein activity and protein-protein interaction attributable to O-GlcNAc and O-phosphate will require site-mapping of these GSK-3β modifications under hypertrophic conditions. The advanced proteomic techniques that allow determination of sites of O-GlcNAc modification and their interplay with phosphorylation on proteins within the signalling pathways for understanding their molecular role in the etiology of diabetes and cardiovascular disease, have recently been reviewed [71].

Gel-independent quantitative protein profiling

Proteomic technologies detecting differences in protein profiles need to be quantitative. MS is inherently not a quantitative technique, because peptides analyzed will produce different signal intensities depending on their chemical composition, the matrix in which they are present, and other poorly understood variables. However, two peptides of the same chemical structure that differ in mass because they differ in isotopic composition are expected, according to stable isotope dilution theory, to generate identical specific signals in a MS [72]. The technique of stable isotope dilution has proven to be highly suitable for quantitative protein profiling. It is based on intrinsic labeling, with a stable isotope (^{2}H, ^{13}C, ^{18}O or ^{15}N), of peptides of one of the two samples to be compared. Subsequently, the samples are mixed and analyzed on the MS. Each peptide will appear as a pair of signals differing in mass. The ratio of the signal intensities precisely indicates the ratio of abundance of the protein from which the peptide originates. The principles of the two stable isotope dilution techniques, ICAT and the ^{18}O to ^{16}O exchange, in comparison to DIGE , are schematically presented in Figure 1.

In one approach, C-terminal labeling is performed by tryptic digestion in $H_2{}^{18}O$ or $H_2{}^{16}O$,

which results e.g. in MALDI-post source dissociation (PSD) mode-MS, peak doublets with 2 Da mass difference [72, 73]. This approach can be very powerful because labeling is universal and high labeling efficiencies can be obtained. A potential complication is that trypsin can continue to exchange ^{18}O or ^{16}O into the peptide at the second oxygen [59]. However, this problem can be solved by starting trypsin cleavage prior to the exchange, resulting in the incorporation of two ^{18}O's generating a mass difference of 4 Da. An analogous strategy is based on a class of reagents termed isotope-coded affinity tags, or ICAT [72]. These reagents consist of an alkylating group (iodoacetic acid) that covalently attaches the reagent (a polyether mass-encoded linker containing 8 hydrogens (d0) or 8 deuteriums (d8)) to reduced cysteine residues. Of course, these need to be present in the peptide that is to be quantitated and identified. Moreover, the reagent contains a biotin affinity tag through which ICAT-labeled peptides, derived from a mixture of two samples, can selectively be enriched by avidin affinity chromatography before analysis on LC-MS/MS. Thus, in a single, automated operation, this method identifies the proteins present in two related samples and determines the relative abundance. The ICAT technology specifically targets the cysteine containing peptides, which has the advantage of substantial reduction in sample complexity, but the disadvantage of lack of analysis of cystein-free peptides. In addition, peptides must contain appropriately spaced protease cleavage sites flanking the cysteine residues. Finally, the ICAT tag is large (about 450 Da) and remains with each peptide throughout the analysis. This can make database searching more difficult, especially for small peptides with limited sequence [16]. Sensitivity may also be a concern, since tagged peptides derived from low-copy proteins are likely to be poorly recovered during the affinity step as a result of non-specific interactions with the avidin-Sepharose, hence uncovering its, in potential, greatest weakness. Furthermore, the hydrophobicity of the biotin moiety is very dominating over the overall elution pattern of the ICAT-labeled peptides. Thereby, the retention behaviour is equalized, such that the peptides labeled with the original ICAT label elute off the column in a fairly small time window. This generally reduces the number of peptides which can be sequenced during a standard LC-MS/MS experiment. Also the detection by MS is not always accurate, especially when the size of the ICAT tag versus the small peptide is taken into account. More recently, the ICAT protocol has been considerably improved [74, 75]: 1) the heavy and light reagents are now ^{13}C-based and the mass difference is 9 Da. instead of 8 Da., eliminating potential confusion between oxidized methionine and doubly labeled peptides; 2) the biotin portion of the ICAT tag is cleaved with acid after the ICAT-reagent labeled peptides are eluted from the avidin columns. Biotin cleavage reduces the size of the tag on the peptides from 442 Da. to 227 Da., which allows analysis of larger peptides and minimizes the effect of the label on the LC elution pattern [74, 75].

Proteomics in the study of heart hypertrophy and failure

Heart failure is a complex multi-factorial disease, ultimately diagnosed on the basis of the inability of the heart to maintain sufficient cardiac output to meet metabolic needs of the body [5]. So far, proteomic investigations of human heart failure have been concentrated on dilated cardiomyopathy (DCM) [30], a disease of unknown etiology, in which contributory factors are genetic factors, prior viral infections, cardiac specific autoantibodies, toxic agents, etc. These studies have been complicated by factors such as differences in underlying causes of disease state, genetic variability, medical history, and therapeutic interventions. Furthermore, heart failure is not only caused by DCM but also originates from ischemia and/or hypertension, or congenital heart defects. Animal models of various forms of heart disease are available and are potentially useful approaches to overcome the above-mentioned complex interfering factors in the human situation. Until now, proteomic studies of heart failure in large animals (e.g. pacing induced heart failure in the dog and bovine hereditary DCM) have been performed [76-79]. Important biochemical similarities to human DCM have been observed in these studies. The causes of contractile dysfunction in heart failure are still largely unknown, but are likely to result from underlying alterations in gene and protein expression level, including modifications [30]. Therefore, proteomic studies are likely to give new insights into cellular mechanisms involved in cardiac dysfunction and may also provide new diagnostic and therapeutic markers. As cardiac myocytes are mainly responsible for contractility and hypertrophic growth, the use of *in vitro* models of more or less homogenous cardiomyocytes (either isolated or in culture) for protein profiling purposes, in combination with the application of stress or the addition of neurohumoral factors (ET-1), may be advantageous.

Current status of proteomic studies on DCM

The etiology of DCM still remains largely unknown, although some of the genetics have been elucidated [80]. Proteomics has been used for molecular characterization of DCM, both at the level of human heart biopsies and animal models. Knecht et al. characterized alterations in DCM protein patterns using conventional 2-DE and silver staining [26, 81, 82]. These studies revealed only few significantly altered proteins of which only a few proteins could be identified. The latter was certainly limited by the lack of MS identification. Pleissner et al. also studied (chamber-specific) DCM protein patterns and presented them in a world-wide-web accessible database [83, 84]. Corbett and colleagues used 2-DE to determine quantitative and qualitative changes in protein expression in heart tissue from patients with DCM compared with ischemic heart disease and undiseased controls [85]. Among the 88 spots, that were found to be downregulated in DCM compared to ischemic cardiopathy, multiple desmin

containing spots were found as well as several metabolic enzymes and stress-related proteins. The involvement of stress proteins in DCM (also compared to ischemic heart failure tissue and normal (LV) controls) is also illustrated by Scheler et al [86, 87]. With the help of immunostaining, differences in HSP-27 patterns between DCM, ischemic heart failure, and controls could be detected. These data suggest that HSP-27 degradation is enhanced in the failing heart [88]. In view of the limiting factors regarding the availability of human DCM tissue, appropriate DCM animal models have been developed. Besides a turkey model of idiopathic DCM [89], several bovine DCM models have been put forward [78, 79, 90, 91]. Weekes et al. performed proteomic analysis on bovine DCM resulting in the identification of 35 up-or downregulated proteins, compared to controls [78]. An interesting finding is the increase of the ubiquitin C-terminal hydrolase enzyme in the diseased ventricles. This enzyme is thought to release free ubiquitin from poly-ubiquinated proteins, thereby increasing the pool of free ubiquitin in the cytoplasm. The authors discuss the possibility that this increased free pool of ubiquitin leads to an increased cellular level of ubiquitin, which in turn can drive inappropriate ubiquitination of proteins. This incongruous ubiquitination can result in the proteolysis of these proteins by the 26S proteasome [92, 93] and can contribute to the development of heart failure [94]. Pacing induced heart failure in dogs can be used as an alternative model for DCM. Heinke et al. presents two 2-DE studies on protein changes in this canine model [76, 77]. By using both a linear immobilized pH gradient (IPG) strip (4-7 pH range) and a non-linear IPG strip (3-10 pH range) a total of 100 proteins were found to be altered (69 alterations in 4-7 IPG strip; 31 alterations in 3-10 IPG strip). Among these protein changes, large numbers of metabolic and mitochondrial proteins were detected.

Above-mentioned studies are examples of the implementation of proteomics in studying heart disease in both human and animal tissue. Inter-comparison of human and animal DCM (-models) reveals similarities although many of the significant protein alterations are not yet identified. The limited use in these studies of MS still hampers proper identification of proteins, and their PTMs. Furthermore, an adequate inter-comparison is still limited due to differences in regional origin of the left ventricular tissue and the limited number of patients studied, together with the limited amount of proteins identified. Also the etiology of heart failure in the human studies versus the animal studies differ considerably (e.g. DCM (i.e. genetic, idiopathic, viral? vs. pacing induced)). Therefore, the significance of protein alterations, especially in human studies, in terms of disease pathogenesis, are not well determined. The use of a more controlled situation, as in an animal model, might be more informative [85].

Figure 2: During the progression of heart disease (from initial event to eventual heart failure) numerous alterations of the cardiac proteome occur, each disease type having its own characteristics. In the initial phase the protein changes are mainly due to PTMs. These PTMS can continue to play a role during the progression of heart disease. During the progression of the disease, alterations in gene and protein expression will predominate eventually. (CHD = Congenital Heart Disease, DCM = Dilated Cardiomyopathy, MI = Myocardial Infarction).

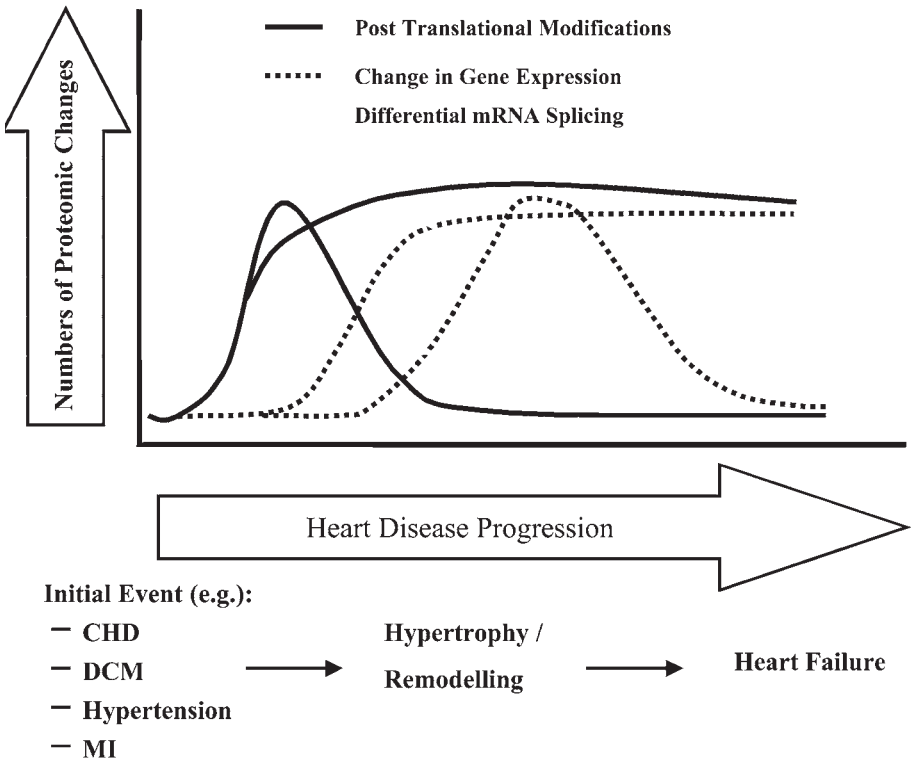

Towards an integrated approach

Theoretically, proteomics-based approaches offer the advantage of a holistic view of relatively abundant proteins that are present in the cell at a given time. With this method, unlike the more conventional "targeted" approach, both expected and unexpected alterations of known and unknown proteins can be found. The major challenge will be to investigate the contribution of these changes to alterations in cellular functions ultimately resulting in cardiac dysfunction. For this purpose, three important interrelated aspects (see also Fig. 2) should be considered: 1) time-related changes. Heart failure is not a fixed state but rather a dynamic and progressive disease, evolving in time; 2) different etiologies. Heart failure can be the result of different types of pathology, including ischemic heart disease, hypertension, and congenital heart

disease. These different underlying causes of heart failure may be reflected in different proteomes; 3) different definitions. Heart failure may be defined on basis of clinical, hemodynamic or biochemical features. Therefore, each measured proteome in fact should be accompanied by a description of the state of the heart failure process. One strategy to investigate the time-related changes that eventually lead to heart failure, is composed of the longitudinal collection of tissue of hearts at risk of failure, and to correlate the proteomic results with measurements of cardiovascular hemodynamics at each time point. These correlations will allow the identification of those protein changes that most likely are of functional importance. As an example of this strategy, we recently conducted a pilot study in which proteomic as well as hemodynamic profiles of the hypertrophied right ventricle of the rat heart were determined [95]. Male Wistar rats underwent either a pulmonary artery banding (PAB) operation or a sham operation. After a sustained period of PAB, the banded animals all developed RV hypertrophy and right atrial enlargement (sham vs. PAB; 0.70 ± 0.04 vs. 1.29 ± 0.05 mg/g RV/BW and 0.10 ± 0.01 vs. 0.25 ± 0.02 mg/g RA/BW, $p<0.05$). Hemodynamics, measured in a parallel group, revealed a compensated state of the RV [96]. All RV tissue was collected from the PAB animals and subsequently pooled and homogenized. The resulting solubilized protein sample was prefractionated into a cytosolic and a myofilament fraction and hence separated via 2-DE (Figure 3). The same process was repeated for the control animals. The gels (ie. PAB and sham) were stained using Coomassie Blue, and matching and analysis was performed using PDQUEST (BioRad) software. A total number of 27 spots were at least 2-fold increased or decreased in intensity. Among these proteins, several metabolic, cytoskeletal, and stress-related proteins could be identified by MALDI-TOF MS. It should be noted that this pilot study was performed on homogenates of the RV that were pooled on equal protein basis. The separate examination of individual samples will not only lead to more accurate protein quantification, but, together with hemodynamic profiling, is also a requirement to study possible correlations between individual hemodynamics and protein expression levels. While already with the pooled homogenates clear changes in protein composition of the pressure overloaded RV were demonstrated, the hemodynamic measurements appeared still compatible with preserved RV contractility and global function. This suggests that the observed protein changes occurred in the absence of heart failure, and are signs of attempted compensation. Moreover, it demonstrates the dynamic nature of heart failure. It also shows that profiling of the stages preceding actual heart failure may provide us with more insight into the mechanisms involved in the progression from (compensated) hypertrophy towards heart failure.

Figure 3: Example of a Coomassie stained 2-DE gel of cytoplasmic fractions of the control versus pressure-overloaded right ventricle of the rat *(see text for more details)*. Zoomed images of two spots representing differentially expressed proteins are shown as examples. L1, L2 and L3 correspond to three landmark proteins.

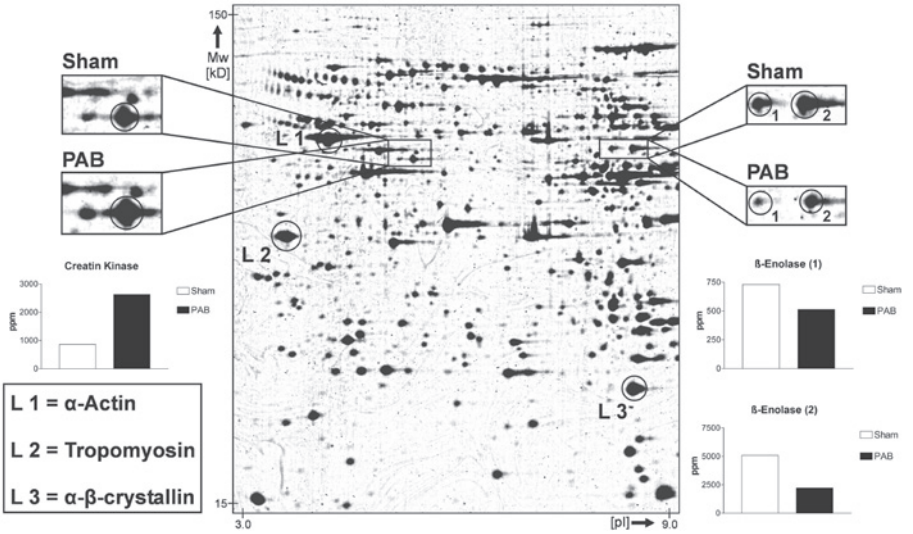

Towards the cellular level

In the heart, like many other organs, various cell types (e.g. the coronary endothelial and smooth muscle cells, fibroblasts and myocytes) exist and, therefore, different cellular phenotypes make up the (patho)physiological responses *in vivo* to e.g. increased stretch and neurohumoral stimulation. Therefore when cardiovascular responses and diseases are investigated in the human situation and/or experimental setting *in vivo,* the interplay between various cell types should always be taken into account as well. Proteomic investigations of cells isolated from the heart are rare and, unfortunately, accessible databases on the internet do not exist [32]. The current approach is to analyse both tissue, separated cells and cells in (co)culture. A first successful attempt was made by Corbett *et al.* [85] who submitted to 2-DE whole tissue samples, endothelial and mesothelial cells, cardiac fibroblasts and myocytes obtained from human patients affected either by dilated DCM or ischaemic heart disease (IHD). The most prominent changes occurred in the contractile protein MLC-2 and in a group of proteins identified as desmin. Interestingly, these proteins were not apparent in electrophoretic separations of vascular tissue or cultured endothelial cells, mesothelial cells or cardiac fibroblasts, which were clearly distinguishable from the 2-DE patterns of whole heart and of isolated cardiac myocytes. Moreover, the observed protein changes did not appear to reflect variations in the cellular

composition of biopsy samples [85]. Likewise, studies at the cellular level are essential to sort out the functional significance of the various PTMs observed in total protein extracts of ventricular tissue. For example, it is known that sustained activation of the β-adrenergic signalling pathways, as occurs during development of heart failure, can exert deleterious effects on the myocardium, promoting hypertrophy, left ventricular dysfunction, apoptosis, etc. Proteomic techniques were recently used in combination with phospholabeling to analyze (-agonist-evoked) protein phosphorylation profiles in isolated mouse cardiomyocytes [41]. Apart from changes in the well-known target proteins such as troponin I and phospholamban, a remarkable finding in this study was the observed phosphorylation of a cardiac isoform of p20 (member of the family of heat shock proteins). Adenovirus-mediated overexpression of cardiac p20 increased cell contractility and intracellular Ca^{2+} transient amplitudes which demonstrates the potential role of this newly discovered protein in cardiac (patho)physiology [41]. Two-DE electrophoresis combined with ^{32}P-autoradiography and MS-protein identification and phosphorylation mapping provides a novel and sensitive platform to analyze cardiac phosphoproteome and its modifications in response to various stimuli and in disease states. To give another example of proteomics at the cellular level, we recently applied differential 2DE combined with MALDI-TOF-MS to cultured neonatal rat cardiomyocytes which is known as a well-established *in vitro* model for cardiac hypertrophy [2, 9, 97]. Methods of isolation of this primary culture have been described in detail [97]. Cells were stimulated for 48 hrs with 10 nM ET-1 to induce the hypertrophic phenotype (Figure 4). Cells were lysed directly in 800 µl rehydration buffer (5M urea, 2M thiourea, 0.25% CHAPS, 0.8% Triton X100, 10% isopropanol, 12.5% water saturated isobutanol, 5% glycerol, 1% DTT, protease inhibitor complete and biolytes and incubated at 25 ^{0}C for 1 hr and stored frozen at -80°C. Thawed extracts, after centrifugation, were subjected to 2-DE, after fixing and staining with colloidal Commassie blue. Gel images were acquired by means of a BioRad GS-800 scanner and differential display analysis performed by PDQUEST 7.1 program (BioRad). For the first time we were able to detect changes in a cluster of protein spots which were all identified as desmin, an intermediate filament (IF) protein known to maintain myofibrillar and mitochondrial positioning in cardiac muscle (Figure 4) [85, 98, 99]. Several authors have reported on desmin changes in cardiac hypertrophic phenotype by applying proteomics on *in vivo* models [85, 100]. Two well-established features for hypertrophy-failure transition are myofibrillar re-and disarrangement and contractile failure. Desmin modifications could impair both myofibrillar arrangement and energy delivery. On the other hand, diverse cytoskeletal mutations have been associated with DCM in both clinical and experimental settings (reviewed by [1, 2]). Based on their specific locations within the cytoskeletal network, distinct classed of cytoskeletal

defects have been uncovered that include components of the dystrophin/dystroglycan complex and mutations in nuclear and IFs, such as desmin and lamin A/C. Since the cytoskeleton serves multiple functions in the cardiomyocyte, a number of theories have been proposed that might link the observed defects with chamber dilation, force generation and transmission, sarcolemmmal integrity, sarcomeric organization/ assembly and intercalated disc stability [1]. As far as cardiac energy metabolism is concerned, it is postulated by Capetanaki *et al.* [99] that desmin may play a role in positioning mitochondria along the sarcomere thus allowing the coupling between energy production and demand. In agreement with the previous observations on Ca^{2+}-activated protease induced IF degradation by Nelson and Traub [101], in our recent *in vitro* study of cultured cardiomyocytes we could confirm changes in desmin molecular mass compatible with a proteolytic PTM-type.

Figure 4: Representative gel images of a total protein extract from control and endothelin-1 (ET-1) stimulated (48 hrs) neonatal rat cardiomyocytes (see text for more details). Interesting spots were excised from gel, destained and in-gel digested with trypsin and used for MALDI-TOF-MS and, if needed LC-tandem MS analysis. Histograms report different expression of 3 desmin species in terms of relative intensity of Coomassie blue staining.

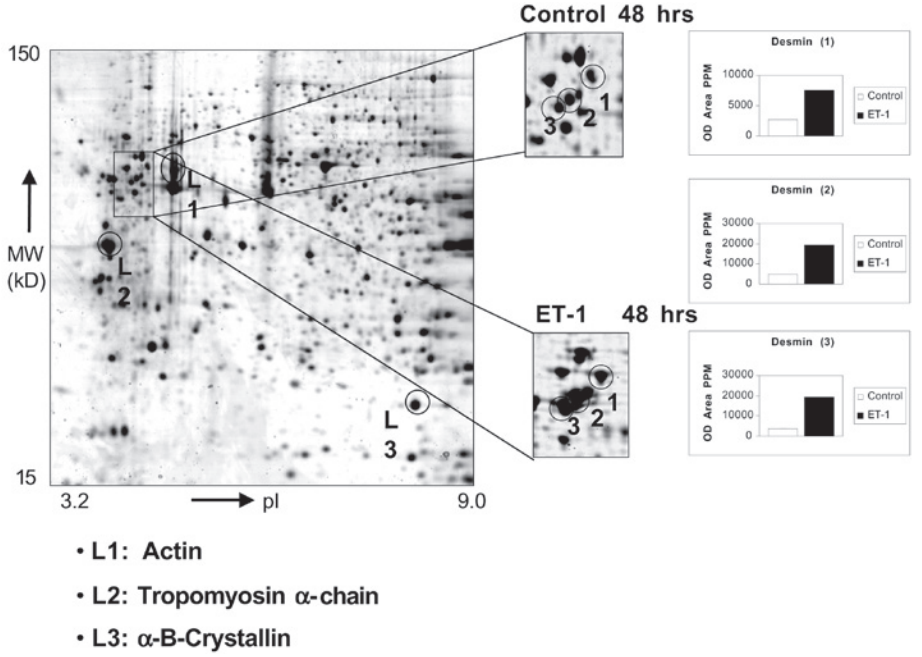

Beyond the first decade of proteomics

In 1995, when for the first time the term proteome was defined as the protein complement of a genome, the process of studying the proteome became known as proteomics. The initial goal of proteomics was the rapid identification of all the proteins expressed by a cell or tissue, a goal that, however, has yet to be achieved for any species [72]. Notwithstanding, the possibility of MS identification of gel-separated proteins led to a renaissance in biochemical approaches to protein function. As described in great extent in the foregoing sections, the current goal of proteomics is more varied and directed to systematic determination of diverse properties of proteins such as sequence, abundance, state of modification, interactions with other proteins, functional activity, subcellular distribution, structure, etc [72]. Many different technologies have been, and still are being, developed to collect the information contained in these diverse properties of proteins. Although, it should be noted that there is no single technology platform that can satisfy all the desired proteomic measurements and that there is no mature, "true" proteomic technology. In practice, proteomic approaches still focus on limited aspects of the broad menu of protein attributes, which in most studies are abundance, identification, and sequence. Comprehensive understanding of the (mal)functioning of living cells will require a quantitative, dynamic description of the stoichiometry of protein complexes or networks, the kinetics and energetics of formation, and the functional consequences of each protein(complex) in a cellular pathway [4].

Several exciting new developments in the field of MS will gain in importance and increase its impact on biological sciences. Although the measurement of sequence tags (ESTs) by LC-MS/MS techniques is a very powerful tool in proteomics for protein identification, alternatives have been introduced which omit the tandem MS step and make use of the fact that many tryptic peptides have unique masses [59]. The group of Smith has pioneered this strategy by making use of high resolution Fourier-transform cyclotron resonance (FT-ICR)-MS [102]. This novel MS application has the potential to expand the scope of proteomics from quantification and identification of the most abundant proteins to real proteome-wide determinations [103, 104].The methodology increases the throughput of measurements at the whole proteome level using peptide accurate mass and time of elution tags (AMT tags) as markers for proteins [103]. The approach has the advantages that it extends the sensitivity, dynamic range, comprehensiveness, and throughput of proteomic measurements [59] For example, Lipton et al. detected more than 50,000 putative peptides in a certain bacterium [105]. They showed also that this approach might be easily combined with stable isotope labelling, making it amenable for quantitative proteomics [59, 105]. When nanoLC–MS/MS and FT-ICR-MS will increasingly be used for high-throughput analysis

of complex protein samples, a major challenge lies in the consistent, objective and transparent analysis of the large amounts of data generated by such experiments and their dissemination and publication [106]. The currently available computational tools have recently been reviewed including discussion of the needs for statistical criteria in the analysis of large proteomic datasets [106].

A second novel MS application is the direct coupling of biomolecular interaction analysis (BIA) with MALDI-TOF-MS or nanoLC-MS/MS. This enables us to link protein detection, capture, and analysis of binding kinetics, with the measurement of protein and peptide masses and protein identification [107, 108]. The unique feature of the BIA-MS technology is the real-time monitoring of protein-protein (protein-DNA or protein-RNA) interactions by surface plasmon resonance and the simultaneous MS or MS/MS identification of the protein components. Another potential of the BIA-MS technology is the discovery of PTMs of the interacting protein, which determines the interaction with other molecules. A third example of an advanced MS technology is surface-enhanced laser desorption-ionization retentate chromatography (SELDI-RC)-MS, by which proteins can be captured on chemically modified chip surfaces (ProteinChip® Array from Ciphergen Biosystems Inc, Fremont CA) that are derivatized with chromatographic separation moieties, such as ion exchange, and hydrophobic surfaces [109-111]. The chip surface serves to fractionate and enrich for subpopulations of proteins from complex protein mixtures, thereby simplifying analysis.

Protein microarrays, another emerging class of proteomic technologies, have broad applications for discovery and quantitative analysis [112]. The concept of protein expression profiling arrays, inspired by the success of DNA microarrays, is now most advanced in its development [113]. Nevertheless, to be successful, design and use must take in consideration enormous analytically challenges. There are several reasons why DNA microarray technology cannot readily be adapted towards development of protein microarrays [113]. In contrast to the straightforward design and synthesis of gene-specific capture probes, based on simple base-pair rules and standard solid phase phosphoramidite chemistry, capture agents for protein arrays are far more complicated and require significantly more time for development. Currently, the preferred capture agents for protein expression profiling arrays are antibodies or antibody fragments which have a very long and costly development time [113]. Furthermore, protein expression levels span a huge range (up to 8 orders of magnitude). To avoid multiple measurements of the same sample at different dilutions, protein capture agents with different affinities have to be developed to address such dramatic differences in expression level. It appears also to be difficult to immobilize protein capture agents onto the array while retaining the integrity of their 3-D structures and binding activity, an issue not relevant to the production of DNA arrays.

Interplay of genomics, transcriptomics and proteomics

The dramatic advances in the nature and throughput of molecular technologies are making possible the global, genome-wide analysis of changes in DNA (genotyping), RNA expression and protein expression. A future approach that integrates various "omic" platforms and their data is key to unravelling the complexity and to gain a comprehensive understanding of physiology and pathophysiologies [114]. The total complement of mRNA in a cell or tissue at any given moment constitutes its transcriptome. A transcriptome forms the template for protein synthesis, resulting in the corresponding proteome. Unlike proteomics, of which the technologies still are in infancy, transcriptomics a rather robust and high through-put technology capable of simultaneously quantifying tens of thousands of defined mRNA species in a miniaturized, automated format [114]. Yet, with the numerous advances in proteomics technologies, a first challenge will be the parallel profiling of transcripts and proteins on a global scale. Despite the obvious attraction of integrating knowledge on global scale from genomic and proteomic technologies, there will be many practical (dynamic range) and biological (mRNA and protein turnover, alternative splicing , PTMs, etc) differences involved in this application. Nevertheless, the transcriptomic date can be compared and contrasted provided the studies are carefully designed and interpreted. Some reports on cross comparison of mRNA and protein expression are already available e.g in yeast *Saccharomyces cerevisi* [115] . These authors identified 997 genes with significantly altered mRNA levels. A mean correlation of $r = 0.6$ was found between corresponding mRNA and protein levels, which is quite high taking into account the above-mentioned considerations.

Both the generation and the analysis of proteomic data are becoming increasingly widespread, and as explained above, the field of proteomics is moving rapidly towards high-throughput approaches. The representation of gene and genome sequence data is already fairly well standardized and the databases and tools for their analysis are widely used [116]. However, the situation is less developed for transcriptome, and especially proteome, data. This is because both fields are relatively young and rapidly evolving and they produce data that are only meaningful in the context. For example, there are many different subsets of total proteome of an organism, just as there are different patterns of transcription, distinguished by cell type and condition. Thus, there exists a need for public repositories that contain details of proteomic experiments as opposed to the gel image databases that exist currently which offer little readily accessible information about where samples came from and how, by whom, spots of a gel were analysed. Recently, some journals have begun to require that papers reporting transcriptome experiment results be accompanied by the MIAME-defined minimum set of information about the microarray experiments [116]. Likewise, a systemic

approach to modelling, capturing, and disseminating proteomics experimental data has been reported. Once these models for transcriptomic and proteomic databases are generally accepted and implemented, the integration of proteomic databases with each other and with other resources, such as sequence databases can proceed. It is evident that linkage between and integration of different protein and nuclei acid databases, along the related annotation, will greatly improve the information content and knowledge base with regards to protein data [117].

References

1. Hoshijima, M and Chien, KR (2002) Mixed signals in heart failure: cancer rules. J Clin Invest, 109, 849-855.
2. Hunter, JJ and Chien, KR (1999) Signaling pathways for cardiac hypertrophy and failure. N Engl J Med, 341, 1276-1283.
3. Venter, JC et al. (2001) The sequence of the human genome. Science, 291, 1304-1351.
4. Neet, KE and Lee, JC (2002) Biophysical characterization of proteins in the post-genomic era of proteomics. Mol Cell Proteomics, 1, 415-420.
5. Dos Remedios, CG, Liew, CC, Allen, PD, Winslow, RL, Van Eyk, JE and Dunn, MJ (2003) Genomics, proteomics and bioinformatics of human heart failure. J Muscle Res Cell Motil, 24, 251-260.
6. Hunter, JJ, Zhu, H, Lee, KJ, Kubalak, S and Chien, KR (1993) Targeting gene expression to specific cardiovascular cell types in transgenic mice. Hypertension, 22, 608-617.
7. Hunter, JJ, Tanaka, N, Rockman, HA, Ross, J, Jr. and Chien, KR (1995) Ventricular expression of a MLC-2v-ras fusion gene induces cardiac hypertrophy and selective diastolic dysfunction in transgenic mice. J Biol Chem, 270, 23173-23178.
8. Wettschureck, N, Rutten, H, Zywietz, A, Gehring, D, Wilkie, TM, Chen, J, Chien, KR and Offermanns, S (2001) Absence of pressure overload induced myocardial hypertrophy after conditional inactivation of Galphaq/Galpha11 in cardiomyocytes. Nat Med, 7, 1236-1240.
9. Sugden, PH and Clerk, A (1998) Cellular mechanisms of cardiac hypertrophy. J Mol Med, 76, 725-746.
10. Van Heugten, HAA and Lamers, JMJ (1997) Changes in cardiac phenotype in hypertrophy and failure: from receptor to gene. Heart Failure Reviews, 2, 95 - 106.
11. Poller, W, Fechner, H, Kurreck, J, Pauschinger, M, Kuhl, U, Erdmann, VA, Lamers, JM and Schultheiss, HP (2004) Nucleic acid-based modulation of cardiac gene expression for the treatment of cardiac diseases. Approaches and perspectives. Z Kardiol, 93, 171-193.
12. Iwanaga, Y, Hoshijima, M, Gu, Y, Iwatate, M, Dieterle, T, Ikeda, Y, Date, MO, Chrast, J, Matsuzaki, M, Peterson, KL, Chien, KR and Ross, J, Jr. (2004) Chronic phospholamban inhibition prevents progressive cardiac dysfunction and pathological remodeling after infarction in rats. J Clin Invest, 113, 727-736.
13. Pandey, A and Mann, M (2000) Proteomics to study genes and genomes. Nature, 405, 837-846.
14. Dunn, MJ (2000) Studying heart disease using the proteomic approach. Drug Discov Today, 5, 76-84.
15. Banks, RE, Dunn, MJ, Hochstrasser, DF, Sanchez, JC, Blackstock, W, Pappin, DJ and Selby, PJ (2000) Proteomics: new perspectives, new biomedical opportunities. Lancet, 356, 1749-1756.
16. Graves, PR and Haystead, TA (2002) Molecular biologist's guide to proteomics. Microbiol Mol Biol Rev, 66, 39-63.
17. Van Eyk, JE (2001) Proteomics: unraveling the complexity of heart disease and striving to change cardiology. Curr Opin Mol Ther, 3, 546-553.
18. Ping, P (2003) Identification of novel signaling complexes by functional proteomics. Circ Res, 93, 595-603.
19. Godovac-Zimmermann, J and Brown, LR (2001) Perspectives for mass spectrometry and functional proteomics. Mass Spectrom Rev, 20, 1-57.
20. Macri, J and Rapundalo, ST (2001) Application of proteomics to the study of cardiovascular biology. Trends Cardiovasc Med, 11, 66-75.
21. Wilkins, MR, Sanchez, JC, Gooley, AA, Appel, RD, Humphery-Smith, I, Hochstrasser, DF and Williams, KL (1996) Progress with proteome projects: why all proteins expressed by a genome should be identified and how to do it. Biotechnol Genet Eng Rev, 13, 19-50.

22. Laemmli, UK (1970) Cleavage of structural proteins during the assembly of the head of bacteriophage T4. Nature, 227, 680-685.

23. O'Farrell, PH (1975) High resolution two-dimensional electrophoresis of proteins. J Biol Chem, 250, 4007-4021.

24. Fenn, JB, Mann, M, Meng, CK, Wong, SF and Whitehouse, CM (1989) Electrospray ionization for mass spectrometry of large biomolecules. Science, 246, 64-71.

25. Tanaka, K, Y, I, S, A, Y, Y and T, Y. (1987) Detection of high mass molecules by laser desorption time-of-flight mass spectrometry. In: Proc. 2nd Japan-China Joint Symp. Mass Spectrom. (eds. H, M and L, X-t), pp 185-188, Osaka, Japan.

26. Jungblut, P, Otto, A, Zeindl-Eberhart, E, Plessner, KP, Knecht, M, Regitz-Zagrosek, V, Fleck, E and Wittmann-Liebold, B (1994) Protein composition of the human heart: the construction of a myocardial two-dimensional electrophoresis database. Electrophoresis, 15, 685-707.

27. Gorg, A, Obermaier, C, Boguth, G, Harder, A, Scheibe, B, Wildgruber, R and Weiss, W (2000) The current state of two-dimensional electrophoresis with immobilized pH gradients. Electrophoresis, 21, 1037-1053.

28. Bjellqvist, B, Pasquali, C, Ravier, F, Sanchez, JC and Hochstrasser, D (1993) A nonlinear wide-range immobilized pH gradient for two-dimensional electrophoresis and its definition in a relevant pH scale. Electrophoresis, 14, 1357-1365.

29. Westbrook, JA, Yan, JX, Wait, R, Welson, SY and Dunn, MJ (2001) Zooming-in on the proteome: very narrow-range immobilised pH gradients reveal more protein species and isoforms. Electrophoresis, 22, 2865-2871.

30. McGregor, E and Dunn, MJ (2003) Proteomics of heart disease. Hum Mol Genet, 12 Spec No 2, R135-144.

31. Santoni, V, Molloy, M and Rabilloud, T (2000) Membrane proteins and proteomics: un amour impossible? Electrophoresis, 21, 1054-1070.

32. Jager, D, Jungblut, PR and Muller-Werdan, U (2002) Separation and identification of human heart proteins. J Chromatogr B Analyt Technol Biomed Life Sci, 771, 131-153.

33. Rabilloud, T (1996) Solubilization of proteins for electrophoretic analyses. Electrophoresis, 17, 813-829.

34. Neuhoff, V, Stamm, R, Pardowitz, I, Arold, N, Ehrhardt, W and Taube, D (1990) Essential problems in quantification of proteins following colloidal staining with coomassie brilliant blue dyes in polyacrylamide gels, and their solution. Electrophoresis, 11, 101-117.

35. Patton, WF (2002) Detection technologies in proteome analysis. J Chromatogr B Analyt Technol Biomed Life Sci, 771, 3-31.

36. Lauber, WM, Carroll, JA, Dufield, DR, Kiesel, JR, Radabaugh, MR and Malone, JP (2001) Mass spectrometry compatibility of two-dimensional gel protein stains. Electrophoresis, 22, 906-918.

37. Switzer, RC, 3rd, Merril, CR and Shifrin, S (1979) A highly sensitive silver stain for detecting proteins and peptides in polyacrylamide gels. Anal Biochem, 98, 231-237.

38. Merril, CR, Goldman, D and Van Keuren, ML (1984) Gel protein stains: silver stain. Methods Enzymol, 104, 441-447.

39. Shevchenko, A, Wilm, M, Vorm, O and Mann, M (1996) Mass spectrometric sequencing of proteins silver-stained polyacrylamide gels. Anal Chem, 68, 850-858.

40. Gharahdaghi, F, Weinberg, CR, Meagher, DA, Imai, BS and Mische, SM (1999) Mass spectrometric identification of proteins from silver-stained polyacrylamide gel: a method for the removal of silver ions to enhance sensitivity. Electrophoresis, 20, 601-605.

41. Chu, G, Egnaczyk, GF, Zhao, W, Jo, SH, Fan, GC, Maggio, JE, Xiao, RP and Kranias, EG (2004) Phosphoproteome analysis of cardiomyocytes subjected to beta-adrenergic stimulation: identification and characterization of a cardiac heat shock protein p20. Circ Res, 94, 184-193.

42. Tonge, R, Shaw, J, Middleton, B, Rowlinson, R, Rayner, S, Young, J, Pognan, F, Hawkins, E, Currie, I and Davison, M (2001) Validation and development of fluorescence two-dimensional differential gel electrophoresis proteomics technology. Proteomics, 1, 377-396.
43. Yan, JX, Devenish, AT, Wait, R, Stone, T, Lewis, S and Fowler, S (2002) Fluorescence two-dimensional difference gel electrophoresis and mass spectrometry based proteomic analysis of Escherichia coli. Proteomics, 2, 1682-1698.
44. Unlu, M, Morgan, ME and Minden, JS (1997) Difference gel electrophoresis: a single gel method for detecting changes in protein extracts. Electrophoresis, 18, 2071-2077.
45. Gharbi, S, Gaffney, P, Yang, A, Zvelebil, MJ, Cramer, R, Waterfield, MD and Timms, JF (2002) Evaluation of two-dimensional differential gel electrophoresis for proteomic expression analysis of a model breast cancer cell system. Mol Cell Proteomics, 1, 91-98.
46. Zhou, G, Li, H, DeCamp, D, Chen, S, Shu, H, Gong, Y, Flaig, M, Gillespie, JW, Hu, N, Taylor, PR, Emmert-Buck, MR, Liotta, LA, Petricoin, EF, 3rd and Zhao, Y (2002) 2D differential in-gel electrophoresis for the identification of esophageal scans cell cancer-specific protein markers. Mol Cell Proteomics, 1, 117-124.
47. Baker, CS, Corbett, JM, May, AJ, Yacoub, MH and Dunn, MJ (1992) A human myocardial two-dimensional electrophoresis database: protein characterisation by microsequencing and immunoblotting. Electrophoresis, 13, 723-726.
48. Jungblut, P, Otto, A, Regitz, V, Fleck, E and Wittmann-Liebold, B (1992) Identification of human myocard proteins separated by two-dimensional electrophoresis. Electrophoresis, 13, 739-741.
49. Corbett, JM, Wheeler, CH, Baker, CS, Yacoub, MH and Dunn, MJ (1994) The human myocardial two-dimensional gel protein database: update 1994. Electrophoresis, 15, 1459-1465.
50. Evans, G, Wheeler, CH, Corbett, JM and Dunn, MJ (1997) Construction of HSC-2DPAGE: a two-dimensional gel electrophoresis database of heart proteins. Electrophoresis, 18, 471-479.
51. Muller, EC, Thiede, B, Zimny-Arndt, U, Scheler, C, Prehm, J, Muller-Werdan, U, Wittmann-Liebold, B, Otto, A and Jungblut, P (1996) High-performance human myocardial two-dimensional electrophoresis database: edition 1996. Electrophoresis, 17, 1700-1712.
52. Huber, LA, Pfaller, K and Vietor, I (2003) Organelle proteomics: implications for subcellular fractionation in proteomics. Circ Res, 92, 962-968.
53. Neverova, I and Van Eyk, JE (2002) Application of reversed phase high performance liquid chromatography for subproteomic analysis of cardiac muscle. Proteomics, 2, 22-31.
54. Edmondson, RD, Vondriska, TM, Biederman, KJ, Zhang, J, Jones, RC, Zheng, Y, Allen, DL, Xiu, JX, Cardwell, EM, Pisano, MR and Ping, P (2002) Protein kinase C epsilon signaling complexes include metabolism- and transcription/translation-related proteins: complimentary separation techniques with LC/MS/MS. Mol Cell Proteomics, 1, 421-433.
55. Wang, H and Hanash, S (2003) Multi-dimensional liquid phase based separations in proteomics. J Chromatogr B Analyt Technol Biomed Life Sci, 787, 11-18.
56. Wagner, K, Racaityte, K, Unger, KK, Miliotis, T, Edholm, LE, Bischoff, R and Marko-Varga, G (2000) Protein mapping by two-dimensional high performance liquid chromatography. J Chromatogr A, 893, 293-305.
57. Chong, BE, Yan, F, Lubman, DM and Miller, FR (2001) Chromatofocusing nonporous reversed-phase high-performance liquid chromatography/electrospray ionization time-of-flight mass spectrometry of proteins from human breast cancer whole cell lysates: a novel two-dimensional liquid chromatography/mass spectrometry method. Rapid Commun Mass Spectrom, 15, 291-296.
58. Opiteck, GJ, Ramirez, SM, Jorgenson, JW and Moseley, MA, 3rd (1998) Comprehensive two-dimensional high-performance liquid chromatography for the isolation of overexpressed proteins and proteome mapping. Anal Biochem, 258, 349-361.

59. Romijn, EP, Krijgsveld, J and Heck, AJ (2003) Recent liquid chromatographic-(tandem) mass spectrometric applications in proteomics. J Chromatogr A, 1000, 589-608.

60. Wu, CC and Yates, JR, 3rd (2003) The application of mass spectrometry to membrane proteomics. Nat Biotechnol, 21, 262-267.

61. Washburn, MP, Ulaszek, R, Deciu, C, Schieltz, DM and Yates, JR, 3rd (2002) Analysis of quantitative proteomic data generated via multidimensional protein identification technology. Anal Chem, 74, 1650-1657.

62. Washburn, MP, Wolters, D and Yates, JR, 3rd (2001) Large-scale analysis of the yeast proteome by multidimensional protein identification technology. Nat Biotechnol, 19, 242-247.

63. Link, AJ, Eng, J, Schieltz, DM, Carmack, E, Mize, GJ, Morris, DR, Garvik, BM and Yates, JR, 3rd (1999) Direct analysis of protein complexes using mass spectrometry. Nat Biotechnol, 17, 676-682.

64. Ghezzi, P and Bonetto, V (2003) Redox proteomics: identification of oxidatively modified proteins. Proteomics, 3, 1145-1153.

65. Yi, D, Smythe, GA, Blount, BC and Duncan, MW (1997) Peroxynitrite-mediated nitration of peptides: characterization of the products by electrospray and combined gas chromatography-mass spectrometry. Arch Biochem Biophys, 344, 253-259.

66. Wells, L, Vosseller, K, Cole, RN, Cronshaw, JM, Matunis, MJ and Hart, GW (2002) Mapping sites of O-GlcNAc modification using affinity tags for serine and threonine post-translational modifications. Mol Cell Proteomics, 1, 791-804.

67. Wells, L and Hart, GW (2003) O-GlcNAc turns twenty: functional implications for post-translational modification of nuclear and cytosolic proteins with a sugar. FEBS Lett, 546, 154-158.

68. Comer, FI and Hart, GW (2001) Reciprocity between O-GlcNAc and O-phosphate on the carboxyl terminal domain of RNA polymerase II. Biochemistry, 40, 7845-7852.

69. Hardt, SE and Sadoshima, J (2002) Glycogen synthase kinase-3beta: a novel regulator of cardiac hypertrophy and development. Circ Res, 90, 1055-1063.

70. Parker, GJ, Lund, KC, Taylor, RP and McClain, DA (2003) Insulin resistance of glycogen synthase mediated by o-linked N-acetylglucosamine. J Biol Chem, 278, 10022-10027.

71. Whelan, SA and Hart, GW (2003) Proteomic approaches to analyze the dynamic relationships between nucleocytoplasmic protein glycosylation and phosphorylation. Circ Res, 93, 1047-1058.

72. Patterson, SD and Aebersold, RH (2003) Proteomics: the first decade and beyond. Nat Genet, 33 Suppl, 311-323.

73. Heller, M, Mattou, H, Menzel, C and Yao, X (2003) Trypsin catalyzed 16O-to-18O exchange for comparative proteomics: tandem mass spectrometry comparison using MALDI-TOF, ESI-QTOF, and ESI-ion trap mass spectrometers. J Am Soc Mass Spectrom, 14, 704-718.

74. Lill, J (2003) Proteomic tools for quantitation by mass spectrometry. Mass Spectrom Rev, 22, 182-194.

75. Li, J, Steen, H and Gygi, SP (2003) Protein Profiling with Cleavable Isotope-coded Affinity Tag (cICAT) Reagents: The Yeast Salinity Stress Response. Mol Cell Proteomics, 2, 1198-1204.

76. Heinke, MY, Wheeler, CH, Chang, D, Einstein, R, Drake-Holland, A, Dunn, MJ and dos Remedios, CG (1998) Protein changes observed in pacing-induced heart failure using two-dimensional electrophoresis. Electrophoresis, 19, 2021-2030.

77. Heinke, MY, Wheeler, CH, Yan, JX, Amin, V, Chang, D, Einstein, R, Dunn, MJ and dos Remedios, CG (1999) Changes in myocardial protein expression in pacing-induced canine heart failure. Electrophoresis, 20, 2086-2093.

78. Weekes, J, Wheeler, CH, Yan, JX, Weil, J, Eschenhagen, T, Scholtysik, G and Dunn, MJ (1999) Bovine dilated cardiomyopathy: proteomic analysis of an animal model of human dilated cardiomyopathy. Electrophoresis, 20, 898-906.

79. Eschenhagen, T, Diederich, M, Kluge, SH, Magnussen, O, Mene, U, Muller, F, Schmitz, W, Scholz, H, Weil, J, Sent, U and et al. (1995) Bovine hereditary cardiomyopathy: an animal model of human dilated cardiomyopathy. J Mol Cell Cardiol, 27, 357-370.

80. Seidman, JG and Seidman, C (2001) The genetic basis for cardiomyopathy: from mutation identification to mechanistic paradigms. Cell, 104, 557-567.

81. Knecht, M, Regitz-Zagrosek, V, Pleissner, KP, Emig, S, Jungblut, P, Hildebrandt, A and Fleck, E (1994) Dilated cardiomyopathy: computer-assisted analysis of endomyocardial biopsy protein patterns by two-dimensional gel electrophoresis. Eur J Clin Chem Clin Biochem, 32, 615-624.

82. Knecht, M, Regitz-Zagrosek, V, Pleissner, KP, Jungblut, P, Steffen, C, Hildebrandt, A and Fleck, E (1994) Characterization of myocardial protein composition in dilated cardiomyopathy by two-dimensional gel electrophoresis. Eur Heart J, 15 Suppl D, 37-44.

83. Pleissner, KP, Regitz-Zagrosek, V, Weise, C, Neuss, M, Krudewagen, B, Soding, P, Buchner, K, Hucho, F, Hildebrandt, A and Fleck, E (1995) Chamber-specific expression of human myocardial proteins detected by two-dimensional gel electrophoresis. Electrophoresis, 16, 841-850.

84. Pleissner, KP, Sander, S, Oswald, H, Regitz-Zagrosek, V and Fleck, E (1997) Towards design and comparison of World Wide Web-accessible myocardial two-dimensional gel electrophoresis protein databases. Electrophoresis, 18, 480-483.

85. Corbett, JM, Why, HJ, Wheeler, CH, Richardson, PJ, Archard, LC, Yacoub, MH and Dunn, MJ (1998) Cardiac protein abnormalities in dilated cardiomyopathy detected by two-dimensional polyacrylamide gel electrophoresis. Electrophoresis, 19, 2031-2042.

86. Scheler, C, Muller, EC, Stahl, J, Muller-Werdan, U, Salnikow, J and Jungblut, P (1997) Identification and characterization of heat shock protein 27 protein species in human myocardial two-dimensional electrophoresis patterns. Electrophoresis, 18, 2823-2831.

87. Scheler, C, Li, XP, Salnikow, J, Dunn, MJ and Jungblut, PR (1999) Comparison of two-dimensional electrophoresis patterns of heat shock protein Hsp27 species in normal and cardiomyopathic hearts. Electrophoresis, 20, 3623-3628.

88. Li, XP, Pleissner, KP, Scheler, C, Regitz-Zagrosek, V, Salnikow, J and Jungblut, PR (1999) A two-dimensional electrophoresis database of rat heart proteins. Electrophoresis, 20, 891-897.

89. Gruver, EJ, Glass, MG, Marsh, JD and Gwathmey, JK (1993) An animal model of dilated cardiomyopathy: characterization of dihydropyridine receptors and contractile performance. Am J Physiol, 265, H1704-1711.

90. Tontis, A, Zwahlen, R, Lobsiger, C and Luginbuhl, H (1990) Pathology of bovine cardiomyopathy. Schweiz Arch Tierheilkd, 132, 105-116.

91. Weil, J, Eschenhagen, T, Magnussen, O, Mittmann, C, Orthey, E, Scholz, H, Schafer, H and Scholtysik, G (1997) Reduction of myocardial myoglobin in bovine dilated cardiomyopathy. J Mol Cell Cardiol, 29, 743-751.

92. Ciechanover, A and Schwartz, AL (1994) The ubiquitin-mediated proteolytic pathway: mechanisms of recognition of the proteolytic substrate and involvement in the degradation of native cellular proteins. Faseb J, 8, 182-191.

93. Goldberg, AL (1995) Functions of the proteasome: the lysis at the end of the tunnel. Science, 268, 522-523.

94. Field, ML and Clark, JF (1997) Inappropriate ubiquitin conjugation: a proposed mechanism contributing to heart failure. Cardiovasc Res, 33, 8-12.

95. Dalinghaus, M, Bezstarosti, K, Lamers, JMJ, Lankhuizen, IM, Schoemaker, RG and Helbing, WA (2003) Differential proteomic profiling of right ventricle after 3 weeks of RV pressure overload in young rats. Cardiology in the Young, 13, suppl. 1, 40.

96. Schneider, MD (2004) First annual symposium of the American Heart Association Council on Basic Cardiovascular Sciences: stress signals, molecular targets, and the genome. Circ Res, 94 (Online data suppl. abstract # 38 M.J. Faber et al., p. 12), 1523.

97. van Heugten, HA, van Setten, MC, Eizema, K, Verdouw, PD and Lamers, JM (1998) Sarcoplasmic reticulum Ca^{2+} ATPase promoter activity during endothelin-1 induced hypertrophy of cultured rat cardiomyocytes. Cardiovasc Res, 37, 503-514.

98. Hein, S, Kostin, S, Heling, A, Maeno, Y and Schaper, J (2000) The role of the cytoskeleton in heart failure. Cardiovasc Res, 45, 273-278.

99. Capetanaki, Y (2002) Desmin cytoskeleton: a potential regulator of muscle mitochondrial behavior and function. Trends Cardiovasc Med, 12, 339-348.

100. Korstjens, IJ, Rouws, CH, van der Laarse, WJ, Van der Zee, L and Stienen, GJ (2002) Myocardial force development and structural changes associated with monocrotaline induced cardiac hypertrophy and heart failure. J Muscle Res Cell Motil, 23, 93-102.

101. Nelson, WJ and Traub, P (1983) Proteolysis of vimentin and desmin by the Ca^{2+}-activated proteinase specific for these intermediate filament proteins. Mol Cell Biol, 3, 1146-1156.

102. Shen, Y, Tolic, N, Masselon, C, Pasa-Tolic, L, Camp, DG, 2nd, Lipton, MS, Anderson, GA and Smith, RD (2004) Nanoscale proteomics. Anal Bioanal Chem, 378, 1037-1045.

103. Page, JS, Masselon, CD and Smith, RD (2004) FTICR mass spectrometry for qualitative and quantitative bioanalyses. Curr Opin Biotechnol, 15, 3-11.

104. Ramstrom, M and Bergquist, J (2004) Miniaturized proteomics and peptidomics using capillary liquid separation and high resolution mass spectrometry. FEBS Lett, 567, 92-95.

105. Lipton, MS, Pasa-Tolic, L, Anderson, GA, Anderson, DJ, Auberry, DL, Battista, JR, Daly, MJ, Fredrickson, J, Hixson, KK, Kostandarithes, H, Masselon, C, Markillie, LM, Moore, RJ, Romine, MF, Shen, Y, Stritmatter, E, Tolic, N, Udseth, HR, Venkateswaran, A, Wong, KK, Zhao, R and Smith, RD (2002) Global analysis of the Deinococcus radiodurans proteome by using accurate mass tags. Proc Natl Acad Sci U S A, 99, 11049-11054.

106. Nesvizhskii, AI and Aebersold, R (2004) Analysis, statistical validation and dissemination of large-scale proteomics datasets generated by tandem MS. Drug Discov Today, 9, 173-181.

107. Mattei, B, Borch, J and Roepstorff, P (2004) Biomolecular interaction analysis and MS. Anal Chem, 76, 19A-25A.

108. Natsume, T, Nakayama, H and Isobe, T (2001) BIA-MS-MS: biomolecular interaction analysis for functional proteomics. Trends Biotechnol, 19, S28-33.

109. Grus, FH, Joachim, SC and Pfeiffer, N (2003) Analysis of complex autoantibody repertoires by surface-enhanced laser desorption/ionization-time of flight mass spectrometry. Proteomics, 3, 957-961.

110. Weinberger, SR, Boschetti, E, Santambien, P and Brenac, V (2002) Surface-enhanced laser desorption-ionization retentate chromatography mass spectrometry (SELDI-RC-MS): a new method for rapid development of process chromatography conditions. J Chromatogr B Analyt Technol Biomed Life Sci, 782, 307-316.

111. Weinberger, SR, Dalmasso, EA and Fung, ET (2002) Current achievements using ProteinChip Array technology. Curr Opin Chem Biol, 6, 86-91.

112. Blagoev, B and Pandey, A (2001) Microarrays go live—new prospects for proteomics. Trends Biochem Sci, 26, 639-641.

113. Espina, V, Mehta, AI, Winters, ME, Calvert, V, Wulfkuhle, J, Petricoin, EF, 3rd and Liotta, LA (2003) Protein microarrays: molecular profiling technologies for clinical specimens. Proteomics, 3, 2091-2100.

114. Hegde, PS, White, IR and Debouck, C (2003) Interplay of transcriptomics and proteomics. Curr Opin Biotechnol, 14, 647-651.

115. Ideker, T, Thorsson, V, Ranish, JA, Christmas, R, Buhler, J, Eng, JK, Bumgarner, R, Goodlett, DR, Aebersold, R and Hood, L (2001) Integrated genomic and proteomic analyses of a systematically perturbed metabolic network. Science, 292, 929-934.

116. Taylor, CF, Paton, NW, Garwood, KL, Kirby, PD, Stead, DA, Yin, Z, Deutsch, EW, Selway, L, Walker, J, Riba-Garcia, I, Mohammed, S, Deery, MJ, Howard, JA, Dunkley, T, Aebersold, R, Kell, DB, Lilley, KS, Roepstorff, P, Yates, JR, 3rd, Brass, A, Brown, AJ, Cash, P, Gaskell, SJ, Hubbard, SJ and Oliver, SG (2003) A systematic approach to modeling, capturing, and disseminating proteomics experimental data. Nat Biotechnol, 21, 247-254.

117. Cavalcoli, JD (2001) Genomic and proteomic databases: large-scale analysis and integration of data. Trends Cardiovasc Med, 11, 76-81.

Chapter 3

Proteomic changes in the pressure overloaded right ventricle after 6 weeks in young rats: correlations with the degree of hypertrophy

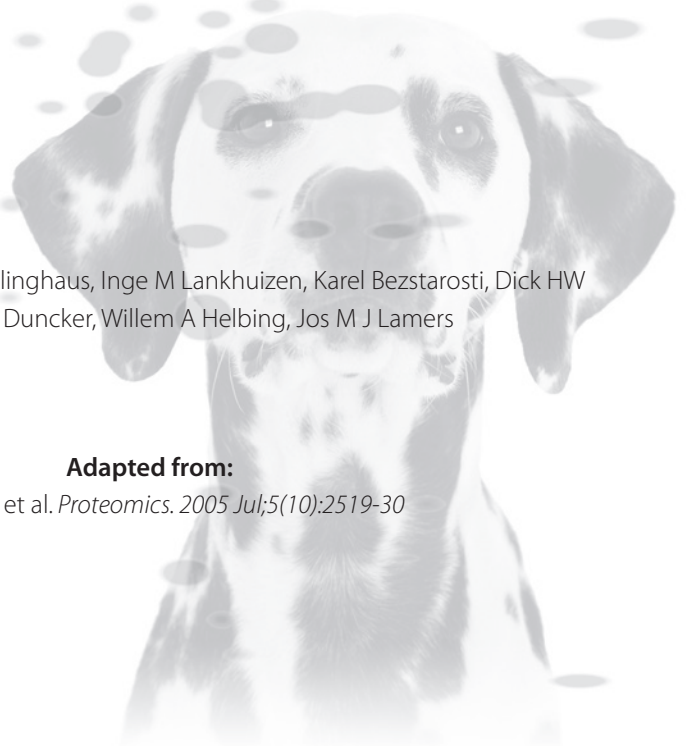

Matthijs J Faber, Michiel Dalinghaus, Inge M Lankhuizen, Karel Bezstarosti, Dick HW Dekkers, Dirk J Duncker, Willem A Helbing, Jos M J Lamers

Adapted from:
M.J. Faber et al. *Proteomics. 2005 Jul;5(10):2519-30*

Abstract

Right ventricular (RV) hypertrophy is an important problem in congenital heart disease. We determined the alterations in phenotype that occur in the initial phase of RV hypertrophy and their possible correlations with the degree of hypertrophy. Therefore we performed a differential proteomic profiling study on RV hypertrophy using an animal model of pulmonary artery banding (PAB) in parallel with hemodynamic characterization. RV homogenates were subfractionated in myofilament and cytoplasmic proteins which subsequently were separated by two-dimensional gel electrophoresis (2-DE), excised and analysed by mass spectrometry (MS). The cytoplasmic fraction showed expression changes in metabolic proteins, indicative for a shift from fatty acid to glucose as substrate for energy supply. Upregulation of three HSP-27's (1.9, 1.7 and 3.5 fold) indicated an altered stress response in RV hypertrophy. Detailed analysis by immunoblotting and MS showed that two of these HSP-27's were at least phosphorylated on Ser15. The myofilament fraction showed upregulation of desmin and α-B-crystallin (1.4 and 1.3 fold respectively). This alteration in desmin was confirmed by 1-DE immunoblots. Certain differentially expressed proteins, such as HSP-27, showed a significant correlation with the RV weight to body weight ratio in the PAB rats, suggesting an association with the degree of hypertrophy.

Introduction

The incidence of congenital heart disease (CHD) is approximately 6 per 1,000 live births [1]. Because of the ongoing improvement in the treatment of patients with CHD, the number of patients reaching adulthood after correction or palliation of complex congenital heart disease is steadily increasing over the last decades [2]. In many of these patients, residual loading abnormalities , including pressure overload, have been imposed on the right ventricle (RV). Thus, RV function has been demonstrated to be an important determinant of long-term outcome after (surgical) correction for complex CHD [3]. Distinct phenotypes could be associated with RV hypertrophy and ultimate RV failure due to RV pressure overload. Specific changes in protein expression could provide us with more insight into the molecular mechanisms involved in (the development of) RV dysfunction. Results of proteomic analysis of the failing human and animal heart are available but most of these studies pertain to the dilated-type of left ventricular (LV) failure [4]. There are no studies that have systematically evaluated the alterations in protein expression and PTMs in the pressure-overloaded RV in vivo. Although proteomic analysis of RV biopsies from CHD patients would be most favorable, this material can rarely be obtained. Furthermore, such study design would be complicated by difficulties in obtaining adequate control tissue.

Therefore, the aim of this animal study was to analyze the changes in the RV proteome resulting from chronic RV pressure overload in parallel with in-depth characterization of RV hemodynamics and hypertrophy. For these purposes we set up a young rat model of RV hypertrophy due to chronic pressure overload by means of pulmonary artery banding (PAB). Invasive hemodynamic measurements using pressure-volume loop analysis were performed before excision of the heart. 2-D-PAGE was used for separation and quantification of proteins. Prior to this, subfractionation of RV homogenates into cytoplasmic and myofilament (-associated) proteins was performed in order to enhance the protein coverage. Proteins that were found to be significantly up- or downregulated in the hypertrophic RV were subsequently analyzed with the MS for identification. The analysis of some of the key protein changes, such as those of HSP-27 and myofilament-associated desmin, were substantiated with immunoblot and/or phosphorylation analysis. Finally, data on relative protein expression were linked to the degree of hypertrophy in order to investigate possible correlations.

Material and methods

All experimental procedures and protocols used in this study were reviewed and approved by the institutional animal care and use committee and are in accordance with the National Institutes of Health "Guide for the care and use of laboratory animals" (NIH publication No. 85-23, revised 1996).

Male Wistar rats (Harlan, Zeist, The Netherlands) underwent PAB or sham operation. The first group consisted of 6 rats that underwent PAB at the age of 8 weeks. A second group consisted of 6 age-matched control rats that received a sham operation at the same age. After the initial operation (Sham or PAB) the animals were housed for a period of 6 weeks at a 12h-light/dark cycle with standard rat chow and water available ad libitum.

Pulmonary artery banding procedure

Anesthesia was induced with pentobarbital (60 mg/kg i.p.). After intubation, the animals were mechanically ventilated via a volume-controlled respirator (3 ml; 45 strokes/min) with oxygen enriched room air. Positive end-expiratory pressure was maintained with 4 cm H_2O. A lateral thoracotomy was performed and the main pulmonary artery (PA) was exposed. An 18 Gauge needle was placed alongside the PA and a 4-0 silk suture was tied around the PA and the needle. Next, the needle was rapidly removed, setting a fixed diameter for the PA. The combination of a fixed banding around the PA and the growth of the animal eventually resulted in a constrictive narrowing of the PA. This will subsequently lead to increased RV pressures (see later). After the banding procedure the thorax was closed in layers and extra oxygen was supplied during the first hour post-operatively in order to let the animals recover from the procedure. The sham animals underwent the same procedures except for banding of the PA.

Hemodynamic measurements

After a housing period of 6 weeks, hemodynamic measurements were performed. The study protocol was the same for both sham and PAB animals. After induction of anesthesia, as described above, the heart was exposed by thoracotomy and a pressure- and conductance catheter were inserted into both ventricles to measure both ventricular pressures and volumes simultaneously. From these measurements, pressure-volume loops of RV and LV were constructed out of which the following parameters were derived: heart rate, cardiac output, stroke work, dP/dt-max, and ventricular end-systolic and end-diastolic pressures. At the end of the hemodynamic measurements the animals were killed and the heart was rapidly removed and divided into RV, LV, right atrium, left atrium and septum. Tissues were weighed and stored at -80°C.

Tissue Sample Preparation

RV tissue was homogenized in 100 µL of sample buffer (15 mM Tris-HCl, 1 mM EGTA, protease inhibitor cocktail Complete™ (Roche, Mannheim, Germany)) with a micro-dismembrator (Braun, Melsungen, Germany). Subsequently, protein concentration was

measured with the DC protein assay (BioRad, Hercules, CA, USA). Homogenates were stored at -80°C. Subfractionation of the homogenates (600 µg) was achieved by adding 5% Triton X100 (v/v 1:4), incubation for 1 hr at 4°C and subsequent centrifugation for 15 min at 13.400 x g (4°C). The first supernatant (cytoplasmic fraction) was collected and the pellet (myofilament fraction) was resuspended in 10 µl 1 % Triton X100 and centrifuged. The second supernatant was added to the first, completing the cytoplasmic fraction.

Two-Dimensional Electrophoresis

Isoelectric focussing was performed using immobilized pH gradient (IPG) strips (Amersham Biosciences, Little Chalfont, Buckinghamshire, UK) with a nonlinear pH range of 3-10. Rehydration buffer (350 µL: 7.8 M urea, 2.2 M thiourea, 0.28 % CHAPS, 0.9 % Triton X100, 11.1 % isopropanol, 13.9 % water saturated isobutanol, 5.6 % glycerol, protease inhibitor cocktail Complete™ (Roche), a few grains of bromophenol blue, 69 mM DTT, 0.6% (v/v) Biolytes) was added to both subfractions. The homogenates were applied to the IPG strips and rehydration was performed overnight at room temperature in a reswelling tray. Next the strips were focused in a Protean IEF Cell (BioRad) according to the following protocol: 250 V; 1hr, 500 V; 1 hr and 8,000 V until 60 kVh was reached. Next, the IPG strips were equilibrated in SDS-equilibration buffer (50 mM Tris-HCl pH 8.8, 6 M urea, 30 % glycerol, 2 % SDS) with the addition of DTT (10 mg/mL) for 15 min, followed by 15 min in the same buffer with the addition of iodoacetamide (25 mg/mL). SDS-PAGE was performed (180 mm x 180 mm x 1 mm polyacrylamide gel (12%)) using the Protean II XL Cell System (BioRad). The IPG strips were sealed in place with a 1 % agarose solution, together with a protein mass standard. The second dimension electrophoresis (2-DE) was carried out at 25 V/gel for 1 hr and next 24 mA/gel and was stopped when the bromophenol blue front reached the bottom of the glass plate (total duration 4-6 hrs). Temperature was kept constant at 25°C by a cooling unit.
After 2-DE separation, the gels were fixed overnight in 40 % ethanol and 10 % acetic acid. Next, the gels were washed in distilled water. Coomassie Blue staining was performed for minimal 24 hr in a 34 % methanol, 17 % $(NH_4)_2SO_4$, 2 % H_3PO_4 and 0.066 % Coomassie Blue G-250 solution.

Analysis of 2-DE gels

The Coomassie Blue stained gels were scanned with a GS-800 calibrated densitometer (BioRad) and imaged and analyzed with PDQUEST software (BioRad). In PDQUEST, the 6 images of the sham RV's and the 6 images of the hypertrophic RV's were compared. Normalization of the gels was based on the total staining density of the image.

Protein identification

Significantly up-or downregulated spots were excised in duplicate from the Coomassie Blue stained gels. Subsequently, these gel-plugs were destained using a destaining solution (1 g $(NH_4)HCO_3$, 175 ml distilled water, 75 ml acetonitril) until colorless. Subsequently, the gel-plugs were dried using a centrifugal evaporator. The gel-plugs were incubated overnight with trypsin (ultra sequencing grade, Promega, Madison, WI, USA) at room temperature. Trypsin digestion was stopped by adding a solution of 1:2 acetonitrile and 0.1 % trifluoroacetic acid to the gel-plugs. This sample solution was co-crystalized with a matrix (6 mg alpha-cyano-cinnamic-acid, 1 ml acetonitrile) onto a 400 µm anchorchip plate and air-dried before loading into the MALDI-TOF MS (Bruker Daltonics, Billerica, MA, USA). When necessary, the QTOF MS/MS (Waters, Milford, MA, USA) was used for generating peptide mass fingerprints. Peptide masses were used to search the MASCOT protein database (http://www.matrixscience.com). The Swiss Prot database (http://www.expasy.org) was searched to obtain further details on the proteins that were identified. When the confidence of identification was minimal or when there was a lack of protein identification the Q-TOF MS/MS was used for protein identification.

Alkaline phosphatase treatment

Alkaline phosphatase (Boehringer Mannheim, Mannheim, Germany) treatment was applied to 3 consecutive spots (1103, 1104, and 2106) which were suspected to be phosphorylated. The enzymatic dephosphorylation protocol was adapted from Larsen et al. [5]. Briefly, the alkaline phosphatase treatment was performed directly on the MALDI target plate. The original samples were spotted (0.5 µL) on the MALDI target plate followed by alkaline phosphatase (0.05 U in 50mM NH_4CO_3) treatment. The treated samples were placed for 30 min. at 37 °C and prevented from drying. Next, the samples were acidified by adding 0.5 µL of 5% TFA and co-crystallized with a matrix (alpha-cyano-cinnamic-acid) . MS spectra from untreated and treated spots were compared.

Western blotting

Western blotting was used to add confidence to the data on the differential expression of two key proteins observed after 2-DE separation of both fractions. From the myofilament fraction the expression of desmin was analyzed. From the cytoplasmic fraction the expression of total and phosporylated (P-Ser-15) HSP-27 was analyzed.

Myofilament fractions were resuspended in 1% SDS with protease inhibitor. An aliquot was mixed with Laemmli loading buffer and heated for 5 minutes at 95°C. Clear supernatants were used to measure protein concentration (BioRad RcDc

kit). The cytosolic fractions were also mixed with the Laemmli loading buffer and subsequently heated at the same temperature as the myofilament fraction. Proteins were separated by 1D-PAGE, using 10% (desmin) and 15% (HSP-27) gradient gels. Samples were reheated for 5 minutes at 95°C and 20 µg of protein was applied per sample. Proteins were blotted overnight at 40V onto PVDF membranes (Immunoblot, BioRad). Blots were blocked in TBS with Tween (TTBS)-buffer (10 mmol/L Tris-HCl pH 7.6, 150 mmol/L NaCl, 0.1% Tween) supplemented with 0.5 % nonfat milk powder for 1 hr at room temperature and incubated with the diluted primary antibodies for 1 hr at room temperature and overnight at 4°C. The following primary antibodies were used: Desmin mouse monoclonal DE-U-10 1:5000 diluted (Sigma, St. Louis, MO, USA), total HSP-27 and P-HSP-27 (Ser15) rabbit polyclonal each 1:1000 diluted (Santa Cruz Biotechnology, Santa Cruz, CA, USA). After washing with TTBS, blots were incubated with 1:4000 diluted goat anti-rabbit conjugated horseradish peroxidase (Pierce) in TTBS buffer. Results were visualized by recording the ECL signal (Pierce Biotechnology, Rockford, IL, USA) on film (Hyperfilm™ ECL, Amersham Biosciences) and quantitated with a GS-800 calibrated densitometer (BioRad).
Additionally, western blotting on 2-DE gel parts, cut out at the 27 kDa mobility region, were performed with the above described antibodies against total and phosphorylated (Ser15) HSP-27 to specifically look at the spot nrs 1103, 1104 and 2106 (compare with Figure 2).

Statistics

The statistical comparison software within PDQUEST (Mann-Whitney) was used for identification of significantly up-or downregulated spots when comparing sham gels to PAB gels. The statistical software program SPSS (version 10.1 for Windows, Microsoft) was used to re-evaluate the Mann-Whitney statistics and to calculate exact p-values. Correlation data between the individual proteomics spot intensities and parameters of RV hypertrophy were also calculated in SPSS by means of a linear regression analysis. Data are presented as mean ± SEM. A p-value < 0.05 was considered statistically significant.

Results

Degree of hypertrophy and hemodynamics.

RV and right atrium weights relative to body weight (BW) were significantly increased (respectively 1.8 an 1.6 –fold) in the PAB animals after 6 weeks, which demonstrates the presence of a robust hypertrophic response (Table 1). RV end-systolic pressures were significantly increased in the PAB animals (29 ± 2 vs. 66 ± 8 mmHg, $p<0.01$) as well as the RV end-diastolic pressures (5 ± 1 vs. 10 ± 2 mmHg, $p<0.01$), stroke work (5472 ±

597 vs. 12515 ± 2176 mmHg·µl, p<0.05) and the dP/dt-max (1442 ± 107 vs. 3435 ± 359 mmHg/s, p<0.01). Heart rate did not differ between sham and PAB animals (309 ± 10 vs. 297 ± 12 bpm, p=NS), as well as the cardiac output (70 ± 4 vs. 57 ± 6 ml/min, p=NS). LV function was not affected as indicated by LV end-systolic pressures (96 ± 7 vs. 107 ± 7 mmHg, p=NS), end-diastolic pressures (13 ± 2 vs. 11 ± 3 mmHg, p=NS), stroke work (16540 ± 1617 vs. 17798 ± 1929 mmHg·µl, p=NS), and the dP/dt-max (6331 ± 503 vs. 5559 ± 795 mmHg/s, p=NS). Clinically, the rats did not show clear signs of RV failure. Moreover, an increase in liver weight was not observed in the PAB group as compared to the sham group (14.0 ± 0.8 vs. 14.6 ± 0.5 g, p=NS). These results indicate a compensated state of hypertrophy.

Table 1: Heart and bodyweight characteristics of the study groups

Weights	Sham (n=6)	PAB (n=6)	P value
BW start (g)	212 ± 5	206 ± 9	NS
BW end (g)	376 ± 16	374 ± 13	NS
RA/BW (mg/g)	0.13 ± 0.01	0.21 ± 0.03	0.02
RV/BW (mg/g)	0.58 ± 0.02	1.03 ± 0.05	< 0.01
LA/BW (mg/g)	0.05 ± 0.00	0.05 ± 0.00	NS
LV/BW (mg/g)	1.38 ± 0.03	1.42 ± 0.05	NS
Septum/BW (mg/g)	0.66 ± 0.02	0.71 ± 0.03	NS

Data presented as average ± SEM. P-value < 0.05 (Student's T-test) was considered significant. BW = body weight, RA = right atrium, RV = right ventricle, LA = left atrium, LV = left ventricle, NS = non-significant

Reproducibility of subfractionation and 2-DE

The reproducibility of the 2-DE was tested. Therefore, 4 gels were run out of one pooled cytoplasmic fraction. With the image analysis, described in Methods, we matched 304 spots across all 4 gels. The coefficient of variation for all spot intensities was found to be 15%, which is well within the acceptable range of technical variation [6]. Furthermore, the spot intensities showed a high correlation (r^2=0.94) among all gels. These gel-to-gel correlations were comparable with data reported in literature [7].

We also evaluated the percentage of spill over between both the cytoplasmic and myofilament extracts. The myosin light chain 1 and 2 proteins are parts of the myofilaments. Our extraction method resulted in an average spill over of these proteins into the cytoplasmic fraction of 2%, which was relatively constant among the 2-DE gels of sham and PAB group. For typical cytosolic proteins such as malate dehydrogenase and lactate dehydrogenase, an average spill over of 6% to the myofilament fraction was observed which likewise was constant comparing all 2-DE gels from both animal groups.

Protein changes in the cytoplasmic fraction

An example of the pattern of proteins from normal rat RV tissue separated by 2-DE is shown in Figure 1. On average a total of 363 protein spots were matched. Several spots were clustered and non-distinguishable and, therefore, were not included in the analysis. Most of these spots reside at the basic side of the gel as can be derived from Figure 1. After comparison of the 2-DE patterns from all sham vs. PAB animals we identified a group of 25 protein spots that were significantly up-or downregulated. Spots in the 2-DE gels unique to either control or PAB 2-DE patterns were not observed.

Figure 1: 2-DE image of RV cytoplasmic fraction

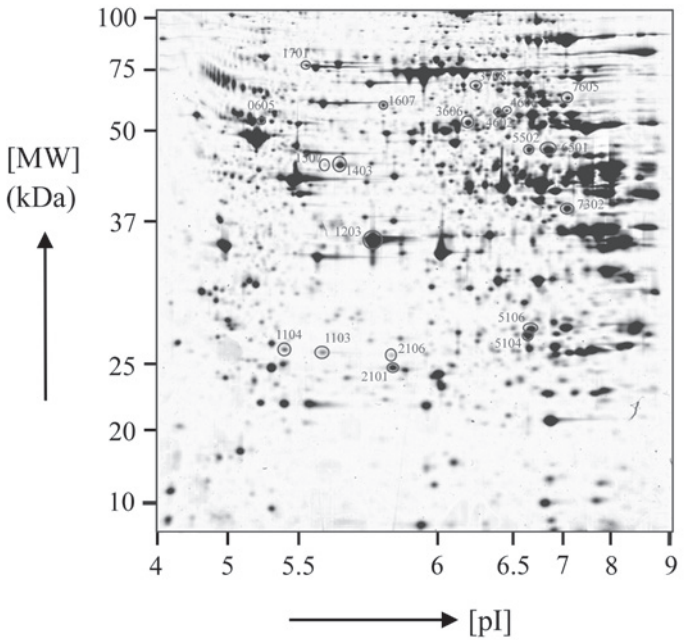

Representative image of a 2-DE gel resembling the cytoplasmic subproteome of a normal rat right ventricle. More information on the labelled protein spots is given in table 2.

Out of the 25 altered protein spots, 20 proteins were identified. For the 5 remaining spots, no adequate peptide mapping could be performed either due to too low amount of protein or to technical limitations. The protein alterations were divided into three categories: 1) metabolic proteins, 2) stress proteins, and 3) miscellaneous. A list of the identified proteins together with their accuracy of identification as indicated by the Mowse score and significance of up- or downregulation is given in Table 2.

Table 2: List of identified differentially expressed proteins in the cytoplasmic fraction

Protein Nr.	Protein Identification	Protein accession number	Change in intensity PAB/ sham	P-value[a]	Theoretical		Mowse Score[b]	% sequence coverage
					Mw	pI		
	Metabolic proteins							
1203	L-Lactate dehydrogenase β-chain	gi|6981146	+ 1.2 ± 0.08 (↑)	0.016	36589	5.70	104	37
1403	Creatine kinase	gi|203474	+ 1.7 ± 0.31 (↑)	0.037	42699	5.33	101	36
1507	Creatine kinase	gi|203474	+ 2.8 ± 0.75 (↑)	0.004	42685	5.33	Indirect[d]	N/A
4602	Propionyl-CoA carboxylase β-chain	gi|51260066	- 1.4 ± 0.10 (↓)	0.004	58641	7.96[e]	122	29
5104	2-enoyl-CoA hydratase	gi|3212683	- 1.5 ± 0.18 (↓)	0.016	28269	6.41	94	42
5106	Phosphoglycerate mutase	gi|112128	+ 1.6 ± 0.13 (↑)	0.004	28814	6.67	73[c]	37
5502	β -enolase	gi|54035288	- 2.0 ± 0.51 (↓)	0.025	46984	7.08	80	24
6501	β -enolase	gi|54035288	- 2.0 ± 0.31 (↓)	0.004	46984	7.08	96	29
7605	Pyruvate kinase M2	gi|206205	+ 1.5 ± 0.22 (↑)	0.010	57744	7.15	111	34
	Stress proteins							
1103	HSP-27	gi|14010865	+ 1.9 ± 0.41 (↑)	0.016	22808	6.12	90	48
1104	HSP-27	gi|14010865	+ 1.7 ± 0.20 (↑)	0.006	22808	6.12[e]	79	36
1701	HSP-8	gi|55250073	+ 1.5 ± 0.20 (↑)	0.016	70827	5.37	64	17
2106	HSP-27	gi|14010865	+ 3.5 ± 1.28 (↑)	0.006	22808	6.12[e]	107	48
	Miscellaneous							
0605	Tubulin β-chain 15	gi|92930	+ 1.6 ± 0.31 (↑)	0.025	49905	4.79[e]	64	26
1607	glucose regulated protein	gi|38382858	+ 1.3 ± 0.13 (↑)	0.025	56588	5.88	169	31
2101	peroxiredoxin 6	gi|6758348	+ 1.5 ± 0.29 (↑)	0.016	24803	5.64	113	40
3606	Selenium binding protein 2	gi|18266692	- 1.4 ± 0.12 (↓)	0.006	52498	6.10	157	34
3708	chaperonin containing TCP1, γ	gi|40018616	+ 1.2 ± 0.10 (↑)	0.025	60608	6.23	71	17
4606	Adenylyl cyclase associated protein	gi|16758742	+ 1.3 ± 0.12 (↑)	0.016	52879	6.69	111	27
7302	Bcat 2 protein	gi|11693174	- 1.5 ± 0.21 (↓)	0.016	44274	8.46[e]	67	19

Identification was achieved using MALDI-MS in combination with the Mascot search engine (www.matrixscience.com). The search was performed in the NCBI database (species: rattus).

[a] Mann-Whitney test was used for statistical comparison

[b] Mascot Mowse score of 58 is the threshold for $p<0.05$

[c] Determined by MSDB database search (instead of NCBI); Mowse score of 54 (instead of 58) is the threshold for $p<0.05$

[d] Identification using (own) 2-DE map comparison

[e] Observed pI different from theoretical pI (Δ pI > 0.5)

One particularly interesting finding was the presence of 3 spots that were identified as HSP-27 (respectively 1.9, 1.7 and 3.5 fold upregulated in the PAB group, see also Figure 2). To add confidence to this observation, western blotting using various antibodies against HSP-27 on 1-DE separated cytoplasmic fractions was performed (Figure 3 A). When using an antibody against total (unphosphorylated and phosphorylated) HSP-27, a 1.5 fold upregulation was found. However, the signals were recorded at a lower molecular mass range (22-23 kDa) compared to the Coomassie blue stained and MS-identified HSP-27 spots on 2-DE. The antibody against a phosphorylated form of HSP-27 (P-Ser15) revealed a marked (3.6 fold) upregulation of recorded signal at the mobility range of 27 kDa. Additionally, western blotting on 2-DE at the mobility range of 27 kDa was performed (Figure 3 B). This analysis showed that all three HSP-27 spots (1103, 1104 and 2106) reacted with the antibody against total HSP-27, whereas only spot nrs. 1103 and 1104 reacted with the antibody against P-HSP-27-Ser15.

Figure 2: Differential expression of three HSP-27's on 2-DE

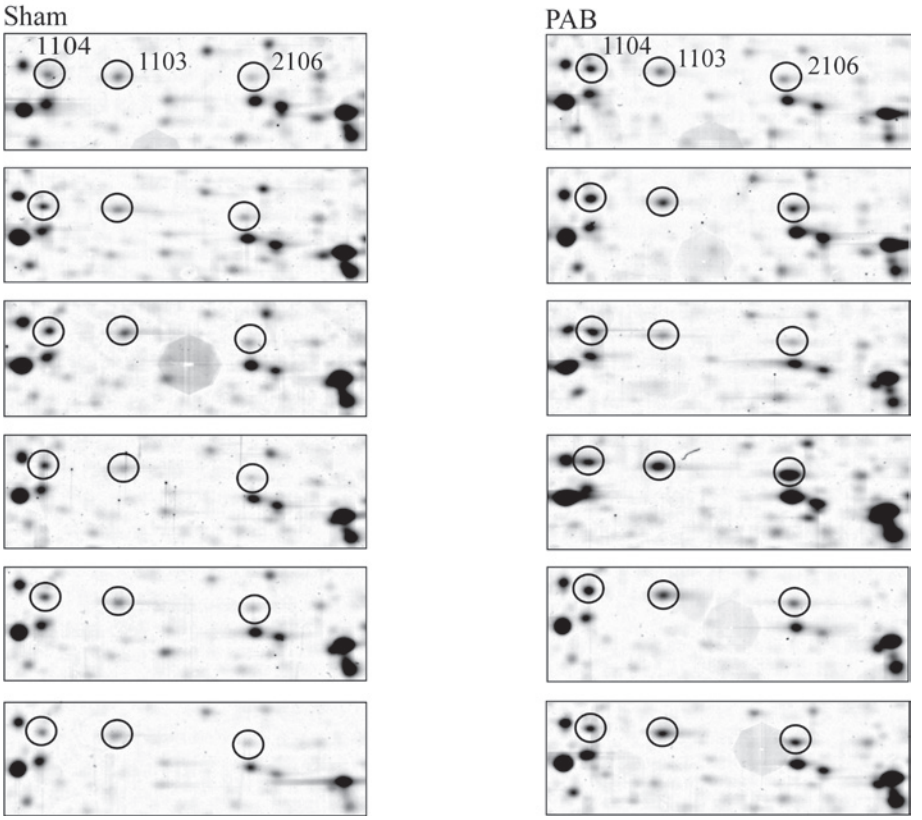

Enlarged 2-DE gel images of the individual right ventricle cytoplasmic subproteomes of 6 sham and 6 PAB rats in order to show the differential expression of three spots identified as HSP-27 at the 27 kDa mobility range with apparent pI values of 5.4, 5.6 and 5.8.

Figure 3: Western blots of desmin and HSP-27 species

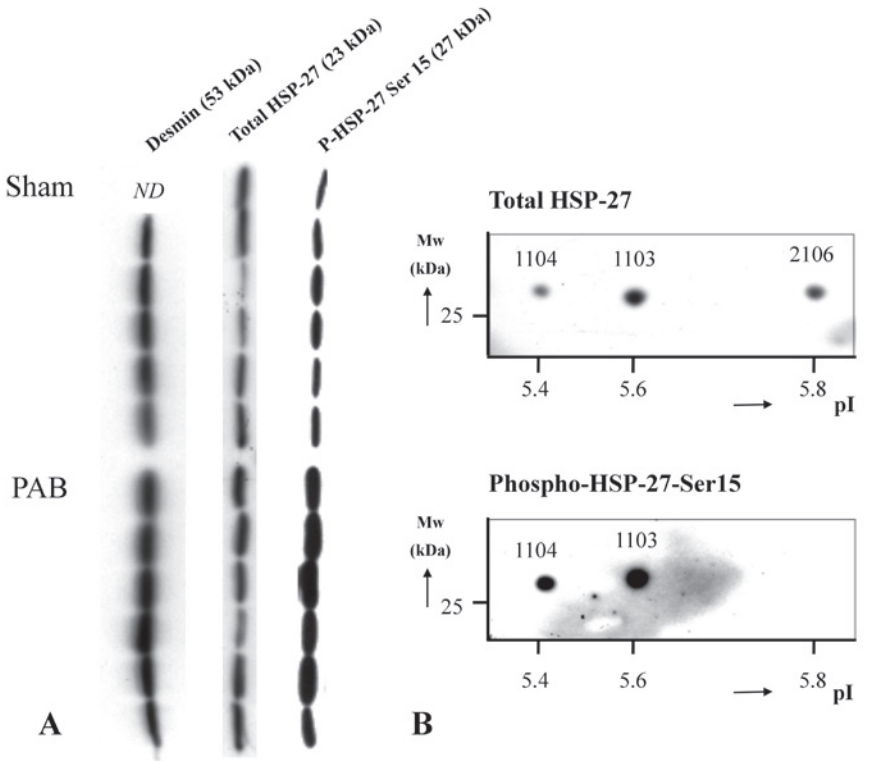

A. Western blots of desmin (myofilament fraction; ECL signal is 1.4 fold upregulated in PAB), total HSP-27 (ECL signal is 1.5 fold upregulated in PAB), HSP-27 phosphorylated at Ser-15 residue (ECL signal is 3.6 fold upregulated in PAB). All HSP-27 1-DE separations are from cytoplasmic fractions. Notice that no ECL signal is found in the 27 kDa mobility range with the antibody against total HSP-27, likely due to the relative low amount of right ventricular cytoplasmic protein which was loaded in the wells of the 1-DE gels (20 µg)
B. Western blots of 27 kDa mobility area of 2-DE gels using the same antibodies as in A. The upper ECL image shows three spots reacting with the antibody against total HSP-27. These spots comigrate with the three HSP-27s detected by Coomassie blue as described in Figure 2. The lower part shows that two out of these three spots are reacting with the antibody against phosphorylated HSP-27 at the Ser-15 residue. Notice that 350 µg of right ventricular cytoplasmic protein is loaded on to the 2-DE gels.

To further strengthen the hypothesis that the HSP-27 spots were phosphorylated we applied on-target enzymatic dephosphorylation of the trypsin digested spots. First, we recorded an MS spectrum from the original sample and thereafter one was made from the alkaline phosphatase treated peptide digest. By comparing these spectra we identified a HSP-27 fragment peptide at a m/z ratio of 2098 in the original spectrum of all spots which shifted leftwards to a m/z ratio of 2018 in the spectrum of the treated sample. This was observed for HSP-27 spot nrs. 1103 and 1104 but not for spot nr. 2106 (Figure 4). The leftward shift of approximately 80 Da is indicative for the presence of a phosphorylated peptide which indeed carries Ser-15.

Figure 4: Identification of the phosphorylation site in the differentially expressed HSP-27's

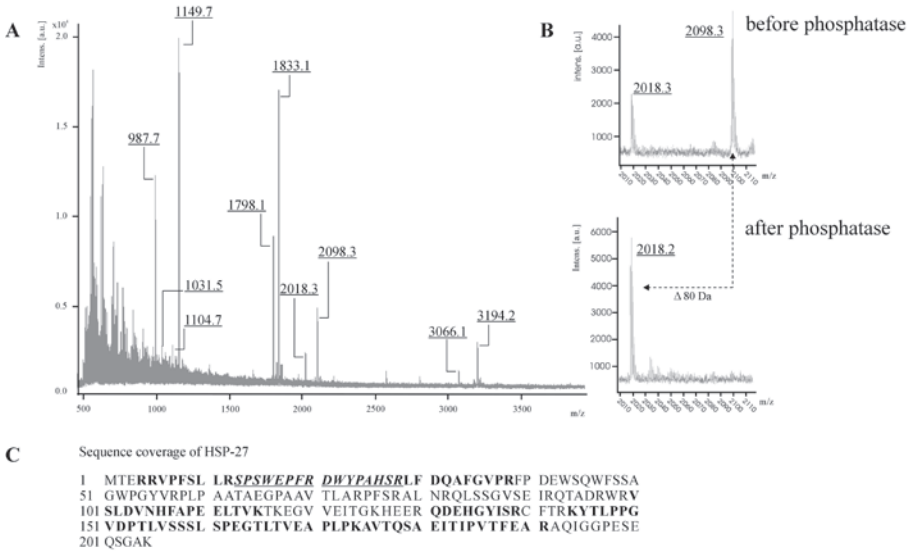

C Sequence coverage of HSP-27

1 MTE**RRVPFSL LR*SPSWEPFR* *DWYPAHSR*LF DQAFGVPR**FP DEWSQWFSSA
51 GWPGYVRPLP AATAEGPAAV TLARPFSRAL NRQLSSGVSE IRQTADRWRV
101 **SLDVNHFAPE ELTVK**TKEGV VEITGKHEER **QDEHGYISR**C FTR**KYTLPPG**
151 **VDPTLVSSSL SPEGTLTVEA PLPKAVTQSA EITIPVTFEA R**AQIGGPESE
201 QSGAK

A. MALDI-MS spectrum of one of the phosphorylated HSP-27 spot after in gel digestion with trypsin. The peaks used for identification (Mascot) are labelled with the precise values.
B. The upper panel shows a part of the MS spectrum of a phosphorylated HSP-27 spot before on-target treatment with alkaline phosphatase. After enzymatic dephosphorylation the peak corresponding to the phosphorylated peptide shifted leftwards (lower panel). This mass shift of 80 Da corresponds with the removal of one phosphate group. Similar phosphopeptide results were obtained with HSP-27 spot nrs 1103 and 1104 which refer to Figure 2.
C. The sequence coverage of HSP-27 from spot nr 1103 (compare Figure 2) by peptide ion signals in the mass spectrum. The peptide sequences corresponding to the z values indicated in A are given in bold. The sequence coverage is 52%. The peptide fragment (referring to value 2098.3 in B), including its most likely phosphorylation site Ser-15, is given in italic and underlined.

Changes in myofilament protein expression

Figure 5 shows a typical example of a 2-DE separation pattern of the myofilament(-associated) proteins from the RV of a sham-operated rat. It became clear that the separation of the myofilament subfraction is complicated by too wide differences in relative expression levels of the bulk of myofilament components, such as myosin binding protein C, actin, tropomyosin and troponins on one hand and the associated proteins, such as those of the cytoskeleton, on the other hand [8, 9]. Nevertheless, on average a total of 211 protein spots could be properly matched. As with the cytoplasmic fraction, many clustered spots were excluded from the analysis. The comparison of the 2-DE maps between sham and PAB animals resulted in the detection of 13 altered protein spots, of which 7 spots were upregulated. With the help of Q-TOF MS/MS we were able to identify 8 protein spots including one which appeared to be a contamination. Interestingly, among the altered proteins, an upregulation of both

desmin and α-B-crystallin (CryAB) was found (1.4 and 1.3 fold respectively) which was substantiated for desmin by immunoblotting of myofilament fractions separated on 1-DE (Figure 3). Besides these respectively intermediate filament and chaperone proteins, also alterations in apparent non-structural proteins like α-enolase were found. Table 3 shows a list of the differentially expressed (identified) proteins, including details on identification accuracy and statistical evaluation.

Figure 5: 2-DE image of RV myofilament fraction

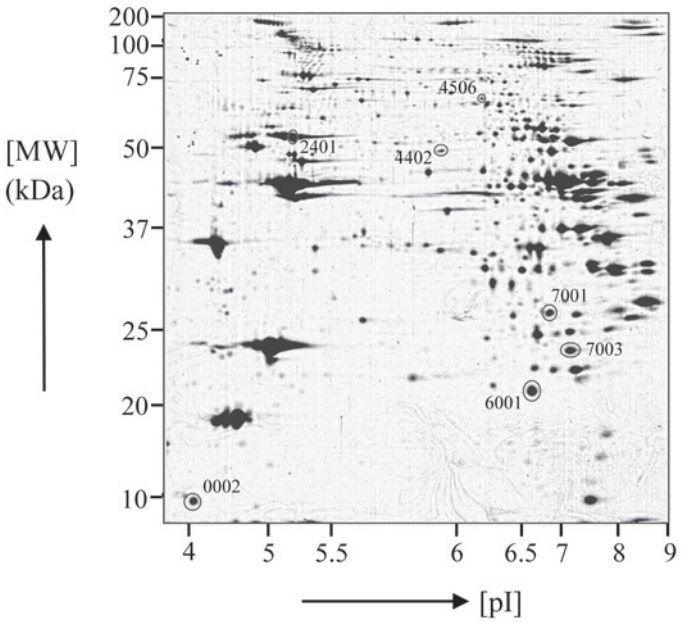

Representative image of a 2-DE gel resembling the myofilament subproteome of a normal rat right ventricle. More information on the labelled protein spots is given in Table 3.

Table 3: List of identified differentially expressed proteins in the myofilament fraction

Protein Nr.	Protein identification	Protein accession number	Change in intensity PAB/sham	P-value[c]	Theoretical		Mowse Score	Mowse threshold p < 0.05	% sequence coverage
					pI	Mw			
0002	ATP synthase delta chain[a]	gi | 20806153	-1.9 ± 0.36 (↓)	0.016	5.16[d]	17584	93	29	13
2401	Desmin[b]	gi | 38197676	1.4 ± 0.18 (↑)	0.010	5.21	53390	87	54	17
4402	Alpha-enolase[a]	gi | 6978809	1.5 ± 0.21 (↑)	0.025	6.16	47428	317	30	21
4506	Pincher[b]	gi | 20135683	2.0 ± 0.40 (↑)	0.025	6.33	61428	62	54	13
6001	Alpha-beta crystallin[a]	gi | 57580	1.3 ± 0.11 (↑)	0.025	6.84	19945	259	30	25
7001	Electron transfer flavoprotein β-subunit[a]	gi | 51948412	-1.9 ± 0.52 (↓)	0.016	7.60[d]	27898	266	31	23
7003	NADH dehydrogenase (ubiquinone) beta subcomplex[a]	gi | 27667934	-2.8 ± 1.10 (↓)	0.037	7.57	21131	286	31	32

Identification was achieved using the Mascot search engine (www.matrixscience.com) using de NCBI database seach (species: rattus)

[a] Identification by Q-TOF MS/MS

[b] Idenification by MALDI-MS

[c] Mann-Whitney test was used for statistical comparison

[d] Observed pI different from theoretical (Δ pI > 0.5)

Correlations with the degree of hypertrophy

In order to investigate potential relationships between the observed protein changes and the degree of hypertrophy, we analyzed the significances of correlations between the proteomic data (individual relative intensities of each spot) and RV weight to BW ratio in the PAB group (Figure 6). This approach resulted in the detection of 4 spots that were significantly correlated with the degree of hypertrophy. One spot, HSP-27 (spot number 1103/cytoplasmic fraction), was positively correlated with the degree of hypertrophy (r^2=0.89, p<0.01). Furthermore, both spots containing β-enolase (5502 and 6501) were negatively correlated with the RV weight to BW ratio (r^2=0.99, p<0.01 and r^2=0.87, p<0.01 respectively). From the myofilament fraction only one spot (7003, NADH dehydrogenase ubiquinone) was found to be negatively correlated with the degree of hypertrophy (r^2=0.76, p<0.05).

Figure 6: Correlation with the degree of hypertrophy

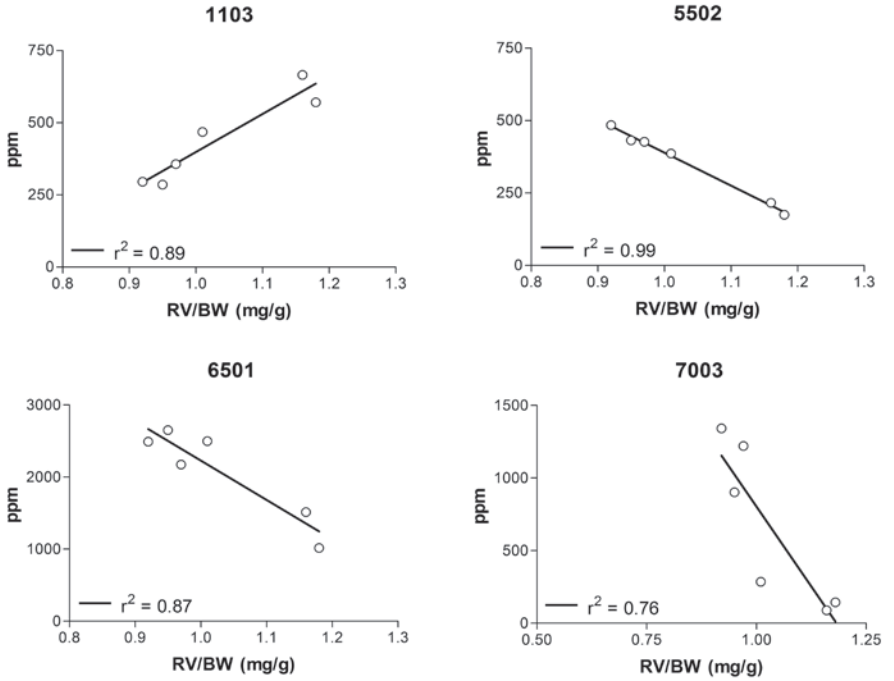

Individual correlations between relative protein intensity (ppm) and the degree of hypertrophy (RV/BW) in PAB animals. Spot 1103 = HSP-27, 5502 = β-Enolase, 6501 = β-Enolase and 7003 = NADH dehydrogenase (ubiquinone) beta subcomplex.

Discussion

In this study we demonstrate, for the first time, that 6 weeks of RV pressure overload in young rats leads to alterations in the proteome as studied by means of a differential 2-DE and MS analysis. Since the RV hypertrophy was well characterized by hemodynamic measurements, these alterations in the proteome are occurring in a compensated state of RV hypertrophy. We showed that the majority of the protein changes that occur in the cytoplasmic fraction of the hypertrophied RV belong to the category of metabolic and stress related proteins. Two out of the three upregulated HSP-27 species appeared to be phosphorylated, most likely on the Ser-15 residue, as shown by immunoblotting and MS analysis. The alterations found in the myofilament subproteome concern metabolic proteins, intermediate filament protein desmin, and the desmin-associated chaperone protein CryAB, which in principle all are myofilament associated proteins. Interestingly, significant correlations between the degree of hypertrophy (RV weight to BW ratio) and relative RV content (% staining intensity on 2-DE gel) of several of the differentially expressed proteins were found.

From Table 2 one can appreciate that at least 20 proteins are changed significantly in the hypertrophic RV compared to the normal RV. The majority of protein changes in the cytoplasmic fraction concern alterations in the metabolic proteins. Metabolism related changes include a decrease in beta-oxidation enzymes (spots 4602 and 5104 as in Table 2) and an increase in glycolytic enzymes (spots 1203, 5106, and 7605 as in Table 2). In the normal heart the myocardium preferentially oxidizes fatty acids [10-12]. In various models of LV hypertrophy it was demonstrated that the energy supplying pathways return to a fetal state of metabolism [13-19]. This shift in metabolism is characterized by a decreased oxidation of fatty acids and an increased glucose metabolism [20-25]. The metabolic shift in energy supply from beta-oxidation towards glycolysis has been less well documented for the RV [26]. The results of our proteomics study can be interpreted to suggest that the shift in energy substrate utilization in the hypertrophic RV resembles the situation in the hypertrophic LV. Several mechanisms have been proposed that should provide an explanation for this metabolic shift, such as an imbalance in O_2 supply/demand ratio in the hypertrophic hearts [27, 28].

Besides alterations in the expression of metabolic proteins, proteins involved in the stress response were also altered in our study. Three altered protein spots could be identified as HSP-27 which suggested the presence of PTMs. HSP-27 is a stress related protein that has received special interest in cardioprotection as well as heart failure. The HSP-27 protein is an actin-cap binding protein that can inhibit actin polymerization [29]. Its function is mainly dependent on its phosphorylation state

and these modifications can therefore play an important role in cardiac remodeling processes. The presence of HSP-27 alterations in cardiovascular diseases has been reported by several groups [30-32]. However, the effect of altered phosphorylation of HSP-27 on the development of RV hypertrophy or its influence on alterations in cardiac function that occur in RV hypertrophy are unknown. In the study of Scheler et al. HSP-27 protein expression patterns of normal and failing hearts (LV) were compared [31]. In that study, HSP-27 expression profiling was performed using 2-DE in combination with immunostaining. Numerous HSP-27 containing spots were detected, which were located in two separate mass series (27-28 kDa and 22-23 kDa) that reacted with the anti-HSP-27 antibody. Multiple spots in the lower mass range were found to be upregulated whereas some spots from the high mass range were downregulated in the LV of dilated cardiomyopathy (DCM) type hearts, suggesting that some form of HSP-27 degradation is occurring in the failing heart [31]. In our present study we did not observe an upregulation of lower mass range HSP-27's by 2-DE. However, an upregulation of lower mass range HSP-27's was found by western blotting of 1-DE separated cytoplasmic fractions using the HSP-27 antibody reacting with the unphosphorylated as well as the phosphorylated form. This indicates that in the rat RV the HSP-27's of 22-23 kDa are less abundant, at least non-detectable with staining by Coomassie blue. Nevertheless, we did find an upregulation of HSP-27's of 27-28 kDa by 2-DE. This latter finding was confirmed by western blotting using a specific antibody against phospho-Ser-15 HSP-27 (Figure 3). Moreover, using MS we could observe a phosphorylation for two HSP-27 spots (1103 and 1104) by comparing spectra before and after enzymatic dephosphorylation of the Ser-15 containing peptide fragment of HSP-27. These data suggest that those two HSP-27 spots are at least phosphorylated at the Ser-15 residue. The third spot (2106) is also very likely to be modified since its observed pI on the gel is still different (approximate pI=5.8) from its theoretical value (pI=6.12). More in depth studies, specifically on the sites and degree of phosphorylation of HSP-27's and its possible association with hemodynamic alterations, are needed to clarify the role of HSP-27 in the hypertrophic RV.

The myofilament fraction revealed 13 protein alterations of which only 7 proteins could be identified as shown in Table 3. Perhaps the most interesting observation are the upregulations found for desmin and CryAB. The CryAB, a protein that was found in both myofilament and cytoplasmic subfractions, is known for its regulatory role in desmin distribution [33, 34]. The CryAB binds to both desmin and cytoplasmic actin and functions as a quality control in the formation of intermediate filaments [35]. An upregulation of CryAB has been found in the LV in DCM, a downregulation in end-stage congestive heart (LV) failure [30] [36-38]. From our model of RV hypertrophy we can conclude that CryAB is also upregulated in the myofilament subproteome of

the RV. Remarkably, the CryAB was unchanged in the cytoplasmic fraction, indicating that the cytoplasmic concentration of this protein is not affected in RV hypertrophy. From several studies by Robbins et al. it can be concluded that specific desmin localization is crucial for optimal cardiac function [33-35, 39]. We observed an increase in myofilament-associated desmin in the hypertrophic RV. Altered desmin expression has been observed in other pressure overloaded types of cardiac hypertrophy, as well as familial cardiomyopathies and DCM [40-42]. However, no discrimination was made between cytoplasmic and myofilament fraction. In the present study we were able to discriminate between both cellular fractions, resulting in the detection of upregulated myofilament-associated desmin. This upregulation was confirmed by western blotting of 1-DE separated myofilament fractions.

Hemodynamic assessment shows that the relative protein expressions were studied in a compensated state of RV hypertrophy. This degree of hypertrophy, as expressed by the RV weight to BW ratio, was correlated with multiple relative protein spot intensities. We correlated protein spot intensities of only the PAB group with this parameter of RV hypertrophy. In the PAB group the RV weight to BW ratio will differ among the individual animals due to slightly different pressure loads and different hypertrophic responsiveness. Therefore, protein spots from the PAB group that show significant correlations between RV weight to BW ratio and the relative protein expression might be important in determining the hypertrophic responsiveness. Two of these proteins that showed such a correlation are β-enolase and HSP-27. Further evaluation of the exact role of these proteins and their modifications in the pathological hypertrophic response of the RV is needed. Nevertheless, the present data suggests that these specific protein spots are part of a protein signature that changes with the degree of hypertrophy. Additional studies with varying degrees of hypertrophy or duration of pressure overload are needed to underscore this hypothesis.

Despite the fact that this study reveals important protein changes in RV hypertrophy, limitations of this approach should also be considered. An extensive review on proteomic studies and the limitations is given by McGregor and Dunn [4]. The staining used in this study, Coomassie blue, is well known for its good downstream compatibility with MS and its linearity and dynamic range making it suitable for quantitation [43-45]. However, the detection sensitivity is moderate compared to silver staining protocols limiting the protein coverage [46]. In the future, more advanced 2-DE gel based proteomic profiling methods may be applied to the field of cardiovascular proteomics, like the DIGE system. Also non-gel based quantitative proteomics methods using stable isotope labeling, such as ICAT, could be promising.

The application of a subfractionation step prior to 2-DE analysis is necessary for whole heart homogenates in order to reduce the sample complexity, increase the quality and resolution of the 2-DE gels, and to enhance the overall protein coverage [47]. In the present study we applied a detergent-extraction of the isolated myofilament fraction to pre-separate at least the myofilament(-associated) proteins from all other cellular proteins.

Specific limitations may apply to the study of myofilament proteins. Although desmin and (to a lesser extent) CryAB are known as myofilament associated proteins, many of the proteins identified in this study would not be expected in the myofilament fraction. Moreover, several myofilament proteins are known to be difficult to separate and/or to be quantitated by 2-DE due to their extreme pI values and/or high molecular weights. On the other hand, immunoblot analysis of the myofilament-associated desmin convincingly demonstrated the agreement between the relative intensity of Coomassie blue staining on 2-DE and the ECL staining on 1-DE (r^2=0.71, $p<0.01$). In addition to these limitations, staining problems with specific myofilament proteins have been reported [48]. To overcome these limitations, RP-HPLC has been proposed in addition to 2-DE, to study the myofilament proteins [48].

In conclusion, we present for the first time, a proteomic analysis of RV hypertrophy in a hemodynamically well characterized rat model. Our study reveals many protein alterations in compensated RV hypertrophy, in both cytoplasmic and myofilament subfractions. The metabolic protein changes are consistent with a shift from fatty acid to glucose as substrate for the energy supply. Furthermore, the increased expression of phosphorylated HSP-27 species is indicative for an altered stress response. Likewise, changes were found in the expression of myofilament-associated proteins, such as desmin and CryAB. Interestingly, some of the differentially expressed proteins, such as HSP-27, showed a significant correlation with the RV weight to BW ratio in PAB rats suggesting an association with the degree of hypertrophy.

References

1. Hoffman, J. I.Kaplan, S., The incidence of congenital heart disease. J Am Coll Cardiol 2002, 39, 1890-1900.
2. Wren, C.O'Sullivan, J. J., Survival with congenital heart disease and need for follow up in adult life. Heart 2001, 85, 438-443.
3. Bolger, A. P., Coats, A. J.Gatzoulis, M. A., Congenital heart disease: the original heart failure syndrome. Eur Heart J 2003, 24, 970-976.
4. McGregor, E.Dunn, M. J., Proteomics of heart disease. Hum Mol Genet 2003, 12 Spec No 2, R135-144.
5. Larsen, M. R., Sorensen, G. L., Fey, S. J., Larsen, P. M., et al., Phospho-proteomics: evaluation of the use of enzymatic de-phosphorylation and differential mass spectrometric peptide mass mapping for site specific phosphorylation assignment in proteins separated by gel electrophoresis. Proteomics 2001, 1, 223-238.
6. Molloy, M. P., Brzezinski, E. E., Hang, J., McDowell, M. T., et al., Overcoming technical variation and biological variation in quantitative proteomics. Proteomics 2003, 3, 1912-1919.
7. Challapalli, K. K., Zabel, C., Schuchhardt, J., Kaindl, A. M., et al., High reproducibility of large-gel two-dimensional electrophoresis. Electrophoresis 2004, 25, 3040-3047.
8. Arrell, D. K., Neverova, I., Fraser, H., Marban, E., et al., Proteomic analysis of pharmacologically preconditioned cardiomyocytes reveals novel phosphorylation of myosin light chain 1. Circ Res 2001, 89, 480-487.
9. McDonough, J. L., Neverova, I.Van Eyk, J. E., Proteomic analysis of human biopsy samples by single two-dimensional electrophoresis: Coomassie, silver, mass spectrometry, and Western blotting. Proteomics 2002, 2, 978-987.
10. Saddik, M.Lopaschuk, G. D., Myocardial triglyceride turnover and contribution to energy substrate utilization in isolated working rat hearts. J Biol Chem 1991, 266, 8162-8170.
11. Henning, S. L., Wambolt, R. B., Schonekess, B. O., Lopaschuk, G. D., et al., Contribution of glycogen to aerobic myocardial glucose utilization. Circulation 1996, 93, 1549-1555.
12. Zierler, K. L., Fatty acids as substrates for heart and skeletal muscle. Circ Res 1976, 38, 459-463.
13. Buttrick, P. M., Kaplan, M., Leinwand, L. A.Scheuer, J., Alterations in gene expression in the rat heart after chronic pathological and physiological loads. J Mol Cell Cardiol 1994, 26, 61-67.
14. Schwartz, K., Boheler, K. R., de la Bastie, D., Lompre, A. M., et al., Switches in cardiac muscle gene expression as a result of pressure and volume overload. Am J Physiol 1992, 262, R364-369.
15. Feldman, A. M., Weinberg, E. O., Ray, P. E.Lorell, B. H., Selective changes in cardiac gene expression during compensated hypertrophy and the transition to cardiac decompensation in rats with chronic aortic banding. Circ Res 1993, 73, 184-192.
16. Charlemagne, D., Maixent, J. M., Preteseille, M.Lelievre, L. G., Ouabain binding sites and (Na+,K+)-ATPase activity in rat cardiac hypertrophy. Expression of the neonatal forms. J Biol Chem 1986, 261, 185-189.
17. Bishop, S. P.Altschuld, R. A., Increased glycolytic metabolism in cardiac hypertrophy and congestive failure. Am J Physiol 1970, 218, 153-159.
18. Taegtmeyer, H.Overturf, M. L., Effects of moderate hypertension on cardiac function and metabolism in the rabbit. Hypertension 1988, 11, 416-426.
19. Massie, B. M., Schaefer, S., Garcia, J., McKirnan, M. D., et al., Myocardial high-energy phosphate and substrate metabolism in swine with moderate left ventricular hypertrophy. Circulation 1995, 91, 1814-1823.
20. Meerson, F. Z., The myocardium in hyperfunction, hypertrophy and heart failure. Circ Res 1969, 25, Suppl 2:1-163.

21. Reibel, D. K., Uboh, C. E.Kent, R. L., Altered coenzyme A and carnitine metabolism in pressure-overload hypertrophied hearts. Am J Physiol 1983, 244, H839-843.
22. Reibel, D. K., O'Rourke, B.Foster, K. A., Mechanisms for altered carnitine content in hypertrophied rat hearts. Am J Physiol 1987, 252, H561-565.
23. Wittels, B.Spann, J. F., Jr., Defective lipid metabolism in the failing heart. J Clin Invest 1968, 47, 1787-1794.
24. Anderson, P. G., Allard, M. F., Thomas, G. D., Bishop, S. P., et al., Increased ischemic injury but decreased hypoxic injury in hypertrophied rat hearts. Circ Res 1990, 67, 948-959.
25. Yonekura, Y., Brill, A. B., Som, P., Yamamoto, K., et al., Regional myocardial substrate uptake in hypertensive rats: a quantitative autoradiographic measurement. Science 1985, 227, 1494-1496.
26. Takeyama, D., Kagaya, Y., Yamane, Y., Shiba, N., et al., Effects of chronic right ventricular pressure overload on myocardial glucose and free fatty acid metabolism in the conscious rat. Cardiovasc Res 1995, 29, 763-767.
27. Carvajal, K.Moreno-Sanchez, R., Heart metabolic disturbances in cardiovascular diseases. Arch Med Res 2003, 34, 89-99.
28. Nascimben, L., Ingwall, J. S., Lorell, B. H., Pinz, I., et al., Mechanisms for increased glycolysis in the hypertrophied rat heart. Hypertension 2004, 44, 662-667
29. Landry, J.Huot, J., Modulation of actin dynamics during stress and physiological stimulation by a signaling pathway involving p38 MAP kinase and heat-shock protein 27. Biochem Cell Biol 1995, 73, 703-707.
30. Scheler, C., Muller, E. C., Stahl, J., Muller-Werdan, U., et al., Identification and characterization of heat shock protein 27 protein species in human myocardial two-dimensional electrophoresis patterns. Electrophoresis 1997, 18, 2823-2831.
31. Scheler, C., Li, X. P., Salnikow, J., Dunn, M. J., et al., Comparison of two-dimensional electrophoresis patterns of heat shock protein Hsp27 species in normal and cardiomyopathic hearts. Electrophoresis 1999, 20, 3623-3628.
32. Knowlton, A. A., Kapadia, S., Torre-Amione, G., Durand, J. B., et al., Differential expression of heat shock proteins in normal and failing human hearts. J Mol Cell Cardiol 1998, 30, 811-818.
33. Wang, X., Osinska, H., Gerdes, A. M.Robbins, J., Desmin filaments and cardiac disease: establishing causality. J Card Fail 2002, 8, S287-292.
34. Wang, X., Osinska, H., Klevitsky, R., Gerdes, A. M., et al., Expression of R120G-alphaB-crystallin causes aberrant desmin and alphaB-crystallin aggregation and cardiomyopathy in mice. Circ Res 2001, 89, 84-91.
35. Sanbe, A., Osinska, H., Saffitz, J. E., Glabe, C. G., et al., Desmin-related cardiomyopathy in transgenic mice: a cardiac amyloidosis. Proc Natl Acad Sci U S A 2004, 101, 10132-10136.
36. Arbustini, E., Morbini, P., Grasso, M., Fasani, R., et al., Restrictive cardiomyopathy, atrioventricular block and mild to subclinical myopathy in patients with desmin-immunoreactive material deposits. J Am Coll Cardiol 1998, 31, 645-653.
37. Yang, J., Moravec, C. S., Sussman, M. A., DiPaola, N. R., et al., Decreased SLIM1 expression and increased gelsolin expression in failing human hearts measured by high-density oligonucleotide arrays. Circulation 2000, 102, 3046-3052.
38. Hwang, D. M., Dempsey, A. A., Wang, R. X., Rezvani, M., et al., A genome-based resource for molecular cardiovascular medicine: toward a compendium of cardiovascular genes. Circulation 1997, 96, 4146-4203.
39. Wang, X., Klevitsky, R., Huang, W., Glasford, J., et al., AlphaB-crystallin modulates protein aggregation of abnormal desmin. Circ Res 2003, 93, 998-1005.
40. Collins, J. F., Pawloski-Dahm, C., Davis, M. G., Ball, N., et al., The role of the cytoskeleton in left ventricular pressure overload hypertrophy and failure. J Mol Cell Cardiol 1996, 28, 1435-1443.

41. Heling, A., Zimmermann, R., Kostin, S., Maeno, Y., et al., Increased expression of cytoskeletal, linkage, and extracellular proteins in failing human myocardium. Circ Res 2000, 86, 846-853.
42. Wang, X., Li, F., Campbell, S. E.Gerdes, A. M., Chronic pressure overload cardiac hypertrophy and failure in guinea pigs: II. Cytoskeletal remodeling. J Mol Cell Cardiol 1999, 31, 319-331.
43. Lauber, W. M., Carroll, J. A., Dufield, D. R., Kiesel, J. R., et al., Mass spectrometry compatibility of two-dimensional gel protein stains. Electrophoresis 2001, 22, 906-918.
44. Patton, W. F., Detection technologies in proteome analysis. J Chromatogr B Analyt Technol Biomed Life Sci 2002, 771, 3-31.
45. Neuhoff, V., Stamm, R., Pardowitz, I., Arold, N., et al., Essential problems in quantification of proteins following colloidal staining with coomassie brilliant blue dyes in polyacrylamide gels, and their solution. Electrophoresis 1990, 11, 101-117.
46. Switzer, R. C., 3rd, Merril, C. R.Shifrin, S., A highly sensitive silver stain for detecting proteins and peptides in polyacrylamide gels. Anal Biochem 1979, 98, 231-237.
47. Huber, L. A., Pfaller, K.Vietor, I., Organelle proteomics: implications for subcellular fractionation in proteomics. Circ Res 2003, 92, 962-968.
48. Neverova, I.Van Eyk, J. E., Application of reversed phase high performance liquid chromatography for subproteomic analysis of cardiac muscle. Proteomics 2002, 2, 22-31.

Chapter 4

Right- and left ventricular function after chronic pulmonary artery banding in rats assessed with biventricular pressure-volume loops

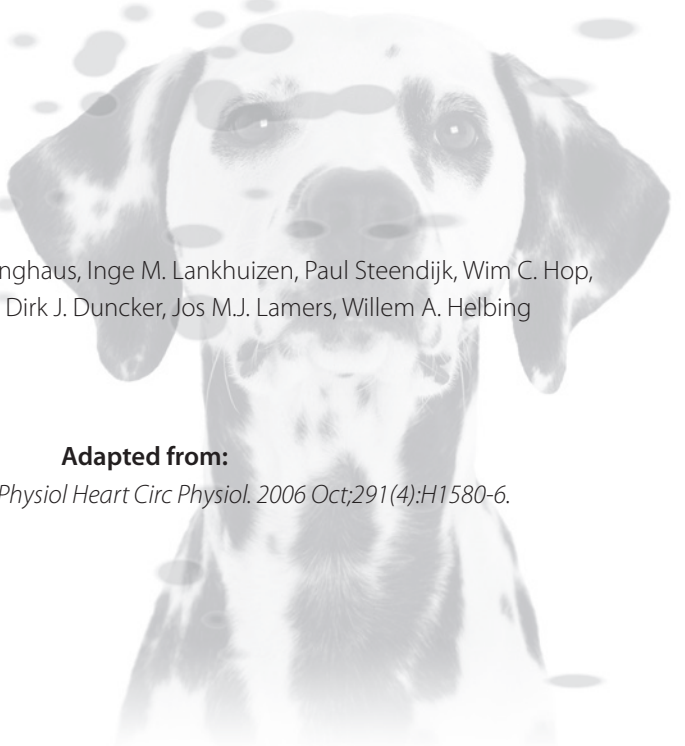

Matthijs J. Faber, Michiel Dalinghaus, Inge M. Lankhuizen, Paul Steendijk, Wim C. Hop, Regien G. Schoemaker, Dirk J. Duncker, Jos M.J. Lamers, Willem A. Helbing

Adapted from:

M.J. Faber et al. *Am J Physiol Heart Circ Physiol. 2006 Oct;291(4):H1580-6.*

Abstract

In many patients with congenital heart disease, the right ventricle (RV) is subjected to abnormal loading conditions. In order to better understand the state of compensated RV hypertrophy, which could eventually progress to decompensation, we studied the effects of RV pressure overload in rats. In the present study we report the biventricular adaptation to 6 weeks of pulmonary artery banding (PAB). PAB resulted in a RV pressure overload to approximately 60% of systemic level and a 2-fold increase in RV mass ($p<0.01$). Systemic hemodynamic parameters were not altered and overt signs of heart failure were absent. Load-independent measures of ventricular function (ESPVR, PRSW, dP/dt_{Max}-Ved), assessed by means of pressure-volume (PV) loops, demonstrated an 2-3 fold increase in RV contractility under baseline conditions in PAB rats. RV contractility increased in response to dobutamine stimulation (2.5 µg/kg/min) both in PAB as in sham operated rats in a similar fashion, indicating preserved RV contractile reserve in PAB rats. Left ventricular (LV) contractility at baseline was unaffected in PAB rats, although LV volume in PAB rats was slightly decreased. LV contractility increased in response to dobutamine (2.5 µg/kg/min) both in PAB and sham rats, while the response to a higher dose of dobutamine (5 µg/kg/min) was blunted in PAB rats. Six weeks of RV pressure overload in rats resulted in a state of compensated RV hypertrophy with preserved RV contractile reserve, while LV contractile state at baseline was not affected. Furthermore, this study demonstrates the feasibility of performing biventricular PV-loop measurements in rats.

Introduction

Right ventricular (RV) function is an important determinant of long-term outcome in patients with complex congenital heart disease, chronic pulmonary obstructive diseases, or pulmonary hypertension. In many of these patients the RV is subjected to (residual) abnormal loading conditions, including pressure overload. Although compensated hypertrophy will develop initially, ultimately RV failure will ensue. The mechanisms underlying the progression from compensated RV hypertrophy to decompensated RV hypertrophy (ie. RV failure) have not been well defined. As the survival of the patients improves, a better understanding of these mechanisms becomes mandatory in order to be able to design preventive strategies and to time surgical (re)intervention in these patients.

To study the mechanisms underlying the transition from a compensated state of hypertrophy to a decompensated state in patients is very difficult, because invasive data cannot be easily obtained. For this purpose animal models may be beneficial. Small experimental animals, such as rats, are widely used in cardiovascular research since they can provide a variety of disease models including heart hypertrophy and failure. A major advantage of the use of these small disease models is that cardiac material can be easily sampled to study critically involved molecular changes over time and the possibility to study effects of transgenesis and gene ablation [2, 5, 22, 23, 34]. Recently, we performed a proteomic profiling study on RV hypertrophy showing multiple expression and post-translational changes in metabolic-, stress-, and myofilament proteins [12]. To interpret these molecular findings in terms of possible mechanisms involved in RV remodelling, an accurate assessment of RV function is required, preferably by using load-independent parameters of cardiac contractility [13, 24, 29, 30]. We present a biventricular hemodynamic characterization using pressure-volume (PV) loops of RV hypertrophy in a rat model induced by 6 weeks of pressure overload as a result of pulmonary artery banding (PAB).

Methods

All experimental procedures and protocols used in this investigation were reviewed and approved by the institutional animal care and use committee and are in accordance with the National Institutes of Health "*Guide for the care and use of laboratory animals*" (NIH publication No. 85-23, revised 1996).

Male Wistar rats (190-220 g, Harlan, Zeist, The Netherlands) underwent PAB or sham operation. Complete hemodynamic studies were performed in 15 animals: 6 rats underwent PAB at the age of 8 weeks, whereas 9 rats underwent a sham operation and

served as control. The animals were housed after the initial operation (ie. sham or PAB) for a period of 6 weeks, prior to the hemodynamic studies, in groups of 2 or 3 animals, on a 12/12-h light/dark cycle with standard rat chow and water *ad libitum*.

Pulmonary artery banding procedure

Anesthesia was induced by pentobarbital (60 mg/kg i.p.). After intubation, the animals were mechanically ventilated with the use of a volume-controlled respirator and oxygen-enriched room air. Positive end-expiratory pressure was maintained at 4 cm H_2O. A left thoracotomy was performed and the pulmonary artery (PA) was carefully dissected free from the aorta. A silk thread was positioned under the PA and an 18 gauge needle was placed alongside the PA. A suture was tied tightly around the needle and the needle was rapidly removed in order to produce a fixed constricted opening in the lumen equal to the diameter of the needle. The combination of a fixed banding around the PA and the growth of the animal will eventually result in a markedly increased RV afterload. After the banding, the thorax was closed in layers and post-operative pain relief was obtained by applying buprenorphine (15 µg/kg s.c.). The sham animals underwent the same procedure except for the banding of the PA.

Hemodynamic instrumentation

After a housing period of 6 weeks, hemodynamic measurements were performed. The study protocol was the same for sham and PAB animals.

After induction of anesthesia (pentobarbital; 60 mg/kg i.p.) the animals were intubated and ventilated as described above. A catheter (PE-50) was placed in the abdominal cavity for i.p. administration of pentobarbital for maintenance of anesthesia. Both femoral veins were canulated with a catheter (PE-50) for the infusion of hypertonic saline for calculation of the parallel conductance (see later) and for the administration of dobutamine. The right carotid artery was canulated with a catheter (PE-50) connected to a fluid-filled pressure transducer to monitor systemic blood pressures and to obtain samples for blood-gas analysis. The right jugular vein was canulated with a catheter (PE-50) for the infusion of Haemaccel (Hoechst, Behring-Werke, Marburg Germany) to maintain adequate fluid levels. A right thoracotomy was performed and an ultrasonic flow-probe (Transonics Systems Inc., Ithaca, NY), connected to a Transonics flow meter (TS420), was placed around the aorta and used for calibration of the conductance catheter (see later). A left thoracotomy was performed for maximal exposure of the left side of the heart to facilitate an adequate catheter insertion in the LV. For preload reduction, required to obtain systolic and diastolic PV-relations, a silk thread was placed around the vena cava inferior, just above the diaphragm. A conductance catheter (CD Leycom, Zoetermeer, The Netherlands) and a pressure-tip catheter (Millar Instruments,

Houston, TX) were inserted in the RV through the ventricular wall, at the level of the outflow tract, and positioned towards the apex. Similarly, conductance and pressure-tip catheters were inserted in the LV apex and positioned along the LV long axis. The conductance catheters consisted of 5 segments of which, on average, 2-3 segments were used for measurement of ventricular volumes. Positioning of the conductance catheters was optimized by observing the pressure and segmental volume signals with appropriate phase relationships. The conductance catheters were connected to a Leycom Sigma-5 DF signal processors (CD Leycom) and the pressure-tip catheters were connected to pressure transducer units (Millar Instruments, Houston, TX). Signals were recorded at a minimal sample rate of 500Hz using the Conduct 2000 data-acquisition hard- and software (CD Leycom) installed on an IBM compatible personal computer.

Conductance catheter calibration

In order to obtain absolute volumes, the conductance catheter derived signals must be calibrated for parallel conductance and slope factor (α). Conductance catheters were calibrated as previously described. Briefly, parallel conductance was determined by the hypertonic saline method and slope factor α by matching uncalibrated conductance stroke volume with stroke volume derived from the aortic flow signal [1, 28].

Hemodynamic study protocol

When hemodynamic stability was reached, a set of measurements was performed to calibrate the conductance catheter method and to assess hemodynamics and contractile performance in baseline conditions. Data were recorded with open chest at steady-state baseline conditions and during transient preload reduction. The parallel conductance of both ventricles was measured (*in duplo*) by injecting 50 µL NaCl 10% intravenously [28]. All measurements were made during short suspension of the ventilation at end-expiration. To determine inotropic reserve we infused dobutamine at 2.5 (dobu-2.5) and 5 µg/kg/min (dobu-5) via a pump. The same set of measurements as described above were performed and started at least 10 minutes after the onset of dobutamine infusion. Moreover, the parallel conductance was re-calculated for each dobutamine step since parallel conductance changes during the administration of dobutamine [33]. Before each set of measurements a blood sample was drawn and analyzed (Roche Diagnostics, Almere, The Netherlands) to ensure proper oxygenation and acid/base balances.

Hemodynamic measurements and calculations

The biventricular signals were analyzed by custom made software (Circlab). The steady state data were averaged over two separate intervals that each consisted of at least five

cardiac cycles. From these steady state data the following parameters were calculated: heart rate, cardiac output, stroke volume (SV), end-systolic pressure, end-diastolic pressure, end-systolic volume, end-diastolic volume, maximal first time-derivative of pressure (dP/dt_{Max}), and stroke work.

PV loops acquired during vena cava occlusion were used to derive ventricular PV relations (Figure 1). The end-systolic point was defined as the point in the cardiac cycle of maximal elastance. Elastance was defined as $P(t)/[V(t)-V_0]$, where P(t) is the instantaneous pressure, V(t) instantaneous volume, and V_0 the theoretical volume at zero pressure [8]. V_0 was determined by an iterative algorithm as previously described by Kono et al [16]. The following relations were determined and used as parameters of systolic function: the end-systolic pressure-volume relation (ESPVR)[29], the dP/dt_{max} -Ved relation[24], and the preload recruitable stroke work relation (PRSW)[13]. Slopes and intercepts of these relations were previously validated as sensitive and relative load-independent parameters of ventricular function.

Figure 1: Representative right-and left ventricular PV loops

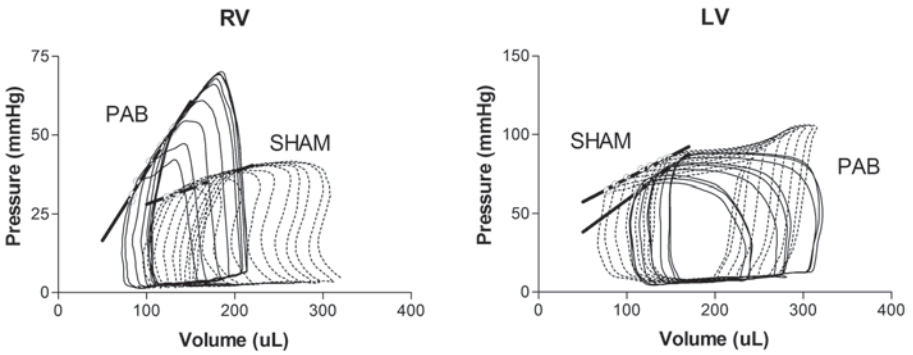

In both sham (dotted loops) and PAB (solid loops) animals during preload reduction. The black solid lines represent the end-systolic PV relations (ESPVR) in both groups.

Statistical analysis

The differences in hemodynamic parameters between the control group and the PAB group at baseline were analyzed using a Student's T-test. The effect of dobutamine stimulation for each group were analyzed using repeated measures ANOVA. Differences in response to dobutamine stimulation between groups were tested by repeated measures 2-way ANOVA. *Post* hoc testing, when appropriate, was performed using the Bonferroni correction. The software packages SPSS and SAS (PROC MIXED) were used for data analysis. A two-sided p-value < 0.05 was considered statistically significant. Data are presented as mean ± SEM

Results

During the banding period, the rats did not show overt signs of heart failure and/or cyanosis. The average body weight of the PAB group at the start of the protocol did not differ significantly from the control (sham) group (resp. 206 ± 9 vs. 210 ± 4 g, p=NS). The weight gain during the 6 week housing period was similar between groups (PAB: 168 ± 9 vs. sham: 172 ± 10 g, p=NS). Right atrial and RV weight were increased in PAB rats, while left heart weights were unaffected (Table 1).

Table 1: Heart weight to body weight characteristics of the study groups.

Weights	Sham (n=9)	PAB (n=6)	p-value
RA/BW (mg/g)	0.13 ± 0.01	0.21 ± 0.03	<0.01
RV/BW (mg/g)	0.59 ± 0.02	1.03 ± 0.05	<0.01
LA/BW (mg/g)	0.05 ± 0.00	0.05 ± 0.00	N.S.
LV/BW (mg/g)	1.37 ± 0.04	1.42 ± 0.05	N.S.
Septum (mg/g)	0.69 ± 0.02	0.71 ± 0.03	N.S.

Values are mean ± SEM. BW=body weight, RA=right atrium, RV=right ventricle, LA=left atrium, LV=left ventricle, PAB=pulmonary artery banding, N.S.= non-significant

Baseline hemodynamics (Table 2)

In baseline conditions the heart rate and cardiac output did not differ between sham and PAB rats. The RV peak-systolic pressures in PAB rats were increased to 60% of peak-systolic LV pressure. RV end-diastolic and end-systolic volumes were slightly decreased in PAB rats, although this did not reach statistical significance (p≥0.26). Both RV stroke work and dP/dt_{max} were increased in the PAB rats as compared to the sham group. The slopes of the ESPVR, PRSW, and the dP/dt_{max} -Ved relations (henceforth called the three PV-relations) were all steeper in the PAB rats, indicating an increased contractile function of the RV (Figure 2).

In the LV the end-systolic and end-diastolic pressures were similar in both groups. The end-diastolic volumes were similar for both groups while the end-systolic volumes were decreased in the LV of the PAB rats. Both LV stroke work and dP/dt_{max} were similar for both sham and PAB rats. The contractility of the LV, as expressed by the three PV-relations, was not altered in the PAB rats.

Table 2: Hemodynamics at baseline and during dobutamine infusion.

	parameters		Baseline	Dobu-2.5	Dobu-5
	HR	sham	310 ± 8	396 ± 6 †	421 ± 10 ‡
		PAB	297 ± 12	379 ± 8 †	407 ± 10 ‡
	CO	sham	51 ± 4	52 ± 4	63 ± 5 ‡
		PAB	49 ±5	51 ± 3	53 ± 4
	SV	sham	164 ± 11	132 ± 11†	149 ± 13 ‡
		PAB	164 ± 13	134 ± 7 †	130 ± 7
	MAP	sham	90 ± 6	89 ± 6	90 ± 6
		PAB	101 ± 6	97 ± 10	92 ± 8
RV	Ved	sham	315 ± 44	218 ± 28†	222 ± 22
		PAB	259 ± 32	223 ± 24	284 ± 36
	Ves	sham	151 ± 34	89 ± 19†	78 ± 10
		PAB	95 ± 30	90 ± 19	118 ± 23
	Pes	sham	29 ± 1	34 ± 3	37 ± 4
		PAB	63 ± 8 *	74 ± 8†	89 ± 7 ‡ [b]
	Ped	sham	5 ± 1	3 ± 1	4 ± 1
		PAB	7 ± 1	9 ± 1†	10 ± 1
	SW	sham	3963 ± 500	3746 ± 506	4879 ± 709 ‡
		PAB	11087 ± 2179 *	9005 ± 1653 † [a]	9911 ± 1618 ‡
	dP/dt_{max}	sham	1429 ± 94	2114 ± 128 †	2708 ± 144 ‡
		PAB	3435 ± 359 *	4278 ± 458 †	4973 ± 623 ‡
LV	Ved	sham	337 ± 26	203 ± 21 †	199 ± 22
		PAB	265 ± 26	168 ± 8 †	169 ± 9
	Ves	sham	172 ± 21	71 ± 12 †	50 ± 12 ‡
		PAB	101 ± 20 *	34 ± 2 †	39 ± 6 [b]
	Pes	sham	93 ± 6	98 ± 12	111 ± 13
		PAB	107 ± 7	107 ± 6	103 ± 7
	Ped	sham	10 ± 2	7 ± 1	8 ± 2
		PAB	10 ± 3	7 ± 2	8 ± 2
	SW	sham	15344 ± 1634	14402 ± 2219	17502 ± 2391
		PAB	18169 ± 2114	15819 ± 1469	15078 ± 1584
	dP/dt_{max}	sham	6331 ± 503	8845 ± 764 †	10629 ± 688 ‡
		PAB	5559 ± 795	8234 ± 1070 †	9109 ± 1068

Values are mean ± SEM. HR=heart rate (beats/min), CO=cardiac output (mL/min), SV=stroke volume (µL), MAP=mean arterial pressure (mmHg), Ved=end-diastolic volume (µL), Ves=end-systolic volume (µL), Pes=end-systolic pressure (mmHg), Ped=end-diastolic pressure (mmHg), SW=stroke work (mmHg· µL), dP/dt_{max}=maximum first time derivative of pressure vs. time ($mmHg \cdot s^{-1}$)

* $p<0.05$ *versus* corresponding control in baseline

† $p<0.05$ *versus* baseline

‡ $p<0.05$ *versus* dobu-2.5

[a] $p<0.05$ difference in dobutamine response (baseline – dobu-2.5) between sham and PAB

[b] $p<0.05$ difference in dobutamine response (dobu-2.5 – dobu-5) between sham and PAB

Hemodynamics during dobutamine stimulation (Table 2)

Heart rate increased significantly at each step of dobutamine infusion in both PAB and sham rats and the magnitude of the response was similar in both groups. Cardiac output did not significantly change in PAB rats and increased in sham rats only at dobu-5. In concert, stroke volumes significantly decreased in both PAB and sham rats to a similar extent at dobu-2.5. Only in sham animals stroke volume increased at dobu-5, but did not return to baseline level. No alteration in systemic blood pressure was observed in response to dobutamine.

In many respects, the responses of the RV to dobutamine stimulation were similar in PAB and sham rats. End-systolic RV pressures increased somewhat in both groups, but only significantly in PAB rats at each level of dobutamine stimulation. End-diastolic volumes decreased in response to dobu-2.5 in both groups, but the response was only significant in sham rats ($p<0.001$, PAB: $p=0.32$). At dobu-5 the end-diastolic volume increased non-significantly in PAB rats ($p=0.18$) and was unaltered in sham rats. Further analysis did not reveal any statistical trends in the response of RV end-diastolic volumes between PAB and sham rats at the two levels of dobutamine stimulation (all $p\geq0.20$). RV dP/dt_{max} increased at each level of dobutamine in both groups. RV SW, however, tended to decrease at dobu-2.5 and subsequently increased at dobu-5. All three PV relations increased significantly in response to dobu-2.5 in both groups (Fig 2). In contrast, at dobu-5 all three PV relations demonstrated no further significant alterations as compared to dobu-2.5. Although, Ees decreased slightly in both groups ($p\geq0.34$) and PRSW and dP/dt_{max}-Ved increased slightly ($p\geq0.32$), no differences in the response between PAB and sham could be demonstrated ($p>0.50$). Together, these results indicate an increased RV contractile response at dobu-2.5, without a further increase at dobu-5.

The LV of the PAB animals also responded in a similar fashion to dobutamine stimulation as compared to its sham counterparts. LV end-diastolic and end-systolic pressures did not change significantly as a result of dobutamine stimulation. The LV end-diastolic volume and end-systolic volumes decreased in both groups equally, mainly as a result of the first dosage of dobutamine. Furthermore, the LV dP/dt_{max} increased in both groups while the stroke work remained unaltered. LV contractility increased in both sham and PAB rats as represented by an increase in the slopes of the PV-relations (Figure 2). At dobu-5 only the LV of sham animals was capable of increasing contractility as represented by an increase in Ees and dP/dt_{max}-Ved. In summary, the LV contractile response to dobutamine stimulation was similar for both groups at dobu-2.5 and the response of the PAB animals at dobu-5 was blunted.

Figure 2: Alterations in three load-independent parameters of contractility at baseline and during dobutamine infusion for the RV (A) and LV (B).

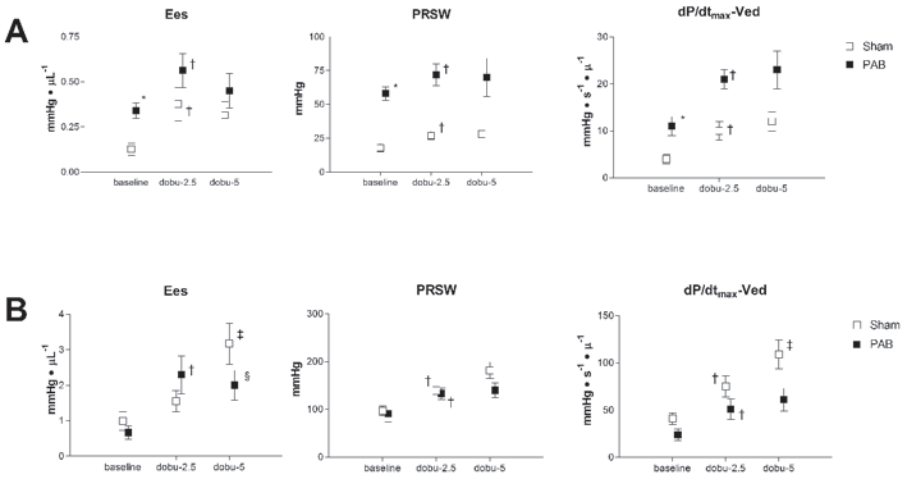

Ees=end-systolic elastance (mmHg· μL^{-1}), PRSW=preload recruitable stroke work (mmHg), dP/dt_{max}-Ved=maximum first time derivative of pressure divided by end-diastolic volume ($mmHg \cdot s^{-1} \cdot \mu L^{-1}$)
* $p<0.05$ *versus* corresponding control in baseline
† $p<0.05$ *versus* baseline
‡ $p<0.05$ *versus* dobu-2.5
§ $p<0.05$ difference in dobutamine response (dobu-2.5 – dobu-5) between sham and PAB

Discussion

Our findings indicate that 6 weeks of RV pressure overload in our rat model resulted in enhanced baseline RV contractility and that RV contractile reserve was maintained indicating a state of compensated RV hypertrophy. Furthermore, baseline LV contractility was unaffected while the LV response to dobutamine stimulation was blunted. These data are in line with the observation that RV pressure overload did not result in alterations in systemic hemodynamic parameters and that overt signs of heart failure were absent.

Assessment of cardiac contractile state by load-independent parameters of LV function by means of the conductance catheter technique is well established [15, 29]. It has been shown that the technique is applicable in the LV of large animals and humans, as well as small animals such as rats [7, 27]. More recently, it was shown that despite the complex geometry of the RV, this approach is also useful in characterizing RV contractile state and reserve in various conditions [3, 4, 8, 10, 17, 19, 25, 31]. Some investigators have used this technique simultaneously in both LV and RV studying LV and RV responses and their interaction in various derangements of the normal

circulation. The application of this biventricular conductance catheter technique so far has been limited to larger animals such as lambs [19]. To our knowledge, this study is the first to apply the biventricular conductance catheter (multi-segment) technique in small experimental animals such as rats.
In our study RV systolic pressure was increased to about 60% of systolic LV pressure, a level of RV pressure overload that is commonly encountered in patients with residual abnormalities after palliative or corrective surgery for complex congenital heart disease. This resulted in a robust hypertrophic response: increasing RV mass 2-fold in the PA banded rats (Table 1). We used three load-independent measures of contractility (ESPVR, PRSW and dP/dt_{max}-Ved) to determine the contractile state of both the RV and LV. These indices all indicated a 2-3 fold increase of RV contractility at baseline in the pressure overloaded RV. Contractile reserve of the RV was demonstrated by a further increase of RV contractility at the lowest dose of dobutamine. Qualitatively, the responses of the RV were similar in the sham and PAB rats. Similarly, baseline LV contractility was the same in sham and PAB rats. At each level of dobutamine stimulation (2.5 and 5 µg/kg/min, resp.) LV contractility increased in sham rats, but in PAB rats LV contractility did not increase further at the highest dose of dobutamine. Qualitatively, the responses of the LV were similar in both sham and PAB rats, except for a blunted response at the highest dose of dobutamine in PAB rats. RV volumes were slightly, but not significantly, lower in PAB rats, while LV end-diastolic volumes tended to be somewhat lower in PAB rats ($p=0.09$).

The effects of pressure overload on RV contractile function have been studied previously under various conditions and by using various techniques. The onset of and the duration of the pressure overload determine the RV hypertrophic response and the effects on RV hemodynamics. For example, in patients with acute RV pressure overload the RV dilates and stroke volume reduces. Initially, the increased end-diastolic RV volume serves to maintain cardiac output, but eventually RV dysfunction results in a diminished cardiac output [14, 26]. In contrast, in young lambs with acute RV pressure overload, RV end-diastolic volume was unaltered, while RV contractile state increased [8, 9]. These studies implicated RV homeometric autoregulation as an important immediate adaptation to RV pressure overload. In patients with chronic RV pressure overload, induced by either COPD or primary pulmonary hypertension, MRI studies have demonstrated an increased RV mass, a decrease of both RV and LV end-diastolic volume, and a maintained RV systolic function [18, 32]. Similar results have been obtained in experimental studies using the conductance catheter technique. Leeuwenburgh and coworkers induced 8 weeks of RV pressure overload in lambs by gradually increasing and maintaining RV pressures at systemic levels [19]. In response,

these lambs developed compensated RV hypertrophy as demonstrated by the increase of RV contractile indices at a normal RV end-diastolic volume. Furthermore, LV contractile function was not affected by the RV hypertrophy, as parameters of LV contractility were unaltered, while LV end-diastolic volume was decreased. The results from these previous studies are in line with the major findings from our study: in response to chronic RV pressure overload RV and LV contractile function is maintained at a normal or somewhat decreased RV end-diastolic volume and a somewhat decreased LV end-diastolic volume.

In their study on chronic RV pressure overload, Leeuwenburgh and coworkers suggested that the increase in RV contractile state was out of proportion to the amount of hypertrophy, indicating a hypercontractile state of the RV. The results of our study are in line with the observations made by Leeuwenburgh and co-workers, although the increase in RV contractile state in our study seemed more in proportion with the amount of hypertrophy. When normalising the three PV-relations for RV weight, no difference was seen in two out the three PV-relations (Figure 3). Although the PV relations increased significantly at dobu-2.5 in the sham animals, the qualitative response in sham and PAB animals to dobutamine was similar. This suggests that the intrinsic RV contractility of the PAB rats is similar or slightly higher as compared to controls and that contractile reserve is maintained.

Figure 3: Right ventricular PV relations corrected for RV weight (see Discussion for more details).

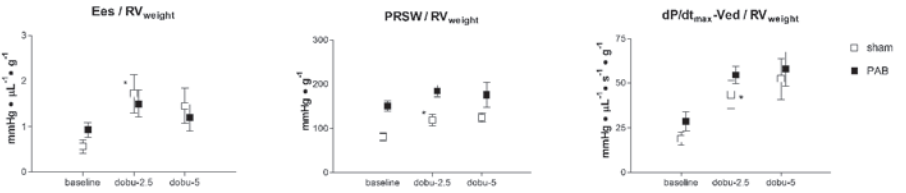

Ees / RV_{weight} =end-systolic elastance divided by RV weight (mmHg· μL^{-1}· g^{-1}), PRSW / RV_{weight} =preload recruitable stroke work divided by RV weight (mmHg· g^{-1}), dP/dt_{max}-Ved / RV_{weight} =maximum first time derivative of pressure divided by end-diastolic volume divided by RV weight (mmHg·s^{-1}· μL^{-1}· g^{-1})

* $p<0.05$ *versus* baseline

Notably, in the study in lambs the LV contractile state was maintained at a lower LV end-diastolic volume, suggesting a slight hypercontractile state of the LV as well. In our study the LV end-diastolic volumes also tended to be lower in the PAB rats. The finding that the baseline LV ESPVR was shifted leftward (LV V_{100} = 194 ± 22 vs. 114 ± 32 sham vs. PAB, p=0.05) also supports a hypercontractile LV function in the PAB rats. The drive for this hypercontractile state is unknown, but we found no signs of

increased systemic sympathetic nervous stimulation. LV response to the 5 µg/kg/min dobutamine stimulation was blunted in the PAB animals. Whether a downregulation of LV β – adrenergic receptors plays a role in this response is uncertain. LV β – adrenergic receptors were downregulated 4 weeks after monocrotaline treatment in rats, while RV β – adrenergic receptors were unaffected [6]. However, other studies have not found a downregulation in LV β – adrenergic receptors in RV hypertrophy [20, 21]. Therefore additional research to elucidate the mechanisms behind this LV blunted response is necessary.

Relevance of the study

Many patients with corrected congenital heart disease, pulmonary hypertension and/or chronic obstructive pulmonary disease have (residual) abnormal RV loading conditions making them prone for the development of RV failure. One of the challenges is to identify the turning point from compensated RV hypertrophy to (irreversible) RV failure. In a previous study, we reported the changes in the myocardial protein expression in response to RV pressure overload [12]. We demonstrated alterations in expression of metabolic proteins, compatible with a shift from fatty acid to carbohydrate metabolism. Furthermore, we found upregulation of several low molecular weight heat shock proteins and could demonstrate the phosphorylation of HSP-27. The expression of several proteins seemed to be correlated with the degree of hypertrophy. For example, a phosphorylated HSP-27 was positively correlated with the degree of hypertrophy (r^2=0.89, $p<0.01$). This study demonstrates the feasibility of characterizing biventricular responses to RV pressure overload in a small animal model. This allows to characterize the progression of RV compensated hypertrophy to RV failure over time and to correlate these findings with alterations in myocardial protein expression. By using this approach relevant changes in myocardial protein expression can be correlated with the onset of RV failure [11]. Therefore, further longitudinal studies are needed to correlate hemodynamics with alterations in the myocardial proteome.

In conclusion, 6 weeks of RV pressure overload in rats resulted in a state of compensated RV hypertrophy, while LV contractile state at baseline was not, or only marginally affected. Furthermore, this study demonstrated the feasibility of performing biventricular measurements using a multi-segment conductance catheter technique in rats. This hemodynamic profiling of the preceding stages of heart failure in a small animal model will facilitate an integration between physiology and biochemistry ultimately leading to a more accurate interpretation of heart hypertrophy and failure.

References:

1. Baan J, van der Velde ET, de Bruin HG, Smeenk GJ, Koops J, van Dijk AD, Temmerman D, Senden J, and Buis B. Continuous measurement of left ventricular volume in animals and humans by conductance catheter. Circulation 70: 812-823, 1984.
2. Bar H, Kreuzer J, Cojoc A, and Jahn L. Upregulation of embryonic transcription factors in right ventricular hypertrophy. Basic Res Cardiol 98: 285-294, 2003.
3. Bishop A, White P, Groves P, Chaturvedi R, Brookes C, Redington A, and Oldershaw P. Right ventricular dysfunction during coronary artery occlusion: pressure-volume analysis using conductance catheters during coronary angioplasty. Heart 78: 480-487, 1997.
4. Bishop A, White P, Oldershaw P, Chaturvedi R, Brookes C, and Redington A. Clinical application of the conductance catheter technique in the adult human right ventricle. Int J Cardiol 58: 211-221, 1997.
5. Braun MU, Szalai P, Strasser RH, and Borst MM. Right ventricular hypertrophy and apoptosis after pulmonary artery banding: regulation of PKC isozymes. Cardiovasc Res 59: 658-667, 2003.
6. Brown L, Miller J, Dagger A, and Sernia C. Cardiac and vascular responses after monocrotaline-induced hypertrophy in rats. J Cardiovasc Pharmacol 31: 108-115, 1998.
7. Cingolani OH, Yang XP, Cavasin MA, and Carretero OA. Increased systolic performance with diastolic dysfunction in adult spontaneously hypertensive rats. Hypertension 41: 249-254, 2003.
8. de Vroomen M, Cardozo RH, Steendijk P, van Bel F, and Baan J. Improved contractile performance of right ventricle in response to increased RV afterload in newborn lamb. Am J Physiol Heart Circ Physiol 278: H100-105, 2000.
9. De Vroomen M, Steendijk P, Lopes Cardozo RH, Brouwers HH, Van Bel F, and Baan J. Enhanced systolic function of the right ventricle during respiratory distress syndrome in newborn lambs. Am J Physiol Heart Circ Physiol 280: H392-400, 2001.
10. Dickstein ML, Yano O, Spotnitz HM, and Burkhoff D. Assessment of right ventricular contractile state with the conductance catheter technique in the pig. Cardiovasc Res 29: 820-826, 1995.
11. Faber MJ, Agnetti G, Bezstarosti K, Lankhuizen IM, Dalinghaus M, Guarnieri C, Caldarera CM, Helbing WA, and Lamers JM. Recent developments in proteomics: implications for the study of cardiac hypertrophy and failure. Cell Biochem Biophys 44: 11-29, 2006.
12. Faber MJ, Dalinghaus M, Lankhuizen IM, Bezstarosti K, Dekkers DH, Duncker DJ, Helbing WA, and Lamers JM. Proteomic changes in the pressure overloaded right ventricle after 6 weeks in young rats: correlations with the degree of hypertrophy. Proteomics 5: 2519-2530, 2005.
13. Glower DD, Spratt JA, Snow ND, Kabas JS, Davis JW, Olsen CO, Tyson GS, Sabiston DC, Jr., and Rankin JS. Linearity of the Frank-Starling relationship in the intact heart: the concept of preload recruitable stroke work. Circulation 71: 994-1009, 1985.
14. Guarracino F, Cariello C, Danella A, Doroni L, Lapolla F, Vullo C, Pasquini C, and Stefani M. Right ventricular failure: physiology and assessment. Minerva Anestesiol 71: 307-312, 2005.
15. Kass DA and Maughan WL. From 'Emax' to pressure-volume relations: a broader view. Circulation 77: 1203-1212, 1988.
16. Kono A, Maughan WL, Sunagawa K, Hamilton K, Sagawa K, and Weisfeldt ML. The use of left ventricular end-ejection pressure and peak pressure in the estimation of the end-systolic pressure-volume relationship. Circulation 70: 1057-1065, 1984.
17. Kuehne T, Saeed M, Gleason K, Turner D, Teitel D, Higgins CB, and Moore P. Effects of pulmonary insufficiency on biventricular function in the developing heart of growing swine. Circulation 108: 2007-2013, 2003.
18. Kuehne T, Yilmaz S, Steendijk P, Moore P, Groenink M, Saaed M, Weber O, Higgins CB, Ewert P, Fleck

E, Nagel E, Schulze-Neick I, and Lange P. Magnetic resonance imaging analysis of right ventricular pressure-volume loops: in vivo validation and clinical application in patients with pulmonary hypertension. Circulation 110: 2010-2016, 2004.

19. Leeuwenburgh BP, Helbing WA, Steendijk P, Schoof PH, and Baan J. Biventricular systolic function in young lambs subject to chronic systemic right ventricular pressure overload. Am J Physiol Heart Circ Physiol 281: H2697-2704, 2001.
20. Leineweber K, Brandt K, Wludyka B, Beilfuss A, Ponicke K, Heinroth-Hoffmann I, and Brodde OE. Ventricular hypertrophy plus neurohumoral activation is necessary to alter the cardiac beta-adrenoceptor system in experimental heart failure. Circ Res 91: 1056-1062, 2002.
21. Leineweber K, Seyfarth T, Abraham G, Gerbershagen HP, Heinroth-Hoffmann I, Ponicke K, and Brodde OE. Cardiac beta-adrenoceptor changes in monocrotaline-treated rats: differences between membrane preparations from whole ventricles and isolated ventricular cardiomyocytes. J Cardiovasc Pharmacol 41: 333-342, 2003.
22. Li HH, Kedar V, Zhang C, McDonough H, Arya R, Wang DZ, and Patterson C. Atrogin-1/muscle atrophy F-box inhibits calcineurin-dependent cardiac hypertrophy by participating in an SCF ubiquitin ligase complex. J Clin Invest 114: 1058-1071, 2004.
23. Li Y, Ha T, Gao X, Kelley J, Williams DL, Browder IW, Kao RL, and Li C. NF-kappaB activation is required for the development of cardiac hypertrophy in vivo. Am J Physiol Heart Circ Physiol 287: H1712-1720, 2004.
24. Little WC. The left ventricular dP/dtmax-end-diastolic volume relation in closed-chest dogs. Circ Res 56: 808-815, 1985.
25. Lopes Cardozo RH, Steendijk P, Baan J, Brouwers HA, De Vroomen M, and Van Bel F. Right ventricular function in respiratory distress syndrome and subsequent partial liquid ventilation. Homeometric autoregulation in the right ventricle of the newborn animal. Am J Respir Crit Care Med 162: 374-379, 2000.
26. Lualdi JC and Goldhaber SZ. Right ventricular dysfunction after acute pulmonary embolism: pathophysiologic factors, detection, and therapeutic implications. Am Heart J 130: 12761282, 1995.
27. Sato T, Shishido T, Kawada T, Miyano H, Miyashita H, Inagaki M, Sugimachi M, and Sunagawa K. ESPVR of in situ rat left ventricle shows contractility-dependent curvilinearity. Am J Physiol 274: H1429-1434, 1998.
28. Steendijk P and Baan J. Comparison of intravenous and pulmonary artery injections of hypertonic saline for the assessment of conductance catheter parallel conductance. Cardiovasc Res 46: 82-89, 2000.
29. Suga H and Sagawa K. Instantaneous pressure-volume relationships and their ratio in the excised, supported canine left ventricle. Circ Res 35: 117-126, 1974.
30. Uemura K, Kawada T, Sugimachi M, Zheng C, Kashihara K, Sato T, and Sunagawa K. A self-calibrating telemetry system for measurement of ventricular pressure volume relations in conscious, freely moving rats. Am J Physiol Heart Circ Physiol 287: H2906-2913, 2004.
31. Vogel M, Derrick G, White PA, Cullen S, Aichner H, Deanfield J, and Redington AN. Systemic ventricular function in patients with transposition of the great arteries after atrial repair: a tissue Doppler and conductance catheter study. J Am Coll Cardiol 43: 100-106, 2004.
32. Vonk-Noordegraaf A, Marcus JT, Holverda S, Roseboom B, and Postmus PE. Early changes of cardiac structure and function in COPD patients with mild hypoxemia. Chest 127:1898-1903, 2005.
33. White PA, Brookes CI, Ravn H, Hjortdal V, Chaturvedi RR, and Redington AN. Validation and utility of novel volume reduction technique for determination of parallel conductance. Am J Physiol Heart Circ Physiol 280: H475-482, 2001.
34. Zaha V, Grohmann J, Gobel H, Geibel A, Beyersdorf F, and Doenst T. Experimental model for heart failure in rats—induction and diagnosis. Thorac Cardiovasc Surg 51: 211-215, 2003.

Chapter 5

Time dependent changes in cytoplasmic proteins of the right ventricle during prolonged pressure overload

Matthijs J. Faber, Michiel Dalinghaus, Inge M. Lankhuizen, Karel Bezstarosti, Adrie J.M. Verhoeven, Dirk J Duncker, Willem A. Helbing, Jos M.J. Lamers

Adapted from:

M.J. Faber et al. J Mol Cell Cardiol. 2007 Aug;43(2):197-209.

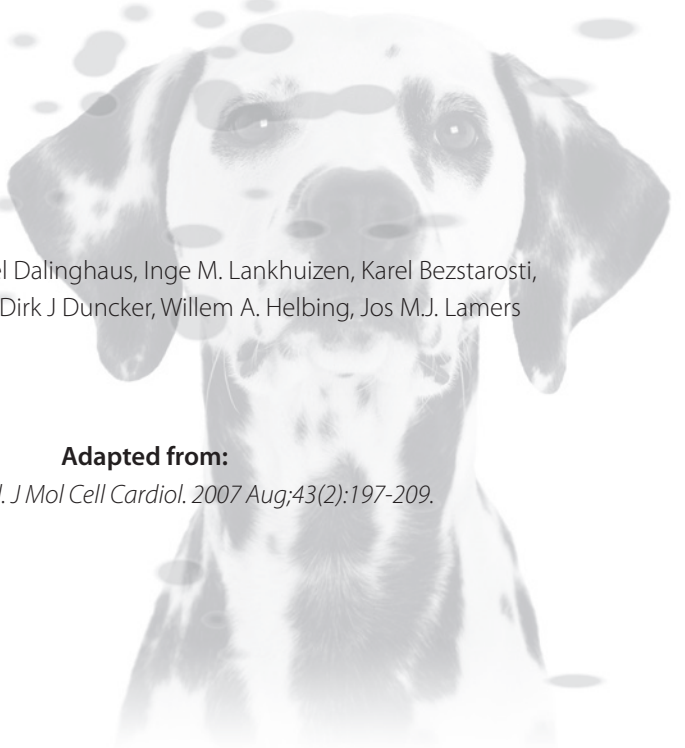

Abstract:

In many forms of congenital heart disease, the right ventricle (RV) is subject to abnormal loading conditions resulting in RV hypertrophy and remodelling. We determined the alterations in RV cytoplasmic proteomic phenotype that occur during prolonged periods of RV pressure overload. We performed a differential proteomic profiling study on RV hypertrophy using an animal model of various durations of pulmonary artery banding (PAB) in parallel with hemodynamic characterization. This hemodynamic evaluation showed that after 6, 12 and 20 weeks of PAB, the RV is in a compensated state of hypertrophy. Overall, the majority of protein changes was metabolism related indicating a shift towards the glycolytic pathway at the expense of β-oxidation in the RV of the PAB animals. The changes in proteins related to the glycolytic pathway, exemplified by enolase and creatine kinase B-chain, tended to precede changes in β-oxidation. In parallel, increases in stress chaperones, exemplified by several phosphorylated HSP-27 species, are present from the 6 week time point, whereas increases in anti-oxidant proteins, exemplified by peroxiredoxin 2 and 6, appears to be restricted to the 12 week time point. The p38 MAPK signal transduction pathway appears not to be activated. Observed protein changes are likely part of a protective mechanism against the development of RV failure.

Introduction

Right ventricular hypertrophy (RV) is an important problem in congenital heart disease (CHD). The ongoing improvement in the treatment of patients with CHD has led to an increased survival but concomitantly has also resulted in increasing numbers of adult patients with residual loading abnormalities, including RV pressure overload [1]. An important determinant of long-term outcome after (surgical) correction for CHD is RV function [2]. The initial adaptation of the RV to abnormal loading conditions includes remodelling and hypertrophy. At this initial stage the function of the RV is still preserved and usually no clinical signs of heart failure are present. This process, referred to as compensated RV hypertrophy, will eventually progress to a point where the RV is unable to counterbalance the increased loading conditions, and will progress towards RV failure. At present not much is known about the underlying protein alterations in the process of compensated RV hypertrophy. We previously demonstrated that differential proteomic profiling is a valuable tool in detecting alterations in protein expression in the hypertrophic rat RV [3]. In that study we demonstrated, after 6 weeks exposure of the RV to pressure overload, altered expression of several metabolic proteins consistent with the well known shift from fatty acid to carbohydrates as a substrate for energy supply. We also found the upregulation of three (post-translationally modified) HSP-27s which are indicative for a compensatory response to altered (oxidative) stress. The aim of the present study was to determine changes in protein composition over time in relation to RV function during prolonged pressure overload. For this purpose we extended the duration of pressure overload to a maximum of 20 weeks in the same rat model of RV hypertrophy caused by pulmonary artery banding (PAB). The various phases of compensated RV hypertrophy were hemodynamically characterized by measuring biventricular pressure-volume loops and proteomic analysis was performed on the RV (6, 12 and 20 weeks) and left ventricle (LV; 20 weeks). The cytoplasmic proteins were separated from the myofilaments and differentially displayed and quantified using two-dimensional gel electrophoresis (2-DE). The proteins that were found to be significantly up-or down-regulated in the hypertrophic RV were subsequently analyzed by mass spectrometry (MS) for identification.

Materials and Methods

All experimental procedures and protocols used in this investigation were reviewed and approved by the institutional animal care and use committee and are in accordance with the National Institutes of Health "Guide for the care and use of laboratory animals" (NIH publication No. 85-23, revised 1996).

Male Wistar rats (190-220 g, Harlan, Zeist, The Netherlands) underwent PAB or sham operation. The animals were housed after the initial operation (ie. sham or PAB), prior to the hemodynamic studies, in groups of 2 or 3 animals, on a 12/12-h light/dark cycle with standard rat chow and water ad libitum. Three different periods of housing were applied: 6, 12 and 20 weeks (resp. n=6 vs. 6, n=8 vs. 9, n=11 vs. 12 (sham vs. PAB)).

Pulmonary artery banding procedure

In order to produce RV pressure overload, the pulmonary artery was banded as described previously [3]. Briefly, after induction of anesthesia (pentobarbital) the rats were intubated and mechanically ventilated. A left thoracotomy was performed and a silk thread was positioned under the pulmonary artery. A suture was tied tightly around an 18 gauge needle that was placed alongside the pulmonary artery. Next, the needle was rapidly removed in order to produce a fixed constricted opening in the lumen equal to the diameter of the needle. The sham animals underwent the same procedure except for the banding of the pulmonary artery.

Hemodynamic measurements

After the housing period of either 6, 12 or 20 weeks, hemodynamic measurements were performed as described previously [4]. The study protocol was the same for both sham and PAB animals. In brief, after induction of anesthesia, the heart was exposed by thoracotomy and pressure- and conductance catheters were inserted into both ventricles to measure ventricular pressures and volumes simultaneously. From these measurements, pressure-volume loops of RV and LV were constructed out of which the following parameters were derived: heart rate, cardiac output, ventricular end-systolic and end-diastolic pressures, dP/dt-max. The end-systolic elastance was used as a parameter of systolic function [4, 5]. At the end of the hemodynamic measurements the animals were killed and the heart was rapidly removed and divided into RV, LV, right atrium, left atrium and septum. Tissues were weighed and stored at -80°C.

Proteomics

The RV tissues of the individual animals were used for proteomics analysis as previously described [3]. In brief, RV tissue was homogenized and subsequently, the homogenate (600 µg) was prefractionated using Triton-X-100 into a cytoplasmic and myofilament fraction. The cytoplasmic fraction was subjected to 2-DE using nonlinear pI strips (pH 3-10, Amersham Biosciences, Little Chalfont, Buckinghamshire, UK) and polyacrylamide gel (SDS-PAGE, 12%). After 2-DE separation the gels were stained with Coomassie Blue and analyzed with PDQUEST (BioRad, Hercules, CA, USA). This analysis leads on the one hand to parts per million (ppm) values as a measure of the staining intensity of

each protein spot relative to the total of the 2-DE gel and on the other hand the fold change of the mean ppm value of a spot due to pressure overload. Significantly up- or downregulated spots as well as several unchanged (landmark) spots were excised, destained and trypsinized prior to protein identification by MALDI-TOF MS (Bruker Daltonics, Billerica, MA, USA) or QTOF MS/MS (Waters, Milford, MA, USA). In addition, for database profiling purposes, several other spots were excised and ultimately identified. The reproducibility of the subfractionation and the 2-DE technique has been shown previously [3]. No technical replicates were used.

Western blotting

Western blotting was used to study the phosphorylation state of HSP-27 at Ser-15 and Ser-86 and to study the p38 MAPK signaling pathway upstream to HSP-27. In brief, proteins were separated by 2D-PAGE (HSP-27) or 1D-PAGE, using 15% gels. The samples were heated for 5 min. at 95º C and 20 µg of protein was applied per sample. The following primary antibodies were used: total HSP-27 (cat. #sc-9012, Santa Cruz Biotechnology, Santa Cruz, Ca, USA) , P-HSP-27 (Ser-15) (cat. #sc-12359-R, Santa Cruz Biotechnology), and P-HSP-27 (Ser86) (cat. #ab17938, Abcam, Cambridge, UK) each 1:1000 diluted, and p38-MAPK 1:4000 diluted (cat. #9212, Cell Signaling Technology, Beverly, MA, USA), p-p38-MAPK (Thr180/Tyr182) 1:2000 diluted (cat. #9211, Cell Signaling Technology). After washing with TBS/Tween, the blots were incubated with 1:5000 (HSP-27s) or 1:2000 (p38 MAPK) diluted goat antirabbit conjugated horseradish peroxidase (Pierce Biotechnology, Rockford, IL, USA)). The results were visualized by recording the ECL signal (Pierce Biotechnology) on film (Hyperfilm™ ECL, Amersham Biosciences) and quantitated with a GS-800 calibrated densitometer (Biorad). The 1D gels were analyzed with QuantityOne software (BioRad).

Phosphopeptide analysis by mass spectrometry

In addition to western blotting, MS was used to study HSP-27 phosphorylation. 2-DE gel plugs were destained and digested overnight with trypsin (Promega, sequencing grade). NanoLC-MS/MS was performed on an Agilent 1100 coupled to an LTQ-Orbitrap mass spectrometer (Thermo Scientific, Waltham, MA, USA), operating in positive mode. Peptide mixtures were trapped on a Jupiter™ C18 reversed phase column (Phenomenex; column dimensions 1.5 cm × 100 µm, packed in-house) at a flow rate of 8 µl/min. Peptide separation was performed on a Reprosil-Pur C18-AQ reversed phase column (Dr Maisch GmbH column dimensions 20 cm × 50 µm, packed in-house) using a linear gradient from 0 to 30% B (A = 0.1 M acetic acid; B = 80% (v/v) acetonitrile, 0.1 M acetic acid) in 70 min and at a constant flow rate of 200 nl/min using a splitter. The column eluent was sprayed directly into the ESI source of the mass spectrometer, which

was operated in the data-dependent mode to automatically switch between MS, MS^2, and MS^3 acquisition. Full MS scans were performed in the Orbitrap and the three most intense ions were fragmented in the linear ion trap by collision induced dissociation. The MS^3 event was triggered upon detection of the neutral loss of phosphoric acid (m/z difference of -98, -49, or -32.7 , for charge states 1^+, 2^+, and 3^+, respectively). MS^2 and MS^3 spectra were searched using the Mascot protein identification software (MatrixScience) against the publicly available NCBRnr database (taxonomy: Rattus) with carbamidomethyl cysteine set as fixed modification and oxidized methionine and phosphorylation (serine, threonine, and tyrosine) set as variable modifications. Searches were done with tryptic specificity allowing two missed cleavages, a precursor mass tolerance of 10 ppm and MS^2 and MS^3 fragment ion tolerance of 0.8 Da.

Statistics

The statistical comparison software within PDQUEST (Mann-Whitney) was used for identification of significantly up-or downregulated spots when comparing sham gels to PAB gels within one time group. The statistical software program SPSS (version 10.1 for Windows, Microsoft) was used to re-evaluate the Mann-Whitney statistics and to calculate exact p-values. Statview (version 5.0, SAS Institute, Cary, NC, USA) software was used to calculate differences in protein expression over time using repeated measures Anova followed by Bonferoni correction. The differences in hemodynamic parameters between the control group and the PAB group at baseline were analyzed using a Student's T-test. A two-sided p-value < 0.05 was considered statistically significant. Data are presented as mean ± SEM.

Results

Degree of hypertrophy

During the banding periods, the rats did not show overt signs of heart failure and/or cyanosis. There were no differences in body mass between sham and PAB animals in each time group. After 6, 12 and 20 weeks of PAB the RV and right atrium mass, relative to body mass, were significantly increased (Table 1).

Table 1: Heart and bodyweight characteristics of the study groups per time point.

		Time group		
		6 wk	**12 wk**	**20 wk**
BW start	sham	212 ± 5	211 ± 6	196 ± 4
	pab	206 ± 9	199 ± 4	190 ± 5
BW end	sham	376 ± 16	435 ± 11	521 ± 19
	pab	374 ± 13	448 ± 8	531 ± 12
RV/BW	sham	0.58 ± 0.02	0.51 ± 0.01	0.46 ± 0.02
	pab	1.03 ± 0.05 *	0.97 ± 0.04 *	0.84 ± 0.02 *
RA/BW	sham	0.13 ± 0.01	0.12 ± 0.01	0.14 ± 0.01
	pab	0.21 ± 0.03 *	0.22 ± 0.02 *	0.24 ± 0.02 *
LV/BW	sham	1.38 ± 0.03	1.34 ± 0.04	1.29 ± 0.04
	pab	1.43 ± 0.05	1.43 ± 0.03	1.32 ± 0.04
LA/BW	sham	0.05 ± 0.00	0.05 ± 0.00	0.05 ± 0.00
	pab	0.05 ± 0.00	0.04 ± 0.01	0.05 ± 0.00
Septum/BW	sham	0.66 ± 0.02	0.63 ± 0.03	0.58 ± 0.02
	pab	0.71 ± 0.03	0.67 ± 0.02	0.61 ± 0.02

Data presented as mean ± SEM. BW = body weight, RV = right ventricle, RA = right atrium, LV = left ventricle, LA = left atrium.

* $p<0.05$ versus corresponding control

Hemodynamics (Table 2)

RV end-systolic pressure in the PAB group was increased to approximately 60% of LV end-systolic pressure in all three time groups. Heart rate decreased in PAB at 12 and 20 weeks and in conjunction, cardiac output tended to be lower in PAB. Parameters of RV contractility, dP/dt-max and end-systolic elastance, were increased in PAB to a similar extent at 6,12, and 20 weeks, indicating preserved systolic RV function. These results in the 12 and 20 week PAB group are similar to our previous results obtained after 6 weeks of PAB and indicate a state of compensated RV hypertrophy up to 20 weeks [4]. In the LV the end-systolic and end-diastolic pressures, dP/dt-max and the end-systolic elastance were similar in both groups.

Table 2: Hemodynamic characterization of the study groups per time point.

		6 wk	12 wk	20 wk
HR	*sham*	310 ± 8	305 ± 7	306 ± 8
	PAB	297 ± 12	283 ± 4*	286 ± 6*
CO	*sham*	51 ± 4	51 ± 3	41 ± 3
	PAB	49 ± 5	38 ± 3*	36 ± 2
SV	*sham*	164 ± 11	168 ± 10	137 ± 10
	PAB	164 ± 13	135 ± 9*	128 ± 6
Right Ventricle				
Pes	*sham*	29 ± 1	29 ± 3	32 ± 3
	PAB	63 ± 8*	57 ± 5*	68 ± 5*
Ped	*sham*	5 ± 1	4 ± 1	6 ± 1
	PAB	7 ± 1	6 ± 2	7 ± 1
dP/dtmax	*sham*	1429 ± 94	1542 ± 68	1261 ± 75
	PAB	3435 ± 359*	2500 ± 214*	2854 ± 136*
Ees	*sham*	0.126 ± 0.034	0.134 ± 0.024	0.168 ± 0.036
	PAB	0.34 ± 0.042*	0.375 ± 0.074*	0.486 ± 0.061*
Left Ventricle				
Pes	*sham*	93 ± 6	112 ± 8	92 ± 4
	PAB	107 ± 7	91 ± 7	92 ± 6
Ped	*sham*	10 ± 2	9 ± 1	8 ± 1
	PAB	10 ± 3	8 ± 1	10 ± 1
dP/dtmax	*sham*	6331 ± 503	5351 ± 488	5008 ± 294
	PAB	5559 ± 795	4542 ± 300	4291 ± 217
Ees	*sham*	0.992 ± 0.255	0.81 ± 0.16	0.921 ± 0.157
	PAB	0.667 ± 0.185	0.886 ± 0.116	0.839 ± 0.105

Values are mean ± SEM. HR=heart rate, CO=cardiac output (mL/min), SV=stroke volume (μL), Pes=end-systolic pressure (mmHg), Ped=end-diastolic pressure (mmHg), dP/dt_{max}=maximum first time derivative of pressure vs. time ($mmHg \cdot s^{-1}$), Ees=end-systolic elastance ($mmHg \cdot \mu L^{-1}$).

* $p<0.05$ versus corresponding control

Differential proteomic profiles over time

From all the sham and PAB 2-DE gels in all time groups, approximately 350 spots were matched. Spots that were differentially regulated and spots that were used for efficient matching of the gels were selected for further analysis (179 spots). From these 179 spots, 119 spots were identified by MS (66%). As a supplement we include a representative 2-DE map of the 179 spots, including a table with the protein names and identification details (Fig 1S and Table 1S).

After comparing and analyzing the 2-DE gels across all time groups and within each time group, we identified a group of 72 spots that were present and matched in all gels of each time group and were different in intensity in at least one group. Of these 72 spots, 12 were significantly up- or down regulated in all three time groups, 22 spots in only two time groups, and 38 in only one time group (Table 3). No spots unique to either sham or PAB rats or time group were observed. The protein alterations were grossly divided into four categories: (1) metabolic proteins, (2) stress- and antioxidant proteins, (3) miscellaneous (including signal transduction and apoptosis related proteins), and (4) not identified. A comprehensive list of RV (and LV) proteins changes, together with identification details and degree of up- or downregulation is provided in Table 3. More technical MS and identification data is provided in Table 1 of the supplement.

Metabolic proteins (Table 3; Figure 1)

About 50-60% of the spots that changed throughout all time groups, were identified as metabolic proteins.

From table 3 we can conclude that already in the early phase of compensated RV hypertrophy (6 weeks), there is a general upregulation of proteins involved in the glycolytic pathway. The enzymes related to the mitochondrial oxidation tended to change mainly at 12 and 20 weeks of RV hypertrophy. In contrast to the carbohydrate metabolism, proteins related to fatty acid oxidation and amino acid metabolism were all downregulated. Overall, these changes suggest a shift towards carbohydrates as energy fuel for the hypertrophied RV at the expense of fatty acids and amino acids.

Among the 12 spots that were significantly altered in all time groups (RV), 7 spots were related to metabolism (Table 3). Two of these spots were identified as β-enolase, spot #17 and #20, and were downregulated in all three time groups ($p<0.05$). The α-enolase (spot #79) did not change at 6 and 12 weeks but was only significantly increased after 20 weeks of PAB (increase 30%, $p<0.05$) (Figure 1). The extent of downregulation of both β-enolase spots tended to increase gradually with the duration of pressure overload (Figure 1; Table 3).Two other spots were identified as creatine kinase B-chain (#9 and #45), which were both increased throughout the study.

Table 3: List of differentially displayed right- and left ventricular cytoplasmic proteins over time.

Suppl. Map	#	Protein ID	RV 6	RV 12	RV 20	ratio (max/min) RV 6 weeks		RV 12 weeks		RV 20 weeks		LV 20 weeks		NCBI Acc.nr.	Theoretical Mr	Theoretical pI
		Metabolic Proteins														
		"Anaerobic" metabolism - glycolysis														
@ 2c	82	Aldose reductase				1,01 ± 0,06	up	1,12 ± 0,07	up	1,16 ± 0.05*	up	1,08 ± 0,06	down	gi|1168407	35643	6,28
@ 1c	79	Alpha Enolase				1,23 ± 0,14	up	1,13 ± 0,13	up	1,30 ± 0.13*	up	1,03 ± 0,06	down	gi|56757324	46955	6,16
@ 1c	17	Beta-enolase				1,99 ± 0.51*	down	2,16 ± 0.32*	down	2,70 ± 0.31*	down	1,06 ± 0,10	down	gi|119346	46800	7.74[a]
@ 1d	20	Beta-enolase				2,01 ± 0.31*	down	2,02 ± 0.29*	down	2,81 ± 0.24*	down	1,11 ± 0,14	down	gi|119346	46800	7,74
@ 2b	9	Creatine-kinase chain B				1,70 ± 0.31*	up	2,36 ± 0.29*	up	1,98 ± 0.20*	up	1,02 ± 0,12	up	gi|125296	42685	5,33
@ 2b	45	Creatine-kinase chain B				2,80 ± 0.75*	up	3,49 ± 0.53*	up	2,29 ± 0.28*	up	1,19 ± 0,21	up	gi|125296	42685	5,33
@ 2d	90	Creatine-kinase M-chain				1,04 ± 0,26	up	1,37 ± 0,25	down	1,45 ± 0.15*	down	1,05 ± 0,08	down	gi|125308	42992	6,58
@ 2b	6	L-lactate dehydrogenase B-chain				1,23 ± 0.08*	up	1,39 ± 0.21*	up	1,00 ± 0,08	up	1,02 ± 0,11	down	gi|1170739	36458	5,70
@ 1c	53	Phosphoglucomutase				1,28 ± 0,29	up	1,62 ± 0.23*	up	1,66 ± 0.14*	up	1,03 ± 0,07	down	gi|730311	61519	6,32
@ 3c	16	Phosphoglycerate mutase B-chain				1,56 ± 0.13*	up	1,35 ± 0,33	up	1,17 ± 0,10	down	1,28 ± 0,23	up	gi|112128	28814	6,67
@ 1d	21	Pyruvate kinase, isozymes M1/M2				1,55 ± 0.22*	up	1,35 ± 0,33	up	2,24 ± 0.35*	up	1,09 ± 0,09	up	gi|125601	57613	7,40
@ 3d	61	Triosephosphate isomerase				1,12 ± 0,07	down	1,20 ± 0.08*	up	1,23 ± 0.09*	up	1,00 ± 0,08	up	gi|1351280	26773	6.51[a]
		Oxidative metabolism - PDH and TCA cycle														
@ 1d	171	3-oxoacid CoA-transferase				1,37 ± 0.20*	up	1,45 ± 0.16*	up	1,52 ± 0.20*	up	1,29 ± 0,20	up	gi|2492999	56371	8.47[a]
@ 2b	44	ATP-specific succinyl-CoA synthetase subunit beta				1,38 ± 0,27	down	1,43 ± 0.23*	down	1,98 ± 0.22*	down	1,16 ± 0,19	down	gi|52788305	50424	6.57[a]
@ 1c	54	Dihydrolipoamide dehydrogenase				1,12 ± 0,12	up	1,26 ± 0.12*	up	1,29 ± 0.06*	up	1,01 ± 0,07	down	gi|81885266	54004	7.96[a]
@ 1b	47	Dihydrolipoamide S-acetyltransferase				1,22 ± 0,20	down	1,81 ± 0.25*	up	1,28 ± 0,15	up	1,21 ± 0,22	down	gi|220838	57645	5.53[b]
@ 1b	158	Dihydrolipoamide S-acetyltransferase				1,03 ± 0,10	down	1,29 ± 0.11*	up	1,22 ± 0.10*	up	1,06 ± 0,13	down	gi|266685	58727	5.7[b]
@ 2d	118	Fumarate hydratase, mit prec.				1,14 ± 0,23	down	1,23 ± 0,14	down	1,36 ± 0.10*	up	1,17 ± 0,09	up	gi|120605	54429	9.06[a]
@ 1d	172	Fumarate hydratase, mit prec.				1,04 ± 0,18	up	1,14 ± 0,08	down	1,25 ± 0.11*	up	1,07 ± 0,07	up	gi|120605	54429	9.06[a]
@ 2b	43	NAD+ specific isocitrate dehydrogenase. a-subunit				1,16 ± 0,11	down	1,28 ± 0.12*	up	1,12 ± 0,10	up	1,11 ± 0,16	down	gi|68565369	40044	6.47[a]
@ 1c	174	Succinate dehydrogenase				1,14 ± 0.09*	up	1,05 ± 0,18	down	1,15 ± 0,19	down	1,22 ± 0.09*	down	gi|52782765	71570	6,75
@ 1c	176	Succinate dehydrogenase				1,07 ± 0,16	up	1,03 ± 0,11	up	1,06 ± 0,13	down	1,27 ± 0.12*	down	gi|52782765	71570	6,75
		Oxidative metabolism - electron transport														
@ 1c	164	ATP synthase alpha chain				1,19 ± 0,10	up	1,20 ± 0,20	up	1,32 ± 0.09*	up	1,04 ± 0,09	down	gi|83300587	59717	9.22[a]
@ 1c	178	Dihydrolipoamide dehydrogenase				1,26 ± 0,21	up	1,16 ± 0,16	up	1,11 ± 0,08	up	1,14 ± 0.06*	down	gi|81885266	54004	7.96[a]
@ 1c	165	Electron-transferring-flavoprotein dehydrogenase				1,07 ± 0,11	down	1,17 ± 0,21	down	1,19 ± 0.08*	down	1,03 ± 0,09	down	gi|52000614	68155	7,33
@ 2c	83	NADH dehydrogenase 1 alpha-subcomplex 10				1,02 ± 0,30	up	1,08 ± 0,31	down	1,25 ± 0,33	down	1,39 ± 0.18*	down	gi|81885291	31681	5.44[a,b]
@ 3d	179	Ubiquinol-cytochrome c reductase				1,00 ± 0,32	up	1,14 ± 0,31	down	1,29 ± 0,23	down	1,57 ± 0.28*	down	gi|52001457	29427	9.04[a,b]
		Oxidative metabolism - fatty acid oxidation														
@ 3c	15	2-enolyl CoA hydratase (A/B chain)				1,45 ± 0.18*	down	1,12 ± 0,16	down	1,18 ± 0,10	down	1,25 ± 0.13*	down	gi|2392292	28141	6,41
@ 2c	84	Acyl-CoA dehydrogenase				1,01 ± 0,13	up	1,07 ± 0,13	down	1,20 ± 0.10*	down	1,10 ± 0,10	down	gi|1168286	44737	8.47[a]
@ 2c	163	Acyl-CoA dehydrogenase				1,09 ± 0,16	up	1,06 ± 0,12	down	1,36 ± 0.12*	down	1,12 ± 0,11	down	gi|1168286	44737	8.47[a]
@ 2c	167	Acyl-CoA thioesterase, mit prec.				1,26 ± 0,19	down	1,24 ± 0,16	down	1,68 ± 0.12*	down	1,03 ± 0,08	down	gi|6166586	49670	7.68[a]
@ 4d	169	Fatty acid binding protein				- - - -		1,21 ± 0,14	down	1,96 ± 0.18*	down	- - - -		gi|2494405	14568	7.93[a]
@ 2c	77	Peroxisomal dienoyl CoA isomerase				1,43 ± 0,19	down	1,46 ± 0.20*	down	2,10 ± 0.15*	down	1,07 ± 0,06	down	gi|6015047	36148	8.13[a]
		Oxidative metabolism - amino acid metabolism														
@ 2b	156	3-methyl-2-oxobutanoate dehydrogenase alpha-chain				1,29 ± 0,24	down	1,12 ± 0,12	down	1,66 ± 0.20*	down	1,22 ± 0,29	down	gi|129032	50133	7.68[a]
@2d	170	Aspartate transaminase				1,15 ± 0,11	down	1,14 ± 0,11	down	1,24 ± 0.08*	down	1,06 ± 0,08	up	gi|91997	46399	6,73
@ 2d	19	Bcat2 protein				1,73 ± 0.31*	down	1,52 ± 0.22*	down	1,49 ± 0.12*	down	1,04 ± 0,14	up	gi|81885326	44138	8.62[a]
@ 2d	64	Bcat2 protein				1,46 ± 0.21*	down	1,68 ± 0.27*	down	1,45 ± 0.12*	down	1,01 ± 0,12	up	gi|81885326	44138	8.62[a]
@ 1d	168	Glutamate dehydrogenase 1				1,03 ± 0,17	up	1,20 ± 0,15	down	1,21 ± 0.09*	down	1,12 ± 0,10	down	gi|92090591	61377	8.05[a]
@ 1c	144	Propionyl-CoA carboxylase				1,45 ± 0.10*	down	1,24 ± 0,13	down	1,17 ± 0,12	down	1,04 ± 0,07	down	gi|129686	58589	7,19
@ 1c	49	Propionyl-CoA carboxylase alpha-chain prec.				1,13 ± 0,14	down	1,30 ± 0,15	down	1,23 ± 0.08*	down	1,05 ± 0,12	down	gi|92654	78190	6,33

		Oxidative metabolism - other substrates																	
@ 1c	159	Aldehyde dehydrogenase		1,16 ± 0,16	up	1,25 ± 0,19	up	1,60 ± 0.12*	up	1,02 ± 0,09	down	gi|81892738	55566	6,69
@ 2d	111	Carbonyl reductase [NADPH] 1		1,15 ± 0,07	down	1,12 ± 0,11	down	1,19 ± 0.05*	down	1,10 ± 0,07	down	gi|1352258	30428	8.21[a]
		Stress- and antioxidant Proteins																	
		Stress - chaperone																	
@ 1a	154	78 kDa glucose-regulated protein precursor		1,06 ± 0,15	down	1,12 ± 0,15	up	1,43 ± 0.10*	up	1,04 ± 0,08	down	gi|121574	72302	5,07
@ 3d	23	Alpha-B-crystallin		1,45 ± 0.14*	up	1,34 ± 0.13*	up	1,43 ± 0.08*	up	1,04 ± 0,06	up	gi|117388	19945	6,67
@ 1a	153	Calreticulin prec		1,00 ± 0,24	up	1,38 ± 0,22	up	1,64 ± 0.17*	up	1,11 ± 0,13	up	gi|117505	47966	4,33
@ 1b	10	dnaK-type molecular chaperone hsc-73		1,51 ± 0.20*	up	1,49 ± 0.17*	up	1,46 ± 0.25*	up	1,09 ± 0,12	down	gi|51702275	71112	5,37
@ 1b	155	dnaK-type molecular chaperone hsc-73		1,02 ± 0,17	up	1,21 ± 0,16	up	1,37 ± 0.13*	up	1,15 ± 0,14	down	gi|347019	70884	5,43
@ 3b	5	HSP-27		1,92 ± 0.41*	up	3,05 ± 0.80*	up	3,93 ± 0.62*	up	1,06 ± 0,14	down	gi|1170367	22808	6.12[a]
@ 3b	11	HSP-27		3,52 ± 1.28*	up	3,05 ± 1,10	up	4,24 ± 0.79*	up	1,08 ± 0,22	down	gi|1170367	22808	6,12
@ 3b	39	HSP-27		1,66 ± 0.20*	up	2,77 ± 0.87*	up	2,86 ± 0.41*	up	1,30 ± 0,28	down	gi|1170367	22808	6.12[a]
@1c	160	HSP-75		1,37 ± 0,20	down	1,35 ± 0,19	down	1,38 ± 0.10*	down	1,02 ± 0,13	up	gi|81910345	80411	6,56
@ 1b	142	Protein disulphide isomerase A3, prec.		1,29 ± 0.13*	up	1,36 ± 0,27	up	1,36 ± 0.14*	up	1,12 ± 0,12	down	gi|1352384	56588	5,88
@ 1c	143	T-complex protein 1, gamma subunit		1,22 ± 0.10*	up	1,11 ± 0,16	up	1,15 ± 0,09	up	1,09 ± 0,20	up	gi|549059	60450	6,23
		Antioxidant																	
@ 1d	57	Catalase		1,16 ± 0,21	down	1,67 ± 0.27*	down	1,15 ± 0,33	down	1,07 ± 0,12	down	gi|115707	59931	7,15
@ 3c	52	Gluthathione peroxidase		1,31 ± 0,19	up	1,94 ± 0.31*	up	1,67 ± 0.14*	up	1,07 ± 0,11	down	gi|121668	22486	7.66[a]
@ 3b	38	Peroxiredoxin 2		1,05 ± 0,23	up	1,53 ± 0.19*	up	1,02 ± 0,12	up	1,21 ± 0,12	up	gi|549132	21941	5,34
@ 3a	151	Peroxiredoxin 2		1,01 ± 0,08	down	1,09 ± 0,11	down	1,39 ± 0.17*	down	1,18 ± 0.11*	down	gi|549132	21770	5,34
@ 4d	59	Peroxiredoxin 5, mit prec		1,28 ± 0,18	down	1,24 ± 0.10*	up	1,09 ± 0,11	down	1,02 ± 0,13	up	gi|20138819	22507	8.94[a,b]
@ 3b	30	Peroxiredoxin 6		1,51 ± 0.29*	up	1,50 ± 0.23*	up	1,20 ± 0,15	up	1,00 ± 0,12	up	gi|5902791	24672	5,65
@ 3c	41	Peroxiredoxin 6		1,06 ± 0,18	down	1,84 ± 0.31*	down	1,76 ± 0.28*	down	1,41 ± 0.17*	down	gi|5902791	24729	5,65
@ 1c	51	Selenium binding protein 2		1,39 ± 0.12*	down	1,39 ± 0.18*	down	1,47 ± 0.09*	down	1,15 ± 0,10	down	gi|81879451	52498	6,10
		Miscellaneous Proteins																	
		Signal transduction - apoptosis - cell growth																	
@ 2a	36	14-3-3 protein epsilon		1,15 ± 0,27	down	2,19 ± 0.63*	up	1,15 ± 0,15	up	1,02 ± 0,18	down	gi|61216932	29326	4,63
@ 3a	33	14-3-3 protein gamma		1,41 ± 0,32	up	1,72 ± 0.30*	up	1,56 ± 0.14*	up	1,10 ± 0,14	up	gi|48428718	28325	4,80
@ 1c	145	Adenylyl cyclase-associated protein		1,29 ± 0.12*	up	1,18 ± 0,33	up	1,63 ± 0.32*	up	1,35 ± 0,24	up	gi|1705586	52879	6,69
@ 2c	56	Annexin I = Lipocortin I		1,54 ± 0.24*	up	1,60 ± 0,30	up	1,46 ± 0.17*	up	1,11 ± 0,18	down	gi|113947	39016	7,14
@ 2a	34	Annexin V = Lipocortin V		1,20 ± 0,35	up	2,44 ± 0.44*	up	1,90 ± 0.20*	up	1,10 ± 0,19	up	gi|4033508	35648	4,93
@ 2a	35	Annexin V = Lipocortin V		1,08 ± 0,18	down	1,17 ± 0.08*	down	1,45 ± 0.17*	down	1,07 ± 0,12	down	gi|4033508	35533	4,93
@ 1c	161	Dihydropyrimidinase related protein-2		1,16 ± 0,18	up	1,12 ± 0,21	up	1,33 ± 0.10*	up	1,01 ± 0,09	down	gi|1351260	62239	5,95
@ 1b	157	Guanine deaminase		1,05 ± 0,28	up	1,99 ± 0,67	up	2,00 ± 0.27*	up	1,05 ± 0,11	up	gi|81868670	50869	5,48
@ 4c	50	Histidine triad nucleotide-binding protein 1		- - - -		1,78 ± 0.40*	up	1,28 ± 0,17	up	- - - -		gi|2495231	13751	6,39
@ 4d	60	Nucleoside diphosphate kinase		1,24 ± 0,28	up	1,81 ± 0.26*	up	1,99 ± 0.18*	up	1,04 ± 0,10	up	gi|127984	17386	6,92
@ 4d	55	Nucleoside diphosphate kinase		1,00 ± 0,09	down	1,33 ± 0.07*	up	1,11 ± 0,06	up	1,01 ± 0,07	up	gi|127984	17386	6,92
		Miscellanous																	
@ 3a	37	MLC-1		1,16 ± 0,11	up	1,35 ± 0.13*	up	1,06 ± 0,09	up	1,06 ± 0,07	up	gi|127151	22125	5,03
@ 1a	4	Tubulin B-chain		1,60 ± 0.31*	up	1,14 ± 0,28	up	1,66 ± 0.32*	up	1,07 ± 0,20	down	gi|92930	49905	4,79
		No identification																	
@ 2d	62	no ID		1,04 ± 0,08	down	1,36 ± 0.13*	down	1,38 ± 0.10*	down	1,23 ± 0,23	down	n/a	n/a	n/a
@ 1b	173	no ID		1,90 ± 0.57*	down	1,65 ± 0,53	down	2,19 ± 0.49*	down	1,59 ± 0.39*	down	n/a	n/a	n/a
@ 1c	175	no ID		1,13 ± 0,12	up	1,16 ± 0,19	up	1,04 ± 0,11	down	1,29 ± 0.11*	down	n/a	n/a	n/a
@ 2c	177	no ID		1,02 ± 0,35	down	1,20 ± 0,33	down	1,12 ± 0,31	down	1,70 ± 0.28*	down	n/a	n/a	n/a

Protein identification was achieved using MALDI-TOF-MS and/or QTOF MS/MS in combination with the Mascot search engine (www.matrixscience.com) using de NCBI database search (species: rattus). The Mann-Whitney test was used for identification of significantly up-or downregulated spots when comparing sham gels to PAB gels within one time group. The color coding refers to significant upregulation (red) or downregulation (blue) of RV proteins at the various time points. The first and second column respectively refer to the position and number of the proteins on the database 2-DE map that can be found in the online supplement. * $p<0.05$ for the change in intensity (PAB/sham)

[a] Observed pI different from theoretical pI (Δ pI > 0.5). [b] Observed Mw different from theoretical Mw (Δ Mw > 10%)

Figure 1: Composition of the heterodimeric enolase in relation to the duration of RV pressure overload.

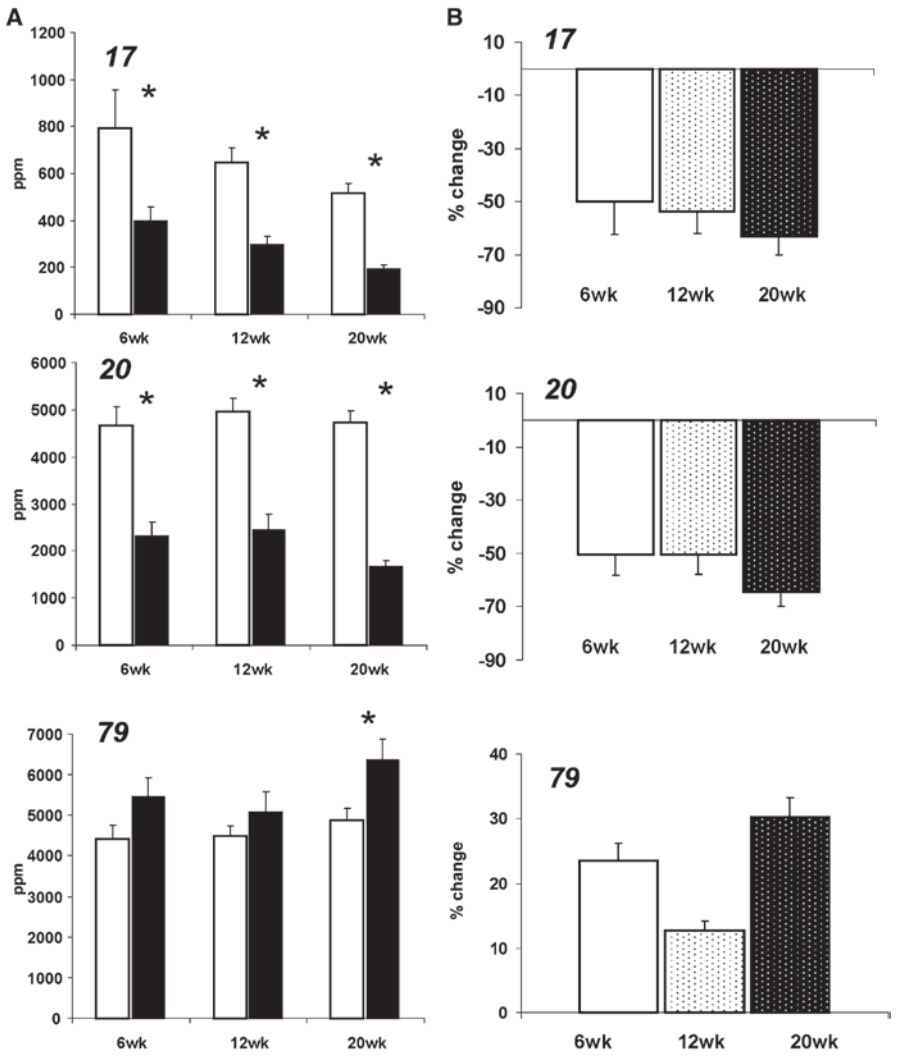

Panel A shows the relative intensity as expressed by a ppm value for both beta-enolase isoforms (spot #17 and #20) and alpha-enolase (spot #79) over time. The relative change (%) over time, is given in panel B.
* p<0.05 sham vs. PAB

Stress- and antioxidant proteins

Phosphorylated HSP-27s and p38 MAPK pathway activation

Five of the 12 spots that were significantly altered in the RV throughout the 3 time groups were stress related, including HSP-27, Hsc-73, α-B-Crystallin (CryAB) and selenium binding protein 2 (Table 3). HSP-27 was identified in three spots that were all

upregulated in all time groups. Interestingly, the extent of upregulation of HSP-27 spots #5 and #39 in the RV increased further with the duration of pressure overload (Figure 2 C). Previously we demonstrated by MS, as well as immunoblotting, that spot #5 and #39 contain HSP-27s that are phosphorylated at least at Ser-15 [3]. Here, we show that spot #5 and #39 also contain HSP-27s phosphorylated at Ser-86 using 2-DE immunoblotting. Analysis by LTQ-Orbitrap also demonstrated the presence of peptides phosphorylated at Ser-15 and Ser-86 (Figure 2 Supplement). In order to examine whether the increase of phosphorylated HSP-27 species in the pressure overloaded RV is caused by the activation of p38-MAPK, we measured the phosphorylation degree of p38-MAPK by immunoblotting. After 6 weeks of PAB, the signals of the p38-MAPK antibody and its phosphorylated form were similar in the RV of sham and PAB animals. When PAB was extended to 20 weeks, both the p38-MAPK and the phosphorylated antibody signal were decreased in the RV of PAB animals. As expected, the levels of p38-MAPK and its phosphorylated form were not altered in the LV in all time groups (Figure 3).

Figure 2: Differential expression of HSP-27 during the progression of RV hypertrophy in rats.

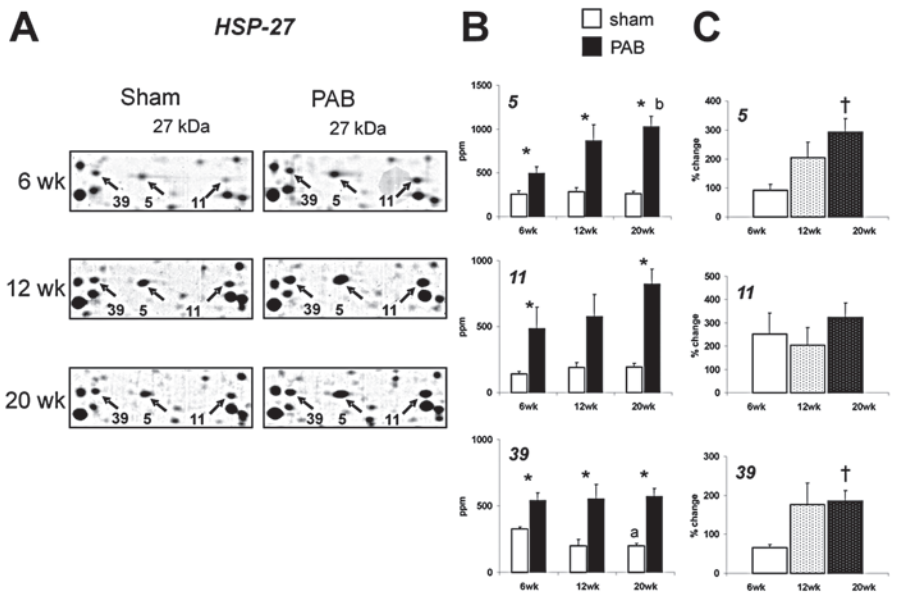

Panel A shows the three separate HSP-27 spots (number 5, 11 and 39 respectively) on a section of a 2DE gel for both sham and PAB rats. Panel B shows the relative intensity as expressed by a ppm value for each spot number over time. The relative change (%) over time, is given in panel C for each spot number.

* p<0.05 sham vs. PAB

† p<0.05 vs. 6wk group

[a] p<0.05 sham 6 wk vs. sham 20 wk

[b] p=0.068 pab 6 wk vs. pab 20 wk

Figure 3: Western blot analysis of p38-MAPK activity

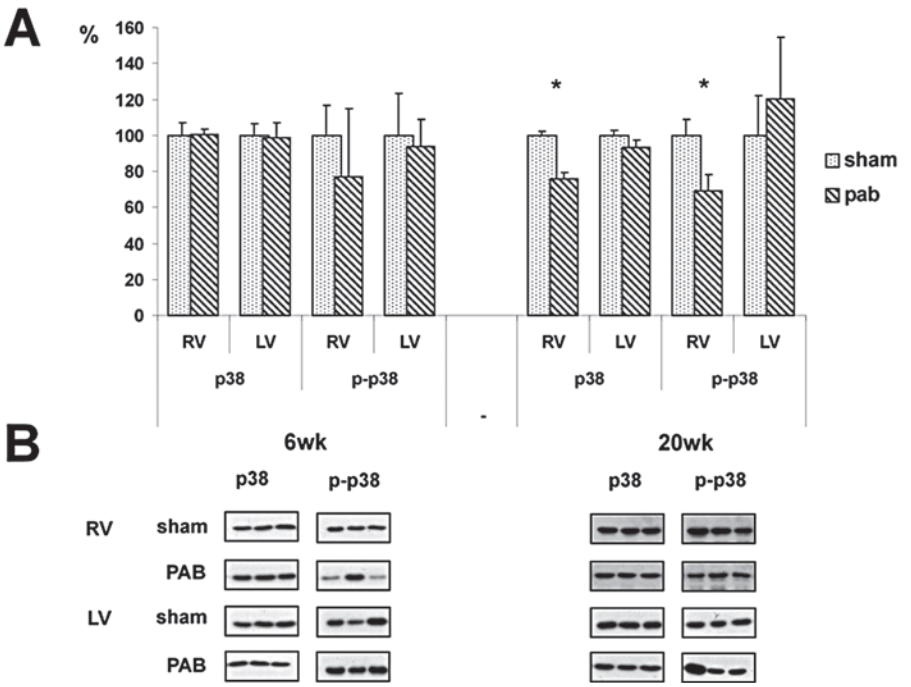

Panel A shows bar graphs representing the differences in expression of p38-MAPK and p-p38 MAPK. The changes in the PAB animals were related to the sham levels which were set at 100%. Representative 1D western blots are given in panel B.
* p<0.05 versus corresponding control

Alterations in the peroxiredoxin system

The subtypes Prx-2, Prx-5, and Prx-6 were significantly altered in the hypertrophic RV. Prx-5 was only upregulated in the 12 wk group (spot #59, Table 3).The subtypes Prx-2 and Prx-6 each were present in two distinct spots, one acidic and one basic. Their alterations over time are shown in Figure 4. The acidic Prx-2 decreased over time by 28% (spot #151, $p<0.05$) while the basic Prx-2 increased at 12 weeks by 53% (spot #38, $p<0.05$). Conversely, the acidic Prx-6 increased by approximately 50% at 6 and 12 weeks to return no near baseline levels at 20 weeks of PAB (spot #30, $p<0.05$). The basic Prx-6 decreased by approximately 45% after 12 and 20 weeks (spot # 41, $p<0.05$).

Figure 4: Differential expression of Prx-2 and Prx-6 during the progression of RV hypertrophy in rats.

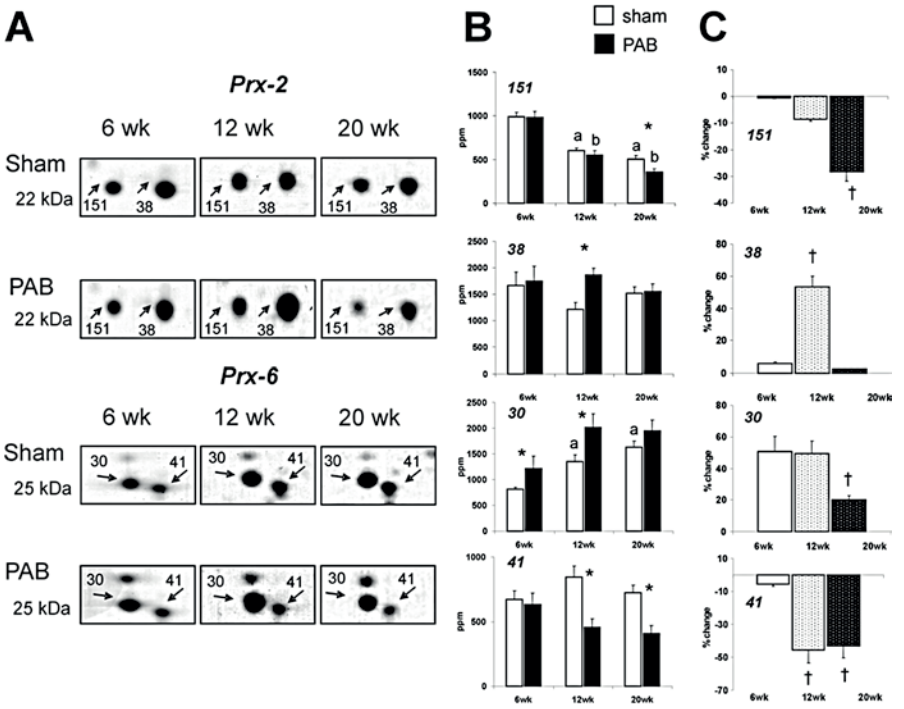

Panel A shows the Prx-2 and Prx-6 spots on a section of a 2DE gel for both sham and PAB rats. Spot #151 (Prx-2) and #30 (Prx-6) are the acidic, oxidized forms. Panel B shows the relative intensity as expressed by a ppm value for each spot over time. The relative change (%) over time, is given in panel C.

* p<0.05 sham vs. PAB

† p<0.05 vs. 6wk group

[a] p<0.05 sham 6 wk vs. sham 12 and 20 wk

[b] p=0.068 pab 6 wk vs. pab 12 and 20 wk

Miscellaneous and not identified proteins

Besides the large and diverse group of metabolism-, stress-, and antioxidant proteins, also changes in other functional groups can be found. In our model, several proteins related to signal transduction, apoptosis and cell growth were found to be altered in response to prolonged RV pressure overload. The majority of these protein changes occur after 12 weeks of PAB (Table 3). Further studies are required to determine the relevance and functional consequences of these changes.

Left ventricular protein changes

In addition to studying protein changes in the compensated RV, we also compared the proteome of the LV between control and PAB animals. Since invasive hemodynamic evaluation showed that the LV of sham and PAB animals behaved functionally similar over time, we chose to study the cytoplasmic proteome of the LV only at the 20 wk time point. The same proteomic analysis as described above was applied to the LV. In contrast to the 56 protein spots that were altered in the RV after 20 weeks of PAB, only 11 spots were significantly up- or downregulated in the LV of PAB animals at 20 wks. From these spots, 6 were only significantly changed in the LV (4 metabolic proteins, 2 no identification) while 5 spots were also found to be changed in the RV (2 metabolic, 2 stress proteins, 1 no identification) for one or two of the time points (Table 3).

Discussion

Here, we present a comprehensive study of the changes in cytoplasmic protein expression after a prolonged period of pressure overload of the RV in a hemodynamically well-characterized rat model. We demonstrated that the majority of the protein expression changes that occur in the cytoplasmic fraction are related to metabolism and (oxidative) stress. In general, we observed protein changes consistent with a shift towards the glycolytic pathway at the expense of the β-oxidation in the RV of the PAB animals. More specifically, the heterodimeric enolase shifted towards a more fetal phenotype as the pressure overload progressed. Furthermore, stress-related proteins such as phosphorylated HSP-27 were upregulated in the hypertrophic RV and were also dependent on the duration of pressure overload. The fact that we also found changes in Prx species, in parallel to HSP-27 alterations, can be seen as an indication of oxidative stress. In all protein categories, the number of affected proteins increases with the duration of PAB. In contrast, the number of affected antioxidant proteins is increased at 12 weeks and decreases again at 20 weeks of PAB. This may suggest that the RV increasingly adapts to the oxidative and/or mechanical stress during prolonged periods of increased workload. We attempted to correlate the temporal changes in protein expression with several hemodynamic parameters but no consistent correlations were found (data not shown).

Metabolic protein changes

The majority of the proteins found to be changing during compensated RV hypertrophy are related to metabolism (Table 3). Overall, there appears to be a shift in metabolism towards carbohydrates as energy fuel for the hypertrophied RV at the expense of fatty acids and amino acids. These observations are in accordance with results obtained in

various models of LV hypertrophy, and may be the result of increased energy demand associated with increased workload [6-12]. In this extended study we observed similar qualitative changes (Table 3). In addition, we found that proteins related to the fatty acid and amino acid metabolism are all downregulated in the RV of PAB animals. Interestingly, the changes in the fatty acid and amino acid oxidation proteins tend to occur after 12 and 20 weeks of PAB, whereas several alterations in proteins related to the glycolytic pathway already occur after 6 weeks.

Another metabolic shift was found in the α and β enolase proteins. The glycolytic enzyme enolase is composed as a homodimer or heterodimer from α, β, and γ subunits with the β subunit being specifically expressed in striated muscle and the γ subunit in nervous tissue [13-16]. In our study, we found two different spots most likely containing β_1 and β_2 -enolase (Table 3) which were both decreased in all three time groups which is in accordance with results obtained in studies on LV hypertrophy [17, 18]. The α-enolase was not significantly changed after 6 and 12 weeks of PAB but increased significantly by 30% in the 20wk group ($p<0.05$). This suggests that the heterodimeric composition of enolase is changing with the duration of RV pressure overload (Figure 1). Heterodimeric enolase composed of relatively more α monomers has been linked to a better association of the complex of glycolytic enzymes with the contractile machinery of hypertrophic cardiac myocytes [18].

Interestingly, the alterations in the LV after 20 weeks of PAB were seen in metabolic proteins. This is in accordance with observations by Schott et al. [19]. In this study, using a monocrotaline model of RV hypertrophy, changes in the LV proteome were analyzed. An upregulation of proteins relevant for energy metabolism was observed. Since changes in the biomechanical load on the LV were not observed, the changes in LV protein expression may be attributed to changes in neurohumoral stimulation [19].

Stress and antioxidant proteins

From table 3 we can appreciate that several stress proteins are upregulated in the early phase of compensated RV hypertrophy (6 weeks of PAB). The antioxidant proteins tend to be activated after 12 weeks of PAB and these levels subsequently decrease at 20 weeks. Two of the stress proteins that were significantly altered in this study were HSP-27 and Hsc-73 (synonym: heat shock 70 kDa protein 8). Both HSP-27 and Hsc-73 were present in multiple spots suggesting post-translational modifications (Table 3). Indeed, for HSP-27 which is likely to have multiple phosphorylation sites, we have previously demonstrated that two out of three spots are at least phosphorylated at the Ser-15 residue [3]. Here, we show that these two spots contain HSP-27 also phosphorylated at Ser-86. This pattern of cardiac HSP-27 phosphorylation induced by stress has also been shown by Cullingford et al. [20]. One interpretation may be that the most acidic spot

(#39) contains HSP-27 that is double phosphorylated at Ser-15 and Ser-86, and that the middle spot (#5) contains HSP-27 phosphorylated at either Ser-15 or Ser-86, whereas the most basic spot (#11) contains HSP-27 that is not phosphorylated at these serine residues. Alternatively, another modification may discriminate between spots #5 and #39. A possible PTM would be an additional phosphorylation of Ser-78. Unfortunately, the peptide containing P-Ser-78 could not be found in the MS spectra but this does not preclude its presence. A specific antibody is not available.

One of the signalling pathways for HSP-27 phosphorylation is known to be the MAPK pathway. We concordantly studied this pathway using antibodies against p38-MAPK and its phosphorylated form (Figure 3) [21, 22]. At 6 wks of PAB the RV levels of p38-MAPK and p-p38-MAPK were similar in both groups. At 20 wks of PAB these levels were not increased in the RV of PAB animals, but even slightly decreased. In a recent study by Buermans et al. it was shown in a monocrotaline model of RV hypertrophy that compensated RV hypertrophy is characterized by an absence of p38-MAPK activation whereas RV failure was associated with an upregulation of p38-MAPK [23]. This is in close agreement with the observation that in our model of compensated RV hypertrophy there is no activation of the p38-MAPK pathway.

Our data suggests that throughout the hypertrophic response the transcription of total HSP-27 is progressively increasing and that the fraction of phosphorylated HSP-27 is also progressively increasing. In our study we did not identify the upstream pathway for HSP-27 phosphorylation. However, the protein kinase C-δ pathway is known to play a role in the development of pathological hypertrophy and has been shown to be activated both in RV and LV pressure overload [24-26]. Furthermore, protein kinase C-δ has been shown to phosphorylate HSP-27 proteins independent of the p38-MAPK pathway [27]. Therefore, it could be speculated that the protein kinase C-δ pathway plays a role in the development of compensated RV hypertrophy and that the p38-MAPK pathway is involved in the transition to decompensated hypertrophy.

In addition to the increased levels of the HSP-27 and Hsc-73 we also observed a consistent increased expression of CryAB over time (approximately +40%, $p<0.05$, table 3 #23). Both the HSPs and the CryAB have an important function in the protein quality control machinery. It has recently been shown that the formation of desmin aggregates, induced by adenoviral mutant-desmin overexpression, impairs the proteolytic function of the ubiquitin proteasome system (UPS) in cardiomyocytes [28]. Both HSP-27 and CryAB have a critical role in preventing the impairment of the proteolytic function of the UPS [28, 29]. The protein quality control and the selective protein degradation through the UPS are critical in the cardiac response to stress [30-32]. Interestingly, the reversibility of the aggregation formation and the subsequent UPS impairment offers new opportunities for pharmacological treatment with the

protein quality control components as a major target. In our model the RV has to deal with increased stress for prolonged period of time. One could speculate that this leads to a delicate process of increased protein synthesis and degradation in order to adapt to the increased loading conditions. This increased protein handling is also subject to the protein quality control machinery, resulting in increased synthesis of chaperone proteins. In our model the RV is still capable of dealing with these increased loading conditions, suggesting that the protein quality control is still functional. More in depth studies are needed to investigate the change in levels or post translational modifications of the numerous chaperones in the transition phase to RV failure.

Several antioxidant proteins, like peroxiredoxin (Prx) and gluthathion peroxidase (glut-Prx), were also significantly changed during the time course of RV hypertrophy which is indicative for increased oxidative stress caused by chronic pressure overload. In a recent study by Cullingford et al., cardiomyocytes exposed to H_2O_2 showed marked changes in the family of Prx proteins in relation to alterations in HSPs and CryAB. Among those changes, an increase in the acidic Prx-2 and Prx-6 and a decrease in the basic component was found. [20]. In our in vivo study, the Prx subtypes Prx-2 and Prx-6 were both significantly changed in the hypertrophic RV. Each of these subtypes were present in 2 distinct spots. In contrast to the in vitro study by Cullingford, we did not observe an acidic shift for the Prx-2. The basic Prx-2 increased with 53% ($p<0.05$) at 12 wks and the acidic Prx-2 decreased over time to -28% at 20 wks ($p<0.05$). However, similar to the in vitro study, we did observe an acidic shift for the Prx-6 subtype. The acidic Prx-6 increased at 6 and 12 wks with approximately 50% ($p<0.05$) returning to near normal levels at 20 wks. The basic Prx-6 decreased with approximately 45% ($p<0.05$) at 12 and 20 wks (Figure 4) This acidic shift is potentially the result of "over-oxidation" to Cys-SO_2H/Cys-SO_3H [33-36]. It has been speculated that this oxidation of Prx proteins, which is reversible, is a mechanism to conserve these proteins and may play an important role in long-term defense against oxidative stress [20, 37]. Our data suggests that the oxidation of Prx-6 reaches its maximum at 12 weeks. Despite the numerous types of Prx, these proteins are nevertheless non-redundant. In a recent study by Nagy et al, it was demonstrated that hearts of Prx-6 -/- mice were more susceptible to ischemic-reperfusion damage [38]. Another Prx protein, glut-Prx, is known to be upregulated in the hypertrophied myocardium [39]. Glut-Prx, in conjunction with HSP's, is suggested to have a protective effect on the contractile properties of the heart [40]. In our study, the fractional change in glut-Prx levels initially increases from 31 to 94% (6 to 12 wks) and subsequently decreases to 67% in 20 wks in the RV of PAB animals (Table 3, #52). Again, this suggests that the protective effects of glut-Prx reaches its maximum at 12 weeks of PAB. Future studies should include

the assessment of the levels of glut-Prx in a more advanced phase of compensated hypertrophy, and eventually in hearts that progress to heart failure.

Limitations

It should be noted that our study addresses only the changes in abundant cytoplasmic proteins. This is due to the cell fractionation and the proteomics techniques used, mainly the choice of IPG strips (pI 3-10) and detection by Coomassie blue staining [41, 42]. Further studies are needed to look at, possible related, protein changes with a lower abundance, for instance by using 2-DE zoom gels and more sensitive protein stains, or proteins that are present in other cell fractions, such as membrane proteins, cytoskeletal and myofibrillar proteins.

Conclusions

In conclusion, we present for the first time, a longitudinal proteomic analysis of hemodynamically characterized compensated RV hypertrophy. We have identified and grouped several protein changes that occur over time and show similar shifts in energy metabolism similar to what has been described for LV hypertrophy [6-12]. We have shown that the expression of (phosphorylated) HSP-27s increases with the duration of PAB despite the absence of an increase in expression of p38-MAPK. Since the RV is still in a state of compensated hypertrophy, the results of the differentially displayed proteome suggests that the increase in stress chaperone and antioxidant proteins is involved in the protection of the RV against development of failure. Further research is needed to study the exact role of these low molecular weight proteins in protein quality control machinery as well as the potential role of these proteins as therapeutic target.

The supplementary data (Figure 1S and 2S and Table1S) associated with this chapter can be found under the Appendix at the end of this chapter

References

1. Wren C, O'Sullivan JJ. Survival with congenital heart disease and need for follow up in adult life. Heart 2001; 85: 438-43.
2. Bolger AP, Coats AJ, Gatzoulis MA. Congenital heart disease: the original heart failure syndrome. Eur Heart J 2003; 24: 970-6.
3. Faber MJ, Dalinghaus M, Lankhuizen IM, Bezstarosti K, Dekkers DH, Duncker DJ et al. Proteomic changes in the pressure overloaded right ventricle after 6 weeks in young rats: correlations with the degree of hypertrophy. Proteomics 2005; 5: 2519-30.
4. Faber MJ, Dalinghaus M, Lankhuizen IM, Steendijk P, Hop WC, Schoemaker RG et al. Right- and left ventricular function after chronic pulmonary artery banding in rats assessed with biventricular pressure-volume loops. Am J Physiol Heart Circ Physiol 2006; 291:H1580-6
5. Suga H, Sagawa K. Instantaneous pressure-volume relationships and their ratio in the excised, supported canine left ventricle. Circ Res 1974; 35: 117-26.
6. Buttrick PM, Kaplan M, Leinwand LA, Scheuer J. Alterations in gene expression in the rat heart after chronic pathological and physiological loads. J Mol Cell Cardiol 1994; 26: 61-7.
7. Schwartz K, Boheler KR, de la Bastie D, Lompre AM, Mercadier JJ. Switches in cardiac muscle gene expression as a result of pressure and volume overload. Am J Physiol 1992; 262: R364-9.
8. Feldman AM, Weinberg EO, Ray PE, Lorell BH. Selective changes in cardiac gene expression during compensated hypertrophy and the transition to cardiac decompensation in rats with chronic aortic banding. Circ Res 1993; 73: 184-92.
9. Charlemagne D, Maixent JM, Preteseille M, Lelievre LG. Ouabain binding sites and (Na+,K+)-ATPase activity in rat cardiac hypertrophy. Expression of the neonatal forms. J Biol Chem 1986; 261: 185-9.
10. Bishop SP, Altschuld RA. Increased glycolytic metabolism in cardiac hypertrophy and congestive failure. Am J Physiol 1970; 218: 153-9.
11. Taegtmeyer H, Overturf ML. Effects of moderate hypertension on cardiac function and metabolism in the rabbit. Hypertension 1988; 11: 416-26.
12. Massie BM, Schaefer S, Garcia J, McKirnan MD, Schwartz GG, Wisneski JA et al. Myocardial high-energy phosphate and substrate metabolism in swine with moderate left ventricular hypertrophy. Circulation 1995; 91: 1814-23.
13. Craig SP, Day IN, Thompson RJ, Craig IW. Localisation of neurone-specific enolase (ENO2) to 12p13. Cytogenet Cell Genet 1990; 54: 71-3.
14. Feo S, Oliva D, Barbieri G, Xu WM, Fried M, Giallongo A. The gene for the muscle-specific enolase is on the short arm of human chromosome 17. Genomics 1990; 6: 192-4.
15. Keller A, Ott MO, Lamande N, Lucas M, Gros F, Buckingham M et al. Activation of the gene encoding the glycolytic enzyme beta-enolase during early myogenesis precedes an increased expression during fetal muscle development. Mech Dev 1992; 38: 41-54.
16. Fletcher L, Rider CC, Taylor CB, Adamson ED, Luke BM, Graham CF. Enolase isoenzymes as markers of differentiation in teratocarcinoma cells and normal tissues of mouse. Dev Biol 1978; 65: 462-75.
17. Merkulova T, Lucas M, Jabet C, Lamande N, Rouzeau JD, Gros F et al. Biochemical characterization of the mouse muscle-specific enolase: developmental changes in electrophoretic variants and selective binding to other proteins. Biochem J 1997; 323 (Pt 3): 791-800.
18. Keller A, Rouzeau JD, Farhadian F, Wisnewsky C, Marotte F, Lamande N et al. Differential expression of alpha- and beta-enolase genes during rat heart development and hypertrophy. Am J Physiol 1995; 269: H1843-51.

19. Schott P, Singer SS, Kogler H, Neddermeier D, Leineweber K, Brodde OE et al. Pressure overload and neurohumoral activation differentially affect the myocardial proteome. Proteomics 2005; 5: 1372-81.
20. Cullingford TE, Wait R, Clerk A, Sugden PH. Effects of oxidative stress on the cardiac myocyte proteome: modifications to peroxiredoxins and small heat shock proteins. J Mol Cell Cardiol 2006; 40: 157-72.
21. Guay J, Lambert H, Gingras-Breton G, Lavoie JN, Huot J, Landry J. Regulation of actin filament dynamics by p38 map kinase-mediated phosphorylation of heat shock protein 27. J Cell Sci 1997; 110 (Pt 3): 357-68.
22. Kacimi R, Chentoufi J, Honbo N, Long CS, Karliner JS. Hypoxia differentially regulates stress proteins in cultured cardiomyocytes: role of the p38 stress-activated kinase signaling cascade, and relation to cytoprotection. Cardiovasc Res 2000; 46: 139-50.
23. Buermans HP, Redout EM, Schiel AE, Musters RJ, Zuidwijk M, Eijk PP et al. Microarray analysis reveals pivotal divergent mRNA expression profiles early in the development of either compensated ventricular hypertrophy or heart failure. Physiol Genomics 2005; 21: 314-23.
24. Sabri A, Steinberg SF. Protein kinase C isoform-selective signals that lead to cardiac hypertrophy and the progression of heart failure. Mol Cell Biochem 2003; 251: 97-101.
25. Braun MU, LaRosee P, Schon S, Borst MM, Strasser RH. Differential regulation of cardiac protein kinase C isozyme expression after aortic banding in rat. Cardiovasc Res 2002; 56: 52-63.
26. Braun MU, Szalai P, Strasser RH, Borst MM. Right ventricular hypertrophy and apoptosis after pulmonary artery banding: regulation of PKC isozymes. Cardiovasc Res 2003; 59: 658-67.
27. Maizels ET, Peters CA, Kline M, Cutler RE, Jr., Shanmugam M, Hunzicker-Dunn M. Heat-shock protein-25/27 phosphorylation by the delta isoform of protein kinase C. Biochem J 1998; 332 (Pt 3): 703-12.
28. Liu J, Tang M, Mestril R, Wang X. Aberrant protein aggregation is essential for a mutant desmin to impair the proteolytic function of the ubiquitin-proteasome system in cardiomyocytes. J Mol Cell Cardiol 2006; 40: 451-4.
29. Chavez Zobel AT, Loranger A, Marceau N, Theriault JR, Lambert H, Landry J. Distinct chaperone mechanisms can delay the formation of aggresomes by the myopathy-causing R120G alphaB-crystallin mutant. Hum Mol Genet 2003; 12: 1609-20.
30. Connell P, Ballinger CA, Jiang J, Wu Y, Thompson LJ, Hohfeld J et al. The co-chaperone CHIP regulates protein triage decisions mediated by heat-shock proteins. Nat Cell Biol 2001; 3: 93-6.
31. Zhang C, Xu Z, He XR, Michael LH, Patterson C. CHIP, a cochaperone/ubiquitin ligase that regulates protein quality control, is required for maximal cardioprotection after myocardial infarction in mice. Am J Physiol Heart Circ Physiol 2005; 288: H2836-42.
32. Patterson C. Search and destroy: the role of protein quality control in maintaining cardiac function. J Mol Cell Cardiol 2006; 40: 438-41.
33. Wagner E, Luche S, Penna L, Chevallet M, Van Dorsselaer A, Leize-Wagner E et al. A method for detection of overoxidation of cysteines: peroxiredoxins are oxidized in vivo at the active-site cysteine during oxidative stress. Biochem J 2002; 366: 777-85.
34. Rabilloud T, Heller M, Gasnier F, Luche S, Rey C, Aebersold R et al. Proteomics analysis of cellular response to oxidative stress. Evidence for in vivo overoxidation of peroxiredoxins at their active site. J Biol Chem 2002; 277: 19396-401.
35. Mitsumoto A, Takanezawa Y, Okawa K, Iwamatsu A, Nakagawa Y. Variants of peroxiredoxins expression in response to hydroperoxide stress. Free Radic Biol Med 2001; 30: 625-35.
36. Baty JW, Hampton MB, Winterbourn CC. Proteomic detection of hydrogen peroxide-sensitive thiol proteins in Jurkat cells. Biochem J 2005; 389: 785-95.

37. Rhee SG, Chae HZ, Kim K. Peroxiredoxins: a historical overview and speculative preview of novel mechanisms and emerging concepts in cell signaling. Free Radic Biol Med 2005; 38: 1543-52.
38. Nagy N, Malik G, Fisher AB, Das DK. Targeted Disruption of Peroxiredoxin 6 Gene Renders the Heart Vulnerable to Ischemia Reperfusion Injury. Am J Physiol Heart Circ Physiol 2006;291:H2636-40
39. Kirshenbaum LA, Hill M, Singal PK. Endogenous antioxidants in isolated hypertrophied cardiac myocytes and hypoxia-reoxygenation injury. J Mol Cell Cardiol 1995; 27: 263-72.
40. Wagner KD, Gmehling G, Gunther J, Stauss HM, Mydlak K, Theres H et al. Contractile function of rat myocardium is less susceptible to hypoxia/reoxygenation after acute infarction. Mol Cell Biochem 2001; 228: 49-55.
41. McGregor E, Dunn MJ. Proteomics of heart disease. Hum Mol Genet 2003; 12 Spec No 2: R135-44.
42. Faber MJ, Agnetti G, Bezstarosti K, Lankhuizen IM, Dalinghaus M, Guarnieri C et al. Recent developments in proteomics: implications for the study of cardiac hypertrophy and failure. Cell Biochem Biophys 2006; 44: 11-29.

Appendix

Figure 1S

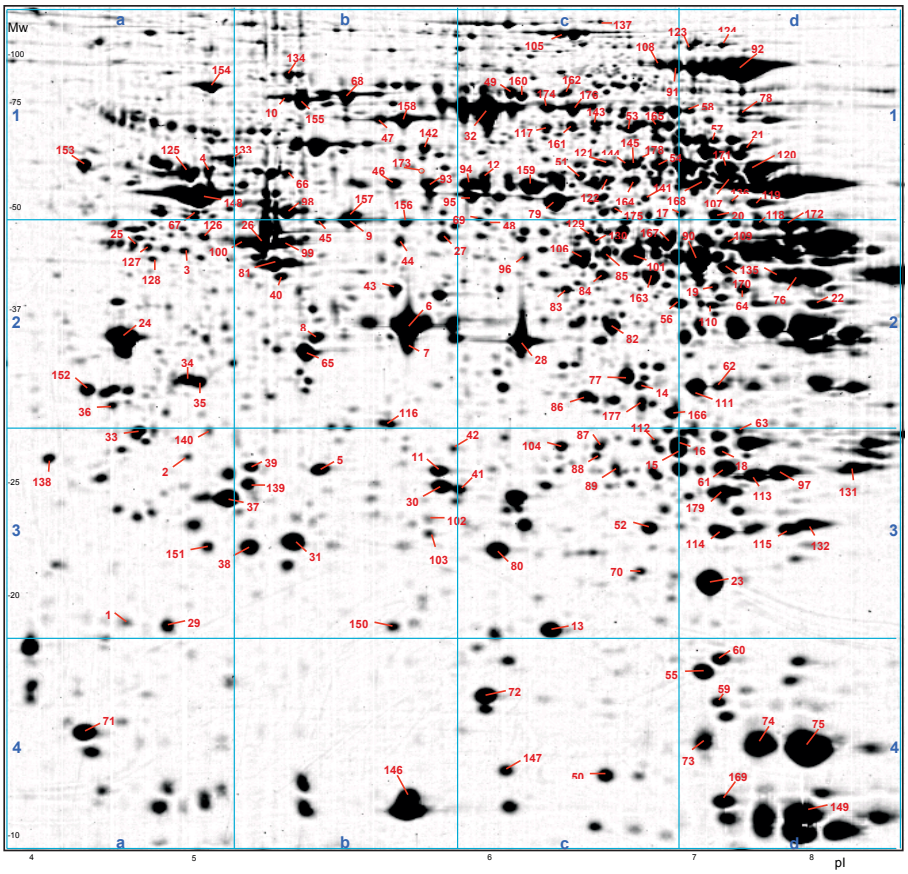

Representative 2-DE map showing 179 spots that were differentially regulated and used for efficient matching of the gels. The numbers correspond with the numbers used in Table 1S.

Figure 2S

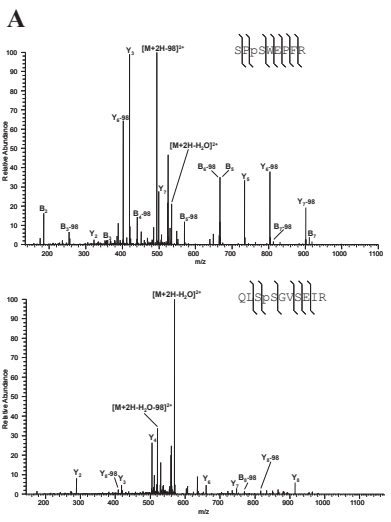

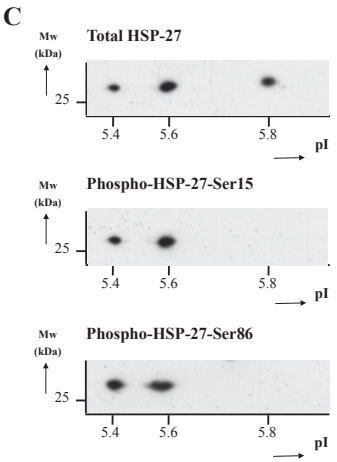

Panel A: LTQ-Orbitrap spectra of HSP-27 peptides. Top spectrum is showing a phosphorylation at Ser-15 residue. The bottom spectrum is showing a phosphorylation at Ser-86.

Panel B shows the amino acid sequence of HSP-27 with the phosphopeptides in bold.

Panel C shows 2-DE westernblots using specific antibodies against total HSP-27 (top), HSP-27 phosphorylated at Ser-15 (middle), and HSP-27 phosphorylated at Ser-86 (bottom).

B

Sequence coverage of HSP-27

1 MTERRVPFSL LR**SPSWEPFR** DWYPAHSRLF DQAFGVPRFP DEWSQWFSSA
51 GWPGYVRPLP AATAEGPAAV TLARPFSRAL NR**QLSSGVSE IR**QTADRWRV
101 SLDVNHFAPE ELTVKTKEGV VEITGKHEER QDEHGYISRC FTRKYTLPPG
151 VDPTLVSSSL SPEGTLTVEA PLPKAVTQSA EITIPVTFEA RAQIGGPESE
201 QSGAK

Table 1S

	Location			ratio (max/min)													NCBI	Theoretical		MOW-SE
#	Map	Protein ID	Cat.	6 wk RV *			12 wk RV *			20 wk RV *			20 wk LV *				Acc.nr.	Mr	pI	score
1	@ 3a	no ID	No ID	2,0	down	$	-	-	-	-	-	-	-	-	-		n/a	n/a	n/a	n/a
2	@ 3a	no ID	No ID	1,8	up	ns	-	-	-	-	-	-	-	-	-		n/a	n/a	n/a	n/a
3	@ 2a	no ID	No ID	2,4	up	$	-	-	-	-	-	-	-	-	-		n/a	n/a	n/a	n/a
4	@ 1a	Tubulin B-chain	Misc.	1,6	up	$	1,1	up	ns	1,7	up	$	1,1	down	ns		gi|92930	49905	4,79	
5	@ 3b	HSP-27	Stress	1,9	up	$	3,0	up	$	3,9	up	$	1,1	down	ns		gi|1170367	22808	6,12	
6	@ 2b	L-lactate dehydrogenase B-chain	Metab.	1,2	up	$	1,4	up	$	1,0	up	ns	1,0	down	ns		gi|1170739	36458	5,70	
7	@ 2b	L-lactate dehydrogenase B-chain	Metab.	1,9	up	$	-	-	ns	1,2	up	ns	1,2	up	ns		gi|1170739	36458	5,70	
8	@ 2b	no ID	No ID	1,9	up	ns	-	-	-	-	-	-	-	-	-		n/a	n/a	n/a	n/a
9	@ 2b	Creatine-kinase chain B	Metab.	1,7	up	$	2,4	up	$	2,0	up	$	1,0	up	ns		gi|125296	42685	5,33	
10	@ 1b	dnaK-type molecular chaperone hsc-73	Stress	1,5	up	$	1,5	up	$	1,5	up	$	1,1	down	ns		gi|51702275	71112	5,37	
11	@ 3b	HSP-27	Stress	3,5	up	$	3,1	up	ns	4,2	up	$	1,1	down	ns		gi|1170367	22808	6,12	
12	@ 1c	no ID	No ID	2,2	up	$	-	-	-	2,1	up	$	-	-	-		n/a	n/a	n/a	n/a
13	@ 3c	P20 protein = HSP-beta-6	Stress	2,5	up	ns	-	-	-	-	-	-	1,1	down	ns		gi|6016271	17494	6,05	
14	@ 2c	no ID	No ID	1,6	down	$	-	-	-	-	-	-	-	-	-		n/a	n/a	n/a	n/a
15	@ 3c	2-enolyl CoA hydratase (A/B chain)	Metab.	1,5	down	$	1,1	down	ns	1,2	down	ns	1,3	down	$		gi|2392292	28141	6,41	
16	@ 3c	Phosphoglycerate mutase B-chain	Metab.	1,6	up	$	1,4	up	ns	1,2	down	ns	1,3	up	ns		gi|112128	28814	6,67	
17	@ 1c	Enolase 3 = Beta-enolase	Metab.	2,0	down	$	2,2	down	$	2,7	down	$	1,1	down	ns		gi|119346	46800	7,74	
18	@ 3d	no ID	No ID	1,9	down	$	-	-	-	-	-	-	-	-	-		n/a	n/a	n/a	n/a
19	@ 2d	Bcat2 protein	Misc.	1,7	down	$	1,5	down	$	1,5	down	$	1,0	up	ns		gi|81885326	44138	8,62	
20	@ 1d	Enolase 3 = Beta-enolase	Metab.	2,0	down	$	2,0	down	$	2,8	down	$	1,1	down	ns		gi|119346	46800	7,74	
21	@ 1d	Pyruvate kinase, isozymes M1/M2	Metab.	1,5	up	$	1,3	up	ns	2,2	up	$	1,1	up	ns		gi|125601	57613	7,40	
22	@ 2d	no ID	No ID	2,1	up	$	-	-	-	-	-	-	-	-	-		n/a	n/a	n/a	n/a
23	@ 3d	Alpha-B-crystallin	Stress	1,5	up	$	1,3	up	$	1,4	up	$	1,0	up	ns		gi|117388	19945	6,67	
24	@ 2a	Tropomyosin 1 alpha chain	Misc.	-	-	-	-	-	-	-	-	-	1,5	down	ns		gi|92090646	32693	4,69	
25	@ 2a	no ID		-	-	-	-	-	-	-	-	-	-	-	-		n/a	n/a	n/a	n/a
26	@ 2b	Actin alpha		-	-	-	-	-	-	-	-	-	-	-	-		gi|54036697	41992	5,30	
27	@ 2b	no ID	No ID	-	-	-	-	-	-	1,7	down	$	-	-	-		n/a	n/a	n/a	n/a
28	@ 2c	Malate dehydrogenase (cytosolic)		-	-	-	-	-	-	-	-	-	-	-	-		gi|81861572	36460	6,16	
29	@ 3a	MLC-2		-	-	-	-	-	-	-	-	-	-	-	-		gi|127167	18737	4,86	
30	@ 3b	Peroxiredoxin 6 = Anti-oxidant protein 2	Stress	1,5	up	$	1,5	up	$	1,2	up	ns	1,0	up	ns		gi|5902791	24672	5,65	
31	@ 3b	no ID		-	-	-	-	-	-	-	-	-	-	-	-		n/a	n/a	n/a	n/a
32	@ 1c	Serum Albumin (precursor)		-	-	-	-	-	-	-	-	-	-	-	-		gi|113580	68674	6,09	
33	@ 3a	14-3-3 protein gamma	Misc.	1,4	up	ns	1,7	up	$	1,6	up	$	1,1	up	ns		gi|48428718	28325	4,80	
34	@ 2a	Annexin V = Lipocortin V	Misc.	1,2	up	ns	2,4	up	$	1,9	up	$	1,1	up	ns		gi|4033508	35648	4,93	
35	@ 2a	Annexin V = Lipocortin V	Misc.	1,1	down	ns	1,2	down	$	1,4	down	$	1,1	down	ns		gi|4033508	35533	4,93	
36	@ 2a	14-3-3 protein epsilon	Misc.	1,2	down	ns	2,2	up	$	1,1	up	ns	1,0	down	ns		gi|61216932	29326	4,63	
37	@ 3a	MLC-1	Misc.	1,2	up	ns	1,3	up	$	1,1	up	ns	1,1	up	ns		gi|127151	22125	5,03	
38	@ 3b	Peroxiredoxin 2 = Thioredoxin peroxidase	Stress	1,1	up	ns	1,5	up	$	1,0	up	ns	1,2	up	ns		gi|549132	21941	5,34	
39	@ 3b	HSP-27	Stress	1,7	up	$	2,8	up	$	2,9	up	$	1,3	down	ns		gi|1170367	22808	6,12	
40	@ 2b	no ID	No ID	-	-	-	1,7	up	$	-	-	-	-	-	-		n/a	n/a	n/a	n/a
41	@ 3c	Peroxiredoxin 6 = Anti-oxidant protein 2	Stress	1,1	down	ns	1,8	down	$	1,8	down	$	1,4	down	$		gi|5902791	24729	5,65	
42	@ 3b	no ID	No ID	-	-	-	-	-	$	2,4	down	$	1,3	down	-		n/a	n/a	n/a	n/a
43	@ 2b	NAD+ specific isocitrate dehydrogenase. a-subunit	Metab.	1,2	down	ns	1,3	up	$	1,1	up	ns	1,1	down	ns		gi|68565369	40044	6,47	
44	@ 2b	ATP-specific succinyl-CoA synthetase subunit beta	Metab.	1,4	down	ns	1,4	down	$	2,0	down	$	1,2	down	ns		gi|52788305	50424	6,57	
45	@ 2b	Creatine-kinase chain B	Metab.	2,8	up	$	3,5	up	$	2,3	up	$	1,2	up	ns		gi|125296	42685	5,33	
46	@ 1b	no ID	No ID	-	-	-	1,4	up	$	-	-	-	-	-	-		n/a	n/a	n/a	n/a

% seq.	Matched		Mann-Whitney*			Parts per million (ppm) values ± SEM															
cover-age	peptides	06R	12R	20R	20L	sham 06 RV		pab 06 RV		sham 12 RV		pab 12 RV		sham 20 RV		pab 20 RV		sham 20 LV		pab 20 LV	
n/a	n/a	$	-	-	-	587	38	288	58	-	-	-	-	-	-	-	-	-	-	-	-
n/a	n/a	ns	-	-	-	183	55	325	29	-	-	-	-	-	-	-	-	-	-	-	-
n/a	n/a	$	-	-	-	214	39	512	90	-	-	-	-	-	-	-	-	-	-	-	-
		$	ns	$	ns	652	90	1046	145	459	41	524	120	517	75	860	108	183	23	171	24
		$	$	$	ns	258	41	497	71	285	45	867	182	261	28	1025	121	495	52	466	35
		$	$	ns	ns	12867	663	15796	618	11189	1301	15597	1573	27656	1311	27720	1915	28290	1938	27756	2284
		$	ns	ns	ns	591	89	1095	108	-	-	-	-	1379	151	1613	423	1617	129	1931	238
n/a	n/a	ns	-	-	-	267	66	512	87	-	-	-	-	-	-	-	-	-	-	-	-
		$	$	$	ns	1018	92	1733	269	1337	127	3150	251	1829	152	3616	196	2375	220	2426	155
		$	$	$	ns	338	32	511	47	395	28	587	50	417	61	608	51	521	40	479	36
		$	ns	$	ns	138	21	486	161	188	41	575	166	194	25	823	112	453	63	420	61
n/a	n/a	$	-	$	-	489	66	1068	130	-	-	-	-	537	60	1117	99	-	-	-	-
		ns	-	-	ns	512	106	1267	371	-	-	-	-	-	-	-	-	840	118	734	130
n/a	n/a	$	-	-	-	640	61	396	58	-	-	-	-	-	-	-	-	-	-	-	-
		$	ns	ns	$	2720	295	1873	111	3776	131	3357	451	2694	138	2289	149	3667	229	2924	250
		$	ns	ns	ns	1582	70	2468	181	1145	178	1551	291	2628	175	2249	132	1607	161	2065	313
		$	$	$	ns	793	164	398	58	646	64	299	33	518	40	192	16	427	27	405	29
n/a	n/a	$	-	-	-	701	65	371	99	-	-	-	-	-	-	-	-	-	-	-	-
		$	$	$	ns	619	84	358	41	569	64	374	34	496	26	333	20	433	39	451	48
		$	$	$	ns	4664	400	2317	300	4955	289	2451	324	4725	256	1680	111	4102	224	3683	400
		$	ns	$	ns	358	44	555	38	250	52	338	46	141	18	316	29	205	14	223	11
n/a	n/a	$	-	-	-	539	95	1109	160	-	-	-	-	-	-	-	-	-	-	-	-
		$	$	$	ns	8111	417	11784	988	10974	376	14749	1392	12912	557	18406	640	13943	393	14439	799
		-	-	-	ns	-	-	-	-	-	-	-	-	-	-	-	-	7176	708	4809	577
n/a	n/a	-	-	-	-	-	-	-	-	-	-	-	-	-	-	-	-	-	-	-	-
		-	-	-	-	-	-	-	-	-	-	-	-	-	-	-	-	-	-	-	-
n/a	n/a	-	-	$	-	-	-	-	-	-	-	-	-	1433	138	861	91	-	-	-	-
		-	-	-	-	-	-	-	-	-	-	-	-	-	-	-	-	-	-	-	-
		-	-	-	-	-	-	-	-	-	-	-	-	-	-	-	-	-	-	-	-
		$	$	ns	ns	814	42	1227	224	1353	124	2023	251	1628	117	1957	198	2008	134	2009	206
n/a	n/a	-	-	-	-	-	-	-	-	-	-	-	-	-	-	-	-	-	-	-	-
		-	-	-	-	-	-	-	-	-	-	-	-	-	-	-	-	-	-	-	-
		ns	$	$	ns	939	198	1325	110	306	29	526	75	292	15	455	32	360	38	396	26
		ns	$	$	ns	753	96	906	238	379	44	925	126	541	45	1025	69	517	69	569	60
		ns	$	$	ns	1427	109	1326	194	1186	57	1015	44	1105	82	764	73	1033	69	964	83
		ns	$	ns	ns	460	58	398	77	158	25	347	84	311	29	357	32	259	28	253	36
		ns	$	ns	ns	3107	280	3608	119	3182	208	4284	311	3702	155	3931	308	3488	173	3698	180
		ns	$	ns	ns	1664	249	1754	270	1217	130	1866	122	1521	117	1559	137	1369	107	1651	91
		$	$	$	ns	326	18	541	56	200	49	553	107	200	19	571	61	247	41	190	26
n/a	n/a	-	$	-	-	-	-	-	-	308	29	522	19	-	-	-	-	-	-	-	-
		ns	$	$	$	672	64	633	88	845	87	459	62	724	60	410	57	1085	78	768	75
n/a	n/a	-	$	$	-	-	-	-	-	-	-	-	-	494	34	207	34	356	33	285	38
		ns	$	ns	ns	502	30	434	33	684	44	878	59	1110	65	1239	82	1202	110	1078	123
		ns	$	$	ns	451	78	326	28	572	79	400	31	839	48	423	41	748	75	645	82
		$	$	$	ns	75	10	210	50	75	7	263	32	102	8	232	21	138	18	165	19
n/a	n/a	-	$	-	-	-	-	-	-	611	35	856	62	-	-	-	-	-	-	-	-

47	@ 1b	Dihydrolipoamide S-acetyltransferase (fragment)	Metab.	1,2	down	ns	1,8	up	$	1,3	up	ns	1,2	down	ns	gi|220838	57645	5,53		
48	@ 2c	no ID	No ID	1,2	down	ns	1,5	down	ns	1,2	down	ns	1,1	up	ns	n/a	n/a	n/a	n/a	
49	@ 1c	Propionyl-CoA carboxylase alpha-chain prec.	Metab.	1,1	down	ns	1,3	down	ns	1,2	down	$	1,0	down	ns	gi|92654	78190	6,33		
50	@ 4c	Histidine triad nucleotide-binding protein 1 = PKC-inhibitor	Misc.	-	-	xx	1,8	up	$	1,3	up	ns	-	-	xx	gi|2495231	13751	6,39		
51	@ 1c	Selenium binding protein 2	Misc.	1,4	down	$	1,4	down	$	1,5	down	$	1,1	down	ns	gi|81879451	52498	6,10		
52	@ 3c	Gluthathione peroxidase	Stress	1,3	up	ns	1,9	up	$	1,7	up	$	1,1	down	ns	gi|121668	22486	7,66		
53	@ 1c	Phosphoglucomutase	Metab.	1,3	up	ns	1,6	up	$	1,7	up	$	1,0	down	ns	gi|730311	61519	6,32		
54	@ 1c	Dihydrolipoamide dehydrogenase	Metab.	1,1	up	ns	1,3	up	$	1,3	up	$	1,0	down	ns	gi|81885266	54004	7,96		
55	@ 4d	Nucleoside diphosphate kinase (B?)	Metab.	1,0	down	ns	1,3	up	$	1,1	up	ns	1,0	up	ns	gi|127984	17386	6,92		
56	@ 2c	Annexin I = Lipocortin I	Misc.	1,5	up	$	1,6	up	ns	1,5	up	$	1,1	down	ns	gi|113947	39016	7,14		
57	@ 1d	Catalase	Stress	1,2	down	ns	1,7	down	$	1,2	down	ns	1,1	down	ns	gi|115707	59931	7,15		
58	@ 1d	Carnitine O-palmitolyltransferase II (prec)	Metab.	1,1	down	ns	1,4	down	ns	1,1	down	ns	1,0	down	ns	gi|117289	74634	6,89		
59	@ 4d	Peroxiredoxin 5, mit prec	Stress	1,3	down	ns	1,2	up	$	1,1	down	ns	1,0	up	ns	gi|20138819	22507	8,94		
60	@ 4d	Nucleoside diphosphate kinase	Metab.	1,2	up	ns	1,8	up	$	2,0	up	$	1,0	up	ns	gi|127984	17386	6,92		
61	@ 3d	Triosephosphate isomerase (fragment)	Metab.	1,1	down	ns	1,2	up	$	1,2	up	$	1,0	up	ns	gi|1351280	26773	6,51		
62	@ 2d	no ID	No ID	1,0	down	ns	1,4	down	$	1,4	down	$	1,2	down	ns	n/a	n/a	n/a	n/a	
63	@ 3d	Adenylate kinase isozyme 2 (mit?)	Metab.	1,4	down	ns	1,3	down	ns	1,1	up	ns	1,2	down	ns	gi|266401	26232	6,36		
64	@ 2d	Bcat2 protein	Misc.	1,5	down	$	1,7	down	$	1,4	down	$	1,0	up	ns	gi|81885326	44138	8,62		
65	@ 2b	Pyruvate dehydrogenase (lipoamide), B-chain		-	-	-	-	-	-	-	-	-	-	-	-	gi|1352624	38823	5,94		
66	@ 1b	Desmin		-	-	-	-	-	-	-	-	-	-	-	-	gi|1352241	53293	5,21		
67	@ 1a	Desmin		-	-	-	-	-	-	-	-	-	-	-	-	gi|11968118	53424	5,21		
68	@ 1b	dnaK-type molecular chaperone GRP75, prec		-	-	-	-	-	-	-	-	-	-	-	-	gi|55584140	73699	5,87		
69	@ 2c	no ID		-	-	-	-	-	-	-	-	-	-	-	-	n/a	n/a	n/a	n/a	
70	@ 3c	Alpha-B-crystallin		-	-	-	-	-	-	-	-	-	-	-	-	gi|2119189	20076	6,76		
71	@ 4a	no ID		-	-	-	-	-	-	-	-	-	-	-	-	n/a	n/a	n/a	n/a	
72	@ 4c	Superoxide dismutase [Cu-Zn]		-	-	-	-	-	-	-	-	-	-	-	-	gi|818029	15569	5,89		
73	@ 4d	Myoglobin		-	-	-	-	-	-	-	-	-	-	-	-	gi|78099013	17146	7,83		
74	@ 4d	Myoglobin		-	-	-	-	-	-	-	-	-	-	-	-	gi|78099013	17146	7,83		
75	@ 4d	Myoglobin		-	-	-	-	-	-	-	-	-	-	-	-	gi|78099013	17146	7,83		
76	@ 2d	Aldolase A		-	-	-	-	-	-	-	-	-	-	-	-	gi|6978487	39327	8,31		
77	@ 2c	Peroxisomal dienoyl CoA isomerase	Metab.	1,4	down	ns	1,5	down	$	2,1	down	$	1,1	down	ns	gi|6015047	36148	8,13		
78	@ 1d	no ID		-	-	-	-	-	-	-	-	-	-	-	-	n/a	n/a	n/a	n/a	
79	@ 1c	Enolase 1 = Alpha Enolase	Metab.	1,2	up	ns	1,1	up	ns	1,3	up	$	1,0	down	ns	gi|56757324	46955	6,16		
80	@ 3c	no ID		-	-	-	-	-	-	-	-	-	-	-	-	n/a	n/a	n/a	n/a	
81	@ 2b	Troponin T, cardiac muscle isoforms		-	-	-	-	-	-	-	-	-	-	-	-	gi|1717772	34431	5,19		
82	@ 2c	Aldose reductase	Metab.	1,0	up	ns	1,1	up	ns	1,2	up	$	1,1	down	ns	gi|1168407	35643	6,28		
83	@ 2c	NADH dehydrogenase 1 alpha-subcomplex 10-like protein	Metab.	1,0	up	ns	1,1	down	ns	1,2	down	ns	1,4	down	$	gi|81885291	31681	5,44		
84	@ 2c	Acyl CoA dehydrogenase, short chain spec mito prec	Metab.	1,0	up	ns	1,1	down	ns	1,2	down	$	1,1	down	ns	gi|1168286	44737	8,47		
85	@ 2c	no ID		-	-	-	-	-	-	-	-	-	-	-	-	n/a	n/a	n/a	n/a	
86	@ 2c	no ID		-	-	-	-	-	-	-	-	-	-	-	-	n/a	n/a	n/a	n/a	
87	@ 3c	no ID		-	-	-	-	-	-	-	-	-	-	-	-	n/a	n/a	n/a	n/a	
88	@ 3c	Proteasome endopeptidase complex, iota chain		-	-	-	-	-	-	-	-	-	-	-	-	gi|46397659	27382	6,34		
89	@ 3c	Hypoxanthine phosphoribosyltransferase		-	-	-	-	-	-	-	-	-	-	-	-	gi|2117729	24462	6,07		
90	@ 2d	Creatine-kinase M-chain	Metab.	1,0	up	ns	1,4	down	ns	1,5	down	$	1,0	down	ns	gi|125308	42992	6,58		
91	@ 1c	Transferrin		-	-	-	-	-	-	-	-	-	-	-	-	gi|6175089	75809	7,57		

		ns	$	ns	ns	210	20	172	23	276	32	501	35	488	33	622	62	679	88	563	70
n/a	n/a	ns	ns	ns	ns	162	28	135	34	208	23	138	20	176	10	144	15	196	19	213	18
		ns	ns	$	ns	1396	125	1238	102	1683	159	1296	90	1554	62	1267	62	1487	128	1420	103
		xx	$	ns	xx	-		-		285	46	508	80	267	22	341	34	-		-	
		$	$	$	ns	838	68	604	14	915	85	656	62	761	29	517	23	711	41	620	42
		ns	$	$	ns	545	29	717	95	383	25	743	107	438	24	734	48	630	26	590	55
		ns	$	$	ns	682	94	875	157	641	70	1037	99	673	40	1117	70	809	47	788	23
		ns	$	$	ns	1237	92	1385	109	1319	87	1660	110	1051	32	1358	50	1186	59	1177	56
		ns	$	ns	ns	1962	67	1962	157	1967	69	2623	115	2169	90	2400	96	2223	67	2240	137
		$	ns	$	ns	513	74	790	52	432	57	692	95	512	44	746	60	403	36	364	48
		ns	$	ns	ns	356	59	306	24	439	61	263	22	452	112	393	58	1330	83	1240	120
		ns	ns	ns	ns	558	39	497	54	544	64	392	28	300	25	269	20	342	23	327	55
		ns	$	ns	ns	636	48	499	59	377	22	469	27	375	26	344	24	510	44	520	48
		ns	$	$	ns	762	97	943	178	618	67	1118	103	472	40	937	34	602	39	625	43
		ns	$	$	ns	2869	168	2570	75	2897	153	3490	157	2489	142	3069	125	3073	123	3086	220
n/a	n/a	ns	$	$	ns	876	51	844	37	739	59	544	31	626	39	452	18	803	130	655	61
		ns	ns	ns	ns	657	60	464	101	441	41	328	29	356	41	377	36	497	30	416	44
		$	$	$	ns	1239	120	851	88	1312	146	780	88	1018	56	704	43	1027	71	1038	101
		-	-	-	-	-	-	-	-	-	-	-	-	-	-	-	-	-	-	-	-
		-	-	-	-	-	-	-	-	-	-	-	-	-	-	-	-	-	-	-	-
		-	-	-	-	-	-	-	-	-	-	-	-	-	-	-	-	-	-	-	-
		-	-	-	-	-	-	-	-	-	-	-	-	-	-	-	-	-	-	-	-
n/a	n/a	-	-	-	-	-	-	-	-	-	-	-	-	-	-	-	-	-	-	-	-
		-	-	-	-	-	-	-	-	-	-	-	-	-	-	-	-	-	-	-	-
n/a	n/a	-	-	-	-	-	-	-	-	-	-	-	-	-	-	-	-	-	-	-	-
		-	-	-	-	-	-	-	-	-	-	-	-	-	-	-	-	-	-	-	-
		-	-	-	-	-	-	-	-	-	-	-	-	-	-	-	-	-	-	-	-
		-	-	-	-	-	-	-	-	-	-	-	-	-	-	-	-	-	-	-	-
		-	-	-	-	-	-	-	-	-	-	-	-	-	-	-	-	-	-	-	-
		-	-	-	-	-	-	-	-	-	-	-	-	-	-	-	-	-	-	-	-
		ns	$	$	ns	3120	330	2184	172	3727	315	2561	288	3410	120	1624	101	3235	99	3034	160
n/a	n/a	-	-	-	-	-	-	-	-	-	-	-	-	-	-	-	-	-	-	-	-
		ns	ns	$	ns	4427	340	5463	475	4507	237	5078	507	4887	299	6361	521	5633	119	5493	277
n/a	n/a	-	-	-	-	-	-	-	-	-	-	-	-	-	-	-	-	-	-	-	-
		-	-	-	-	-	-	-	-	-	-	-	-	-	-	-	-	-	-	-	-
		ns	ns	$	ns	2899	89	2938	158	3351	145	3768	147	3454	103	3997	138	3392	120	3148	141
		ns	ns	ns	$	608	151	617	103	633	140	588	109	374	73	299	52	563	48	406	42
		ns	ns	$	ns	712	70	722	62	812	65	762	67	627	34	522	31	773	51	705	46
n/a	n/a	-	-	-	-	-	-	-	-	-	-	-	-	-	-	-	-	-	-	-	-
n/a	n/a	-	-	-	-	-	-	-	-	-	-	-	-	-	-	-	-	-	-	-	-
n/a	n/a	-	-	-	-	-	-	-	-	-	-	-	-	-	-	-	-	-	-	-	-
		-	-	-	-	-	-	-	-	-	-	-	-	-	-	-	-	-	-	-	-
		-	-	-	-	-	-	-	-	-	-	-	-	-	-	-	-	-	-	-	-
		ns	ns	$	ns	13684	3017	14259	1697	15541	1781	11378	1593	26994	1265	18596	1772	22883	1372	21845	1146
		-	-	-	-	-	-	-	-	-	-	-	-	-	-	-	-	-	-	-	-

92	@ 1d	Aconitase, mit, prec		-	-	-	-	-	-	-	-	-	-	-	-	gi|13242312	85421	7,87		
93	@ 1b	no ID		-	-	-	-	-	-	-	-	-	-	-	-	n/a	n/a	n/a	n/a	
94	@ 1c	Aldehyde dehydrogenase / ALDH , mit, prec.		-	-	-	-	-	-	-	-	-	-	-	-	gi|16073616	48239	6,06		
95	@ 1c	no ID		-	-	-	-	-	-	-	-	-	-	-	-	n/a	n/a	n/a	n/a	
96	@ 2c	no ID		-	-	-	-	-	-	-	-	-	-	-	-	n/a	n/a	n/a	n/a	
97	@ 3d	no ID		-	-	-	-	-	-	-	-	-	-	-	-	n/a	n/a	n/a	n/a	
98	@ 1b	no ID		-	-	-	-	-	-	-	-	-	-	-	-	n/a	n/a	n/a	n/a	
99	@ 2b	no ID		-	-	-	-	-	-	-	-	-	-	-	-	n/a	n/a	n/a	n/a	
100	@ 2b	Actin alpha		-	-	-	-	-	-	-	-	-	-	-	-	gi|54036698	41758	5,30		
101	@ 2c	Acyl-CoA dehydrogenase, long chain, prec		-	-	-	-	-	-	-	-	-	-	-	-	gi|113016	47842	7,63		
102	@ 3b	no ID		-	-	-	-	-	-	-	-	-	-	-	-	n/a	n/a	n/a	n/a	
103	@ 3b	Adenine phosphoribosyltransferase		-	-	-	-	-	-	-	-	-	-	-	-	gi|202964	19533	6,17		
104	@ 3c	Hypoxantine phosphoribosyltransferase		-	-	-	-	-	-	-	-	-	-	-	-	gi|2117729	24462	6,07		
105	@ 1c	no ID		-	-	-	-	-	-	-	-	-	-	-	-	n/a	n/a	n/a	n/a	
106	@ 2c	no ID		-	-	-	-	-	-	-	-	-	-	-	-	n/a	n/a	n/a	n/a	
107	@ 1d	Methylmalonate-semialdehyde dehydrogenase (acylating)		-	-	-	-	-	-	-	-	-	-	-	-	gi|400269	57771	8,47		
108	@ 1c	Transferrin		-	-	-	-	-	-	-	-	-	-	-	-	gi|1854476	76314	6,94		
109	@ 2d	Creatine kinase, sarcomeric mitochondrial, prec ?		-	-	-	-	-	-	-	-	-	-	-	-	gi|125313	47355	8,76		
110	@ 2d	Alcohol dehydrogenase [NADP+]		-	-	-	-	-	-	-	-	-	-	-	-	gi|1703237	36352	6,81		
111	@ 2d	Carbonyl reductase [NADPH] 1	Metab.	1,1	down	ns	1,1	down	ns	1,2	down	$	1,1	down	ns	gi|1352258	30428	8,21		
112	@ 3c	no ID		-	-	-	-	-	-	-	-	-	-	-	-	n/a	n/a	n/a	n/a	
113	@ 3d	Glutathion S-transferase YB2		-	-	-	-	-	-	-	-	-	-	-	-	gi|121719	25555	7,30		
114	@ 3d	Adenylate kinase isozyme 1		-	-	-	-	-	-	-	-	-	-	-	-	gi|23831184	21588	7,71		
115	@ 3d	Superoxide dismutase [Mn], mit, prec		-	-	-	-	-	-	-	-	-	-	-	-	gi|134678	24659	8,96		
116	@ 2b	no ID		-	-	-	-	-	-	-	-	-	-	-	-	n/a	n/a	n/a	n/a	
117	@ 1c	Dihydropyrimidinase related protein-2	Misc.	1,2	up	ns	1,5	down	ns	1,3	up	ns	-	-	-	gi|1351260	62239	5,95		
118	@ 2d	Fumarate hydratase, mit prec.	Metab.	1,1	down	ns	1,2	down	ns	1,4	up	$	1,2	up	ns	gi|120605	54429	9,06		
119	@ 1d	no ID		-	-	-	-	-	-	-	-	-	-	-	-	n/a	n/a	n/a	n/a	
120	@ 1d	no ID	No ID	1,4	up	ns	1,0	up	ns	2,3	up	$	1,1	down	ns	n/a	n/a	n/a	n/a	
121	@ 1c	Propionyl-CoA carboxylase, beta chain mit prec	Metab.	1,1	up	ns	1,3	up	ns	-	-	-	-	-	-	gi|129686|	58589	7,19		
122	@ 1c	no ID		-	-	-	-	-	-	-	-	-	-	-	-	n/a	n/a	n/a	n/a	
123	@ 1d	no ID		-	-	-	-	-	-	-	-	-	-	-	-	n/a	n/a	n/a	n/a	
124	@ 1d	Aconitase, mit, prec		-	-	-	-	-	-	-	-	-	-	-	-	gi|13242312	85421	7,87		
125	@ 1a	no ID		-	-	-	-	-	-	-	-	-	-	-	-	n/a	n/a	n/a	n/a	
126	@ 2a	no ID		-	-	-	-	-	-	-	-	-	-	-	-	n/a	n/a	n/a	n/a	
127	@ 2a	no ID		-	-	-	-	-	-	-	-	-	-	-	-	n/a	n/a	n/a	n/a	
128	@ 2a	no ID		-	-	-	-	-	-	-	-	-	-	-	-	n/a	n/a	n/a	n/a	
129	@ 2c	no ID		-	-	-	-	-	-	-	-	-	-	-	-	n/a	n/a	n/a	n/a	
130	@ 2c	no ID		-	-	-	-	-	-	-	-	-	-	-	-	n/a	n/a	n/a	n/a	
131	@ 3d	no ID		-	-	-	-	-	-	-	-	-	-	-	-	n/a	n/a	n/a	n/a	
132	@ 3d	no ID		-	-	-	-	-	-	-	-	-	-	-	-	n/a	n/a	n/a	n/a	
133	@ 1a	Vimentin	Misc.	-	-	-	-	-	-	-	-	-	-	-	-	gi|14389299	53700	5,06		
134	@ 1b	no ID		-	-	-	-	-	-	-	-	-	-	-	-	n/a	n/a	n/a	n/a	
135	@ 2d	no ID		-	-	-	-	-	-	-	-	-	-	-	-	n/a	n/a	n/a	n/a	
136	@ 1d	no ID		-	-	-	-	-	-	-	-	-	-	-	-	n/a	n/a	n/a	n/a	
137	@ 1c	no ID		-	-	-	-	-	-	-	-	-	-	-	-	n/a	n/a	n/a	n/a	
138	@ 3a	no ID		-	-	-	-	-	-	-	-	-	-	-	-	n/a	n/a	n/a	n/a	
139	@ 3b	no ID		-	-	-	-	-	-	-	-	-	-	-	-	n/a	n/a	n/a	n/a	
140	@ 3a	no ID		-	-	-	-	-	-	-	-	-	-	-	-	n/a	n/a	n/a	n/a	
141	@ 3a	no ID		-	-	-	-	-	-	-	-	-	-	-	-	n/a	n/a	n/a	n/a	
142	@ 1b	Protein disulphide isomerase A3, prec.	Misc.	1,3	up	$	1,4	up	ns	1,4	up	$	1,1	down	ns	gi|1352384	56588	5,88		
143	@ 1c	T-complex protein 1, gamma subunit	Misc.	1,2	up	$	1,1	up	ns	1,2	up	ns	1,1	up	ns	gi|549059	60450	6,23		
144	@ 1c	Propionyl-CoA carboxylase, beta chain mit prec	Metab.	1,4	down	$	1,2	down	ns	1,2	down	ns	1,0	down	ns	gi|129686	58589	7,19		
145	@ 1c	Adenylyl cyclase-associated protein	Misc.	1,3	up	$	1,2	up	ns	1,6	up	$	1,3	up	ns	gi|1705586	52879	6,69		

			-	-	-	-	-	-	-	-	-	-	-	-	-	-	-	-	-	-	-	-
	n/a	n/a	-	-	-	-	-	-	-	-	-	-	-	-	-	-	-	-	-	-	-	-
			-	-	-	-	-	-	-	-	-	-	-	-	-	-	-	-	-	-	-	-
	n/a	n/a	-	-	-	-	-	-	-	-	-	-	-	-	-	-	-	-	-	-	-	-
	n/a	n/a	-	-	-	-	-	-	-	-	-	-	-	-	-	-	-	-	-	-	-	-
	n/a	n/a	-	-	-	-	-	-	-	-	-	-	-	-	-	-	-	-	-	-	-	-
	n/a	n/a	-	-	-	-	-	-	-	-	-	-	-	-	-	-	-	-	-	-	-	-
	n/a	n/a	-	-	-	-	-	-	-	-	-	-	-	-	-	-	-	-	-	-	-	-
			-	-	-	-	-	-	-	-	-	-	-	-	-	-	-	-	-	-	-	-
			-	-	-	-	-	-	-	-	-	-	-	-	-	-	-	-	-	-	-	-
	n/a	n/a	-	-	-	-	-	-	-	-	-	-	-	-	-	-	-	-	-	-	-	-
			-	-	-	-	-	-	-	-	-	-	-	-	-	-	-	-	-	-	-	-
			-	-	-	-	-	-	-	-	-	-	-	-	-	-	-	-	-	-	-	-
	n/a	n/a	-	-	-	-	-	-	-	-	-	-	-	-	-	-	-	-	-	-	-	-
	n/a	n/a	-	-	-	-	-	-	-	-	-	-	-	-	-	-	-	-	-	-	-	-
			-	-	-	-	-	-	-	-	-	-	-	-	-	-	-	-	-	-	-	-
			-	-	-	-	-	-	-	-	-	-	-	-	-	-	-	-	-	-	-	-
			-	-	-	-	-	-	-	-	-	-	-	-	-	-	-	-	-	-	-	-
			-	-	-	-	-	-	-	-	-	-	-	-	-	-	-	-	-	-	-	-
			ns	ns	$	ns	6421	356	5597	153	7237	420	6438	483	7658	260	6462	171	7612	191	6934	415
	n/a	n/a	-	-	-	-	-	-	-	-	-	-	-	-	-	-	-	-	-	-	-	-
			-	-	-	-	-	-	-	-	-	-	-	-	-	-	-	-	-	-	-	-
			-	-	-	-	-	-	-	-	-	-	-	-	-	-	-	-	-	-	-	-
			-	-	-	-	-	-	-	-	-	-	-	-	-	-	-	-	-	-	-	-
	n/a	n/a	-	-	-	-	-	-	-	-	-	-	-	-	-	-	-	-	-	-	-	-
			ns	ns	ns	-	102	5	119	16	268	60	181	38	125	16	160	27	-	-	-	-
			ns	ns	$	ns	1110	170	975	129	1159	55	945	99	726	33	989	62	1196	70	1396	65
	n/a	n/a	-	-	-	-	-	-	-	-	-	-	-	-	-	-	-	-	-	-	-	-
	n/a	n/a	ns	ns	$	ns	3933	437	5622	955	4524	815	4533	560	4962	475	11197	762	6854	258	6176	524
			ns	ns	-	-	250	18	264	17	262	37	329	33	-	-	-	-	-	-	-	-
	n/a	n/a	-	-	-	-	-	-	-	-	-	-	-	-	-	-	-	-	-	-	-	-
	n/a	n/a	-	-	-	-	-	-	-	-	-	-	-	-	-	-	-	-	-	-	-	-
			-	-	-	-	-	-	-	-	-	-	-	-	-	-	-	-	-	-	-	-
	n/a	n/a	-	-	-	-	-	-	-	-	-	-	-	-	-	-	-	-	-	-	-	-
	n/a	n/a	-	-	-	-	-	-	-	-	-	-	-	-	-	-	-	-	-	-	-	-
	n/a	n/a	-	-	-	-	-	-	-	-	-	-	-	-	-	-	-	-	-	-	-	-
	n/a	n/a	-	-	-	-	-	-	-	-	-	-	-	-	-	-	-	-	-	-	-	-
	n/a	n/a	-	-	-	-	-	-	-	-	-	-	-	-	-	-	-	-	-	-	-	-
	n/a	n/a	-	-	-	-	-	-	-	-	-	-	-	-	-	-	-	-	-	-	-	-
	n/a	n/a	-	-	-	-	-	-	-	-	-	-	-	-	-	-	-	-	-	-	-	-
	n/a	n/a	-	-	-	-	-	-	-	-	-	-	-	-	-	-	-	-	-	-	-	-
			-	-	-	-	-	-	-	-	-	-	-	-	-	-	-	-	-	-	-	-
	n/a	n/a	-	-	-	-	-	-	-	-	-	-	-	-	-	-	-	-	-	-	-	-
	n/a	n/a	-	-	-	-	-	-	-	-	-	-	-	-	-	-	-	-	-	-	-	-
	n/a	n/a	-	-	-	-	-	-	-	-	-	-	-	-	-	-	-	-	-	-	-	-
	n/a	n/a	-	-	-	-	-	-	-	-	-	-	-	-	-	-	-	-	-	-	-	-
	n/a	n/a	-	-	-	-	-	-	-	-	-	-	-	-	-	-	-	-	-	-	-	-
	n/a	n/a	-	-	-	-	-	-	-	-	-	-	-	-	-	-	-	-	-	-	-	-
	n/a	n/a	-	-	-	-	-	-	-	-	-	-	-	-	-	-	-	-	-	-	-	-
	n/a	n/a	-	-	-	-	-	-	-	-	-	-	-	-	-	-	-	-	-	-	-	-
			$	ns	$	ns	317	15	409	37	348	48	475	65	493	30	671	55	472	31	420	35
			$	ns	ns	ns	263	17	321	14	176	22	195	15	128	7	147	9	140	6	154	27
			$	ns	ns	ns	1218	69	842	35	1084	105	876	37	926	56	791	62	951	44	918	46
			$	ns	$	ns	158	10	203	14	88	23	104	9	75	9	122	19	102	10	137	21

146	@ 4b	Fatty acid binding protein	Metab.	-	-	-	-	-	-	-	-	-	-	-	-	n/a	n/a	n/a	
147	@ 4c	Transthyretin prec (prealbumin)	Misc.	-	-	-	-	-	-	-	-	-	-	-	-	n/a	n/a	n/a	
148	@ 1a	ATP synthase beta-subunit, mit prec	Metab.	-	-	-	-	-	-	-	-	-	-	-	-	n/a	n/a	n/a	
149	@ 4d	Hemoglobin B-chain	Misc.	-	-	-	-	-	-	-	-	-	-	-	-	n/a	n/a	n/a	
150	@ 3b	Endothelin 3 prec	Misc.	-	-	-	-	-	-	-	-	-	-	-	-	n/a	n/a	n/a	
151	@ 3a	Peroxiredoxin 2 = Thioredoxin peroxidase	Stress	1,0	down	ns	1,1	down	ns	1,4	down	$	1,2	down	$	gi|549132	21770	5,34	
152	@ 2a	no ID	No ID	-	-	-	-	-	-	1,2	up	$	1,0	up	ns	n/a	n/a	n/a	n/a
153	@ 1a	Calreticulin prec	Stress	1,0	up	ns	1,4	up	ns	1,6	up	$	1,1	up	ns	gi|117505	47966	4,33	
154	@ 1a	dnaK-type molecular chaperone prec	Stress	1,1	down	ns	1,1	up	ns	1,4	up	$	1,0	down	ns	gi|121574	72302	5,07	
155	@ 1b	dnaK-type molecular chaperone hsc-73	Stress	1,0	up	ns	1,2	up	ns	1,4	up	$	1,2	down	ns	gi|347019	70884	5,43	
156	@ 2b	3-methyl-2-oxobutanoate dehydrogenase (lipoamide) alpha-chain prec	Metab.	1,3	down	ns	1,1	down	ns	1,7	down	$	1,2	down	ns	gi|129032	50133	7,68	
157	@ 1b	Guanine deaminase	Misc.	1,0	up	ns	2,0	up	ns	2,0	up	$	1,1	up	ns	gi|81868670	50869	5,48	
158	@ 1b	Dihydrolipoamide S-acetyltransferase (fragment)	Metab.	1,0	down	ns	1,3	up	$	1,2	up	$	1,1	down	ns	gi|266685	58727	5,70	
159	@ 1c	Aldehyde dehydrogenase, mit (fragment)	Metab.	1,2	up	ns	1,3	up	ns	1,6	up	$	1,0	down	ns	gi|81892738	55566	6,69	
160	@1c	TNF receptor-associated protein 1	Misc.	1,4	down	ns	1,3	down	ns	1,4	down	$	1,0	up	ns	gi|81910345	80411	6,56	
161	@ 1c	Dihydropyrimidinase related protein-2	Misc.	1,2	up	ns	1,1	up	ns	1,3	up	$	1,0	down	ns	gi|1351260	62239	5,95	
162	@ 1c	no ID	No ID	-	-	-	-	-	-	2,4	down	$	1,0	up	ns	n/a	n/a	n/a	n/a
163	@ 2c	Acyl-CoA dehydrogenase, short chain specific, mit prec	Metab.	1,1	up	ns	1,1	down	ns	1,4	down	$	1,1	down	ns	gi|1168286	44737	8,47	
164	@ 1c	ATP synthase, H+ transporting, mitochondrial F1 complex, alpha subunit, isoform 1	Metab.	1,2	up	ns	1,2	up	ns	1,3	up	$	1,0	down	ns	gi|83300587	59717	9,22	
165	@ 1c	Electron-transferring-flavoprotein dehydrogenase	Misc.	1,1	down	ns	1,2	down	ns	1,2	down	$	1,0	down	ns	gi|52000614	68155	7,33	
166	@ 2c	no ID	No ID	-	-	-	-	-	-	1,1	down	$	1,1	down	ns	n/a	n/a	n/a	n/a
167	@ 2c	Acyl coA thioesterase, mit prec.	Metab.	1,3	down	ns	1,2	down	ns	1,7	down	$	1,0	down	ns	gi|6166586	49670	7,68	
168	@ 1d	Glutamate dehydrogenase 1	Metab.	1,0	up	ns	1,2	down	ns	1,2	down	$	1,1	down	ns	gi|92090591	61377	8,05	
169	@ 4d	Fatty acid binding protein, adiposite (AFABP)	Metab.	-	-	-	1,2	down	ns	2,0	down	$	-	-	-	gi|2494405	14568	7,93	
170	@2d	Aspartate transaminase	Metab.	1,2	down	ns	1,1	down	ns	1,2	down	$	1,1	up	ns	gi|91997	46399	6,73	
171	@ 1d	3-oxoacid CoA-transferase	Metab.	1,4	up	$	1,4	up	$	1,5	up	$	1,3	up	ns	gi|2492999	56371	8,47	
172	@ 1d	Fumarate hydratase, mit prec.	Metab.	1,0	up	ns	1,1	down	ns	1,2	up	$	1,1	up	ns	gi|120605	54429	9,06	
173	@ 1b	no ID	No ID	1,9	down	$	1,7	down	ns	2,2	down	$	1,6	down	$	n/a	n/a	n/a	n/a
174	@ 1c	Succinate dehydrogenase [ubiquinone] flavoprotein subunit, mit, prec	Metab.	1,1	up	$	1,1	down	ns	1,2	down	ns	1,2	down	$	gi|52782765	71570	6,75	
175	@ 1c	no ID	No ID	1,1	up	ns	1,2	up	ns	1,0	down	ns	1,3	down	$	n/a	n/a	n/a	n/a
176	@ 1c	Succinate dehydrogenase [ubiquinone] flavoprotein subunit, mit, prec	Metab.	1,1	up	ns	1,0	up	ns	1,1	down	ns	1,3	down	$	gi|52782765	71570	6,75	
177	@ 2c	no ID	No ID	1,0	down	ns	1,2	down	ns	1,1	down	ns	1,7	down	$	n/a	n/a	n/a	n/a
178	@ 1c	Dihydrolipoamide dehydrogenase	Metab.	1,3	up	ns	1,2	up	ns	1,1	up	ns	1,1	down	$	gi|81885266	54004	7,96	
179	@ 3d	Ubiquinol-cytochrome c reductase iron-sulfur subunit, mit, prec.	Metab.	1,0	up	ns	1,1	down	ns	1,3	down	ns	1,6	down	$	gi|52001457	29427	9,04	

Protein database corresponding to 2-DE map presented in Figure 1S.
$= p<0.05 and ns=non-significant.

literature comparison		-	-	-	-	-	-	-	-	-	-	-	-	-	-	-	-	-	-	-	-
literature comparison		-	-	-	-	-	-	-	-	-	-	-	-	-	-	-	-	-	-	-	-
literature comparison		-	-	-	-	-	-	-	-	-	-	-	-	-	-	-	-	-	-	-	-
literature comparison		-	-	-	-	-	-	-	-	-	-	-	-	-	-	-	-	-	-	-	-
literature comparison		-	-	-	-	-	-	-	-	-	-	-	-	-	-	-	-	-	-	-	-
		ns	ns	$	$	991	47	985	65	605	28	553	48	505	40	362	33	860	60	727	41
n/a	n/a	-	-	$	ns	-	-	-	-	-	-	-	-	919	40	1067	27	965	45	1001	39
		ns	ns	$	ns	1188	159	1193	229	888	96	1222	143	921	77	1506	85	536	56	595	34
		ns	ns	$	ns	1441	124	1363	147	1278	156	1434	72	1237	48	1764	99	1378	81	1324	60
		ns	ns	$	ns	2585	235	2637	381	3145	231	3800	419	3865	277	5307	321	4051	360	3514	285
		ns	ns	$	ns	429	64	333	36	594	40	531	46	811	80	490	37	741	107	606	117
		ns	ns	$	ns	153	36	160	20	151	32	300	79	218	19	435	44	205	12	215	18
		ns	$	$	ns	1901	139	1854	108	2312	126	2982	185	3976	230	4866	292	4543	399	4280	353
		ns	ns	$	ns	3591	346	4154	413	3658	485	4580	312	3681	113	5897	417	4317	289	4217	270
		ns	ns	$	ns	1675	194	1226	112	1890	212	1404	120	1229	74	892	37	1370	131	1397	114
		ns	ns	$	ns	541	51	630	77	555	90	624	57	413	17	548	33	431	25	428	28
n/a	n/a	-	-	$	ns	-	-	-	-	-	-	-	-	807	91	334	28	539	68	560	53
		ns	ns	$	ns	3305	364	3614	361	4259	289	4006	345	4172	248	3068	215	4641	287	4162	304
		ns	ns	$	ns	533	36	633	33	468	43	561	77	467	23	618	29	458	32	442	21
		ns	ns	$	ns	1376	128	1285	49	1551	249	1326	112	1906	106	1608	68	1690	85	1634	112
n/a	n/a	-	-	$	ns	-	-	-	-	-	-	-	-	912	30	821	26	802	45	710	51
		ns	ns	$	ns	2378	315	1888	145	2988	296	2402	188	3648	158	2178	118	3412	164	3317	195
		ns	ns	$	ns	1994	171	2058	287	2710	220	2261	215	3067	163	2525	134	2500	126	2227	156
		xx	ns	$	xx	-		-		2691	248	2232	155	3097	212	1580	92	-		-	
		ns	ns	$	ns	3954	217	3434	283	4645	383	4087	196	5254	241	4224	176	4959	299	5273	273
		$	$	$	ns	2233	270	3051	235	3008	274	4356	266	2812	327	4265	283	2635	109	3408	519
		ns	ns	$	ns	2088	179	2175	320	3408	142	2991	178	2359	155	2938	183	3538	170	3775	178
n/a	n/a	$	ns	$	$	92	13	48	13	131	34	79	15	161	19	73	14	252	31	158	33
		$	ns	ns	$	1241	62	1417	88	1155	161	1096	112	1060	167	921	51	1289	64	1052	58
n/a	n/a	ns	ns	ns	$	263	24	298	14	186	28	216	15	154	8	148	14	198	15	154	6
		ns	ns	ns	$	3674	383	3936	410	2617	207	2688	188	2950	317	2771	146	3504	167	2765	234
n/a	n/a	ns	ns	ns	$	600	161	591	125	453	109	378	53	319	76	284	40	507	60	298	35
		ns	ns	ns	$	511	75	642	51	722	68	833	82	700	42	775	31	617	25	542	19
		ns	ns	ns	$	2229	633	2238	343	3044	662	2681	428	1813	216	1403	187	2346	187	1499	239

* Mann-Whitney statistics were used to compare sham vs. PAB within one time group.

Chapter 6

Preserved biventricular function after long-term pulmonary artery banding despite progressive molecular alterations

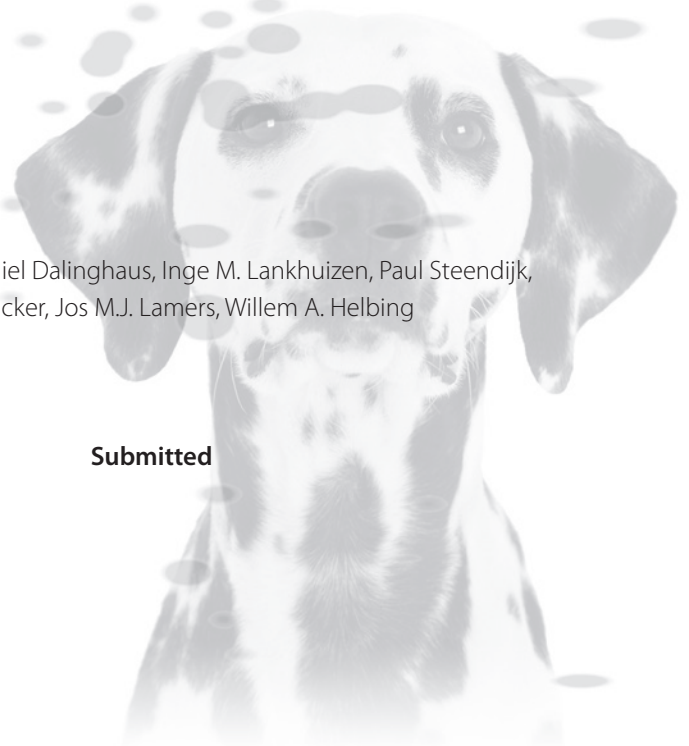

Matthijs J. Faber, Michiel Dalinghaus, Inge M. Lankhuizen, Paul Steendijk, Dirk J. Duncker, Jos M.J. Lamers, Willem A. Helbing

Submitted

Abstract

Aims: In several types of congenital heart disease, as well as in pulmonary hypertension, RV hypertrophy may develop that could ultimately progress to RV failure. In this study we sought to determine hemodynamic signs of imminent RV failure in a model of pulmonary artery banding (PAB).

Methods: Rats received sham (n=28) or PAB (n=27) surgery and were housed for 6, 12 and 20 weeks respectively. After the housing period, baseline diastolic function was measured using pressure-volume loops and dobutamine infusions were used to test systolic and diastolic reserve. In addition, molecular determinants of β-adrenergic signalling, Ca^{2+}-cycling and the degree of fibrosis were measured.

Results: In PAB rats RV systolic function was 3-fold increased in all three time groups ($p<0.01$) and dobutamine response was unimpaired. RV diastolic function parameters indicated both impaired early ($p<0.01$) and late ($p<0.01$) diastolic function, with similar response to dobutamine in PAB and sham. LV systolic and diastolic function was unaffected. The RV β-ARs decreased at 20 weeks, while GRK-2 decreased at 6 and 20 weeks ($p<0.05$). At 6 and 20 weeks the NCX1/SERCA2 ratio was increased ($p<0.05$). There were no signs of increased RV fibrosis in PAB.

Conclusions: Prolonged PAB resulted in compensated RV hypertrophy, with maintained RV systolic function and impaired diastolic function. LV function was not affected. The decrease in β-ARs and SERCA2, commonly found in heart failure, were compensated for by decreases in GRK-2 and PLB, respectively, and an increase in NCX1. These molecular alterations are compatible with our hemodynamic findings of compensated hypertrophy.

Introduction

In several types of (corrected) congenital heart disease, as well as in pulmonary hypertension, the right ventricle (RV) can be subjected to (residual) pressure overload [1]. As a result, compensated RV hypertrophy will develop, that may progress to a decompensated state of hypertrophy (ie. RV failure). This impaired cardiac function is not strictly limited to the RV. The left ventricle (LV) can be involved as well either through neurohumoral pathways or by direct mechanical interaction [2,3]. As the survival of patients with congenital heart disease has improved, a better understanding of the biventricular response to RV pressure overload over time is mandatory enabling us to design preventive strategies and to time surgical (re)intervention.

At present, most studies have addressed the effects of RV pressure overload at one point in time. However, little is known about the time-related changes that occur in the RV and LV during prolonged RV pressure overload. Previously, we reported that RV systolic function after 6 weeks of pulmonary artery banding (PAB) in rats was increased and that RV contractile reserve was maintained [4]. Subsequently, we demonstrated progressive alterations in cytoplasmic metabolic and anti-oxidant proteins after 6, 12 and 20 weeks of RV pressure overload [5]. Despite these molecular changes baseline RV systolic function was unaffected, suggesting compensated RV hypertrophy up to 20 weeks of RV pressure overload. However, early signs of systolic impairment may only be demonstrable during increased systolic demands.

Furthermore, clinical signs of heart failure in the face of prolonged ventricular hypertrophy may also develop secondary to diastolic impairment, as has extensively been demonstrated for the LV. Diastolic dysfunction in these circumstances may be related to alterations in active relaxation as well as alterations in passive diastolic properties due to increased ventricular mass and/or fibrosis. At the molecular level changes in both diastolic as well as systolic function, may be intimately related with alterations in Ca^{2+} cycling and in β-adrenergic signalling.

In this present study, we therefore aim to analyze RV (systolic) contractile reserve as well as biventricular diastolic function after prolonged PAB. Here, we tested the hypothesis that prolonged RV pressure overload up to 20 weeks in rats will eventually result in impaired RV contractile reserve and impaired diastolic function. Furthermore we suspect that LV diastolic function will be preserved. For this purpose, we performed biventricular pressure-volume (PV) loops to assess systolic and diastolic function in rest and under dobutamine stimulation [4-8]. In order to link these potential hemodynamic changes to molecular mechanisms, several components of the Ca^{2+} storage/release system and β_1-adrenergic signaling were studied, as well as the degree of fibrosis.

Methods

Ethical Approval

All experimental procedures and protocols used in this investigation were reviewed and approved by the institutional animal care and use committee of the Erasmus MC and are in accordance with the National Institutes of Health "Guide for the care and use of laboratory animals" (NIH publication No. 85-23, revised 1996).

Male Wistar rats (190-220 g, Harlan, Zeist, The Netherlands) underwent PAB or sham operation. The animals were housed after the initial operation (i.e. sham or PAB), prior to the hemodynamic studies, in groups of 2 or 3 animals, on a 12/12-h light/dark cycle with standard rat chow and water ad libitum. Three different periods of housing were applied: 6, 12 and 20 weeks (resp. n=9 vs. 6, n=8 vs. 9, n=11 vs. 12 (sham vs. PAB)). The instrumentation of the animals as well as the hemodynamic measurements that we used, were exactly the same as previously reported [4] and will only be described briefly.

Pulmonary artery banding procedure

After induction of anesthesia a left thoracotomy was performed and a silk thread was positioned under the pulmonary artery. A suture was tied tightly around an 18 gauge needle that was placed alongside the pulmonary artery. Next, the needle was rapidly removed in order to produce a fixed constricted opening in the lumen equal to the diameter of the needle. The sham animals underwent the same procedure except for the banding of the pulmonary artery.

Hemodynamic instrumentation

Six, 12 or 20 weeks after sham or PAB operations animals were instrumented for hemodynamic measurements. After induction of anesthesia a right thoracotomy was performed and an ultrasonic flow-probe (Transonics Systems Inc., Ithaca, NY), was placed around the aorta. A left thoracotomy was performed for maximal exposure of the left side of the heart. For preload reduction, required to obtain systolic and diastolic PV-relations, a silk thread was placed around the vena cava inferior. Conductance catheters (CD Leycom, Zoetermeer, The Netherlands) and pressure-tip catheters (Millar Instruments, Houston, TX) were inserted in the RV and LV. Signals were recorded at a sample rate of 500Hz using the Conduct 2000 data-acquisition hard- and software (CD Leycom). Conductance catheters were calibrated as previously described [9].

Hemodynamic study protocol

When hemodynamic stability was reached, a set of measurements was performed to calibrate the conductance catheter and to assess hemodynamics and contractile performance in baseline conditions and during dobutamine stimulation (2.5 µg/kg/min (dobu-2.5) and 5 µg/kg/min (dobu-5)). Data were recorded with open chest at steady-state baseline conditions and during transient preload reduction. All measurements were made during short suspension of the ventilation at end-expiration.

Hemodynamic measurements and calculations

The biventricular signals were analyzed by custom made software (Circlab (P.S.)). From the steady state data the following parameters were calculated: heart rate, cardiac output, stroke volume, end-systolic pressure, end-diastolic pressure, end-systolic volume, end-diastolic volume, as reported previously [5].

The following parameters were obtained: end-systolic pressure-volume relation (ESPVR), dP/dt_{max} –end-diastolic volume ($dPdt_{max}$-Ved) relation, and preload recruitable stroke work relation (PRSW) [6-8]. The end-systolic point was defined as the point in the cardiac cycle of maximal elastance. Elastance was defined as $P(t)/[V(t)-V_0]$, where P(t) is the instantaneous pressure, V(t) instantaneous volume, and V_0 the theoretical volume at zero pressure [10]. V_0 was determined by an iterative algorithm as previously described by Kono et al [11].

The diastolic function was described with the following three parameters: dP/dt_{min}, tau and chamber stiffness constant derived from the end-diastolic pressure volume relation (EDPVR) [12,13]. The dP/dt_{min} and tau were calculated from the baseline PV loops whereas the EDPVR was constructed during transient preload reduction. The tau was calculated as time constant of mono-exponential pressure decay during isovolumic relaxation. The isovolumic period was defined as the period between dP/dt_{min} and the point where the dP/dt reached 10% of the dP/dt_{min} [14]. The late-phase of diastole is characterized by passive chamber properties which is reflected by the EDPVR. This EDPVR was constructed by integrating the end-diastolic pressures and volumes in a linear fashion. The slope of this relationship was used as the chamber stiffness constant.

Western blotting

Western blotting was used to study, in RV and LV after 6 and 20 weeks, the levels of β_1-adrenergic receptor (β_1-AR) and its regulator β-adrenergic receptor kinase (GRK-2). In addition, several Ca^{2+} handling proteins were studied. These included the sarcoplasmic reticulum Ca^{2+} ATPase (SERCA2), phospholamban (PLB), and the $Na+/Ca^{2+}$ exchanger (NCX1). In brief, proteins were extracted from homogenized RV and LV tissues as

described before [15]. Next, proteins were separated by 1D-PAGE, using 10% (β_1-AR, GRK-2, NCX1) or 12% (SERCA2, PLB) gels. The samples were heated for 5 min. at 95° C (β_1-AR, GRK-2) or 37° C (SERCA2, PLB, NCX1). Subsequently 20 µg of protein was applied per sample. The following primary antibodies were used: β_1-AR 1:4000 diluted (Santa Cruz Biotechnology, Santa Cruz, CA, USA), GRK-2 1:4000 diluted (Santa Cruz Biotechnology), SERCA2 1:30000 diluted (Abcam, Cambridge, MA, USA), PLB 1:100000 diluted (Affinity BioReagents, Golden, CO, USA) and NCX1 1:1000 diluted (Abcam). The blots were incubated with either GARPO (β_1-AR, GRK-2, SERCA2, resp. 1:4000, 1:4000, 1:30.000) or GAMPO (PLB, NCX1, resp. 1:10.000, 1:100.000). The results were visualized on film (Hyperfilm™ ECL, Amersham Biosciences) and quantitated and analyzed with a GS-800 calibrated densitometer and QuantityOne software (Biorad, Hercules, CA, USA).

Histology

Following the hemodynamic measurements, the heart was dissected and a slice of the RV was fixed in 10% formaldehyde and subsequently dehydrated in several steps of ethanol and xylene followed by embedding in paraffin. Sections of 4.5 µm were deparaffinated in several steps of xylene and ethanol. A routine Heamatoxylin-Eosin staining was performed to assess the orientation of the cardiomyocytes and other structures. A Gomori negative staining was used to assess myocytes cross sectional area, a lectin staining was used for assessing capillary density, and a Picro Sirius red staining was used for quantification of myocardial fibrosis.

Data and statistical analysis

To test contractile reserve in rats after 12 and 20 weeks of PAB we used the following approach. Data on baseline systolic function, that we previously reported [4], as well as the responses to dobutamine after 6 weeks of PAB [4] were all analysed together with dobutamine responses after 12 and 20 weeks of PAB that we report here. We took this approach in order to detect alterations in contractile reserve throughout 6 to 20 weeks of PAB. For the purpose of clarity some of those previously reported data are reiterated here in tables and figures.

Similarly, the diastolic function data (not previously reported) were analysed for all three time groups.

The differences in hemodynamic parameters between the control group and the PAB group at baseline were analyzed using a Student's T-test. Repeated measures 3-way ANOVA was used to study the various interactions between 1) type (ie. sham and PAB), 2) time (ie. 6, 12, and 20 weeks), and 3) dobutamine (i.e. baseline, dobu-2.5, dobu-5). Interactions studied were: type*time, type*dobutamine, time*dobutamine, and type*time*dobutamine. If following the 3-way ANOVA any of these interactions

was found to have a p-value <0.05, subsequent testing was performed using (2-way) ANOVA. Post hoc testing, when appropriate, was performed using the Bonferroni correction. The software package Statview (version 5.0, SAS Institute, Cary, NC, USA) was used for data analysis. For the histological measurements, the data was analyzed using a 2-way ANOVA and when appropriate post hoc testing using the Bonferroni correction. A two-sided p-value < 0.05 was considered statistically significant. Data are presented as mean ± SEM

Results

There were no differences in body mass between sham and PAB animals in each time group and PAB rats did not show any signs of heart failure and/or cyanosis. RV and right atrium weights, relative to body weight, were significantly increased [5].

Table 1: Baseline hemodynamic response to various durations of RV pressure overload.

		Baseline Conditions		
General		6 wk	12 wk	20 wk
HR	sham	310 ± 8	305 ± 7	306 ± 8
	PAB	297 ± 12	283 ± 4*	286 ± 6
CO	sham	51 ± 4	51 ± 3	41 ± 3
	PAB	49 ± 5	38 ± 3*	36 ± 2
SV	sham	164 ± 11	168 ± 10	137 ± 10
	PAB	164 ± 13	135 ± 9	128 ± 6
Right Ventricle				
Pes	sham	29 ± 1	29 ± 3	32 ± 3
	PAB	63 ± 8*	57 ± 5*	68 ± 5*
Ped	sham	4.6 ± 0.8	4.4 ± 1.1	6.3 ± 0.8
	PAB	6.8 ± 0.5	6.1 ± 1.7	7.2 ± 0.9
Ved	sham	315 ± 44	351 ± 31	295 ± 21
	PAB	259 ± 32	195 ± 18*	233 ± 14*

Values are mean ± SEM. HR=heart rate (beats/min), CO=cardiac output (mL/min), SV=stroke volume (μL), Pes=end-systolic pressure (mmHg), Ped=end-diastolic pressure (mmHg), Ved=end-diastolic volume (μL). *p<0.05 versus corresponding control

Global hemodynamic function and RV (systolic) contractile reserve

In all three time groups RV end-systolic pressures were increased in PAB animals to approximately 60% of LV end-systolic pressures. Heart rate and cardiac output were slightly lower in the PAB animals, but stroke volumes were similar (Table 1). Indices of

baseline RV systolic performance were increased in PAB in all time groups to a similar extent (Figure 1)

In response to dobutamine heart rate increased, cardiac output tended to increase, whereas stroke volume tended to decrease in all sham and PAB animals. These responses were independent of the presence and duration of PAB (Table 2). Furthermore, RV end-systolic pressure increased in both sham and PAB and the increase tended to be higher in PAB. In the animals that had PAB in place for 12 and 20 weeks the three indices of systolic performance all increased in response to dobutamine (Figure 1). These responses were similar to those previously reported after 6 weeks of PAB. These results indicate that up to 20 weeks of PAB the animals in our study demonstrated increased baseline RV systolic performance and maintained contractile reserve.

Similarly, indices of LV systolic performance increased in response to dobutamine stimulation after 12 and 20 weeks in a similar fashion as previously reported after 6 weeks of PAB (data not shown).

Table 2: Hemodynamic response to dobutamine infusion after various durations of RV pressure overload.

		6 weeks		12 weeks		20 weeks	
General		**dobu-2.5**	**dobu-5**	**dobu-2.5**	**dobu-5**	**dobu-2.5**	**dobu-5**
HR	*sham*	28± 4*	36± 4	28± 3*	38± 4*†	30± 4*	41± 4*†
	PAB	28± 5*	38± 6*†	32± 4*	43± 4*†	24± 2*	36± 3*†
CO	*sham*	3± 5	20± 7*†	10± 9	16± 11	18± 4*	33± 7*†
	PAB	6± 7	12± 10	33± 21	52± 21*	24± 5*	35± 5*†
SV	*sham*	-20± 4*	-12± 6†	-14± 6	-17± 7	-9± 3	-5± 5
	PAB	-17± 3*	-19± 5*	0± 15	6± 13	-1± 5	-2± 4
Right Ventricle							
Pes	*sham*	15± 6	23± 12*	-1± 8	22± 12*†	39± 6*	57± 6*†
	PAB	19± 14	45± 16*†$	38± 7*#	84± 8*†$	36± 6*	58± 11*†$
Ped	*sham*	-31± 19	4± 54	-17± 32	-24± 35	49± 17	28± 17
	PAB	36± 18	47± 24	10± 31	63± 46	33± 25	79± 43
Ved	*sham*	-22± 15*	-14± 20*	-31± 6*	-41± 8*	-29± 5*	-31± 6*
	PAB	-11± 7	15± 19	-9± 6#	-1± 8$	-9± 5#	-6± 6

Values are presented as percent change ± SEM. HR=heart rate (beats/min), CO=cardiac output (mL/min), SV=stroke volume (µL), Pes=end-systolic pressure (mmHg), Ped=end-diastolic pressure (mmHg), Ved=end-diastolic volume (µL).

*p<0.05 versus baseline

†p<0.05 versus dobu-2.5

#p<0.05 effect of banding baseline versus dobu-2.5

$p<0.05 effect of banding dobu-2.5 versus dobu-5

Δp<0.05 effect of banding baseline versus dobu-5

Figure 1: Alterations in RV systolic function parameters at baseline and during dobutamine infusion.

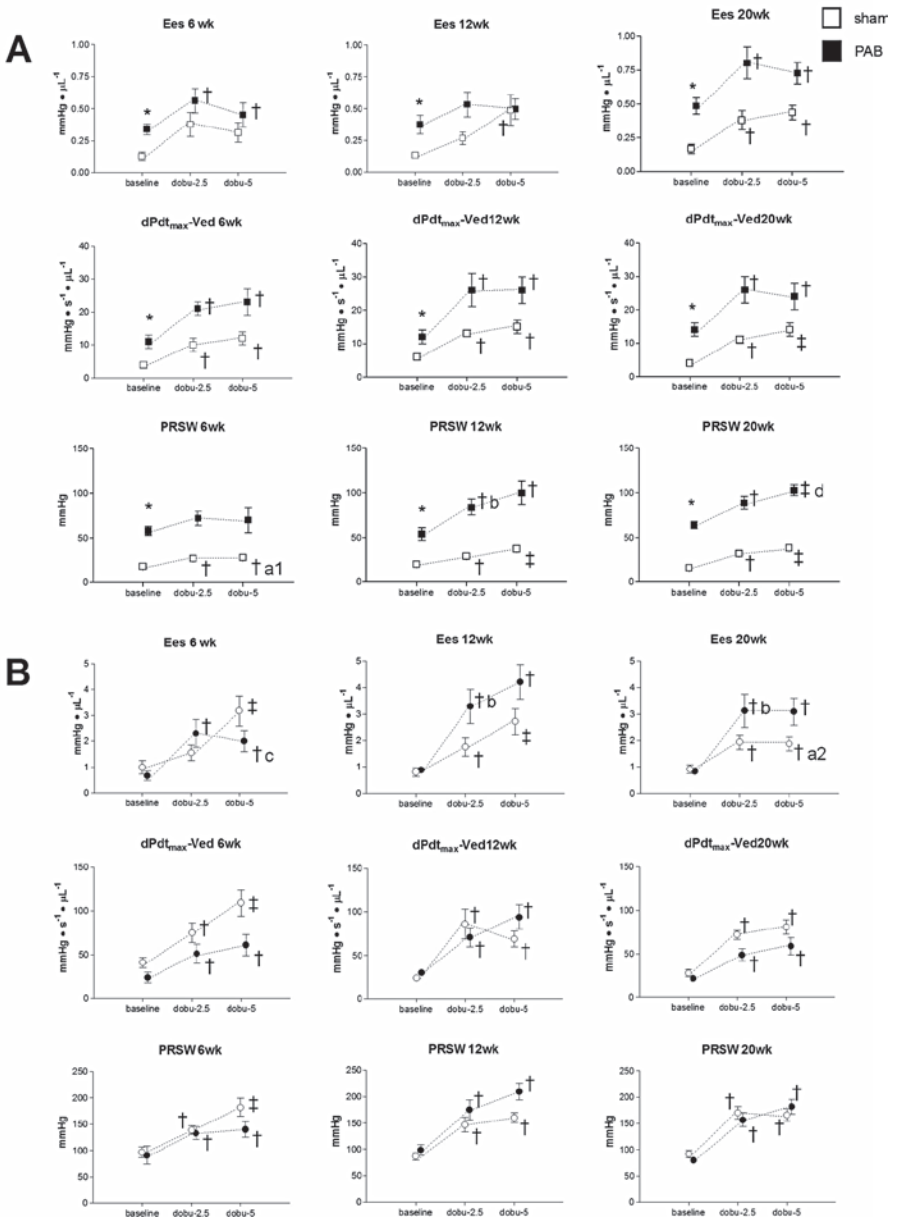

Ees=end-systolic elastance (mmHg·µL^{-1}), PRSW=preload recruitable stroke work (mmHg), dP/dt$_{max}$-Ved=maximum first time derivative of pressure divided by end-diastolic volume (mmHg·s^{-1}·µL^{-1})
*p<0.05 versus corresponding control in baseline
†p<0.05 versus baseline and ‡ p<0.05 versus dobu-2.5
[a]p<0.05 6 wk dobutamine response versus response at 12 and 20 wks
[b]p<0.05 banding effect baseline – dobu-2.5
[c]p<0.05 banding effect baseline – dobu-5

Figure 2: Alterations in diastolic function parameters at baseline and during dobutamine infusion for the RV (A; squares) and LV (B; circles).

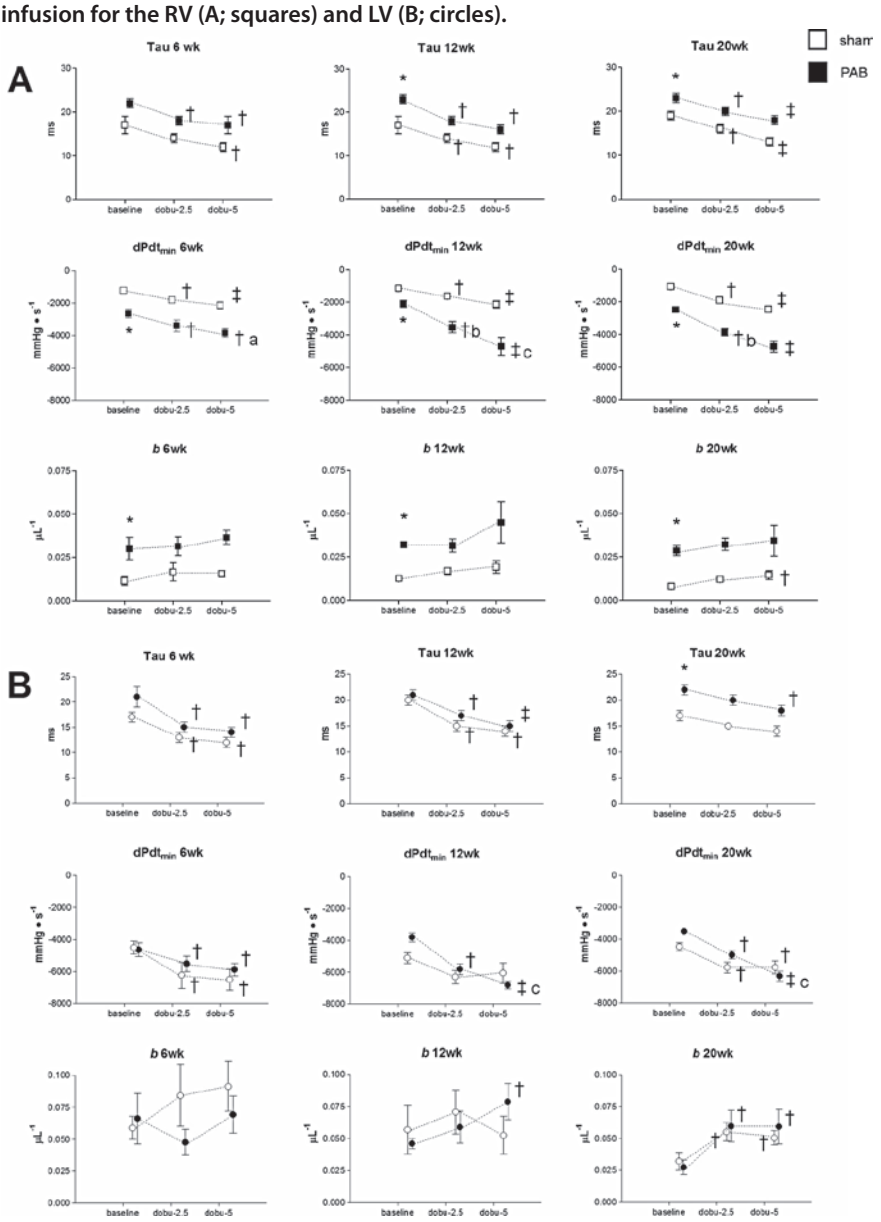

Tau=time constant of isovolumic relaxation (ms), $dPdt_{min}$=minimum first time derivative of pressure vs. time ($mmHg \cdot s^{-1}$), b=chamber stiffness constant derived from end-diastolic pressure-volume relation (μL^{-1}).
*p<0.05 versus corresponding control in baseline
†p<0.05 versus baseline and ‡ p<0.05 versus dobu-2.5
[a]p<0.05 6 wk dobutamine response versus response at 12 and 20 wks
[b]p<0.05 banding effect baseline – dobu-2.5
[c]p<0.05 banding effect dobu-2.5 – dobu-5

Diastolic properties of the RV and LV

Baseline (Table 1; Figure 2)

For all time groups, the RV end-diastolic pressures were similar between PAB and sham. The end-diastolic volume was similar for sham and PAB in after 6 wk banding, but lower after 12 and 20 weeks of PAB (Table 1). At baseline RV dP/dt_{min} was decreased and tau was increased in PAB animals, both indicating a decrease in early diastolic function. Over time (6-20 wk), these parameters did not change in sham and PAB animals (Fig. 2). The chamber stiffness constant b, derived from the EDPVR, was increased in PAB, indicating an impaired late diastolic function (passive stiffness). However, when corrected for RV mass, this passive stiffness of the RV of PAB animals was not increased. Over time the chamber stiffness constant did not change in sham nor PAB animals.

In the LV, the end-diastolic pressures and the end-diastolic volumes were similar for sham and PAB animals. The baseline indices of diastolic function were similar for sham and PAB in all three time groups, except for a minor increase in LV tau at 20 weeks PAB.

Response to dobutamine (Figure 3)

In response to dobutamine, both RV dP/dt_{min} and tau decreased in sham and PAB rats to a similar extent. Furthermore, no consistent changes in the RV chamber stiffness constant were observed. Since the tau is not entirely load-indepent, we corrected the changes in tau during dobutamine stimulation for the Pes. For the RV the slope of the tau-Pes relation was significantly less steep (slope -0.313 ± 0.080 vs. -0.116 ± 0.001 sham vs. PAB RV 20 wk), indicating a true decrease in active relaxation.

The LV dP/dt_{min} and tau responded similar to dobutamine in sham and PAB animals in all three time groups. The slopes of the tau-Pes relation for the LV were not significantly altered (slope -0.087 ± 0.003 vs. -0.060 ± 0.005 sham vs. PAB LV 20 wk). The LV chamber stiffness constant was similar between sham and PAB in response to dobutamine.

Figure 3: dPdtmin-Pes and Tau-Pes corrected relations in the RV and LV after 20 weeks of PAB

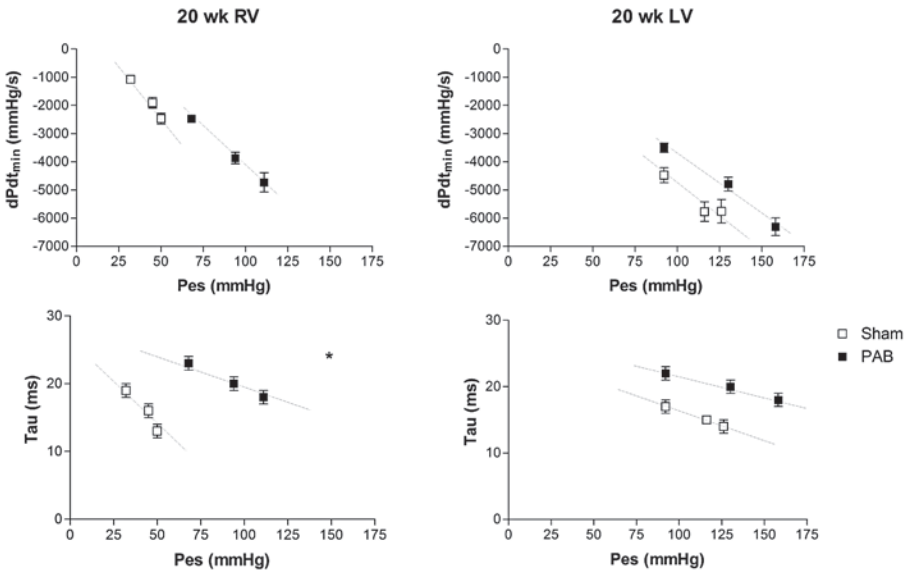

The left panel shows the alterations in dPdtmin and Tau during dobutamine stimulation (from left to right: baseline, dobu-2.5 and dobu-5) for the RV after 20 weeks of PAB corrected for end systolic pressure (Pes). After 20 weeks the slope of the Tau-Pes relation is significantly less steep for the PAB animals ($p<0.05$, see Results). The right panel shows the dPdtmin-Pes and Tau-Pes relation for the LV after 20 weeks of PAB with no difference in slope between sham and PAB.

Western blots (Figure 4)

Since the hemodynamics are relatively constant over time we only performed western blotting in the 6 and 20 weeks. The RV β_1-AR levels were similar after 6 weeks of PAB, but deceased after 20-week PAB-animals by 32% ($p<0.05$, Figure 4A). The RV GRK-2 was decreased by 27% ($p<0.05$) in 6-week PAB animals and decreased even further (-48%, $p<0.05$) after 20-weeks. Over time, changes were found in several Ca^{2+} handling proteins. RV SERCA2 (Figure 4B) was decreased in 6- and 20-week PAB animals by 30% and 41%, respectively (both $p<0.05$). The regulator of SERCA2, PLB, was also downregulated in 6- and 20-week PAB by 14% and 32%, respectively (both $p<0.05$). The levels of RV NCX1 (Fig 4C) were significantly increased in both 6- and 20-week PAB (41% and 90% respectively, both $p<0.05$).

In the LV, the β_1-AR levels were approximately 30% higher in PAB animals after 6 and 20 weeks ($p<0.05$). The LV levels of GRK-2 did not change significantly over time. LV SERCA2 levels were decreased in 6- and 20-week PAB animals (-17% and -14%, respectively, both $p<0.05$). No changes were found in LV PLB levels. The level of LV NCX1 was unaltered after 6 weeks of PAB but was increased by 31% ($p<0.05$) after 20 wk of PAB.

Figure 4: Time-related changes in several Ca^{2+}-handling proteins and components of the β_1-adrenergic signalling system.

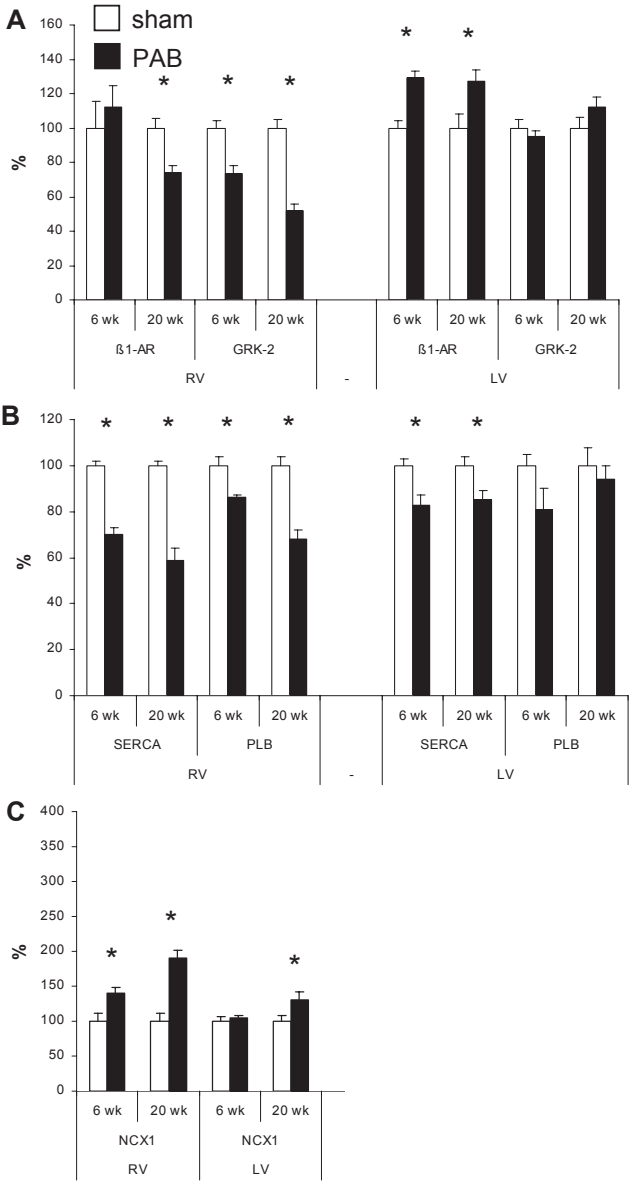

Panel A shows bar graphs representing the differences in expression of the β_1-adrenergic receptor (β_1-AR) and G-protein coupled receptor kinase 2 (GRK-2) in RV and LV after 6 and 20 weeks of RV pressure overload. The changes in the PAB animals were related to the sham levels which were set at 100%. Similar data presentation was used for Panel B which shows changes in the sarcoplasmic reticulum Ca^{2+}-ATPase (SERCA2) and phospholamban (PLB). Panel C shows alterations in the sodium-calcium exchanger (NCX1).
*p<0.05 versus corresponding control

Histology (Figure 5)

The RV myocytes size increased significantly in the PAB animals in all three time groups. Furthermore, the myocyte size increased over time in only the PAB animals. The capillary density after 6 weeks of PAB was similar in sham and PAB animals. When the period of PAB was extended to 12 and 20 weeks, the capillary density was decreased in the PAB animals. The degree of interstitial fibrosis was similar in sham and PAB animals for all three time groups.

Figure 5. Morphological changes in the RV after various durations of RV pressure overload.

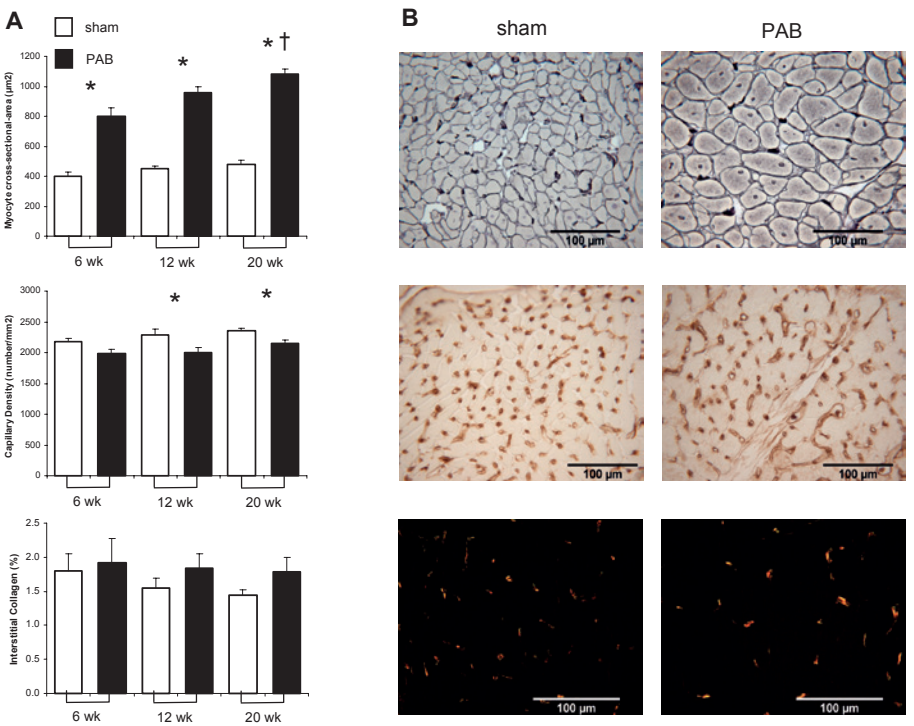

Panel A shows bar graphs representing differences in (from top to bottom) RV myocytes cross-sectional area, capillary density, and interstitial collagen deposition between sham and PAB. Representative tissue sections with the appropriate staining (see methods) are shown in panel B (sham versus PAB).
*p<0.05 versus corresponding control
†p<0.05 change over time; PAB versus sham

Discussion

This present study, together with previous observations, shows that prolonged PAB up to 20 weeks resulted in compensated RV hypertrophy, characterized by enhanced RV systolic function and maintained contractile reserve [5]. Baseline RV diastolic function was impaired but the response to dobutamine stimulation was unaffected. Furthermore, LV systolic function and contractile reserve in general were unaffected. Despite the limited hemodynamic consequences of prolonged PAB, temporal changes were found in several molecular components, potentially compensatory in nature, to preserve systolic and diastolic function of both RV and LV.

RV - Systolic function

In our studies we used relatively load-insensitive measures of contractility to characterize the response of RV and LV to prolonged RV pressure overload induced by PAB. As shown previously, the three indices of systolic function (Figure 1) indicated a similar increase in systolic performance of the RV of PAB animals at baseline [5]. So far, only few investigators have used models of prolonged PAB (>12 weeks) and the extensive hemodynamic analyses, such as presented in this paper, have not previously been performed at different time points after prolonged PAB [16,17].

Several studies have addressed the adaptation of the RV to acute or chronic pressure overload. In acute RV pressure overload, cardiac output was maintained by enhanced RV contractile performance while end-diastolic volumes remained stable [10]. Observations in chronic RV pressure overload are, in general, in line with our study. For example, after 12 weeks of PAB in dogs, cardiac output was maintained and the slope of the ESPVR was three-fold increased [18]. In lambs, after 6 weeks of PAB, RV contractility was enhanced even after correction for RV mass, indicating a hypercontractile state of the RV [19]. In our study, however, RV contractility corrected for mass was increased only after 20 weeks of PAB. The response to dobutamine was unaffected, indicating maintained contractile reserve of the RV up to 20 weeks of PAB. In contrast to our findings, in a study in rats with similar degree of PAB as in our study, LekanneDeprez et al. found heart failure developing after 12 weeks based on clinical signs [17]. Based on those results we extended the PAB up to 20 weeks, but we could not replicate their observations.

Other investigators have used monocrotaline-induced pulmonary hypertension to study the development of (de)compensated RV hypertrophy [20,21]. In many of these studies (severe) RV failure develops after a few weeks [20,22]. Recently, in monocrotaline treated rats developing compensated RV hypertrophy, Hessel et al, found increased RV volumes and unchanged parameters of contractility [21]. The differences in RV contractile performance in the PAB as compared to the monocrotaline model might

be explained by differences in β-adrenergic signalling [21,23,24]. In our study, the RV β_1-AR level as well as the GRK-2 level was decreased after 20 weeks of PAB. In contrast, in monocrotaline induced RV failure in rats, decreased β_1-AR levels and increased GRK-2 levels have been found [23,24]. A simultaneous decrease of β_1-AR and increase of GRK-2 levels, has been implicated in the decreased β-adrenergic signalling in heart failure [25]. In the hypertrophic or senescent heart β-adrenergic signalling could be improved by interventions that reduced the level of GRK-2, while β-adrenergic levels were unaffected [26,27]. Thus, decreasing the level of GRK-2 seems a favourable adaptation to maintain β-adrenergic signalling. We suspect that this is an important compensatory mechanism in our PAB rats, as the responses to adrenergic stimulation were unaffected up to 20 weeks of PAB.

RV - Diastolic function

Early relaxation was prolonged and RV stiffness was increased, indicating an impairment of diastolic function. We used dP/dtmin and tau as early diastolic function parameters and both pointed in the same direction. However, interpretation of these parameters should be done carefully as the dP/dtmin is load-dependent. Similarly, tau is not entirely load-independent and the period of isovolumic relaxation in the RV is less well defined [14,28]. Nevertheless, tau has been used frequently to describe early RV relaxation in animal models, as well as in patients [14,29-31]. In acute RV pressure overload it was shown that RV tau was prolonged and it was suggested that this might be related to the decreased expression of NCX1 [31]. In chronic RV pressure overload a similar impairment of early relaxation, as found in our study, has been shown. For example, after 8 weeks of monocrotaline-induced pulmonary hypertension in dogs a prolonged tau in the RV was found [29]. Similarly, PAB-induced chronic RV pressure overload in lambs also resulted in a prolonged tau [14]. In line with this latter study, we have also analyzed the Tau-Pes (end-systolic pressure) relation at baseline and during dobutamine infusions for the RV and LV, showing that tau decreases less in response to higher end-systolic pressures in the RV of PAB animals (Figure 3). Although catecholaminergic stimulation by dobutamine infusion itself enhances the calcium cycling and hence contributes to increased active relaxation, the differences in response between PAB and sham occurred at same dosages. Therefore, the decreased active relaxation in response to an alteration in load, reflects a true difference in active relaxation in the RV of PAB animals.

Our study further adds to these observations by demonstrating a stable impairment of early relaxation over the entire observation of 20 weeks, but simultaneously demonstrating progressive changes at the molecular level. The expression levels of SERCA2 and PLB in the RV were progressively decreasing, while NCX1 expression

levels progressively increased. The alterations in PLB and NCX1 may be interpreted as a compensatory mechanism to maintain Ca^{2+}-cycling, in the face of a decreased SERCA2 expression. A similar decrease in SERCA2 in combination with signs of impaired relaxation, has been reported in rats with monocrotaline-induced RV hypertrophy [22]. An increase of NCX1 may improve early relaxation, but may also negatively affect contractile function by virtue of underloading of the sarcoplasmic reticulum with Ca^{2+} [32]. However, in small mammals like rats the contribution of NCX1 to the decrease in intracellular [Ca^{2+}] in early diastole is only small and an increase in NCX1 expression therefore may not have such profound effects as in larger mammals [33]. The effects of these changes on Ca^{2+}-transients in our PAB rats are unknown. We interpret the alterations in the Ca^{2+}-handling proteins in our PAB rats as being compensatory and compatible with compensated RV hypertrophy.

Late diastolic function was impaired in PAB animals as reflected by an increased chamber stiffness constant. As a result the RV end-diastolic volume was lower in RV pressure overload. Other studies on chronic RV pressure overload have found similar increases in RV stiffness [14,18]. The results from the morphometric analysis of RV tissues do not indicate significant fibrosis in PAB rats, suggesting that the increased RV mass per se explains the impaired late diastolic function. This is also supported by the observation that the RV EDPVR, when corrected for RV mass, was not increased in PAB animals.

This present study is the first to provide an in-depth analysis of biventricular function over an extended range of durations of PAB. Despite the relatively stable hemodynamics during prolonged RV pressure overload, alterations occur at the molecular level, as shown for β-adrenergic signalling and Ca^{2+}-handling proteins. In addition, we previously demonstrated a time-dependent increase in components of the protein quality control machinery, such as (phosphorylated) heat shock protein 27, as well as alterations in several anti-oxidant enzymes [5]. In rats with monocrotaline-induced RV hypertrophy, the development of congestive heart failure has been specifically associated with the activation of the p38 MAPK pathway [20]. Previously, we demonstrated the p38 MAPK pathway not to be activated in our PAB rats [5]. We speculate that the development of decompensated RV hypertrophy (RV failure) may ensue with a further disruption of, for example, the Ca^{2+}-cycling pathway, the protein quality control machinery, the oxidant/anti-oxidant balance, or activation of the p38-MAPK pathway.

LV - Diastolic function

LV diastolic function remained stable over time. Only after 20 weeks of PAB there was an increase in tau, suggesting impaired early relaxation. At the molecular level,

an increase was found in the NCX1/SERCA2 ratio, which could be related to the prolonged relaxation [34]. However, our hemodynamic data are compatible with only a minor impaired diastolic function and maintained systolic function. Furthermore, during stimulation with catecholamines both diastolic and systolic function further improved in both sham and PAB rats in a similar fashion, suggesting intact Ca^{2+}-cycling. The passive stiffness of the LV was unaltered in our model. This is different from observations by Lamberts et al. who showed an increased stiffness of the LV together with increased collagen depositions in a monocrotaline model of RV hypertrophy [35]. These differences may be related to the degree of hypertrophy, since the LV/body weight and the RV/body weight were approximately 2-fold higher as compared to our study.

Conclusions

This study demonstrates that prolonged RV pressure overload, induced by PAB in rats, leads to compensated hypertrophy, characterized by maintained RV (and LV) systolic function and a slight impairment of diastolic function, that are stable throughout the observation period of 20 weeks. Concurrently, time-dependent alterations occur at the molecular level, for example in the β-adrenergic signalling, Ca^{2+}-handling, the protein quality control machinery, the oxidant/anti-oxidant balance, and the absence of p38-MAPK pathway activation [5]. We suggest that these alterations are necessary for the heart to maintain its function. The progressive nature of these alterations underlines the concept that compensated hypertrophy is not a static situation, but rather is a dynamic, slowly progressive process in which the heart is able to maintain its function by employing compensatory mechanisms. We speculate that the disruption of these compensatory changes at the molecular level may herald the onset of RV failure.

Acknowledgment: We would like to thank Ms. Linda Kievit for her technical assistance with respect to the histological analysis.

References

1. Graham, T. P., Jr. (1991). Ventricular performance in congenital heart disease. Circulation 84, 2259-2274.
2. Slinker, B. K., Chagas, A. C. & Glantz, S. A. (1987). Chronic pressure overload hypertrophy decreases direct ventricular interaction. Am J Physiol 253, H347-357.
3. Brunner, F. (1999). Cardiac endothelin and big endothelin in right-heart hypertrophy due to monocrotaline-induced pulmonary hypertension in rat. Cardiovasc Res 44, 197-206.
4. Faber, M. J., Dalinghaus, M., Lankhuizen, I. M., Steendijk, P., Hop, W. C., Schoemaker, R. G., Duncker, D. J., Lamers, J. M. & Helbing, W. A. (2006). Right- and left ventricular function after chronic pulmonary artery banding in rats assessed with biventricular pressure-volume loops. Am J Physiol Heart Circ Physiol 291, H1580-H1586.
5. Faber, M. J., Dalinghaus, M., Lankhuizen, I. M., Bezstarosti, K., Verhoeven, A. J., Duncker, D. J., Helbing, W. A. & Lamers, J. M. (2007). Time dependent changes in cytoplasmic proteins of the right ventricle during prolonged pressure overload. J Mol Cell Cardiol 43, 197-209.
6. Suga, H. & Sagawa, K. (1974). Instantaneous pressure-volume relationships and their ratio in the excised, supported canine left ventricle. Circ Res 35, 117-126.
7. Glower, D. D., Spratt, J. A., Snow, N. D., Kabas, J. S., Davis, J. W., Olsen, C. O., Tyson, G. S., Sabiston, D. C., Jr. & Rankin, J. S. (1985). Linearity of the Frank-Starling relationship in the intact heart: the concept of preload recruitable stroke work. Circulation 71, 994-1009.
8. Little, W. C. (1985). The left ventricular dP/dtmax-end-diastolic volume relation in closed-chest dogs. Circ Res 56, 808-815.
9. Steendijk, P. & Baan, J. (2000). Comparison of intravenous and pulmonary artery injections of hypertonic saline for the assessment of conductance catheter parallel conductance. Cardiovasc Res 46, 82-89.
10. de Vroomen, M., Cardozo, R. H., Steendijk, P., van Bel, F. & Baan, J. (2000). Improved contractile performance of right ventricle in response to increased RV afterload in newborn lamb. Am J Physiol Heart Circ Physiol 278, H100-105.
11. Kono, A., Maughan, W. L., Sunagawa, K., Hamilton, K., Sagawa, K. & Weisfeldt, M. L. (1984). The use of left ventricular end-ejection pressure and peak pressure in the estimation of the end-systolic pressure-volume relationship. Circulation 70, 1057-1065.
12. Weiss, J. L., Frederiksen, J. W. & Weisfeldt, M. L. (1976). Hemodynamic determinants of the time-course of fall in canine left ventricular pressure. J Clin Invest 58, 751-760.
13. Grossman, W. & Barry, W. H. (1980). Diastolic pressure-volume relations in the diseased heart. Fed Proc 39, 148-155.
14. Leeuwenburgh, B. P., Steendijk, P., Helbing, W. A. & Baan, J. (2002). Indexes of diastolic RV function: load dependence and changes after chronic RV pressure overload in lambs. Am J Physiol Heart Circ Physiol 282, H1350-1358.
15. Faber, M. J., Dalinghaus, M., Lankhuizen, I. M., Bezstarosti, K., Dekkers, D. H., Duncker, D. J., Helbing, W. A. & Lamers, J. M. (2005). Proteomic changes in the pressure overloaded right ventricle after 6 weeks in young rats: correlations with the degree of hypertrophy. Proteomics 5, 2519-2530.
16. Olivetti, G., Ricci, R., Lagrasta, C., Maniga, E., Sonnenblick, E. H. & Anversa, P. (1988). Cellular basis of wall remodeling in long-term pressure overload-induced right ventricular hypertrophy in rats. Circ Res 63, 648-657.
17. LekanneDeprez, R. H., van den Hoff, M. J., de Boer, P. A., Ruijter, P. M., Maas, A. A., Chamuleau, R. A., Lamers, W. H. & Moorman, A. F. (1998). Changing patterns of gene expression in the pulmonary trunk-banded rat heart. J Mol Cell Cardiol 30, 1877-1888.
18. Gaynor, S. L., Maniar, H. S., Bloch, J. B., Steendijk, P. & Moon, M. R. (2005). Right atrial and ventricular adaptation to chronic right ventricular pressure overload. Circulation 112, I212-218.

19. Leeuwenburgh, B. P., Helbing, W. A., Steendijk, P., Schoof, P. H. & Baan, J. (2001). Biventricular systolic function in young lambs subject to chronic systemic right ventricular pressure overload. Am J Physiol Heart Circ Physiol 281, H2697-2704.
20. Buermans, H. P., Redout, E. M., Schiel, A. E., Musters, R. J., Zuidwijk, M., Eijk, P. P., van Hardeveld, C., Kasanmoentalib, S., Visser, F. C., Ylstra, B. & Simonides, W. S. (2005). Microarray analysis reveals pivotal divergent mRNA expression profiles early in the development of either compensated ventricular hypertrophy or heart failure. Physiol Genomics 21, 314-323.
21. Hessel, M. H., Steendijk, P., den Adel, B., Schutte, C. I. & van der Laarse, A. (2006). Characterization of right ventricular function after monocrotaline-induced pulmonary hypertension in the intact rat. Am J Physiol Heart Circ Physiol 291, H2424-2430.
22. Kogler, H., Hartmann, O., Leineweber, K., Nguyen van, P., Schott, P., Brodde, O. E. & Hasenfuss, G. (2003). Mechanical load-dependent regulation of gene expression in monocrotaline-induced right ventricular hypertrophy in the rat. Circ Res 93, 230-237.
23. Leineweber, K., Brandt, K., Wludyka, B., Beilfuss, A., Ponicke, K., Heinroth-Hoffmann, I. & Brodde, O. E. (2002). Ventricular hypertrophy plus neurohumoral activation is necessary to alter the cardiac beta-adrenoceptor system in experimental heart failure. Circ Res 91, 1056-1062.
24. Leineweber, K., Seyfarth, T., Abraham, G., Gerbershagen, H. P., Heinroth-Hoffmann, I., Ponicke, K. & Brodde, O. E. (2003). Cardiac beta-adrenoceptor changes in monocrotaline-treated rats: differences between membrane preparations from whole ventricles and isolated ventricular cardiomyocytes. J Cardiovasc Pharmacol 41, 333-342.
25. Rockman, H. A., Koch, W. J. & Lefkowitz, R. J. (2002). Seven-transmembrane-spanning receptors and heart function. Nature 415, 206-212.
26. MacDonnell, S. M., Kubo, H., Crabbe, D. L., Renna, B. F., Reger, P. O., Mohara, J., Smithwick, L. A., Koch, W. J., Houser, S. R. & Libonati, J. R. (2005). Improved myocardial beta-adrenergic responsiveness and signaling with exercise training in hypertension. Circulation 111, 3420-3428.
27. Leosco, D., Rengo, G., Iaccarino, G., Filippelli, A., Lymperopoulos, A., Zincarelli, C., Fortunato, F., Golino, L., Marchese, M., Esposito, G., Rapacciuolo, A., Rinaldi, B., Ferrara, N., Koch, W. J. & Rengo, F. (2007). Exercise training and beta-blocker treatment ameliorate age-dependent impairment of beta-adrenergic receptor signaling and enhance cardiac responsiveness to adrenergic stimulation. Am J Physiol Heart Circ Physiol 293, H1596-1603.
28. Stein, P. D., Sabbah, H. N., Mazilli, M. & Anbe, D. T. (1980). Effect of chronic pressure overload on the maximal rate of pressure fall of the right ventricle. Chest 78, 10-15.
29. Chen, E. P., Craig, D. M., Bittner, H. B., Davis, R. D. & Van Trigt, P. (1998). Pharmacological strategies for improving diastolic dysfunction in the setting of chronic pulmonary hypertension. Circulation 97, 1606-1612.
30. Maeda, M., Yamakado, T. & Nakano, T. (1999). Right ventricular diastolic function in patients with hypertrophic cardiomyopathy--an invasive study. Jpn Circ J 63, 681-687.
31. Correia Pinto, J., Henriques-Coelho, T., Roncon-Albuquerque, R., Jr. & Leite-Moreira, A. F. (2006). Differential right and left ventricular diastolic tolerance to acute afterload and NCX gene expression in Wistar rats. Physiol Res 55, 513-526.
32. Bers, D. M., Pogwizd, S. M. & Schlotthauer, K. (2002). Upregulated Na/Ca exchange is involved in both contractile dysfunction and arrhythmogenesis in heart failure. Basic Res Cardiol 97 Suppl 1, I36-42.
33. Houser, S. R., Piacentino, V., 3rd, Mattiello, J., Weisser, J. & Gaughan, J. P. (2000). Functional properties of failing human ventricular myocytes. Trends Cardiovasc Med 10, 101-107.
34. Weisser-Thomas, J., Kubo, H., Hefner, C. A., Gaughan, J. P., McGowan, B. S., Ross, R., Meyer, M., Dillmann, W. & Houser, S. R. (2005). The Na+/Ca2+ exchanger/SR Ca2+ ATPase transport capacity regulates the contractility of normal and hypertrophied feline ventricular myocytes. J Card Fail 11, 380-387.
35. Lamberts, R. R., Vaessen, R. J., Westerhof, N. & Stienen, G. J. (2007). Right ventricular hypertrophy causes impairment of left ventricular diastolic function in the rat. Basic Res Cardiol 102, 19-27.

Chapter 7

Cardiac myofilament proteome: determination by reversed phase protein separation

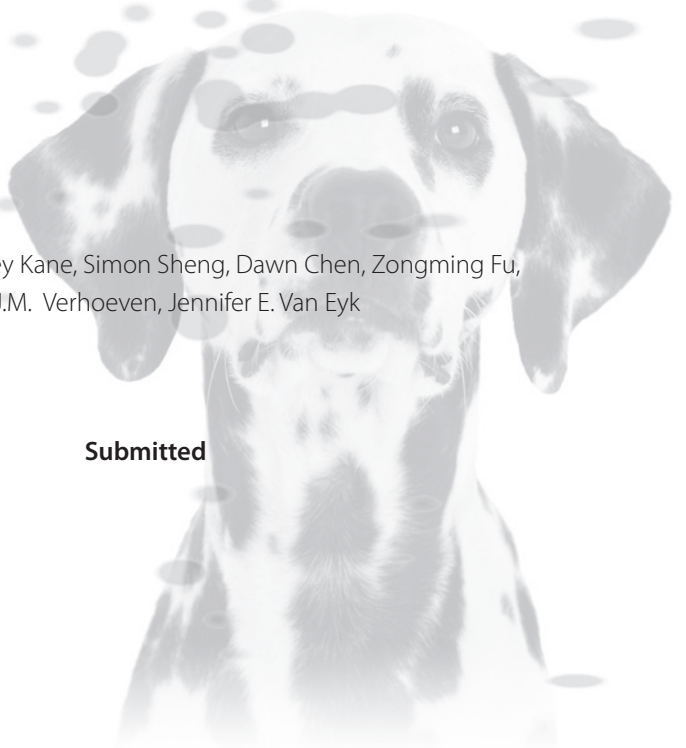

Matthijs J. Faber, Lesley Kane, Simon Sheng, Dawn Chen, Zongming Fu,
Adrie J.M. Verhoeven, Jennifer E. Van Eyk

Submitted

Abstract

Nowadays cardiovascular disease are along the most common causes of morbidity and mortality in the Western world. Increased understanding of the underlying protein changes can be achieved using proteomic technologies. The main component of the cardiomyocyte is the myofilament machinery, responsible for the contractile properties of the heart. Proteomic analysis of the myofilaments is difficult due to intrinsic proterties of these proteins. In this study reverse-phase HPLC was used to determine the myofilament proteome.

First, optimization of the RP-HPLC technique was achieved by testing several solvents and gradients. Second, using HPLC techniques the myofilament proteins were separated from prefractionated rat heart samples and analysed using mass spectrometry. Finally, 122 non-redundant proteins were found including 24 myofilament proteins.

In conclusion, RP-HPLC can be used to separate the myofilament proteins from rat hearts with high reproducibility. Using this method a myofilament subproteome was described. Complementary proteomic techniques are necessary to further increase the protein coverage of the myofilament subproteome.

Introduction

Cardiovascular disease is an important determinant of morbidity and mortality in developed countries. The cardiac proteome is dominated by the myofilaments, which are responsible for the contractile properties of the heart and consists of sarcomeric as well as sarcomere-associated proteins. The thick filaments consist of the myosin heavy and light chains and myosin binding protein C, and the thin filaments are comprised of alpha-actin, F-actin capping protein, tropomyosin (alpha or beta) and the cardiac specific troponin complex (TnI, TnT and TnC) [1-3]. The sarcomere further consists of Z-line proteins, including α-actinin, myozenin, filamin and spectrin,M-line proteins, including M-protein, myomesin and skelemin, and additional proteins responsible for structural integrity of the filaments, including titin and nebulin. Among the sarcomere-associated proteins are the intermediate filaments (e.g. desmins), which link the myofilaments to the plasma membrane and the nucleus [4]. However, a full complement of the myofilamental subproteome has not yet been established.

Analysis of the myofilamental subproteome is notoriously difficult, mainly due to the intrinsic properties of the constituent proteins. Separation on the basis of pI and size by classical two-dimensional electrophoresis (2-DE) has long been the method of choice. However, 2-DE analysis is hampered by the extreme pI values and high molecular weights of many of these proteins. Associated proteins are difficult to identify due to their relatively low abundance. Moreover, many myofilamental proteins do not stain well with the general protein stains used in 2-DE [5, 6]. Nevertheless, several studies have shown changes of myofilamental proteins during heart hypertrophy and heart failure using classical 2-DE analysis [7-10].

Separation of proteins on the basis of hydrophobicity by reverse-phase high performance liquid chromatography (RP-HPLC) has been shown to be a good alternative for 2-DE in determining subcellular proteomes, including the myofilamental proteins from swine hearts [6, 11-13]. In addition RP-HPLC has been shown to be a useful tool in studying troponin crosslinking and identifying a competitive protein antagonist for F-actin [14, 15] . In our study into the effect of pulmonal hypertension on cardiac function in rats, we decided to determine the complement of myofilamental proteins of right ventricular heart tissue. We chose to separate the myofilamental proteins by RP-HPLC before their identification by mass spectrometry. Here, we present an optimized RP-HPLC protocol for rat myofilament proteins, and the detailed myofilament subproteome of the right ventricle generated with this technique.

Methods and Results

Right ventricle (RV) tissue from 28-weeks old male Wistar rats (Harlan, Zeist, The Netherlands) was frozen in liquid N_2 immediately after dissection, and stored at –80ºC until use. The myofilament subproteome was extracted using the "IN Sequence" protocol [6, 16]. In brief, individual RV tissues were homogenized in 20mM HEPES (pH 7.4) and 0.5 mM EDTA, 1 µM leupeptin, 1 µM pepstatin, 0.26 µM aprotinin, 50 mM NaF, 0.2 mM Na_3VO_4, and 0.5 mM PMSF at 4º C at a 1:4 ratio of tissue weight:buffer volume. The whole-tissue homogenate was centrifuged at 4º C for 15 min at 18000g. The pellet was resuspended in 1% aqueous TFA v/v and 0.1% Tris(2-carboxyethyl)-phosphine hydrochloride (initial tissue weight:buffer volume = 1:3) at 4º C. The sample was centrifuged (15 min at 18000g), and the pellet was reextracted with the same buffer. Both supernatants were combined and taken as the myofilament extract. Protein concentrations were determined by BCA protein assay (Pierce). The extracts were stored at -80º C until analysis. Myofilament proteins (0.1mg) were separated on a C8 reverse-phase column (4.6mm id x 76mm, 80 Å pore size, particle size 3µm, Beckman Coulter , Fullerton, CA, USA) with a flow rate of 0.5 mL/min. Protein elution profiles were monitored by extinction at 214 nm. The 32Karat software package (Beckman Coulter) was used to analyse data on an IBM compatible computer.

The reproducibility of column performance was tested by running a mixture of standard proteins (SDS-7, Sigma-Aldrich, St. Louis, MO, USA). The coefficient of variation for the 4 most prominent protein peaks in 6 runs was 0.750.20 % for elution time and 1715% for peak height. To optimize protein separation, a number of different solvent gradient conditions were tested (Table 1 and Figure 1) using the elution profile developed by Neverova as starting point [6]. This consists of a linear 1% per min gradient of B in A followed by C in A at a flow rate of 1.0 mL/min, in which solvent A was 0.05% aqueous TFA, solvent B was 0.05% TFA in isopropanol:ACN (1:9 v/v) and solvent C was 0.05% TFA in acetonitrile. This resulted in poor separation as most of the proteins eluted as a broad peak between 55 and 60 min (Figure 1-A). In addition, the elution profile deteriorated after a few runs and the columns were difficult to recover even by extensive rinsing. The optimal separation was achieved using a linear 0-70 % B gradient in A and a flow rate of 0.5 mL/min, in which solvent A consisted of 0.6% aqueous TFA and solvent B was 0.45 % TFA in ACN (Figure 1-D). To prevent clogging of the column, an extensive column-wash prior to re-equilibration was performed using a 70-100 % linear gradient of solvent C (2% TFA in isopropanol:ACN (1:4 v/v)) in A over 7 min. After each fourth run an additional column rinsing step was performed using a linear 0-70% B in A gradient in 30 min. Using this protocol we separated the myofilament proteins extracted from rat RV tissue (Figure 1).

Table 1: Optimization of reverse-phase HPLC elution profiles

Profile[a]	Solvent			Gradient		Flow characteristics		Resolution [b]
	A	B	C	A-B	A-C	rate (mL/min)	duration (min)	
1	0.05% TFA (aq)	0.05% TFA in isopropanol: ACN 1:9 v/v	0.05% TFA in ACN	0-42%	40-80%	10	90	+/-
2	2% TFA (aq)	2% TFA in ACN	-	0-100%	-	5	30	- -
3	1% TFA (aq)	1% TFA in ACN	-	0-100%	-	5	30.	-
4	0.6% TFA (aq)	0.45% TFA in ACN	-	0-70%	-	5	80	++

[a]: profiles 1 to 4 correspond to elution profiles in Figure 1 A to D, respectively

[b]: resolution was judged from protein profiles, ranging from poor (- -) to good (++)

In three separate runs, the coefficient of variation of 15 major peaks in the elution profile was 0.10 0.05% for retention time, and 13 5% for peak height . Fractions (0.5 ml) were collected and stored at -80ºC until processing. After protein quantitation, the reverse phase fractions (150 L) were concentrated using a SpeedVac (Thermo Scientific, Waltham, MA, USA) to 5-10 L. NH_4HCO_3 (1 M) was added to the residue to pH 8.0. After addition of sequencing grade modified trypsin (Promega, Madison, WI) at a 1:50 enzyme to substrate ratio, the sample was incubated overnight at 37 ºC. The digestion was stopped by addition of TFA [13]. Subsequently, the digests were analyzed using a LTQ ion trap MS/MS instrument (Thermo Finnigan, San Jose, CA, USA) at the Johns Hopkins Proteomics Core Facility. The data obtained from the MS spectra were searched using the NCBI database using the Mascot Deamon search engine (Matrix Science Mascot Daemon, V2.2.0; maximal 2 missed cleavages; peptide and MS/MS tolerance 1.5 Da and 0.8 Da, respectively; common posttranslational modifications; $p < 0.05$). In addition, for Mascot result validation, the raw datafiles were uploaded to the Proteomics Analyzer Software System (PASS, Integrated Analysis Inc).

In three independent runs, 124 non redundant proteins were identified (supplement Table 1). Of these proteins, roughly 20 % belongs to the functional category of myofilament- and cytoskeleton-associated proteins (Figure 2). More than 50 % of the proteins were of mitochondrial and nuclear origin, which may reflect contamination of the myofilament extracts or may be due to the interaction of these organelles with myofilaments, either directly or via the intermediate filaments [17]. Yet, this method of separation allowed coverage of many of the sarcomere proteins (Table 2)

including proteins which are difficult to separate by 2DE because of their high MW, such as titin. Of the major sarcomere proteins, notably of actin and myosin light chain, several isoforms exists with a high degree of sequence similarity (Table 2). For each of these proteins at least two unique peptides were identified in the tryptic digest. In addition, post-translational modifications were found at several peptides for most of the identified proteins (supplement Table 1).

Figure 1: Optimization of reverse-phase HPLC myofilament protein separation

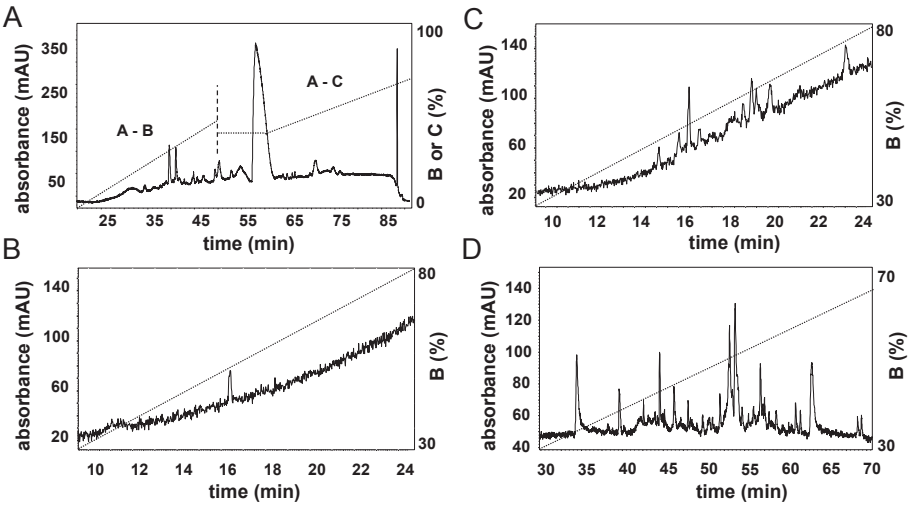

The elution profiles A-D were achieved by using the gradients described in Table 1, profile 1-4 respectively.

Discussion

In this study, we have first separated the myofilamental from the cytoplasmic proteins according to the "IN sequence" protocol. This extraction procedure dramatically reduced complexity of the myofilament extract relative to the whole RV proteome. The subsequent HPLC analysis not only revealed many abundant sarcomeric proteins, but also relatively low abundant proteins such as PDZ and LIM domain 5 and nesprin isoforms. Besides sarcomere proteins, intermediate filaments were found together with mitochondrial proteins. The presence of this latter group of proteins might be explained by the linkage of intermediate filaments such as desmin and vimentin with the mitochondrial apparatus [4, 18, 19]. Previously, we have reported on the rat RV myofilament subproteome based on 2-DE analysis but with a slightly different prefractionation protocol [7]. Many proteins identified with the 2-DE analysis were also found by HPLC, but the latter technique led to the identification of many additional proteins. Interestingly, the desmin proteins identified with the 2-DE method were not

found with HPLC. McDonald et al. previously showed a strikingly low overlap between subproteomes derived by 2-DE and HPLC separation, and concluded that both techniques are complementary in achieving full protein coverage of subproteomes [13]. In addition, other studies also showed that parallel proteomics is needed to improve coverage of the proteome [20, 21].

In conclusion, we have shown that RP-HPLC can be used to fractionate the myofilamental proteins from rat hearts with high reproducibility and is suitable for subsequent mass spectrometry analysis. With this method, we have described the myofilamental subproteome of right ventricles from adult rats. However, complementary proteomic techniques are necessary to further increase the protein coverage of the myofilament subproteome. This method may prove useful in the detection and quantification of protein changes in various forms of cardiac disease.

The supplementary data (Table1S) associated with this chapter can be found under the Appendix at the end of this chapter

Figure 2: Number of non-redundant proteins identified in the rat RV myofilamental extract.

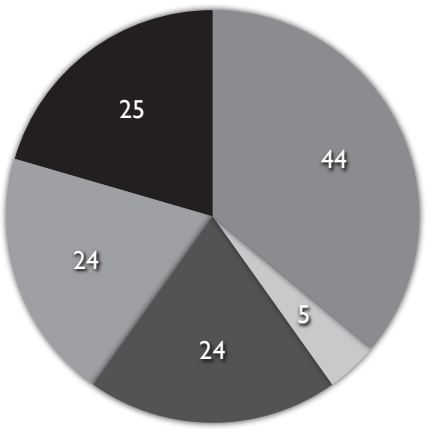

44 Nuclear/transcription/translation/cell-cycle-related proteins + signaling
5 Protection/heat shock/oxygen stress-related proteins
24 Other/unknown
24 Myofilament/intermediate filament/motility systems
25 Mitochondrial and metabolic proteins

Table 2: Myofilament protein list

Accession #	Protein Name	Found PTMs	Protein Weight[a]	Protein Length[b]	Avg Unique Peptides	Total SC[c]
Q8N0Z2	Actin-binding Rho-activating protein	carbamidomethyl (C),oxidation (M),Other PTM	43117	381	2	2
P68032	Actin, alpha cardiac muscle 1	oxidation (M),Other PTM	42019	377	17	38
P68133	Actin, alpha skeletal muscle	oxidation (M),phosphorylation (T),Other PTM	42051	377	6	6
B2RPJ1	Actin, beta-like 2	carbamidomethyl (C),oxidation (M),dioxidation (M),Other PTM	42003	376	4	4
Q59FD9	Actinin, alpha 2 variant	Other PTM	76998	664	3	3
Q9UQV1	Alpha-myosin heavy chain	oxidation (M),phosphorylation (S),phosphorylation (Y),Other PTM	3676	32	72	100
A8TX70	Collagen alpha-5(VI) chain		289926	2615	2	2
Q8TD57	Dynein heavy chain 3, axonemal		470771	4116	3	3
Q9P0U8	Extraocular myosin heavy chain	oxidation (M),phosphorylation (S),Other PTM	19224	167	4	4
Q6ZR29	Furry homolog-like protein.	oxidation (M),phosphorylation (S),phosphorylation (T),Other PTM	160155	1433	3	3
Q2M1N2	Laminin, gamma 2	carbamidomethyl (C),Other PTM	121634	1111	2	2
Q7Z3Z1	Myosin light chain 2	oxidation (M),dioxidation (M),Other PTM	18732	165	9	62
P08590	Myosin light chain 3	oxidation (M),Other PTM	21932	195	18	61
P12829	Myosin light chain 4		21565	197	2	2
P12882	Myosin-1	Other PTM	223145	1939	3	3
Q9UKX2	Myosin-2	phosphorylation (S),Other PTM	223044	1941	2	2

Q8NF91	Nesprin-1	carbamidomethyl (C),oxidation (M),oxidation (W),phosphorylation (S),phosphorylation (T),phosphorylation (Y),dioxidation (M),Other PTM	1011028	8797	10	14
Q8WXH0	Nesprin-2	carbamidomethyl (C),phosphorylation (S)	796442	6885	2	2
Q8WVK0	PDZ and LIM domain 5	oxidation (M)	23823	214	2	3
Q8WZ42	Titin	oxidation (M)	3816188	34350	6	3
P09493	Tropomyosin alpha-1 chain	carbamidomethyl (C),oxidation (M),dioxidation (M),Other PTM	32709	284	13	40
P63316	Troponin C, slow skeletal and cardiac muscles	oxidation (M),dioxidation (M),Other PTM	18403	161	6	8
P48787	Troponin I, cardiac muscle	oxidation (M),Other PTM	24259	211	5	13
P45379	Troponin T, cardiac muscle	dioxidation (M),Other PTM	35924	298	10	14

Myofilament protein list. [a] *protein weight in Daltons;* [b] *Protein length in amino acids;* [c] *Total sequence coverage (SC, %)*

References

1. Solaro, R.J. and H.M. Rarick, Troponin and tropomyosin: proteins that switch on and tune in the activity of cardiac myofilaments. Circ Res, 1998. 83(5): p. 471-80.
2. Solaro, R.J. and J. Van Eyk, Altered interactions among thin filament proteins modulate cardiac function. J Mol Cell Cardiol, 1996. 28(2): p. 217-30.
3. Gordon, A.M., E. Homsher, and M. Regnier, Regulation of contraction in striated muscle. Physiol Rev, 2000. 80(2): p. 853-924.
4. Capetanaki, Y., et al., Muscle intermediate filaments and their links to membranes and membranous organelles. Exp Cell Res, 2007. 313(10): p. 2063-76.
5. Labugger, R., et al., Solubilization, two-dimensional separation and detection of the cardiac myofilament protein troponin T. Proteomics, 2002. 2(6): p. 673-8.
6. Neverova, I. and J.E. Van Eyk, Application of reversed phase high performance liquid chromatography for subproteomic analysis of cardiac muscle. Proteomics, 2002. 2(1): p. 22-31.
7. Faber, M.J., et al., Proteomic changes in the pressure overloaded right ventricle after 6 weeks in young rats: correlations with the degree of hypertrophy. Proteomics, 2005. 5(10): p. 2519-30.
8. Heinke, M.Y., et al., Protein changes observed in pacing-induced heart failure using two-dimensional electrophoresis. Electrophoresis, 1998. 19(11): p. 2021-30.
9. Weekes, J., et al., Bovine dilated cardiomyopathy: proteomic analysis of an animal model of human dilated cardiomyopathy. Electrophoresis, 1999. 20(4-5): p. 898-906.
10. Thiede, B., et al., Identification of human myocardial proteins separated by two-dimensional electrophoresis with matrix-assisted laser desorption/ionization mass spectrometry. Electrophoresis, 1996. 17(3): p. 588-99.
11. Tripet, B., J.E. Van Eyk, and R.S. Hodges, Mapping of a second actin-tropomyosin and a second troponin C binding site within the C terminus of troponin I, and their importance in the Ca2+-dependent regulation of muscle contraction. J Mol Biol, 1997. 271(5): p. 728-50.
12. Van Eyk, J.E., et al., Distinct regions of troponin I regulate Ca2+-dependent activation and Ca2+ sensitivity of the acto-S1-TM ATPase activity of the thin filament. J Biol Chem, 1997. 272(16): p. 10529-37.
13. McDonald, T., et al., Expanding the subproteome of the inner mitochondria using protein separation technologies: one- and two-dimensional liquid chromatography and two-dimensional gel electrophoresis. Mol Cell Proteomics, 2006. 5(12): p. 2392-411.
14. Brown, J.W. and C.J. McKnight, Identifying competitive protein antagonists for F-actin with reverse-phase high-performance liquid chromatography. Anal Biochem. 398(1): p. 117-9.
15. Warren, C.M., T. Kobayashi, and R.J. Solaro, Sites of intra- and intermolecular cross-linking of the N-terminal extension of troponin I in human cardiac whole troponin complex. J Biol Chem, 2009. 284(21): p. 14258-66.
16. Kane, L.A., I. Neverova, and J.E. Van Eyk, Subfractionation of heart tissue: the "in sequence" myofilament protein extraction of myocardial tissue. Methods Mol Biol, 2007. 357: p. 87-90.
17. Cooper, G.t., Cytoskeletal networks and the regulation of cardiac contractility: microtubules, hypertrophy, and cardiac dysfunction. Am J Physiol Heart Circ Physiol, 2006. 291(3): p. H1003-14.
18. Paulin, D. and Z. Li, Desmin: a major intermediate filament protein essential for the structural integrity and function of muscle. Exp Cell Res, 2004. 301(1): p. 1-7.
19. Tang, H.L., et al., Vimentin supports mitochondrial morphology and organization. Biochem J, 2008. 410(1): p. 141-6.
20. Gundry, R.L., et al., Expanding the mouse embryonic stem cell proteome: combining three proteomic approaches. Proteomics. 10(14): p. 2728-32.
21. White, M.Y., et al., Parallel proteomics to improve coverage and confidence in the partially annotated Oryctolagus cuniculus mitochondrial proteome. Mol Cell Proteomics. 10(2): p. M110 004291.

Appendix. Table 1 Supplement: Non-redundant protein list

Protein Name	Found PTMs	Protein Weight (Daltons)	Protein Length (# AA)	Avg Unique Peptides	Category
16 kDa protein	phosphorylation (S),phosphorylation (T)	–	156	3	unknown
18 kDa protein		–	147	2	unknown
24 kDa protein		–	211	2	unknown
252 kDa protein	oxidation (M)	–	2274	3	unknown
40S ribosomal protein S6		28681	249	2	cell cycle
52 kDa protein		–	447	3	unknown
60S ribosomal protein L27	oxidation (M),Other PTM	15798	136	2	cell cycle
Actin, alpha cardiac muscle 1	oxidation (M),Other PTM	42019	377	17	myofilament
Actin, alpha skeletal muscle	oxidation (M),phosphorylation (T),Other PTM	42051	377	6	myofilament
Actin, beta-like 2	carbamidomethyl (C),oxidation (M),dioxidation (M),Other PTM	42003	376	4	myofilament
Actin-binding Rho-activating protein	carbamidomethyl (C),oxidation (M),Other PTM	43117	381	2	myofilament
Actinin, alpha 2 variant	Other PTM	76998	664	3	myofilament
Adenosine deaminase domain-containing protein 2	carbamidomethyl (C),oxidation (M),phosphorylation (S),phosphorylation (Y),Other PTM	61755	583	2	mitochondrial/ metabolic
ADP-ribosylation factor-like protein 6-interacting protein 4		38395	360	2	mitochondrial/ metabolic
Aldehyde oxidase 1	carbamidomethyl (C),oxidation (M),phosphorylation (T),phosphorylation (Y),dioxidation (M),Other PTM	147918	1338	4	mitochondrial/ metabolic
Alpha-myosin heavy chain	oxidation (M),phosphorylation (S),phosphorylation (Y),Other PTM	3676	32	72	myofilament
Antigen NY-CO-43	phosphorylation (S),Other PTM	38859	366	2	unknown

Protein Name	Found PTMs	Protein Weight (Daltons)	Protein Length (# AA)	Avg Unique Peptides	Category
ATP synthase subunit alpha, mitochondrial	oxidation (M),Other PTM	59751	553	6	mitochondrial/ metabolic
ATP synthase subunit beta, mitochondrial	oxidation (M),dioxidation (M),Other PTM	56300	529	10	mitochondrial/ metabolic
ATP synthase subunit O, mitochondrial	phosphorylation (S),phosphorylation (T),Other PTM	23277	213	3	mitochondrial/ metabolic
BTBD2 protein	oxidation (M)	37152	333	2	signaling
Calcium channel, voltage-dependent, alpha 1E subunit variant	carbamidomethyl (C),phosphorylation (T),Other PTM	211937	1869	2	signaling
cDNA FLJ11129 fis, clone PLACE1006239, weakly similar to BONE PROTEOGLYCAN II		30832	273	2	signaling
cDNA FLJ16750 fis, clone ADRGL2011190, highly similar to cGMP-dependent 3',5'-cyclic phosphodiesterase (EC 3.1.4.17)	oxidation (M),dioxidation (M),Other PTM	78177	685	2	mitochondrial/ metabolic
cDNA FLJ54686, highly similar to Homo sapiens Rho GTPase activating protein 21 (ARHGAP21), mRNA	phosphorylation (S),phosphorylation (Y),Other PTM	136250	1217	2	mitochondrial/ metabolic
cDNA FLJ57602, highly similar to Creatine kinase M-type (EC 2.7.3.2)	phosphorylation (S),phosphorylation (T),Other PTM	29941	267	2	mitochondrial/ metabolic
CHD4 protein		39182	355	3	signaling
Chromatin assembly factor 1 subunit A	carbamidomethyl (C),oxidation (M),Other PTM	106926	956	2	signaling
Chromodomain-helicase-DNA-binding protein 6	phosphorylation (S),phosphorylation (T),Other PTM	305412	2715	3	signaling
Citrate synthase, mitochondrial	oxidation (M),Other PTM	51712	466	2	mitochondrial/ metabolic
Collagen alpha-5(VI) chain		289926	2615	2	myofilament
Collectin-12	oxidation (M),dioxidation (M)	81525	742	2	heat shock

Conserved hypothetical protein	oxidation (M),phosphorylation (S),phosphorylation (T)	0	60	2	unknown
Creatine kinase S-type, mitochondrial	dioxidation (M),Other PTM	47504	419	5	mitochondrial/ metabolic
Cytochrome c	Other PTM	3196	28	3	mitochondrial/ metabolic
Death-inducer obliterator 1	oxidation (M)	243873	2240	2	signaling
Docking protein 3	carbamidomethyl (C)	53288	496	2	heat shock
Dynein heavy chain 3, axonemal		470771	4116	3	myofilament
E3 ubiquitin-protein ligase UBR4		573841	5183	2	heat shock
Egf-like module containing, mucin-like, hormone receptor-like sequence 2 isoform e variant	carbamidomethyl (C),oxidation (M)	89233	810	2	signaling
Elongation factor 1-alpha 2		50470	463	2	signaling
Extraocular myosin heavy chain	oxidation (M),phosphorylation (S),Other PTM	19224	167	4	myofilament
FBL protein		28449	260	2	signaling
Fructose-bisphosphate aldolase	Other PTM	39371	364	3	mitochondrial/ metabolic
Furry homolog-like protein.	oxidation (M),phosphorylation (S),phosphorylation (T),Other PTM	160155	1433	3	myofilament
HEATR1 protein		39921	349	4	signaling
High-mobility group box 2	oxidation (M),Other PTM	23905	208	2	signaling
HIRA-interacting protein 3	Other PTM	61957	556	2	signaling
Histone H1.2		21365	213	4	cell cycle
Histone H1.5		22580	226	3	cell cycle
Histone H2A	Other PTM	14135	130	6	cell cycle
Histone H2B type 1-M	oxidation (M),Other PTM	13989	126	13	cell cycle
Histone H2B type 1-N	oxidation (M),oxidation (W),Other PTM	13922	126	6	cell cycle

Protein Name	Found PTMs	Protein Weight (Daltons)	Protein Length (# AA)	Avg Unique Peptides	Category
Histone H2B type 2-E	oxidation (M)	13920	126	2	cell cycle
Histone H4	oxidation (M)	4916	43	4	cell cycle
Histone-lysine N-methyltransferase, H3 lysine-79 specific	phosphorylation (T),Other PTM	184853	1739	2	cell cycle
hypothetical protein LOC646960	carbamidomethyl (C),phosphorylation (S)	0	541	2	unknown
hypothetical protein XP_002342432	phosphorylation (Y),Other PTM	0	100	2	unknown
Hypothetical rhabdomyosarcoma antigen MU-RMS-40.3	phosphorylation (S),dioxidation (M),Other PTM	109361	941	3	unknown
IPI00883770	carbamidomethyl (C),phosphorylation (S)			2	unknown
KCTD2 protein		27443	245	2	signaling
Laminin, gamma 2	carbamidomethyl (C),Other PTM	121634	1111	2	myofilament
Long-chain-fatty-acid--CoA ligase ACSBG2	carbamidomethyl (C),oxidation (M)	74326	666	2	mitochondrial/ metabolic
Malate dehydrogenase	oxidation (M)	33229	316	4	mitochondrial/ metabolic
Methyl-CpG-binding domain protein 4	carbamidomethyl (C),oxidation (M),phosphorylation (S),Other PTM	66051	580	2	signaling
Multidrug and toxin extrusion protein 2		65085	602	2	unknown
Myosin light chain 2	oxidation (M),dioxidation (M),Other PTM	18732	165	9	myofilament
Myosin light chain 3	oxidation (M),Other PTM	21932	195	18	myofilament
Myosin light chain 4		21565	197	2	myofilament
Myosin-1	Other PTM	223145	1939	3	myofilament
Myosin-2	phosphorylation (S),Other PTM	223044	1941	2	myofilament
MYT1 protein	oxidation (M),oxidation (W),phosphorylation (S),Other PTM	92117	846	3	cell cycle

Nephrin		134742	1241	2	unknown
Nesprin-1	carbamidomethyl (C),oxidation (M),oxidation (W),phosphorylation (S),phosphorylation (T),phosphorylation (Y),dioxidation (M),Other PTM	1011028	8797	10	myofilament
Nesprin-2	carbamidomethyl (C),phosphorylation (S)	796442	6885	2	myofilament
Neuropeptide FF receptor 2		60270	522	2	signaling
Nik-related protein kinase	phosphorylation (S),phosphorylation (Y),Other PTM	178479	1582	2	signaling
ORF protein	oxidation (M)	59966	570	2	signaling
p120	oxidation (M),phosphorylation (Y),Other PTM	19911	191	2	unknown
PDZ and LIM domain 5	oxidation (M)	23823	214	2	myofilament
PHD finger protein 2		120775	1096	2	signaling
PIK4CA variant protein		238697	2121	2	mitochondrial/ metabolic
POTE ankyrin domain family member E	oxidation (M),Other PTM	121363	1075	2	unknown
PRO2179	carbamidomethyl (C),oxidation (M)	15609	140	2	unknown
Probable methylcytosine dioxygenase TET3	carbamidomethyl (C),Other PTM	179350	1660	2	mitochondrial/ metabolic
Protein SMG8	carbamidomethyl (C),oxidation (M),Other PTM	109684	991	2	signaling
PTPRM protein	carbamidomethyl (C),Other PTM	156937	1390	2	mitochondrial/ metabolic
Putative RNA-binding protein 15	phosphorylation (S),Other PTM	107189	977	2	signaling
Putative uncharacterized protein DKFZp313C0640	phosphorylation (T),phosphorylation (Y),Other PTM	44353	403	2	unknown
Putative uncharacterized protein DKFZp434K213	carbamidomethyl (C),phosphorylation (S),Other PTM	120893	1059	5	unknown
Putative uncharacterized protein DKFZp761D171	Other PTM	87359	793	2	unknown

Protein Name	Found PTMs	Protein Weight (Daltons)	Protein Length (# AA)	Avg Unique Peptides	Category
Putative uncharacterized protein ENSP00000382190	carbamidomethyl (C),phosphorylation (S),Other PTM	14910	135	2	unknown
Putative uncharacterized protein LOC152225	carbamidomethyl (C),oxidation (M),Other PTM	10763	95	2	unknown
Putative zinc finger protein 75C	phosphorylation (S),Other PTM	49753	426	2	cell cycle
Ras-like protein family member 11B		27508	248	2	signaling
Rhabdomyosarcoma antigen MU-RMS-40.7B	oxidation (M),phosphorylation (S),phosphorylation (Y),Other PTM	137191	1179	31	unknown
RNA-binding motif protein X-linked-like 1 (Kynurenine aminotransferase III) (Protein RBM1).	phosphorylation (S)	42142	390	2	cell cycle
Sacsin	carbamidomethyl (C)	521126	4579	2	heat shock
Semaphorin-5A	carbamidomethyl (C),oxidation (M),Other PTM	120615	1074	3	signaling
Serine/threonine-protein kinase WNK1	oxidation (M)	250756	2382	2	mitochondrial/ metabolic
Sestrin-3	oxidation (M),Other PTM	57291	492	2	signaling
SH3 and multiple ankyrin repeat domains protein 3		186295	1741	2	signaling
Short heat shock protein 60 Hsp60s2	oxidation (M)	27096	258	2	heat shock
Similar to AFG3 ATPase family gene 3-like 2 (Yeast)	phosphorylation (S)	90194	812	3	mitochondrial/ metabolic
SLIT-ROBO Rho GTPase-activating protein 1	carbamidomethyl (C),oxidation (M),phosphorylation (S),phosphorylation (T),phosphorylation (Y),Other PTM	124264	1085	2	mitochondrial/ metabolic
Sorting nexin-29	Other PTM	48338	428	2	signaling
Splicing factor U2AF 35 kDa subunit	carbamidomethyl (C),oxidation (M),phosphorylation (T),phosphorylation (Y),Other PTM	27872	240	4	signaling

Succinate dehydrogenase complex, subunit A, flavoprotein variant	carbamidomethyl (C),oxidation (M),phosphorylation (S),Other PTM	73176	670	2	mitochondrial/ metabolic
Synaptotagmin-like protein 3	phosphorylation (S),phosphorylation (T),Other PTM	68560	610	2	signaling
TATA-binding protein-associated factor 2N		61830	592	2	cell cycle
Testis-expressed sequence 10 protein	carbamidomethyl (C),Other PTM	105674	929	2	unknown
Thyroid peroxidase	oxidation (M)	102963	933	2	mitochondrial/ metabolic
Titin	oxidation (M)	3816188	34350	6	myofilament
Trifunctional enzyme subunit beta, mitochondrial		51294	474	3	mitochondrial/ metabolic
Tropomyosin alpha-1 chain	carbamidomethyl (C),oxidation (M),dioxidation (M),Other PTM	32709	284	13	myofilament
Troponin C, slow skeletal and cardiac muscles	oxidation (M),dioxidation (M),Other PTM	18403	161	6	myofilament
Troponin I, cardiac muscle	oxidation (M),Other PTM	24259	211	5	myofilament
Troponin T, cardiac muscle	dioxidation (M),Other PTM	35924	298	10	myofilament
U4/U6.U5 tri-snRNP-associated protein 1		90255	800	2	cell cycle
Ubiquitin carboxyl-terminal hydrolase 34	carbamidomethyl (C),oxidation (M),phosphorylation (S),phosphorylation (T),phosphorylation (Y),dioxidation (M),Other PTM	404233	3546	7	mitochondrial/ metabolic
Uncharacterized protein C8orf41		56915	508	2	unknown
Zinc finger homeobox protein 2	carbamidomethyl (C),oxidation (W)	152101	1427	3	signaling

Chapter 8

General Discussion

Discussion

RV pressure overload may be the clinical consequence of (repaired or palliated) congenital heart disease, pulmonary hypertension or chronic pulmonary disease. The RV differs from the LV with regard to embryology, genetics, anatomy, coronary circulation, contraction pattern and the basic role in the circulation [1-4]. In this thesis we have described the hemodynamic alterations that occur after prolonged RV pressure overload. We have used biventricular PV-loops to describe baseline hemodynamics, such as ventricular pressure and volume, as well as contractile function using several parameters. Combined with dobutamine stimulation this allowed relatively load-independent assessment of ventricular function and reserve [5-7]. In addition, proteomic technologies were used to study concomitant protein alterations.

Our results indicate that in response to prolonged pressure overload, the RV hypertrophies by increasing the mass of the RV free wall. Systolic RV function at baseline is increased as measured by end-systolic elastance (Ees) and is further enhanced during catecholaminergic stimulation. Furthermore, both early and late diastolic RV function is affected. This is demonstrated by prolongation of early relaxation, as measured by tau and dP/dt_{min}, as well as an increased passive stiffness, as measured by the late phase of the end-diastolic pressure-volume relationship.

In addition, LV mass and both its systolic and diastolic function are unimpaired after prolonged RV pressure overload. Finally, throughout the observation of 20 weeks of pressure overload, the hemodynamic responses did not change much. At the protein level, distinct changes were found, including alterations in metabolic- and stress related proteins.

Hemodynamic response to prolonged RV pressure overload

The effect of increased RV afterload on the development of RV hypertrophy and RV failure has been studied under various experimental conditions.

The first approach that has been used is banding of the pulmonary artery, similar to the approach described in this thesis [7-10]. From these studies we have learned that an acute increase of afterload on the RV is tolerated as long as RV systolic pressure is not increased to more than approximately 60% of systemic pressure [11]. Higher pressure loads have led to acute ventricular failure and unacceptably high mortality [12]. Interestingly, this is quite compatible with observations in patients with congenital heart disease, where acutely increasing the pressure load upon the subpulmonary ventricle (either with right or left ventricular morphology) to higher levels leads to ventricular failure and /or the need for debanding [13, 14].

The adaptation to an acute increase of RV afterload is through homeometric autoregulation, with an increase in end-diastolic and end-systolic volume [15, 16].

Prolonged pressure overload induced by pulmonary artery banding (PAB) leads to a hypertrophic response of the RV. In the studies that have used a similar approach as described in this thesis, i.e. one-time banding and allowing animals "to grow into their banding", have generally led to RV peak systolic pressure at subsystemic levels. Other investigators, that have used adjustable bands around the pulmonary artery, allowing the RV systolic pressure to be gradually increased over time, have generally reached near-systemic peak-systolic pressures in the RV. Irrespective of the approach used, the data from these banding studies are all compatible with our results. There is a vigorous hypertrophic response from the RV, almost exclusively by an increased mass of the free wall of the RV, while the interventricular septum and the LV free wall mass are unaffected [17, 18]. The contractile function of the RV is generally well maintained with a 3-4-fold increase of Ees in baseline conditions when PAB was maintained for up to 12 weeks using various animal models including rats, lambs and dogs [7, 9, 18, 19]. In those instances where contractile reserve was studied, all studies have demonstrated a further (modest) increase of Ees [7, 18]. Collectively these responses, which we also demonstrated in our studies, indicate that in most instances of prolonged RV pressure overload compensated RV hypertrophy will develop. In some cases the increase in Ees was out of proportion in relation to the increase in RV mass, suggesting a hypercontractile state of the RV, but this has not been a consistent finding in all studies [7]. Only few studies have described the clinical signs of heart failure after PA banding. In one such study in rats clinical signs of heart failure developed after 20 weeks of PA banding, but invasive hemodynamic measurements were not obtained [10]. Based on that study we included the group with 20 weeks of PA banding, expecting to obtain failure and to characterise hemodynamic and protein changes that accompany the transition from compensated hypertrophy to failure. However, we were unable to replicate these findings.
The effects of the increased RV afterload on RV and LV volumes differ somewhat in the various studies. In some studies, like ours, a decrease in RV and LV end-diastolic volumes has been found, while other studies described an moderate increase in these volumes [7, 20]. However, severe dilatation of either RV of LV is not a normal finding after PA banding.

A second approach that has been widely used by investigators, primarily interested in pulmonary arterial hypertension, is monocrotaline induced pulmonary arterial hypertension. In general, two different responses have been described in these studies. The first is an increase in pulmonary arterial pressure with the development of a compensated state of right ventricular hypertrophy. The second response is a progressive increase in pulmonary artery pressure with the development of severe

right heart failure and death within a few weeks. The differential responses seem to be dose-related with dosages up to 30-40 mg/kg leading to a compensated state and higher dosages, generally 60-80 mg/kg leading to a decompensated state and RV failure [21-24].
In all studies there is a vigorous RV hypertrophic response with an increase RV free wall mass, while the interventricular septum and LV free wall are unaffected. The increase in RV mass is higher in animals developing RV failure.
In most studies RV peak-systolic pressure remains at subsystemic level, irrespective of the development of compensated or decompensated RV hypertrophy. Only a few studies addressed the hemodynamic adjustments in this model in some more detail. In contrast to the results of our studies, Hessel et al. demonstrated that in monocrotaline-treated rats, end-systolic and end-diastolic volumes progressively increased, as compared to controls, dependant on whether compensated or decompensated RV hypertrophy developed [24]. Furthermore, baseline Ees of the RV, both in the compensated as well as in the decompensated state, was not increased as compared to controls, whereas this is normally found in all banding studies. In isolated RV myocardial trabeculae from rats showing clinical signs of heart failure the force generated at baseline was increased, but the force frequency response was grossly abnormal. Furthermore, the contractile response to catecholaminergic stimulation was decreased [22].

The third approach that has been used is (simulated) high-altitude to induce pulmonary arterial hypertension. This not only exposes the right ventricle to an increased afterload, but also to the effects of arterial hypoxemia [25-30]. In many of these studies the differential effects of hypoxemia alone (upon the LV) and of hypoxemia and pressure load (upon the RV) have been studied. Many studies have addressed research questions regarding capillary density and biochemical or molecular adaptations. However, extensive hemodynamic characterization has usually not been performed, apart from characterization of the RV pressure response.

Prolonged pressure overload upon the RV also induced alterations in diastolic function, indicating that the RV became less compliant. In our study early relaxation, a process dependant on Ca^{2+} re-uptake in the sarcoplasmatic reticulum, was prolonged in the pressure overloaded RV. Even though early relaxation improved during catecholaminergic stimulation, suggesting that Ca^{2+}-cycling was enhanced in these conditions, it was still slower than in normal RV under catecholaminergic stimulation. A decrease in early relaxation has also been observed after PA banding in lambs [31] and after monocrotaline-induced RV hypertrophy in dogs [32]. Global diastolic function

was impaired in RV trabeculae from rats with RV failure after monocrotaline treatment [22]. Similarly, late diastolic function was impaired in these studies as well as in the rats in our study. In our study fibrosis was excluded as an important cause of late diastolic impairment, but our analysis suggested the increased RV mass as an important cause for the diastolic dysfunction.

The effect of RV hypertrophy on LV mass, volumes and function seem to be negligible. Most studies using one of the three above-mentioned approaches have failed to demonstrate significant interference with LV behaviour.

Molecular alterations following prolonged RV pressure overload

As presented in this thesis, many protein alterations occur over time when the RV is subjected to increased afterload [19, 33]. The majority of these changes were related to cardiac metabolism. In general, a shift of proteins related to carbohydrate metabolism and away from fatty acid was observed suggesting a shift towards carbohydrates as preferred energy source. This shift in energy metabolism has already been well documented in LV hypertrophy [34-38]. Earlier, Takeyama reported that glucose uptake is increased in the RV in a model of acute (4 weeks PAB) RV pressure overload [39]. This shift may be the result of an increased energy demand associated with increased workload.

A second set of protein changes in RV hypertrophy included the stress- and antioxidant proteins. These heat shock proteins are known to play a role in adaptation processes to various forms of stress and have a cytoprotective function [40]. We have shown that several stress proteins are upregulated in the early phase of RV hypertrophy (ie. 6 weeks PAB) [33]. This enhanced expression continued throughout the study period of 20 weeks PAB and included the presence of multiple posttranslational modifications [19]. These posttranslational modifications, such as phosphorylation, are thought to be essential for their protective roles [41-43]. For instance, the phosphorylation of HSP-27 has been suggested to play an important role in maintaining the microfilament integrity in response to oxidative stress. In our studies, HSP-27 was found to be upregulated in the hypertrophied RV. In addition, the HSP-27 was found to be phosphorylated at different residues [19]. Several studies have shown the activation of heat shock proteins in the stressed RV. Rafiee et al. studied the expression of the inducible heat shock protein 70 (Hsp-70) in cardiac (right atrium) tissue of children undergoing corrective surgery for cardiac birth defects [44]. One of the main results was the 4-5 fold elevation of Hsp-70 levels in the hearts of children with cyanotic heart disease, while the levels of constitutive Hsp70 were unaffected. Similar results were obtained in their hypoxic animal model, where rabbits were exposed to hypoxia after

birth for a period of 10 days. The presence of selective regulation of HSP levels in the adaptive response to hypoxia-induced stress was also shown in cultured myocytes [42]. Brar et al. showed that selective over expression of HSP by transfection of plasmid constructs in vitro and in vivo resulted in protection against apoptosis-inducing stimuli as well as hypoxic stress [45].

The upstream signalling pathway for HSP-27 phosphorylation includes the MAPK pathway [42, 46]. In our study we found that after 6 wk of RV pressure overload, the levels of p-38 MAPK and its phosphorylated form were similar between controls and PAB animals [19]. After 20 weeks of PAB these levels were slightly decreased, despite the increased HSP-27 transcription, suggesting that another pathway is also involved in HSP-27 transcription and phosphorylation. In addition, the absence of p-38 MAPK activation in our model correlates with the observations done by Buermans et al. [23]. Their study involved prolonged RV pressure overload induced by monocrotaline in rats. The RV with compensated hypertrophy did not show p-38 MAPK activation whereas the RV with signs of hemodynamic failure did. On the other hand, studies on p-38 MAPK signalling in hypoxic hearts revealed early activation of this pathway [42, 47]. Together with our observations, these data suggest that other pathways are involved in HSP-27 phosphorylation. For instance, the protein kinase C-δ pathway has been known to play a role in the development of pathological hypertrophy and has been shown to be activated both in RV and LV pressure overload [48-50]. Furthermore, protein kinase C-δ has been shown to phosphorylate HSP-27 proteins independent of the p38-MAPK pathway [51]. Additional studies are needed to determine the role of the different upstream signalling pathways in (pathological) RV hypertrophy.

Furthermore, changes in cardiac myofilament proteome can be an important part of adaptation to prolonged increased afterload. Conventional proteomic techniques, such as 2-DE protein separation, may not be able to study these changes properly [52]. New techniques, including reversed phase protein separation may be useful techniques for this purpose.

Development of compensated RV hypertrophy versus RV failure.

In order to understand how RV failure develops, one may wonder what the difference between the various experimental approaches is. Why does RV failure almost never develop in PA banding and why is it so common after exposure to high-dose monocrotaline? One possible explanation is that investigators are just not patient enough to await RV failure to develop. In both PA banding and (simulated) high altitude studies, some reports can be identified where failure developed after prolonged exposure to increased RV afterload [8, 10].

In monocrotaline induced pulmonary arterial hypertension and, Buermans et al

demonstrated that treatment with high-dose monocrotaline was associated with early activation of the p38-MAPK pathway, even before the development of RV failure. In contrast, in rats with treated with low-dose monocrotaline, developing compensated RV hypertrophy, p38-MAPK was deactivated by MKP-1, a MAPK specific phosphatase [53]. These authors suggested the development of pathological hypertrophy was predetermined by the activation of the p38-MAPK pathway even before heart failure developed.

In monocrotaline-induced pulmonary arterial hypertension it is generally believed that the active form of the alkaloid, after hepatic conversion, only reaches the pulmonary microvasculature and induces a local vasculitis. However, a recent study demonstrated that vascular responses are also observed in the coronary circulation, suggesting that a monocrotaline-induced vascular response in the RV myocardium might contribute to the development of RV failure [53].

Other investigators have suggested that the development of heart failure in response to pressure overload may be related to a mismatch between the degree of hypertrophy and neo-angiogenesis in the affected myocardium. In this way myocyte oxygen demand may exceed oxygen delivery, thus leading to persistent oxidative stress. In such circumstances the cellular anti-oxidant mechanisms, that we demonstrated to be up-regulated during compensated hypertrophy, may be overwhelmed and activation of intracellular pathways leading to pathological hypertrophy and apoptosis may ensue [54].

In a recent study van de Bogaard et al. demonstrated that the development of RV failure was associated with abnormal capillary formation and with increased RV fibrosis [8]. The loss of capillaries in the failing RV myocardium, that was only seen after the combined exposure to hypoxia and a VEGF receptor blocker, was associated with increased HIF-1α signalling, but decreased VEGF-signalling. These responses were not encountered after pulmonary artery banding and capillary density was maintained in the RV after PA banding. Their observations after PA banding are similar to the results of our study. Furthermore, these authors demonstrated that various dietary interventions that interfered with defence mechanisms against oxidative stress could induce the development of RV failure. Conversely, interventions that boosted defence mechanisms could prevent the development of RV failure [8].

Similar observations have been obtained in the pressure overloaded left ventricle. In experimentally induced LV hypertrophy the development of pathological LV hypertrophy and failure was attenuated or prevented after treatment that enhanced angiogenesis [55-58].

We suspect that RV failure is almost never seen in experimental studies where PA banding is applied, because the acute increase in RV pressure that is tolerated during the banding procedure, leads to a favourable balance between local oxygen demand and supply. This will allow a favourable adjustment at cellular level, like we have demonstrated in our studies. In the experimental model we used the potential interference with coronary angiogenesis from toxic substances, that may be present in other models, is lacking. For the application of our results to many forms of congenital heart disease, it must be borne in mind that pressure overload upon the RV often has been present from birth on and/or increases only gradually. Cyanosis may be an integral part of congenital heart disease and pressure overload upon the RV. Studies in infant humans and rabbits have suggested that the presence of cyanosis may induce further protective adjustments against oxidative stress in the myocardium [44, 47]. Others have suggested that the transcription of pathways of adaptive remodeling was lower in the RV compared with the LV in different types of congenital heart disease with outflow obstruction [4]. Further studies are needed to clarify the role of different mechanisms in the right ventricle related to adaptation to increased afterload and hypoxemia.

Clinical implications

RV pressure overload may be the clinical consequence of (repaired or palliated) congenital heart disease, pulmonary hypertension or chronic pulmonary disease.

For patients with pure (congenital) pulmonary valve stenosis the long-term outcome is generally good, although the natural history of moderate to severe obstruction is generally modified by intervention [59]. Residual obstruction in the RV outflow tract may be a consequence of repaired or palliated complex congenital heart disease, like for example Tetralogy of Fallot, transposition of the great arteries or more complex lesions. In many instances residual lesions induce combined pressure and volume loads upon the right ventricle. The presence and severity of symptoms of heart failure in adults with congenital heart disease correlates with neurohumoral levels, but also with signs of abnormal left heart and right heart function [60]. However, isolated RV systolic failure as a cause of heart failure is rare in these complex lesions. We suspect, therefore, that the alterations in the proteome of the pressure overloaded RV in our rats, improving the ability to withstand increased oxidative stress is also relevant for patient with residual pressure overload upon their RV.

Another aspect of the adjustment to RV pressure overload is the effect on diastolic function. The decrease in both early and late diastolic function in experimental studies of RV pressure overload has been a consistent finding. This may lead to either a decrease in RV end-diastolic volume, as in our study, or an increase in diastolic filling

pressures. Furthermore, the results of our study indicate that an abnormal structure of the RV, for example by increased fibrosis, may not be necessary for the presence of the diastolic dysfunction. Rather, our results suggest that the abnormalities in the late diastolic function of the RV are a direct consequence of an increased RV mass. This may limit the possibility for therapeutical interventions to improve diastolic function, other than by reducing RV mass.

The consequences for the diastolic dysfunction of the RV on systemic output may not be so clear at rest, but may become relevant during exercise. In our experimental set-up, RV end-diastolic volume and stroke volume decreased during catecholaminergic stimulation, and cardiac output did not increase. Although effects of dobutamine stimulation are not similar to the effects of physical stress in patients, , our experiments suggest that limitation of cardiac output in patients with RV hypertrophy may be a consequence of the diastolic rather than the systolic dysfunction.

References

1. Moorman, A.F., et al., The heart-forming fields: one or multiple? Philos Trans R Soc Lond B Biol Sci, 2007. 362(1484): p. 1257-65.
2. Haber, I., et al., Three-dimensional systolic kinematics of the right ventricle. Am J Physiol Heart Circ Physiol, 2005. 289(5): p. H1826-33.
3. Torrado, M., et al., Identification of candidate genes potentially relevant to chamber-specific remodeling in postnatal ventricular myocardium. J Biomed Biotechnol. 2010: p. 603159.
4. Kaufman, B.D., et al., Genomic profiling of left and right ventricular hypertrophy in congenital heart disease. J Card Fail, 2008. 14(9): p. 760-7.
5. Baan, J., E.T. van der Velde, and P. Steendijk, Ventricular pressure-volume relations in vivo. Eur Heart J, 1992. 13 Suppl E: p. 2-6.
6. Steendijk, P., et al., Effects of critical coronary stenosis on global systolic left ventricular function quantified by pressure-volume relations during dobutamine stress in the canine heart. J Am Coll Cardiol, 1998. 32(3): p. 816-26.
7. Leeuwenburgh, B.P., et al., Biventricular systolic function in young lambs subject to chronic systemic right ventricular pressure overload. Am J Physiol Heart Circ Physiol, 2001. 281(6): p. H2697-704.
8. Bogaard, H.J., et al., Chronic pulmonary artery pressure elevation is insufficient to explain right heart failure. Circulation, 2009. 120(20): p. 1951-60.
9. Gaynor, S.L., et al., Right atrial and ventricular adaptation to chronic right ventricular pressure overload. Circulation, 2005. 112(9 Suppl): p. I212-8.
10. LekanneDeprez, R.H., et al., Changing patterns of gene expression in the pulmonary trunk-banded rat heart. J Mol Cell Cardiol, 1998. 30(9): p. 1877-88.
11. Hon, J.K., et al., Influence of clenbuterol treatment during six weeks of chronic right ventricular pressure overload as studied with pressure-volume analysis. J Thorac Cardiovasc Surg, 2001. 122(4): p. 767-74.
12. Vlahakes, G.J., K. Turley, and J.I. Hoffman, The pathophysiology of failure in acute right ventricular hypertension: hemodynamic and biochemical correlations. Circulation, 1981. 63(1): p. 87-95.
13. Wernovsky, G., et al., Course in the intensive care unit after 'preparatory' pulmonary artery banding and aortopulmonary shunt placement for transposition of the great arteries with low left ventricular pressure. Circulation, 1992. 86(5 Suppl): p. II133-9.
14. Ilbawi, M.N., et al., Preparation of the left ventricle for anatomical correction in patients with simple transposition of the great arteries. Surgical guidelines. J Thorac Cardiovasc Surg, 1987. 94(1): p. 87-94.
15. de Vroomen, M., et al., Improved contractile performance of right ventricle in response to increased RV afterload in newborn lamb. Am J Physiol Heart Circ Physiol, 2000. 278(1): p. H100-5.
16. De Vroomen, M., et al., Enhanced systolic function of the right ventricle during respiratory distress syndrome in newborn lambs. Am J Physiol Heart Circ Physiol, 2001. 280(1): p. H392-400.
17. Lindpaintner, K., D.D. Lund, and P.G. Schmid, Effects of chronic progressive myocardial hypertrophy on indexes of cardiac autonomic innervation. Circ Res, 1987. 61(1): p. 55-62.
18. Faber, M.J., et al., Right- and left ventricular function after chronic pulmonary artery banding in rats assessed with biventricular pressure-volume loops. Am J Physiol Heart Circ Physiol, 2006. 291: p. H1580-H1586.
19. Faber, M.J., et al., Time dependent changes in cytoplasmic proteins of the right ventricle during prolonged pressure overload. J Mol Cell Cardiol, 2007. 43(2): p. 197-209.

20. Yerebakan, C., et al., Acute and chronic response of the right ventricle to surgically induced pressure and volume overload--an analysis of pressure-volume relations. Interact Cardiovasc Thorac Surg. 10(4): p. 519-25.
21. Jones, J.E., et al., Serial noninvasive assessment of progressive pulmonary hypertension in a rat model. Am J Physiol Heart Circ Physiol, 2002. 283(1): p. H364-71.
22. Kogler, H., et al., Mechanical load-dependent regulation of gene expression in monocrotaline-induced right ventricular hypertrophy in the rat. Circ Res, 2003. 93(3): p. 230-7.
23. Buermans, H.P., et al., Microarray analysis reveals pivotal divergent mRNA expression profiles early in the development of either compensated ventricular hypertrophy or heart failure. Physiol Genomics, 2005. 21(3): p. 314-23.
24. Hessel, M.H., et al., Characterization of right ventricular function after monocrotaline-induced pulmonary hypertension in the intact rat. Am J Physiol Heart Circ Physiol, 2006. 291(5): p. H2424-30.
25. Clark, D.R. and P. Smith, Capillary density and muscle fibre size in the hearts of rats subjected to stimulated high altitude. Cardiovasc Res, 1978. 12(10): p. 578-84.
26. Lemler, M.S., et al., Myocyte cytoskeletal disorganization and right heart failure in hypoxia-induced neonatal pulmonary hypertension. Am J Physiol Heart Circ Physiol, 2000. 279(3): p. H1365-76.
27. Nakanishi, K., et al., Changes in atrial natriuretic peptide and brain natriuretic peptide associated with hypobaric hypoxia-induced pulmonary hypertension in rats. Virchows Arch, 2001. 439(6): p. 808-17.
28. Birot, O.J., et al., Vascular endothelial growth factor expression in heart of rats exposed to hypobaric hypoxia: differential response between mRNA and protein. J Cell Physiol, 2004. 200(1): p. 107-15.
29. Chouabe, C., et al., Effects of aging on the cardiac remodeling induced by chronic high-altitude hypoxia in rat. Am J Physiol Heart Circ Physiol, 2004. 287(3): p. H1246-53.
30. La Padula, P. and L.E. Costa, Effect of sustained hypobaric hypoxia during maturation and aging on rat myocardium. I. Mechanical activity. J Appl Physiol, 2005. 98(6): p. 2363-9.
31. Leeuwenburgh, B.P., et al., Indexes of diastolic RV function: load dependence and changes after chronic RV pressure overload in lambs. Am J Physiol Heart Circ Physiol, 2002. 282(4): p. H1350-8.
32. Chen, E.P., et al., Pharmacological strategies for improving diastolic dysfunction in the setting of chronic pulmonary hypertension. Circulation, 1998. 97(16): p. 1606-12.
33. Faber, M.J., et al., Proteomic changes in the pressure overloaded right ventricle after 6 weeks in young rats: correlations with the degree of hypertrophy. Proteomics, 2005. 5(10): p. 2519-30.
34. Bishop, S.P. and R.A. Altschuld, Increased glycolytic metabolism in cardiac hypertrophy and congestive failure. Am J Physiol, 1970. 218(1): p. 153-9.
35. Taegtmeyer, H. and M.L. Overturf, Effects of moderate hypertension on cardiac function and metabolism in the rabbit. Hypertension, 1988. 11(5): p. 416-26.
36. Schwartz, K., et al., Switches in cardiac muscle gene expression as a result of pressure and volume overload. Am J Physiol, 1992. 262(3 Pt 2): p. R364-9.
37. Feldman, A.M., et al., Selective changes in cardiac gene expression during compensated hypertrophy and the transition to cardiac decompensation in rats with chronic aortic banding. Circ Res, 1993. 73(1): p. 184-92.
38. Buttrick, P.M., et al., Alterations in gene expression in the rat heart after chronic pathological and physiological loads. J Mol Cell Cardiol, 1994. 26(1): p. 61-7.
39. Takeyama, D., et al., Effects of chronic right ventricular pressure overload on myocardial glucose and free fatty acid metabolism in the conscious rat. Cardiovasc Res, 1995. 29(6): p. 763-7.

40. Snoeckx, L.H., et al., Heat shock proteins and cardiovascular pathophysiology. Physiol Rev, 2001. 81(4): p. 1461-97.
41. Huot, J., et al., HSP27 phosphorylation-mediated resistance against actin fragmentation and cell death induced by oxidative stress. Cancer Res, 1996. 56(2): p. 273-9.
42. Kacimi, R., et al., Hypoxia differentially regulates stress proteins in cultured cardiomyocytes: role of the p38 stress-activated kinase signaling cascade, and relation to cytoprotection. Cardiovasc Res, 2000. 46(1): p. 139-50.
43. Eaton, P., et al., AlphaB crystallin translocation and phosphorylation: signal transduction pathways and preconditioning in the isolated rat heart. J Mol Cell Cardiol, 2001. 33(9): p. 1659-71.
44. Rafiee, P., et al., Cellular redistribution of inducible Hsp70 protein in the human and rabbit heart in response to the stress of chronic hypoxia: role of protein kinases. J Biol Chem, 2003. 278(44): p. 43636-44.
45. Brar, B.K., et al., Heat shock proteins delivered with a virus vector can protect cardiac cells against apoptosis as well as against thermal or hypoxic stress. J Mol Cell Cardiol, 1999. 31(1): p. 135-46.
46. Guay, J., et al., Regulation of actin filament dynamics by p38 map kinase-mediated phosphorylation of heat shock protein 27. J Cell Sci, 1997. 110 (Pt 3): p. 357-68.
47. Rafiee, P., et al., Activation of protein kinases in chronically hypoxic infant human and rabbit hearts: role in cardioprotection. Circulation, 2002. 106(2): p. 239-45.
48. Braun, M.U., et al., Differential regulation of cardiac protein kinase C isozyme expression after aortic banding in rat. Cardiovasc Res, 2002. 56(1): p. 52-63.
49. Braun, M.U., et al., Right ventricular hypertrophy and apoptosis after pulmonary artery banding: regulation of PKC isozymes. Cardiovasc Res, 2003. 59(3): p. 658-67.
50. Sabri, A. and S.F. Steinberg, Protein kinase C isoform-selective signals that lead to cardiac hypertrophy and the progression of heart failure. Mol Cell Biochem, 2003. 251(1-2): p. 97-101.
51. Maizels, E.T., et al., Heat-shock protein-25/27 phosphorylation by the delta isoform of protein kinase C. Biochem J, 1998. 332 (Pt 3): p. 703-12.
52. Neverova, I. and J.E. Van Eyk, Application of reversed phase high performance liquid chromatography for subproteomic analysis of cardiac muscle. Proteomics, 2002. 2(1): p. 22-31.
53. Akhavein, F., et al., Decreased left ventricular function, myocarditis, and coronary arteriolar medial thickening following monocrotaline administration in adult rats. J Appl Physiol, 2007. 103(1): p. 287-95.
54. Dorn, G.W., 2nd, Myocardial angiogenesis: its absence makes the growing heart founder. Cell Metab, 2007. 5(5): p. 326-7.
55. Shiojima, I., et al., Disruption of coordinated cardiac hypertrophy and angiogenesis contributes to the transition to heart failure. J Clin Invest, 2005. 115(8): p. 2108-18.
56. Sano, M., et al., p53-induced inhibition of Hif-1 causes cardiac dysfunction during pressure overload. Nature, 2007. 446(7134): p. 444-8.
57. Friehs, I., et al., Vascular endothelial growth factor prevents apoptosis and preserves contractile function in hypertrophied infant heart. Circulation, 2006. 114(1 Suppl): p. I290-5.
58. Friehs, I., et al., Promoting angiogenesis protects severely hypertrophied hearts from ischemic injury. Ann Thorac Surg, 2004. 77(6): p. 2004-10; discussion 2011.
59. Hayes, C.J., et al., Second natural history study of congenital heart defects. Results of treatment of patients with pulmonary valvar stenosis. Circulation, 1993. 87(2 Suppl): p. I28-37.
60. Bolger, A.P., A.J. Coats, and M.A. Gatzoulis, Congenital heart disease: the original heart failure syndrome. Eur Heart J, 2003. 24(10): p. 970-6.

Chapter 9

Summary

Samenvatting

Summary

This thesis describes studies on the effects of prolonged right ventricular (RV) pressure-overload on hemodynamics as well as protein changes. In **Chapter 1**, the rationale for this research project is presented. Congenital heart disease is a common birth defect with great impact on morbidity and mortality in children. The ongoing improvement in surgical techniques has led to an increased survival of children with certain congenital heart anomalies. In addition, death resulting from congenital heart disease is shifting from newborns towards (young) adults. In a selected group of these patients, such as Tetralogy of Fallot, left hypoplastic heart syndrome or congenitally corrected transposition of the great vessels, the RV is subjected to increased loading conditions. In addition, other diseases such as pulmonary hypertension or even ischemic heart disease can result in increased RV pressure overload. The effects of prolonged RV pressure overload on the heart's function, as well as the effects on molecular and cellular level is not yet fully understood.

One way to study changes at molecular level is the use of proteomics technologies. Proteomics is the study of the proteome, ie. the entire set of proteins expressed by a genome, cell, tissue or organism. **Chapter 2** describes the different proteomics technologies and strategies and its implementation in the study of cardiac hypertrophy and failure.

In **Chapter 3** an animal model of RV hypertrophy as a result of pulmonary artery banding (PAB) is presented. Besides basic hemodynamic measurements a proteomics approach was used to study the protein alterations in compensated RV hypertrophy (after 6 weeks of PAB). Cytoplasmic protein changes were observed including a shift in metabolism from fatty acids to glucose as a substrate for energy supply. In addition, upregulation of heat-shock protein (HSP) 27 was found in the hypertrophied RV, indicating an altered stress response. Proteomic analysis of the myofilament proteins showed upregulation of desmin and α-β-crystallin.

In **Chapter 4** we report the biventricular adaptation to 6 weeks of PAB. In this study biventricular pressure-volume loops were obtained in our rat model. With the help of these invasive measurements many hemodynamic parameters could be obtained. These include basic parameters such as pressure, volume, and heart rate, as well as load-independent measures of contractility, such as the end-systolic pressure-volume relation. In general, systemic hemodynamic parameters were not altered and overt signs of heart failure were absent. RV contractility was enhanced in the PAB rats. In addition, dobutamine stimulation revealed preserved RV contractile reserve,

supporting the concept that 6 weeks of PAB in our model leads to a compensated state of RV hypertrophy.

As our initial studies focussed on the development of the RV hypertrophy model and the use of biventricular pressure-volume loops as well as the application of proteomics technologies, the next two studies were aimed at capturing the transition from compensated to decompensated RV hypertrophie, ie. heart failure. Therefore we extended the duration of PAB to 12 and 20 weeks.
Chapter 5 describes the longitudinal protein alterations in the cytoplasmic fraction. Basic hemodynamic measurements however revealed that the RV is still in a compensated state after 20 weeks of PAB. Nevertheless, many differentially regulated proteins were found including metabolism related proteins as well as stress proteins including HSP-27 en peroxiredoxin species. The observed protein changes are likely part of a protective mechanism against the development of RV failure.

In parallel to the proteomics studies, hemodynamic characterization was performed. **Chapter 6** describes changes in systolic and diastolic function during prolonged PAB (up to 20 weeks), as well as molecular alterations. In the hypertrophied RV, the systolic function of the RV and the left ventricle was maintained. Diastolic (RV) function, which was measured using the end-diastolic pressure-volume relation and tau, was impaired in the early and late phase of diastole but remained stable throughout the observation period. The RV hemodynamic alterations were linked to alterations in several molecular components of the Ca^{2+} cycling and β_1-adrenergic signalling as well as the degree of fibrosis. We suggest that these alterations are necessary for the heart to maintain its function. The progressive nature of these alterations underlines the concept that compensated hypertrophy is not a static situation, but rather is a dynamic, slowly progressive process in which the heart is able to maintain its function by employing compensatory mechanisms.

The contractile properties of the heart ultimately are based on the myofilament machinery that is present in the cardiomyocyte. Alterations in the myofilaments is therefore likely to have its effects on cardiac function. The study of myofilament protein alterations using proteomics technologies is difficult due to the intrinsic properties of these proteins. In **Chapter 7** we present a method for myofilament protein separation using reversed-phase high performance liquid chromatography. The optimization and reproducibility is presented, as well as myofilament subproteome.

In **Chapter 8** the main findings from the preceding chapters were summarized and placed in a broader context. Clinical implications are also discussed.

Samenvatting

Dit proefschrift beschrijft studies over de effecten van langdurige rechter hartkamer (RV) druk overbelasting op de hemodynamiek alsmede de veranderingen in eiwitten. In **Hoofdstuk 1** wordt de achtergrond van het onderzoek beschreven. Aangeboren hartafwijkingen komen frequent voor en hebben derhalve gevolgen voor de morbiditeit en mortaliteit bij kinderen. Dankzij nieuwe en verbeterde chirurgische methoden is er sprake van een betere overleving bij kinderen met bepaalde aangeboren hartafwijkingen. Daarnaast zien we dat overlijden ten gevolge van een aangeboren hartafwijking meer aan het verschuiven is van pas geborenen naar (jonge) volwassenen. In een bepaalde groep van deze patiënten, zoals kinderen met een Tetralogie van Fallot, hypoplastisch linkerhart syndroom of congenitaal gecorrigeerde transpositie van de grote vaten, staat de RV bloot aan hogere drukken dan de normale situatie. Ook andere ziekten zoals pulmonale hypertensie of soms zelf ischemische hartziekten kunnen leiden tot een hogere drukbelasting van de RV. Wat het precieze effect is van de druk overbelasting op de functie van het hart alsmede de effecten op cellulair en moleculair niveau is nog niet volledig bekend.

Een methode om veranderingen op moleculair niveau te bestuderen is het zogenaamde proteomics onderzoek. Proteomics is de studie van het proteoom, dat wil zeggen de studie naar alle eiwitten die voortkomen uit het genoom en die aanwezig zijn in een cel, weefsel of organisme. **Hoofdstuk 2** beschrijft de verschillende proteomics technieken en strategieën en de toepassing daarvan in onderzoek naar hart hypertrofie en falen.

In **Hoofdstuk 3** presenteren we een diermodel met RV hypertrofie ten gevolge van het plaatsen van een bandje om de pulmonaal arterie (PAB). Naast basale hemodynamische metingen werden proteomics technieken gebruikt om eiwitveranderingen in gecompenseerde RV hypertrofie in kaart te brengen (na 6 weken PAB). Er werden veranderingen gevonden in verschillende cytoplasmatische eiwitten waaronder veranderingen in eiwitten betrokken bij het metabolisme. Een verschuiving in energie substraten, van vetzuren naar glucose, werd gevonden. Daarnaast werden er aanwijzingen gezien voor een veranderde stress reactie in de hypertrofische RV gezien de verhoogde aanwezigheid van heat-shock proteïne (HSP) 27. De analyse van myofilament eiwitten liet een toename zien van desmine en α-β-crystalline.

In **Hoofdstuk 4** beschrijven we de adaptatie van beide hartkamers na 6 weken PAB. In deze studie werden druk-volume relaties verkregen in ons diermodel. Dankzij deze invasieve metingen konden diverse hemodynamische parameters worden verkregen

zoals de basale parameters druk, volume en hart frequentie. Ook konden (belasting-onafhankelijke) parameters geëxtraheerd worden die iets zeggen over de contractilteit van het hart, zoals de eind-systolische druk-volume relatie. In het algemeen werden na 6 weken PAB geen veranderingen gezien in de basale hemodynamische parameters. Ook werden geen duidelijke klinische tekenen van hartfalen gezien. De contractiliteit was echter verhoogd in de hypertrofische RV. Na stimulatie met dobutamine bleef de contractiliteitsreserve gehandhaafd. Dit ondersteunt de gedacht dat 6 weken PAB leidt tot een gecompenseerde staat van RV hypertrofie.

Deze voorgaande studies richtten zich meer op de ontwikkeling van het diermodel en het gebruik van druk-volume relaties en de toepassing van proteomics technieken. De volgende studies waren meer gericht op het bestuderen van het overgangspunt van gecompenseerde hypertrofie naar hart falen. Om dit te bewerkstelligen werd de duur van PAB uitgebreid naar 12 en 20 weken. **Hoofdstuk 5** beschrijft longitudinale veranderingen in eiwitten in de cytoplasmatische fractie. Ondanks de uitbreiding van de PAB naar 12 en 20 weken laten basale hemodynamische metingen zien dat de RV nog steeds in een gecompenseerde hypertrofische toestand verkeert. Ondanks deze observatie zien we toch dat er meerdere eiwitveranderingen optreden welke tijdsafhankelijk zijn. Er werden oa. veranderingen gevonden in eiwitten betrokken bij het metabolisme alsmede stress eiwitten zoals HSP-27 en peroxiredixine. Deze eiwitveranderingen maken mogelijk deel uit van een beschermend mechanisme tegen de ontwikkeling van hartfalen.

Naast de proteomics studies werd ook uitgebreid gekeken naar de hemodynamische veranderingen. **Hoofdstuk 6** beschrijft veranderingen in systolische en diastolische functie ten gevolge van langdurige PAB (tot 20 weken), alsmede veranderingen op moleculair niveau. De systolische functie van de RV en de linker hartkamer blijft intact na langdurige PAB. De diastolische functie, zoals weergegeven door de eind-diastolische druk-volume relatie en de tau, is echter afgenomen in zowel de vroege als late fase van de diastole. De geobserveerde veranderingen in RV hemodynamiek werden gekoppeld aan veranderingen in verschillende componenten van calcium huishouding en β_1-adrenerge signaaltransductie alsmede de mate van fibrosering in het hart. Wij denken dat al deze veranderingen nodig zijn voor het hart om zijn functie te waarborgen. Veel van deze veranderingen in eiwitten zijn progressief of tijdsafhankelijk. Dit onderstreept het concept dat gecompenseerde hypertrofie niet een statische toestand is maar juist een dynamisch, langzaam progressief proces waarbij het hart allerlei compensatie mechanismen inzet om zijn functie te behouden.

De contractiele eigenschappen van het hart zijn uiteindelijk gebaseerd op de myofilament eiwitten welke de basis vormen van het contractiliteitsapparaat in de hartspiercellen. Veranderingen in deze eiwitten hebben derhalve dus effect op de functie van het hart. Het bestuderen van myofilament eiwitten gebruikmakend van de proteomics technieken is lastig vanwege de eigenschappen van deze eiwitten. In **Hoofdstuk 7** presenteren we een methode waarbij we myofilament eiwitten bestuderen gebruikmakend van zogenaamde "reversed-phase" vloeistof chromatografie. De optimalisatie en reproduceerbaarheid worden besproken. Ook word een myofilament subproteoom gepresenteerd.

In **Hoofdstuk 8** zijn de belangrijkste bevindingen uit de voorgaande hoofdstukken samengevat en in een bredere context geplaatst. Daarnaast wordt er aandacht gegeven aan de klinische implicatie van dit onderzoek.

Appendix

Dankwoord

Curriculum Vitae

Dankwoord

Het aloude adagium "promoveren doe je niet alleen" is zonder meer waar. Graag zou ik op deze plek een aantal mensen willen bedanken voor hun bijdrage.

Allereerst Prof.dr. W.A. Helbing, beste Wim, hartelijk dank dat je mij de mogelijkheid hebt gegeven om te werken aan dit fantastische project. Ik denk een mooi begin van het basale wetenschappelijk onderzoek binnen de kindercardiologie in Rotterdam. De discussies over de onderzoeksopzet, de resultaten en ook klinische implicatie heb ik erg kunnen waarderen. Fijn dat je me altijd de mogelijkheid hebt geboden om ons werk (inter)nationaal te presenteren.

Prof.dr. J.M.J. Lamers, beste Jos, hartelijk dank dat ik de mogelijkheid heb gekregen om in jouw lab te mogen werken aan het proteomics gedeelte. Na je trainingsrondje van 10-tallen kilometers in de ochtend was je immer bereidt om samen te discussiëren over ons werk. Je inspiratie en motivatie hebben mij zeker geholpen. Helaas ben je door noodlottige omstandigheden niet in staat geweest om het laatste stukje wetenschap mee te maken. Ik hoop van harte dat je wel aanwezig kunt zijn bij de verdediging.

Dr. M. Dalinghaus, beste Michiel, ontzettend veel dank voor je niet-aflatende steun in de reis die promoveren heet. Je was altijd nauw betrokken bij de voortgang en ontwikkelingen. De discussies over druk-volume relaties maar zeker ook de proteomics zijn voor mij zeer nuttig geweest. Dank voor je geduld.

Prof.dr. D.J.G.M. Duncker, beste Dirk, hartelijk dank voor het beschikbaar stellen van een deel van je lab om onze experimenten uit te voeren. Geweldig om te zien hoe je steeds weer, vol enthousiasme en inspiratie, een frisse blik kon werpen op onze studies. Dank ook voor het zitting nemen in de kleine commissie, het beoordelen van mijn proefschrift en je deelname aan de oppositie.

Graag wil ik de overige leden van de kleine commissie, Prof.dr. D. Tibboel en Prof.dr. J.W. Roos-Hesselink, bedanken voor het beoordelen van het manuscript.

Dr. A. Verhoeven, beste Adrie, bedankt dat je in de laatste fase van mijn boekje bereidt bent geweest om mee te denken. Met name je inzet voor het HPLC werk heb ik erg gewaardeerd.

Ook de overige leden van de grote commissie, Prof.dr. I.K.M. Reiss, Prof.dr. A.J. Van der Heijden, Prof.dr. R.M.F. Berger en Prof.dr. W.S. Simonides wil ik van harte bedanken voor hun deelname aan de oppositie.

Dr. P. Steendijk, beste Paul, hartelijk dank voor je inhoudelijke maar ook technische ondersteuning (Circlab) bij onze P-V studies. Fijn dat je altijd bereid was om mee te denken.

The Baltimore group:
Prof. J.E. Van Eyk, dear Jenny, thanks so much for having me around in your lab. Your enthousiasm and hospitality are incredible. Simon Sheng, thanks for your technical assistance with all the RP-HPLC, 2D-LC and Mass spectrometry equipment. Thanks to all other lab members for helping me around.

Inge Lankhuizen, mijn steun en toeverlaat bij alle experimenten. We hebben aardig wat uurtjes doorgebracht in het lab met de ratten, de gels, de paraffine blokjes enzovoort. Hartelijk dank voor je technische assistentie maar zeker ook je inhoudelijke commentaren op ons werk.

Karel Bezstarosti en Dick Dekkers, hartelijk dank voor jullie hulp bij de 2D gels, westernblots en uiteraard de massa spectrometrie.

Jochem, Wilfred, Daniëlle, Diederik en alle andere onderzoekers, bedankt voor de leuke tijd! De gezamenlijke lunches, bakjes koffie met de bijbehorende verhalen...prima!

Mijn collega's in het Sint Franciscus Gasthuis wil ik bedanken voor hun gezelligheid die het maakt dat ik daar een fantastische opleidingstijd heb. Binnenkort naar het Erasmus MC! Ik kom zeker nog eens "Snorren".

Lieve vrienden, teamgenootjes, bedankt voor jullie interesse, steun en begrip (als ik weer eens niet op de training was...) tijdens dit hele traject. Maar bovenal bedankt voor alles wat niks met onderzoek te maken heeft! Remco en Melchior, fijn dat jullie mijn paranimfen willen zijn.

Mijn familie en met name mijn ouders wil ik bedanken voor hun onvoorwaardelijke steun, interesse, en liefde. Ja pa, na al die tijd is de afronding nabij, it giet oan!

Lieve Eline, bedankt dat je er voor me bent. Nu dit afgerond is hebben we gelukkig weer meer tijd voor elkaar. Tijd voor vakantie! Kus!

Matthijs

Februari, 2012

Curriculum Vitae

Matthijs Jan Faber was born on August the 17th of 1980 in Terneuzen, the Netherlands. After graduating from high school at the Zeldenrust-Steelant College in Terneuzen he started Medical School at the Erasmus University Rotterdam in 1998. In 2002 he performed research at the Department of Pediatric Cardiology at the Johns Hopkins University, Baltimore, MD, USA (Dr. J.I. Brenner). In 2003 he started working as a PhD student at the Department of Pediatric Cardiology at the Erasmus MC (Rotterdam, the Netherlands) under supervision of Prof. dr. W.A. Helbing and Dr. M. Dalinghaus. His studies focussed on the effects of right ventricular pressure overload on hemodynamics as well as proteomic changes. The latter part was in close collaboration with the Department of Biochemistry (Prof. dr. J.M.J. Lamers, Dr. AJ.M. Verhoeven). During this period he spent 6 months as a research trainee at the Proteomics Center of the Johns Hopkins University (Prof. J.E. van Eyk). In 2006 he started his internships and graduated from Medical School in 2008. Afterwards he started working as a surgical resident at the Sint Franciscus Gasthuis in Rotterdam where he started his surgical training in July 2009 (Dr. A.J.H. Kerver, Dr. G.H. Mannaerts and Prof. dr. J.N.M. Ijzermans).